LA-UR-21-24825
Approved for public release; distribution is unlimited.

Title: 2020 Virtual Theoretical Division Lightning Talk Series

Author(s): Ramsey, Marilyn Leann; Albright, Apollo James Yin; Andrews, Elizabeth Marie; Csicsery-Ronay, Jennifer Ann; Darwin, Leah Jewell; Fedik, Nikita Sergeyevich; Forde, Aaron Arthur; George, Andrew; Gonzales, Theodore Gary; Kolade, Beauty Ayomide; Kulichenko, Maksim; Kupets, William Redpath; Mallela, Abhishek; Mora Perez, Carlos Adrian; Morency, Marie Yamilee Natalie; Patrick, Amanda C.; Sakano, Michael Neil; Sud, James Patrick; Tkachenko, Nikolay; Wang, Ying; Wu, Shanshan; et al.

Intended for: Report

Issued: 2021-05-18

2020 Virtual Theoretical Division Lightning Talk Series

Marilyn L. Ramsey

Albright, A.
Andrews, E.
Csicsery-Ronay, J.
Darwin, L.
Fedik, N.
Forde, A.
George, A.
Gonzales, T.
Kupets, W.
Kolade,B.
Kulichenko,M.
Kupets, W.
Mallela, A.
Mora Perez, C.
Morency, Y.
Patrick, A.
Sakano, M.
Sud, J.
Tkachenko, N.
Wang, Y.
Wu, S.

2020 Virtual Theoretical Division Lightning Talk Series

LANL Host: Marilyn L. Ramsey
WebEx Meeting Link: https://lanl-us.webex.com/lanl-us/j.php?MTID=me40cde05abed7de3e8413cc6fb64af13
WebEx Meeting ID: 133 665 4525
WebEx Password: F4NiNEn443P

All members of the T Division Community, students, staff members, group leaders, division management and other interested individuals are **invited to come and support** the following student(s) during their Lightning Talk presentation.
*The Lightning Talk Series is a forum for T Division students to present information about their current projects

Tuesday, July 14, 2020, **10:00 a.m.–11:00 a.m.**
Webex Meeting ID: 133 854 0103
Webex Possword: A3Ayv3cr2G

Student Speakers: James Sud, UGS
School Affiliation: University of California, Berkeley
Group: T-4, Physics of Condensed Matter and Complex Systems
Mentors: Lukasz Cincio (T-4), Yu Zhang (T-1), Pavel Dub (C-IIAC)

Student Speakers: Nikolay Tkachenko, GRA
School Affiliation: Utah State University
Group: T-4, Physics of Condensed Matter and Complex Systems
Mentors: Lukasz Cincio (T-4), Yu Zhang (T-1), Pavel Dub (C-IIAC)

Title: ***Reducing Complexity of Variational Quantum Eigensolver for Quantum Chemistry***

Abstract: The solution of electronic structure problem is thought to be the nearest future implementation of small, noisy quantum computers. While the complexity of the exact solution of electronic structure problems on classical computers grows exponentially with the number of electrons, we can use the advantage of quantum calculations to make the problem complexity polynomial with respect to the number of simulated particles. Due to the noise inherent in quantum computers, one approach is to use variational quantum-classical algorithms (VQCAs), although a concern for VQCAs is the large number of measurements needed for convergence, especially to within chemical accuracy. Our group uses two techniques to reduce the number of measurements. The first is Rosalin, a shot-frugal algorithm that measures qubits with probabilities based on the coefficients of corresponding terms in the Hamiltonian. The second is permuting qubits in the fermionic Hamiltonian to make the qubit assignment more appropriate for a given architecture and/or ansatz function, which also decreases the required circuit depth. In our study we attempt to combine the powers of these two methods to push VQE algorithms to molecules previously incalculable due to exceedingly high measurement counts and circuit depths.

Tuesday, August 4, 2020, **10:00 a.m –11:00 a.mStudent Speaker: Andrew George, GRA**
Group: T-5, Material and Physical Data
School affiliation: University of Houston, PhD. Student
Mentors: Nathan Garland(T-5) and Mark Zammit(T-1)

Title: Uncertainty Quantification of Atomic Data for Collisional-radiative Modeling of Fusion Plasma*s*

Abstract: Knowing plasma properties such as ion populations and radiated power are crucial in both standard, steady-state and non-standard, instability or disruption scenarios of tokamak plasmas. A superconfiguration collisional-radiative model which is predicated on simple fit cross sections can be used to describe radiative processes and also allow effective completeness in state space. The approximate cross sections have an

inherit uncertainty due to the approximations utilized400 in cross section formulas. Dakota, an uncertainty quantification package can asses these uncertainties by performing a range of UQ studies on multiple collision processes for various atomic targets. The results of the analysis will allow us understand error approximate CR models by comparing simple fit cross section formulas to the ones derived from fine structure models.

Student Speaker: Willem Kupets*, GRA
Group: *T-1: Physics and Chemistry of Materialsand T-5: Materials and Physical Data
School Affiliation: St. John's College Santa Fe
Mentors: Mark Zammit*, Nathan Garland^, James Colgan

Title: Electron Stopping Powers and Mean Excitation Energy of Atoms and Ions using the Los Alamos Atomic Physics Suite of Codes

Abstract: Electron-impact excitation and ionization cross sections of atoms and ions are crucial for modeling plasmas that are in non local thermodynamic equilibrium during tokamak disruption events. Here we utilize cross sections calculated from the Los Alamos Atomic Physics Suite of Codes to calculate electron stopping powers and mean excitation energies for a variety of atoms and ions. We also utilize the Bragg's additive rule to approximate stopping power of molecules. We validate the calculated stopping powers against the convergent close-coupling data for H and H2 before being integrated into the Los Alamos Suite of Codes.

Student Speaker: Leah Darwin, UGS
Group: T-6, Theoretical Biology and Biophysics
School Affiliation: Arizona State University
Mentors: Chris Neale

Title: Computational Search for Cancer Treatments

Abstract: Cancer is a class of diseases where cells grow uncontrollably and form tumors. Untreated tumors can be lethal, making cancer a leading cause of death worldwide. Up to 30% of all human cancers are found to have a mutation in a protein involved in cell growth known as Ras. Mutations to Ras can cause it to be stuck in an on state, where it continuously signals that more cells need to be made, resulting in uncontrollable cell growth. My research focuses on repairing the mechanism that allows Ras to switch to an off state using new drugs. I use molecular dynamics simulations to emulate drugs interacting with Ras and a well-studied model system. After I optimize our system, I will search large chemical libraries to find drug candidates that will be tested at Frederick National Lab to determine their potential to become new treatments for cancer.

Student Speaker: Amanda Patrick, GRA
Group: T-6, Theoretical Biology and Biophysics
School Affiliation: University of Texas at Arlington, PhD. Student
Mentors: Nick Hengartner and Imelda Trejo

Title*: Nonparametric estimation of force of infection in a generalized SEIR model*

Abstract: The rate at which susceptible individuals become infected is known as the rate of infection. The rate of infection will be assumed as a function of time. The foundation of this estimation will be explored using a generalized SEIR model with known distributions for time to recovery and exposure time. Coronavirus data will be applied to the system to obtain numerical results. How the rate of infection can be estimated will be explored

Thursday, August 6, 2020, **10:00 a.m. –11:00 a.m**

Student Speaker: Carlos Mora Perez, GRA
School affiliation: University of Southern California (USC) Department of Chemistry
Group: T-1, Physics and Chemistry of Materials
Mentor(s): Amanda Neukirch & Dibyajyoti Ghosh

Title: TDDFT Characterization of a CsPbBr3 Clusters' Optical Properties

Abstract: $CsPbBr_3$ perovskite quantum dots (QDs) have recently become promising candidates for photovoltaic applications such as light-emitting diodes (LEDs) but the nature of their optical properties have yet to be fully characterized. In this work, we utilize Time-Dependent Density Functional Theory (TDDFT) within the Gaussian16 package to characterize the excitation states transition energies of a small $CsPbBr_3$ cluster. Several charged vacancy defects and a charge build-up in the system were modeled to gain insight into their perturbative effect on electronic properties. The simulated UV-Vis spectrums outline the extent to which Br vacancies and charge systems (+1 or -1) lower absorption, and why they should be avoided for high performing QDs. The findings provide a guide for the tunability of $CsPbBr_3$ QDs optical properties by understanding the nature of the excitations.

Student Speaker: Apollo Albright, UGS
School Affiliation: Reed College
Group: T-5, Applied Mathematics and Plasma Physics
Mentor(s): Nathan Lemons

Student Speaker: Theodore Gonzales
School Affiliation: University of Colorado-Boulder
Group: T-5, Applied Mathematics and Plasma Physics
Mentor(s): Nathan Lemons

Title*: Detecting Anomalies in Graphs*

Abstract: We present a graph-based mathematical framework to do high dimensional, combinatorial hypothesis testing. The modeling framework has many potential applications, including water testing, outbreak detection, anomalous computer detection, and more. Within this framework, we review three specific tests over lattices that generalize to other graphs.

Thursday, August 13, 2020, **10:00 a.m.–11:00 a.m.**

Student Speaker: Jennifer A. Csicsery-Ronay, UGS
School Affiliation: University of Houston, School of Natural Sciences & Mathematics
Group: T-6, Theoretical Biology and Biophysics
Mentor: William S. Hlavacek

Title: *de novo* Assembly of a Reference Genome Sequence for *Pterophyllum spp.* & the Search for Evolutionary Insights

Abstract: *Pterophyllum* is the genus of fish commonly known as angelfish, an iconic member of the aquatic hobbyist's aquarium. By generating a *Pterophyllum* reference-based genome sequence and subsequently the sequences of additional wild and domestic individuals of varying populations, we will identify how the genome structure of the domestic angelfish is affected by anthropogenic hybridization, as it is believed to be a hybrid of closely related species such as *P. scalare and P. leopoldi*. Comparisons of the genomes will lead to identifying the original sources of the domestic angelfish in the wild, as well as pondering a deeper understanding of how hybridization affects its morphological features.

Student Speaker: Beauty Kolade, UGS
School affiliation: CUNY,Lehman College
Group: T-CNLS, Center for Non-Linear Studies and B-11
Mentor(s): Jacob Miner & Robert F. Williams

Title: Validating Experimental Results of toxins using Cheminformatics and Quantum Chemistry

Abstract: Cardiac glycosides are classes of drugs used in the treatment of heart failure. Developing experimental and computational techniques for predicting the range of conformers that can be adopted by these molecules can provide valuable insight into their chemical potency. Previous studies, including efforts by our group, have focused on using ion-mobility mass spectrometry (IM-MS) and molecular dynamics (MD) to describe arrival times average collisional cross sections (CCS) values associated with many different classes of biomolecules, including cardiac glycoside such as Digitoxin. Our goal in this project is to develop a new computational pipeline for generating conformers for validation against experimental results. Using cheminformatics software (RDKit) and open-source quantum chemistry software (psi4) we are able to generate ensembles of digitoxin, analyze results, and generate CCS values more rapidly than we could previously with molecular dynamics. Using geometric criteria of these structures, and those of simple buckyballs and nanotubes, we are able to identify the most salient geometric features that affect calculated CCS values. We aim to apply this approach to other cardiac glycosides so that we can create a library of ion-mobility-based data for cardiac glycosides that other scientists can use to carry out toxicological investigations of unknown compounds.

Student Speaker: Ying Wang, GRA
School affiliation: University of Southern California
Group: T-1, Physics and Chemistry of Materials
Mentor: Amanda Neukirch

Title: Electron-Hole recombination of Hybrid Dion-Jacobson 2D Lead Iodide Perovskite: Nonadiabatic Molecular Dynamics Analysis

Abstract: 2D hybrid organic-inorganic halide perovskites attracts increasing research attention because of the higher moisture stability and tunabilities of electronic and optical properties. Recently, Dion-Jacobson 2D lead iodide perovskites have been applied to solar cells, exhibiting considerable application prospects. In this project, we focus on two basic hybrid Dion-Jacobson 2D lead iodide perovskite structures, (3AMP)$(MA)_3Pb_4I_{13}$ and (4AMP)$(MA)_3Pb_4I_{13}$ with power conversion efficiency (PCE) as solar cells, 7%, %5, respectively. Experimental work has indicated that the less distorted inorganic lattice in(3AMP)$(MA)_3Pb_4I_{13}$ results in a narrower band gap. The shortest I···I interlayer distance among reported 2D lead iodide perovskites leads to the enhancement in charge transport performance. In order to investigate optoelectrical behavior of these materials and improve the PCE, we adopt ab initio calculation and nonadiabatic molecular dynamics simulation. Through ab initio calculation, we investigate the relationship between optoelectric properties and structures of these materials in ground state, especially the high carrier mobility along the staking direction. The comparison between radiative lifetimes and nonradiative lifetimes of these perovskites rationalizes their PCE difference. Our study helps us have a better understanding of 2D hybrid organic-inorganic halide perovskites from a structure to property aspect and guide the direction for solar cells design with improved PCE.

Student Speaker: Shanshan Wu, GRA
School affiliation: University of Illinois at Chicago
Group name: T-1, Physics and Chemistry of Materials.
Mentors: Danny Perez, Ping Yang

Title: Long-timescale simulations of morphological changes in ThO_2 nanoparticles

Abstract: Thorium dioxide (ThO_2) nanomaterials have gained increasing attention due to their various application, including catalysis and ceramics. As early actinide oxide, ThO_2 is also of interest for nuclear applications, in and of itself, or as a surrogate for later actinides. Understanding the morphological and dynamical properties of ThO_2 is therefore very important. Molecular dynamics (MD) simulations are an ideal tool to do so, as they provide fully-resolved atomistic trajectories. My research focuses on studying morphological changes of ThO_2nanoparticles using Accelerated MD, a class of methods that significantly extend the time scale of MD. In this talk, I will first introduce the method I used, and then discuss the morphological and dynamical properties of very small ThO_2 nanoparticles, such as those that would form soon after nucleation. In particular, I will show that some nanoparticles experience very slow shape transitions between different classes of structures.

Tuesday, August 18, 2020, **10:00 a.m.–11:00 a.m.**

Student Speaker: Yamilee Morency, GRA
School Affiliation: University of Pennsylvania
Group: T-1, Physics and Chemistry of Materials
Mentor: Justin Smith

Title: ***Physics-based Machine Learning Potential Report Card***

Abstract: Potential energy surfaces are essential to solving many problems in chemistry. They are however limited by costly ab initio methods. Machine learning potentials provide a cost-efficient alternative to ab initio methods with little to no loss in accuracy. However, these models have no physical basis. To evaluate their ability to reproduce complex physical phenomena, we propose a physics-based machine learning report card. This report card will be a test suite made up if archetypal problems in chemistry it will also attempt to answer the question of whether failure of the model is caused by the poor parameterization or model descriptors. This talk is a first step towards this report card. It is an analysis of the short-range dependency of the necessary cutoff radius of ANI models in terms of conjugated hydrocarbons.

Student Speaker: Nikita Fedik, GRA
Group: T-1, Physics and Chemistry of Materials
School: Utah State University, Chemistry and Biochemistry Department
Mentors: Benjamin Nebgen, Sergei Tretiak

Title: ***Machine learning parametrization of empirical and semiempirical methods for improving transition metal chemistry***

Abstract: Transition metals (TM) and their complexes are of paramount importance for organometallics, environmental study, catalysis, and industrial applications. However, large scale modeling of TM complexes is very limited by the performance of contemporary methods such as Density Functional Theory (DFT). Fast semiempirical quantum mechanical methods (SEQM), which are of two order of magnitude faster than DFT, often produce errors about 100 kcal/mol for simple organometallic complexes. Additionally, many such SEQM methods completely lack parameters for TM, sometimes neglecting d-oribitals entirely. In this talk, we aim to develop classic machine learning (ML) model for transition metals using the HIPNN architecture. Additionally, we attempt to generate a SEQM parameterization scheme utilizing ML dynamic parameterization to simultaneously improve the accuracy of SEQM methods and rapidly parameterize previously unstudied transition metal.

Student Speaker: Maksim Kulichenko
School Affiliation: Utah State University
Group: T-1, Physics and Chemistry of Materials
Mentors: Justin Smith, Sergei Tretiak

Title*: Diversification of ML Datasets Using Bias Potential as Function of "Uncertainty*"

Abstract: One of the central issues in machine learning is a dataset. Its diversity, size, and preparation time are the variables which researchers always aim to optimize. The purpose of this work is to capture as much chemical space as possible using active learning and biased potentials embedded in the molecular dynamics. Active learning is the technique which allows to keep the dataset as diverse as possible using the ensemble of neural networks. Within MD framework this means augmentation of dataset with only those MD steps where ensemble of neural networks feels uncertain. By constructing biased potentials which are functions of the "uncertainty", we want to make poorly sampled regions more energetically favorable. Thus, artificially forcing the MD to avoid well sampled regions, bias potentials within active learning may significantly accelerate datasets preparation time while increasing the data diversity.

Student Speaker: Yamilee Morency, GRA
School Affiliation: University of Pennsylvania
Group: T-1, Physics and Chemistry of Materials
Mentor: Justin Smith

Title: ***Physics-based Machine Learning Potential Report Card***

Abstract: Potential energy surfaces are essential to solving many problems in chemistry. They are however limited by costly ab initio methods. Machine learning potentials provide a cost-efficient alternative to ab initio methods with little to no loss in accuracy. However, these models have no physical basis. To evaluate their ability to reproduce complex physical phenomena, we propose a physics-based machine learning report card. This report card will be a test suite made up if archetypal problems in chemistry it will also attempt to answer the question of whether failure of the model is caused by the poor parameterization or model descriptors. This talk is a first step towards this report card. It is an analysis of the short-range dependency of the necessary cutoff radius of ANI models in terms of conjugated hydrocarbons.

Wednesday, August 19, 2020, **10:00 a.m. –11:00 a.m.**

Student Speaker: Elizabeth Andrews, GRA
Group: T-CNLS, Center for Non-Linear Studies and EES-16
School affiliation: PhD Candidate at Colorado School of Mines
Mentors: Jeffrey Hyman, Matthew Sweeney, David Moulton

Title: *How many years can a mountain exist before it's washed to the sea: Investigating weathering of fractured rocks*

Abstract: Weathering plays a critical role in our daily lives and the global climate cycle. It provides the soils which we depend on to grow food, and over longer timescales, it consumes atmospheric CO_2 which regulates the Earth's climate. Many studies have been completed to understand the rate that weathering occurs at the Earth's surface, including field studies and laboratory studies. However, there is a consistent discrepancy between rates measured in the lab and those measured in the field, sometimes the difference is several orders of magnitude. If the rates measured in the lab were widespread in field systems, we might expect that mountains would have fully weathered away. Despite many attempts to reconcile this difference in rates, we still do not fully understand the mechanisms that create the observed large discrepancy. This study investigates how heterogeneous flow paths in fractured bedrock control the weathering rates observed at the hillslope scale using reactive transport simulations. Fractures are modeled discretely using dfnWorks, coupled

to PFLOTRAN to simulate weathering in 3D domains. We will use these simulations to understand the spatial distribution of weathering rates in fractured rock systems. We will also determine how fracture density impacts measured weathering rates at the hillslope scale.

Student Speaker: Michael Sakano, GRA
Group: T-1, Physics and Chemistry of Materials
School Affiliation: Purdue University, PhD Student
Mentors: Edward Kober

Title: ***Comparing RDX and HMX reduced chemistry models applied to 1-D hot spot simulations***

Abstract: Both shock-to-detonation and deflagration-to-detonation transitions are important phenomena in the field of high-energy materials research as their behaviors are still not well understood after decades of experimental and theoretical work. Previous efforts focused on connecting gas-phase energetics with shock and thermal experiments to develop simplified, yet plausible chemistry models. However, it is relatively unknown how well these reaction schemes generalize the overall chemical decomposition process, or if they are even applicable to condensed-phase materials. In this study, we refine our preliminary “reduced order” chemistry models for condensed-phase RDX and HMX single crystals obtained from reactive molecular dynamics simulation with the ReaxFF-lg force field. Data was collected from various small-scale temperature and pressure homogeneous isothermal simulations and these results were analyzed using the non-negative matrix factorization algorithm. The computed chemistry components, which were in good agreement with published literature, added greater detail and insight over prevailing theories. We mapped these components onto larger 1-D hot spot simulations to understand how the system evolves from reactants to gaseous products both spatially and temporally. We observed trends in the relationship between variations in chemistry and loading conditions, and eventually plan to implement these simplified models into continuum-level simulation codes.

Student Speaker: Abhishek Mallela
School Affiliation: Department of Mathematics, University of California Davis
Group name: T-6, Theoretical Biology and Biophysics
Mentor name: William S. Hlavacek

Title: ***Bayesian Uncertainty Quantification for COVID-19 Situational Awa***reness

Abstract: To increase situational awareness and support evidence-based policy-making, we formulated two types of mathematical models for COVID-19 transmission within a regional population. One is a fitting function that can be calibrated to reproduce an epidemic curve with two timescales (e.g., fast growth and slow decay). The other is a compartmental model that accounts for quarantine, self-isolation, social distancing, a non-exponentially distributed incubation period, asymptomatic individuals, and mild and severe forms of symptomatic disease. Using Bayesian inference, we have been calibrating our models daily for consistency with new reports of confirmed cases from the 15 most populous metropolitan statistical areas in the United States and quantifying uncertainty in parameter estimates and predictions of future case reports. This online learning approach allows for early identification of new trends despite considerable variability in case reporting. We infer new significant upward trends for five of the metropolitan areas starting between 19-April-2020 and 12-June-2020.

Thursday, August 27, 2020,**10:00 a.m. –11:00 a.m.**

Student Speaker: Aaron Forde (GRA)
School Affiliation: Materials and Nanotechnology, North Dakota State University
Group name: T-1, Physics and Chemistry of Materials
Mentor: Amanda J. Neukirch, Dibya Ghosh

Title: ***Chiroptical Properties Induced into a Lead-Halide Perovskite Cluster Through Surface Chemistry***

Abstract: Chiroptical properties of materials is of interest for various applications, such as structure determination, photo-detectors for polarized light, highly polarized photoluminescence, and spintronics. Chiroptical activity of organic molecules has been a long studied subject due the enantiomer structures which break mirror symmetry, allowing for distinct magnetic-dipole interactions. Inducing chiroptical activity into semiconductor materials has been a challenge due to the difficulty of creating crystal structures that break mirror symmetry. One proposed method to induce chirality into semiconductor materials is to use chiral organic molecules as capping ligands for inorganic nanocrystals. Experimentally it is observed that chiral capped nanocrystals show circular dichroism and polarized photoluminescence, but the atomistic details as to how these molecules impart chiral-optical signatures is not well understood. Is it suspected that the chiral signatures are activated from chiral templating of the nanocrystal surface or through charge-transfer excitations. Here we implement atomistic modeling using time-dependent density functional theory calculations to explore the photo-physical pathways that give rise to circular dichroism for a $CsPbCl_3$ lead-halide perovskite cluster that is passivated with chiral methylbenzylamine and diaminocyclohexane molecules. We find that when the chiral molecules are anchored to the cluster surface there are chiroptical signatures which are distinct from the molecule and cluster themselves. We also find the chirpticalo signatures to be contributions of charge-transfer excitations from the molecule to the cluster and from cluster-to-cluster transitions. This suggests there are competing photo-physical pathways giving rise to circular dichroism in chiral passivated clusters.

Detecting Anomalies in Graphs

Los Alamos National Laboratory
Mentor: Nathan Lemons

Apollo Albright [1] Teddy Gonzales [2]

[1] Reed College

[2] University of Colorado Boulder

August 06, 2020

Can You Find the Path of Elevated Mean?

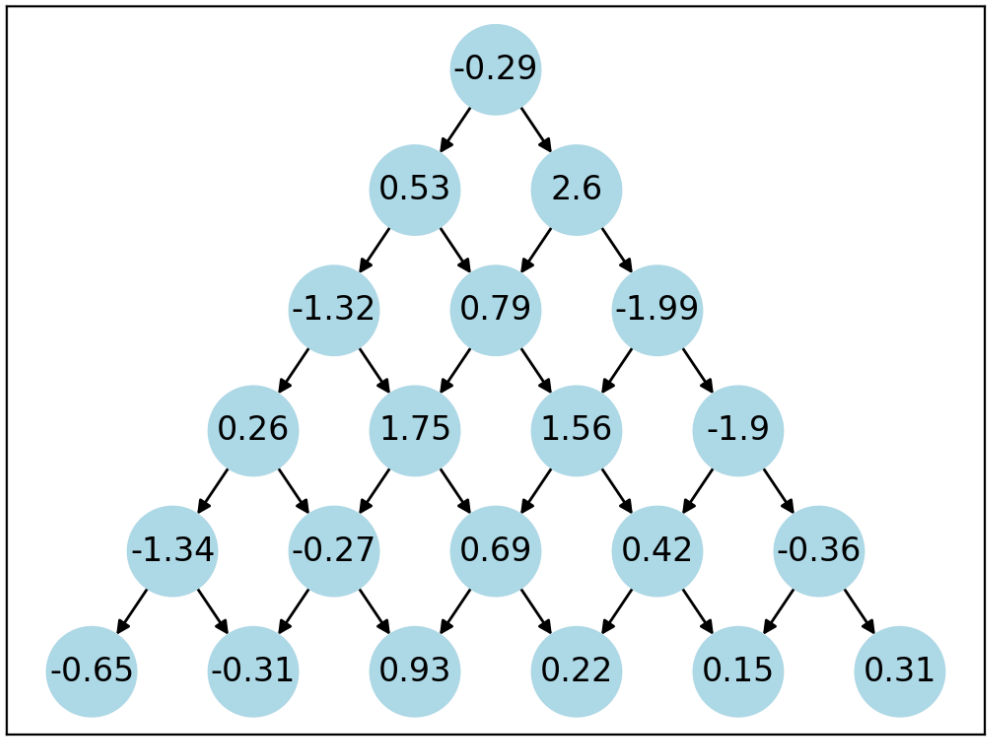

Figure: Lattice With Path of Elevated Mean

Can You Find the Path of Elevated Mean?

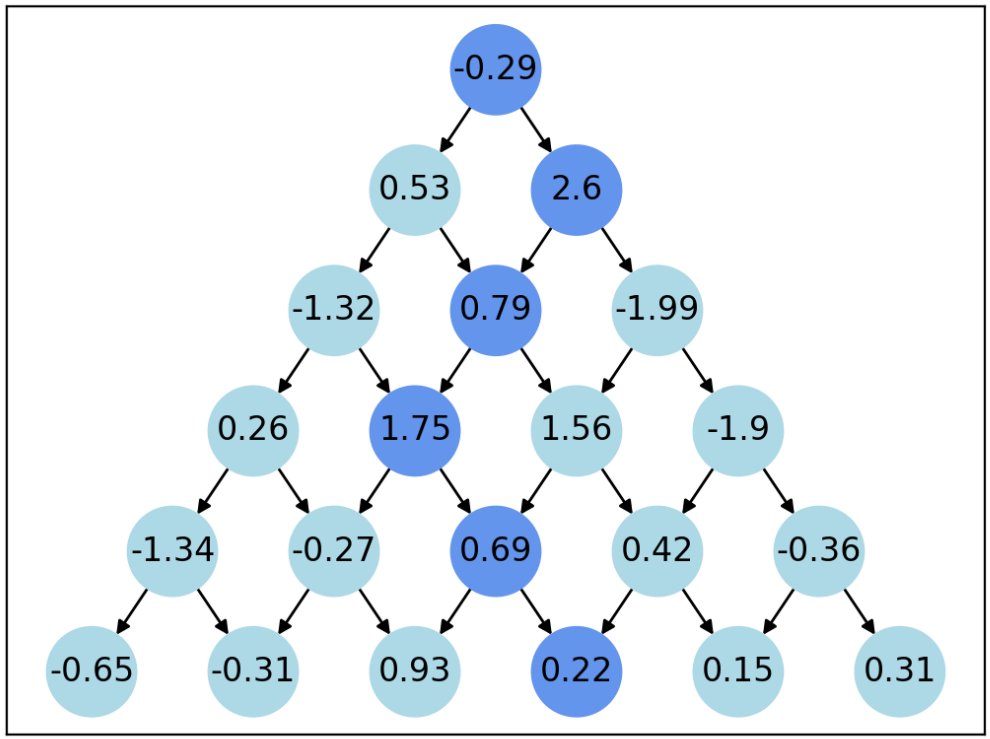

Figure: Lattice With Path of Elevated Mean

Introduction To Framework: Motivation

Potential Applications:

- Chemical spill
- Image patterns
- Anomalous Computers
- Disease outbreak
- Anomalous event in temporal data

Introduction To Framework: Water Quality

1. Sensors are placed at each branching in a river system.
2. At each node *i*, a sensor detects the concentration $\boldsymbol{X}_i$ of an unwanted chemical $\boldsymbol{X}$.
3. Using this data, a test or series of tests determines if a path of elevated chemical concentration exists in the river network.

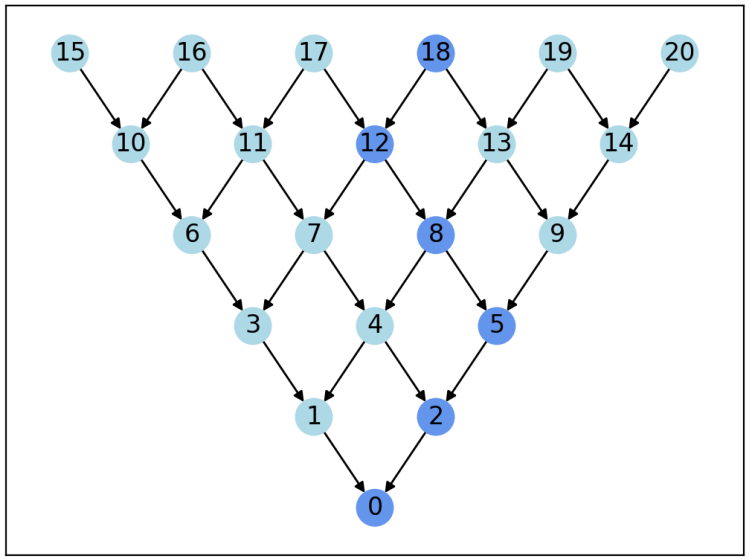

Figure: Example of a Contaminated Stream

Introduction to Framework: In General

- Given $\boldsymbol{X} \subset \{0, 1, 2, \ldots, n-1\}^m$ with some graph structure and with each component a random variable, we would like to distinguish between [1]:
  - H_0 : Every $x \in \boldsymbol{X}$ comes from $N(0, 1)$
  - H_1 : Some subset $P \subseteq \boldsymbol{X}$ from a class $\mathcal{C}$ of subsets has an elevated mean $N(\mu, 1)$
- As $n \to \infty$, we would like to find a threshold for μ, above which, some test T can distinguish between H_0 and H_1, and below which, no test or sequence of tests can distinguish H_0 and H_1.

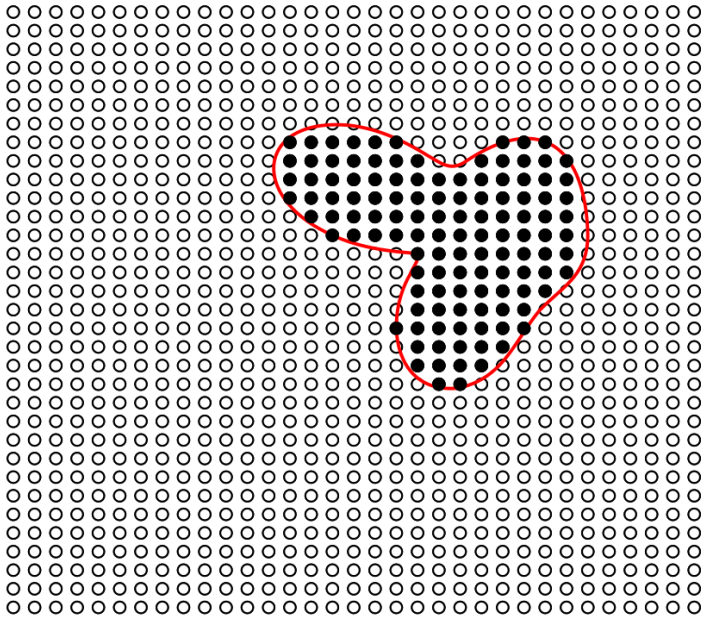

Figure: More General Cluster

Introduction To Framework: Notation

- From here on, we focus on the case of a two-dimensional lattice.
- The lattice has depth (number of levels) m.
- We are interested in $P \in \mathscr{P}_m$, where $\mathscr{P}_m$ is all paths of length m within the lattice.
- A test $T : \boldsymbol{X} \to \{0, 1\}$ distinguishes between the presence or absence of a path with elevated mean.
  - H_0 : Every $x \in \boldsymbol{X} \sim N(0, 1)$
  - H_1 : A path $P \in \mathscr{P}_m \sim N(\mu, 1)$; all $x \notin P \sim N(0, 1)$

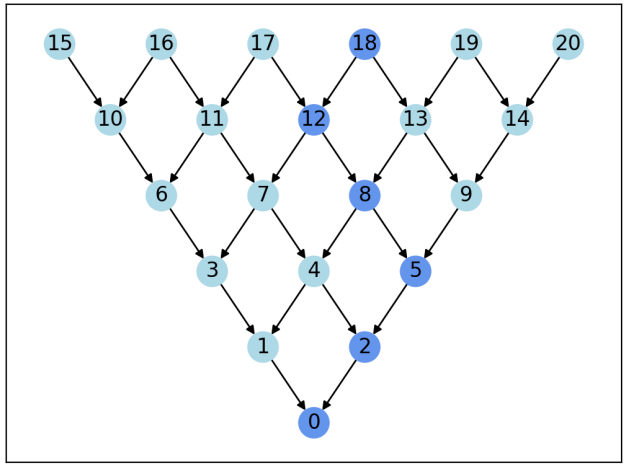

Figure: Lattice with $m = 6$

Three Questions

- What values of μ allow us to distinguish between H_0 and H_1?
- Which tests can work for this?
- What are the computational complexities of these tests?

Types of Tests: Averaging Test

- The Averaging Test is perhaps the simplest [1]:
  - Reject H_0 if $\sum_{x \in \boldsymbol{X}} \geq \frac{1}{2}\mu m$
- Benefits:
  - The Averaging Test is computationally very fast, making it the easiest to use on very large graphs.
  - Can be used to detect any pattern in the graph, not just paths.
- Drawbacks:
  - Its detection threshold is far from optimal, and the value of μ required to detect anomalies can grow quite quickly with some graph types.
  - Cannot find the exact location of a path, only its presence.

Types of Tests: Strip Test

- Strip Test [3]:
  - Reject H_0 if $\sum_{v \in V} X_v > \frac{1}{2}\mu m$ with V the set of nodes which are within the strip of radius $2\sqrt{m} + 1$ around the root node.
- Benefits:
  - Checks significantly fewer nodes ($\approx 4m^{3/2}$) than the averaging test ($\approx m^2/2$).
- Drawbacks:
  - Same drawbacks as the averaging test.
  - Limited to 2 Dimensions
  - Poor performance if path is outside strip, susceptible to adversarial attacks.

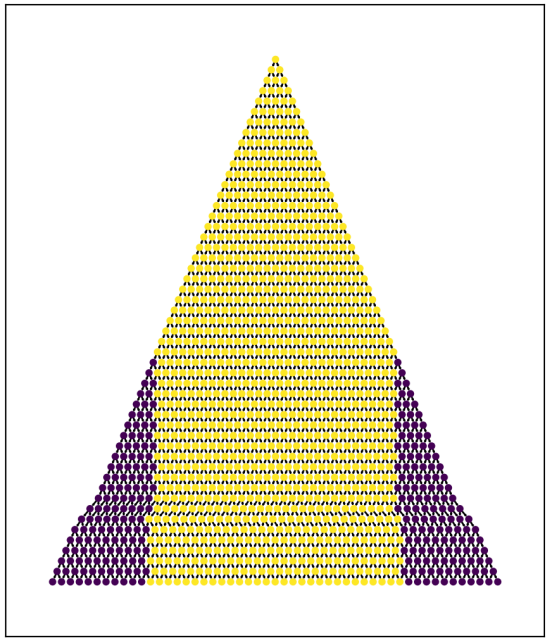

Figure: Strip Over a Lattice

Types of Tests: Bayes Test

- Bayes Test [3]:
  - Assume paths are generated according to some prior distribution π
  - Reject H_0 if $L_m(X) = P(H_1|\pi)/P(H_0|\pi) > 1$.
- Benefits:
  - The Bayes Test can be computed relatively quickly using a recursive algorithm on any acyclic directed graph.
  - If the distribution of paths is known, it has an optimal detection threshold for μ [3].
- Drawbacks:
  - Detecting paths of unknown length can be slow.
  - It assumes paths are generated according to a given prior distribution and is susceptible to adversarial attacks.

Types of Tests: GLRT

- Generalized Likelihood Ratio Test [3]:
  - Reject H_0 if $\max_{p \in \mathscr{P}_m}(\sum_{i \in p} X_i) \geq m\sqrt{2\log(2)}$
- Benefits:
  - Can be applied to find more general shapes in many graphs
  - Path distribution not required
  - Can be used to determine path location
- Drawbacks:
  - Detecting paths of unknown length can be slow.
  - Threshold is not clear when generalizing to other graph and path structures.
  - Often computationally difficult to scan over all “windows”.

Comparison of Tests over 2-D Lattices

- Because the value of μ required to separate H_0 and H_1 can change based on m, we define μ_m to be the value of μ for a given m.

Test	Separable	Inseparable	Runtime	$\mu_{0.95}$
Averaging	$\mu \to \infty$	$\mu \to 0$	$O(m^2)$	2.4
Strip	$\mu_m m^{1/4} \to \infty$	$\mu_m m^{1/4} \to 0$	$O(m^{3/2})$	2.25
GLRT	N/A	N/A	$O(m^2)$	1.25
Bayes	$\mu_m m^{1/4} \to \infty$	$\mu_m m^{1/4} \to 0$	$O(m^2)$	0.85

Table: Bounds for separability and inseparability, runtime scaling as a function of m, and the value of μ required for 95% accuracy with $m = 50$.

Comparison of Tests Over Lattices

Figure: Success Rate vs μ for Various Tests, $m = 100$

- In our testing, with probability 0.5, a path p was picked uniformly at random.
- Under these circumstances, the Bayes test performs the best, followed by the GLRT.
- The Strip and Averaging Tests perform very similarly.

More General Methods

- Generalizations:
  - These methods apply to more than just a 2-D lattice: random geometric graphs, binary trees, and higher dimensional lattices [3, 2].
  - Similar approaches can be used if the random weights are not normally distributed [3].
  - We worked on a few methods of detecting paths of unknown length.
  - These methods, particularly the GLRT, can be applied to detect more general clusters [2].
  - However, without some form of structure to the data, it remains impossible or impractical to detect such clusters as the size of the data set increases.

Thank You for Your Time!

Thank you to our mentor Nathan Lemons who has helped us with this project throughout the summer!

References

- Louigi Addario-Berry, Nicolas Broutin, Luc Devroye, and Gábor Lugosi.
  On combinatorial testing problems.
  The Annals of Statistics, 38, 08 2009.
- Ery Arias-Castro, Emmanuel Candès, and Arnaud Durand.
  Detection of an anomalous cluster in a network.
  Annals of Statistics - ANN STATIST, 39, 01 2010.
- Ery Arias-Castro, Emmanuel Candès, Hannes Helgason, and Ofer Zeitouni.
  Searching for a trail of evidence in a maze.
  The Annals of Statistics, 36, 02 2007.

HOW MANY YEARS CAN A MOUNTAIN EXIST BEFORE IT'S WASHED TO THE SEA: INVESTIGATING WEATHERING OF FRACTURED ROCK SYSTEMS

ELIZABETH ANDREWS[1,2,3], MATT SWEENEY[2,], DAVID MOULTON[4], ALEXIS NAVARRE-SITCHLER[1], JEFFREY HYMAN[2]

1. COLORADO SCHOOL OF MINES
2. EES-16
3. CNLS
4. T-5

COLORADOSCHOOLOFMINES
EARTH • ENERGY • ENVIRONMENT

Los Alamos
NATIONAL LABORATORY
EST. 1943

WHAT IS WEATHERING?

Chemical - dissolution

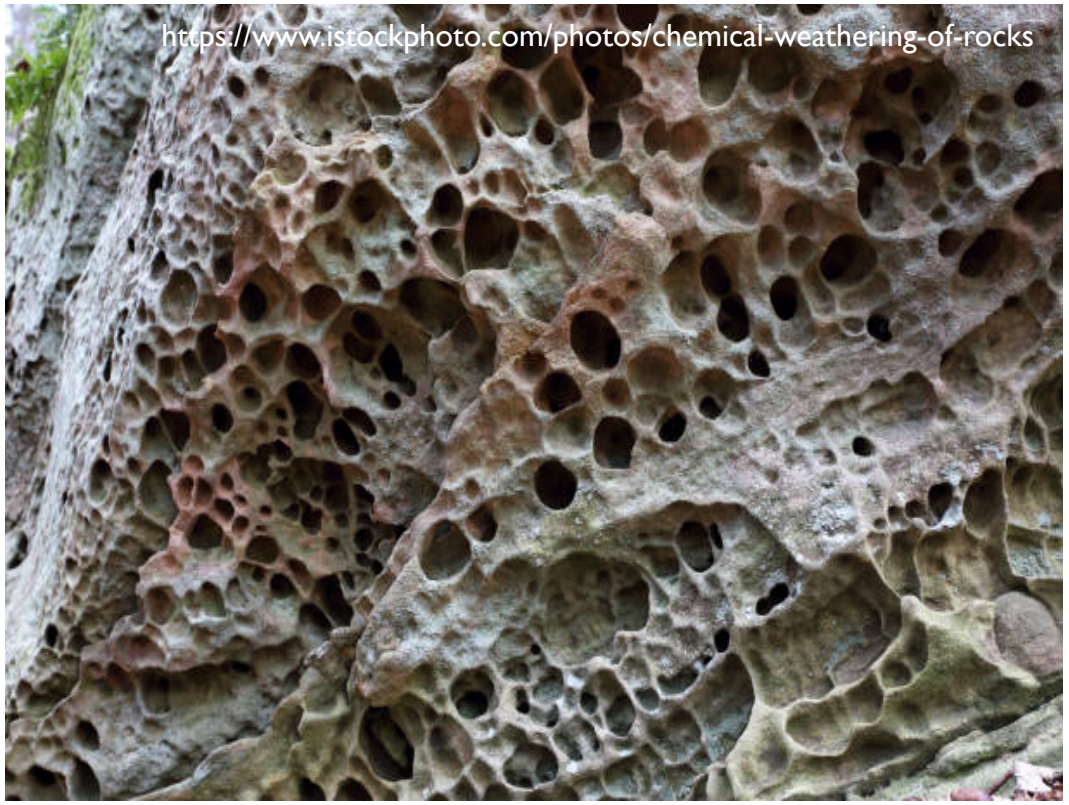

Physical – breaking of rock

WHY IS WEATHERING IMPORTANT?

- Agriculture depends on soil
- Silicate weathering is a long-term climate regulator

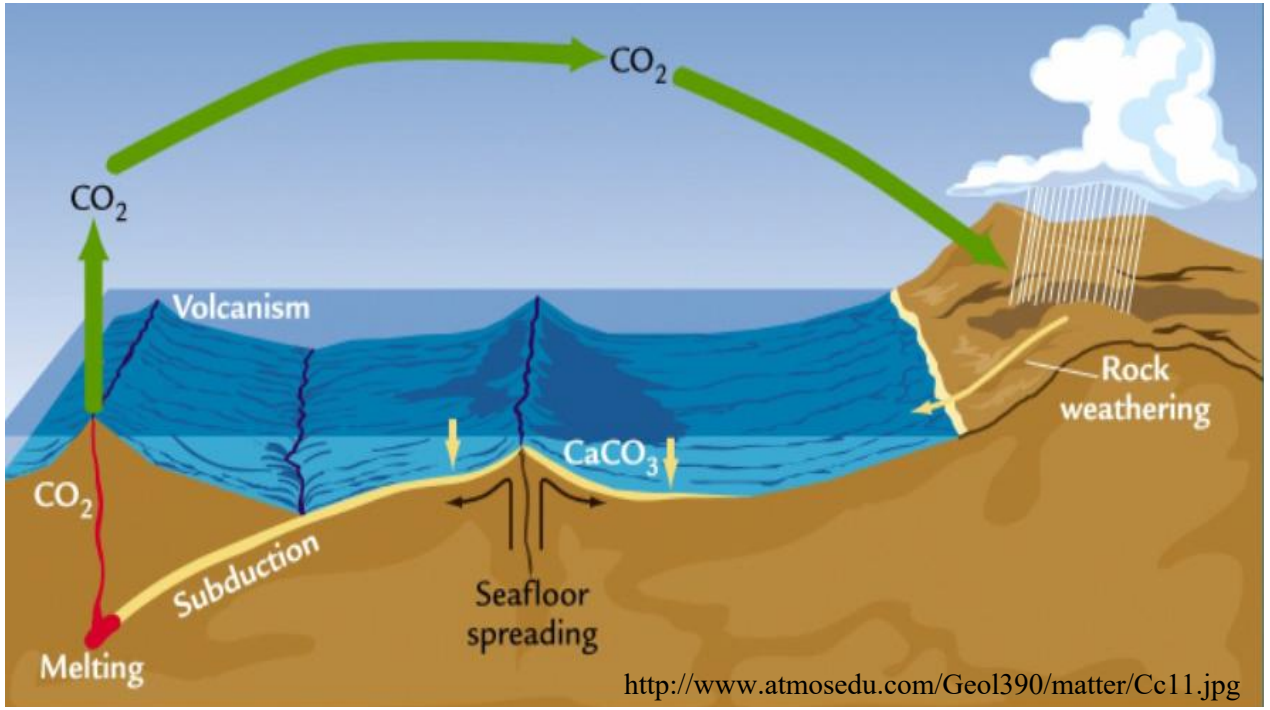

http://www.atmosedu.com/Geol390/matter/Cc11.jpg

WEATHERING RATES MEASURED IN THE LAB ARE SIGNIFICANTLY FASTER THAN FIELD RATES

- Lab conditions?
  - High water:rock ratio?
  - Solution far from equilibrium?
  - Too much surface area?
- Or, is it because of the heterogeneity in the natural system?
  - Heterogeneous flow paths through fractured rock?

Lab

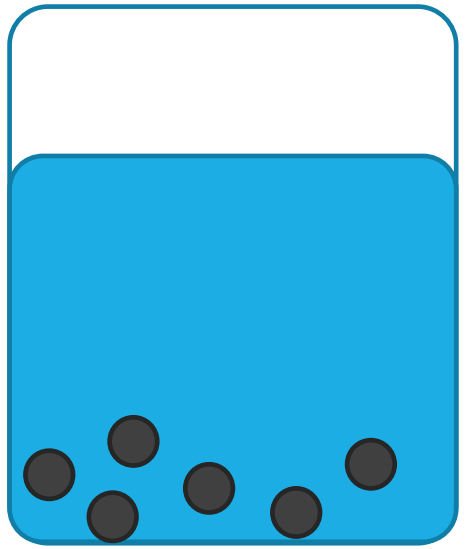

Field

RESEARCH QUESTIONS:

Can flow through fractures explain the difference between lab rates and field rates?

How does fracture density impact the dissolution rate?

DOMAIN SETUP

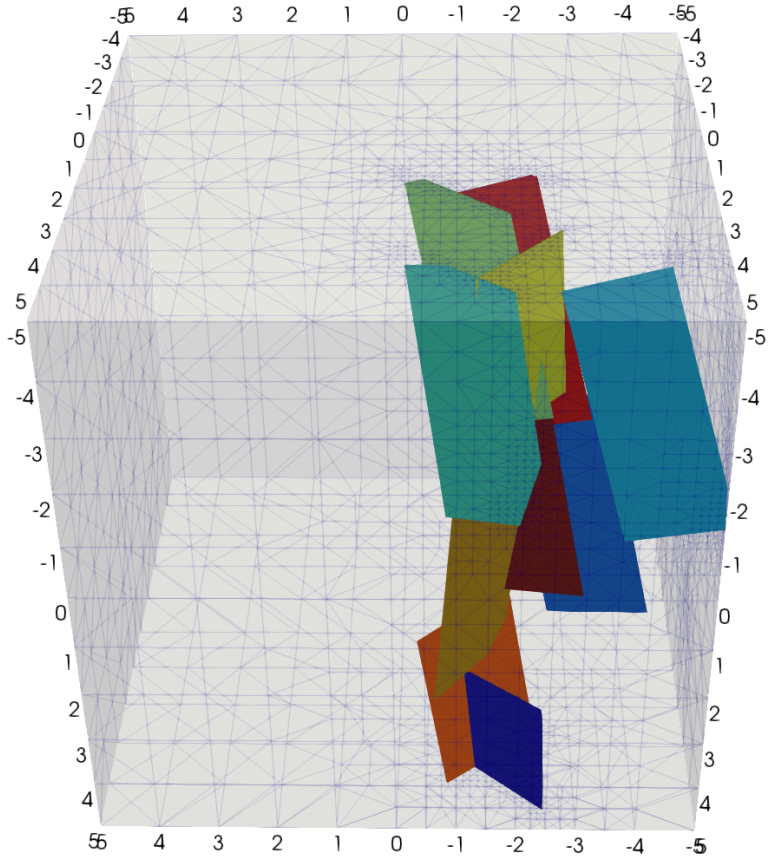

- dfnWorks coupled to PFLOTRAN
- Octree refined domain
- Fluid enters and exits the domain through fractures
- Reactions: Albite dissolution, kaolinite precipitation
  - Albite ($NaAlSi_3O_8$) + $4H^+$ → Na^+ + Al^{3+} + $3SiO_2$ + $2H_2O$
  - $2Al^{3+}$ + $2SiO_2$ + $5H_2O$ → Kaolinite ($Al_2Si_2O_5(OH)_4$) + $6H^+$

SIMULATIONS: 2 DOMAINS

Low density: 11 fractures

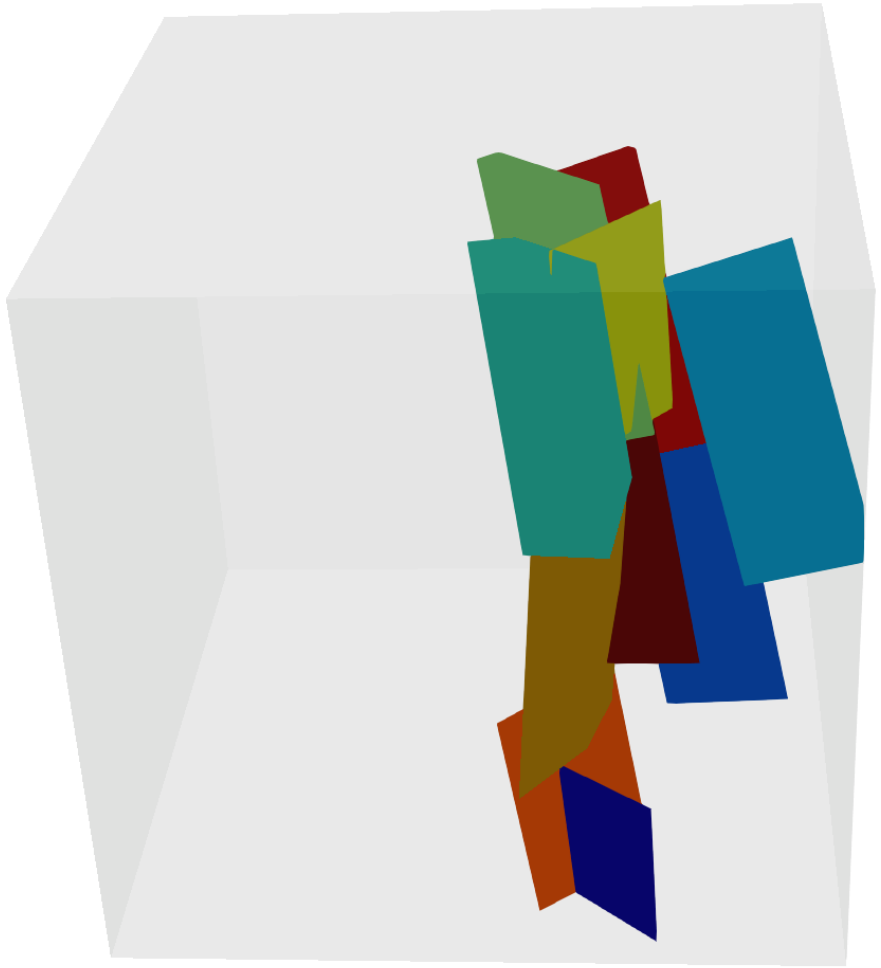

High density: 71 fractures

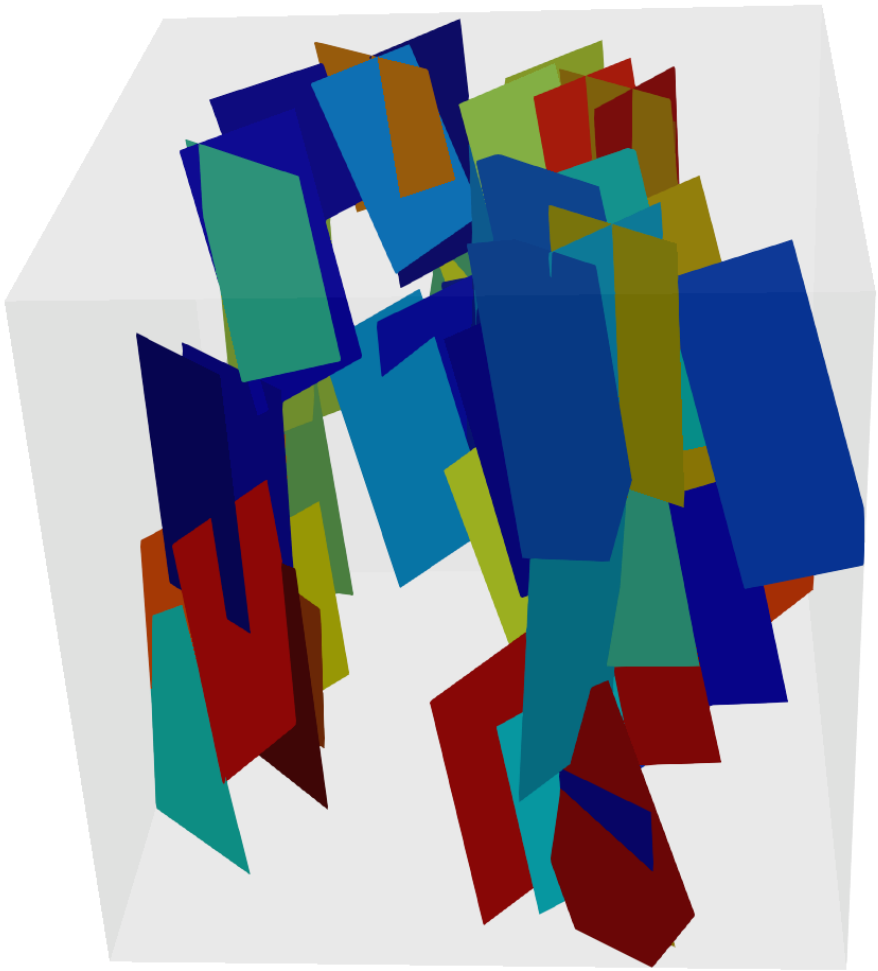

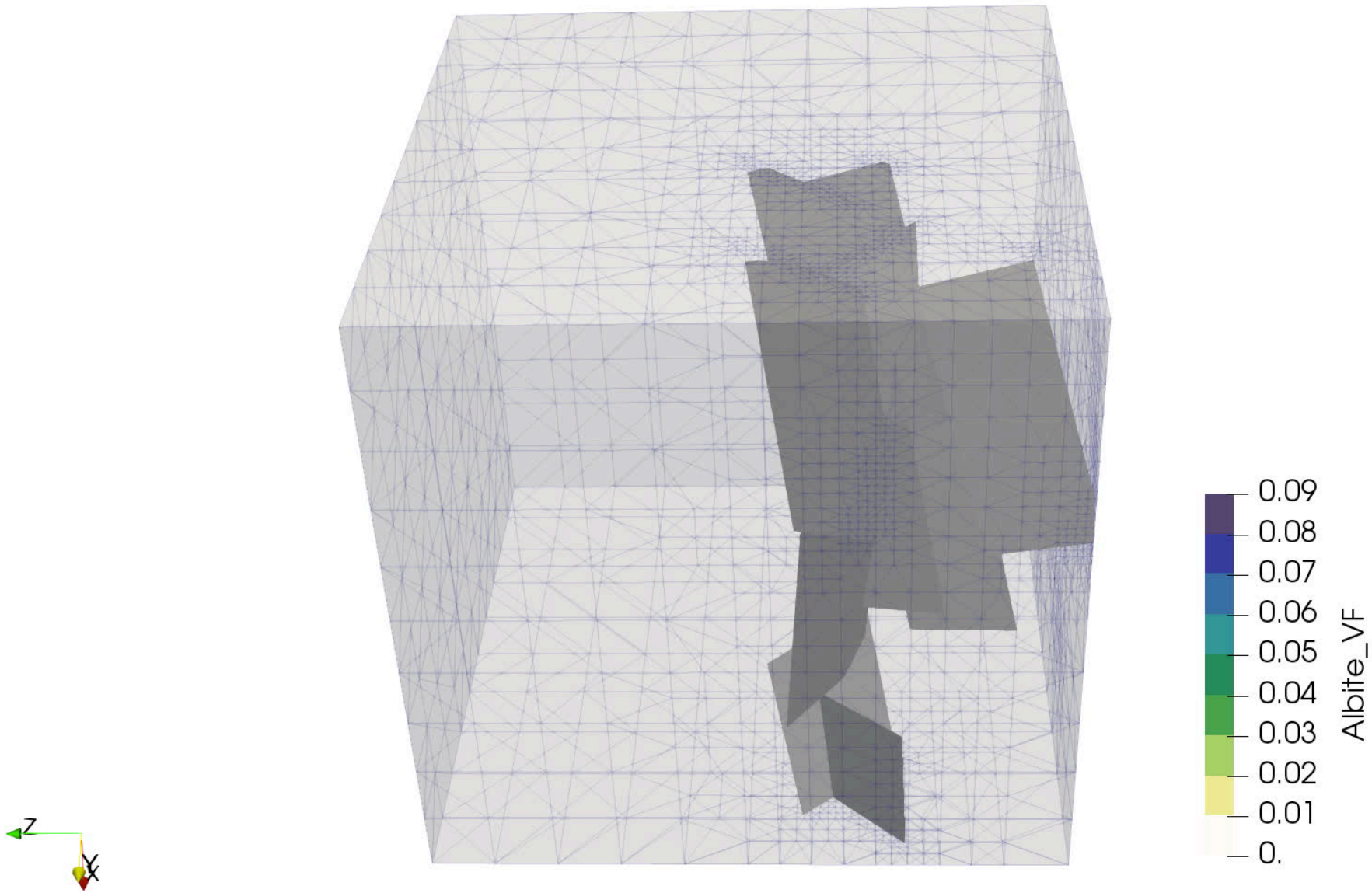
0.09
0.08
0.07
0.06
0.05
0.04
0.03
0.02
0.01
0.
Albite_VF
Z
Y
X

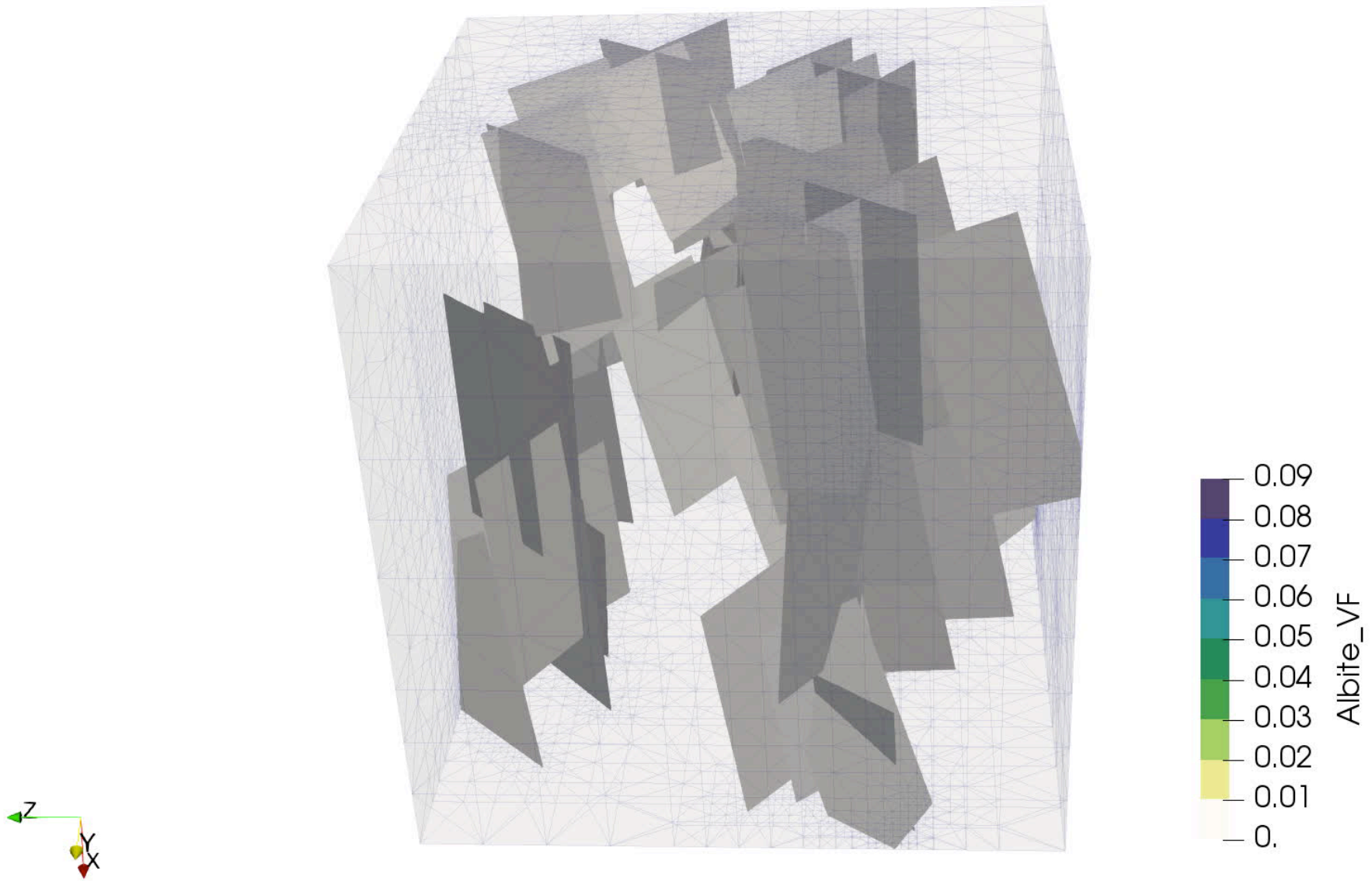
0.09
0.08
0.07
0.06
0.05
0.04
0.03
0.02
0.01
0.
Albite_VF
Z
Y
X

RESULTS

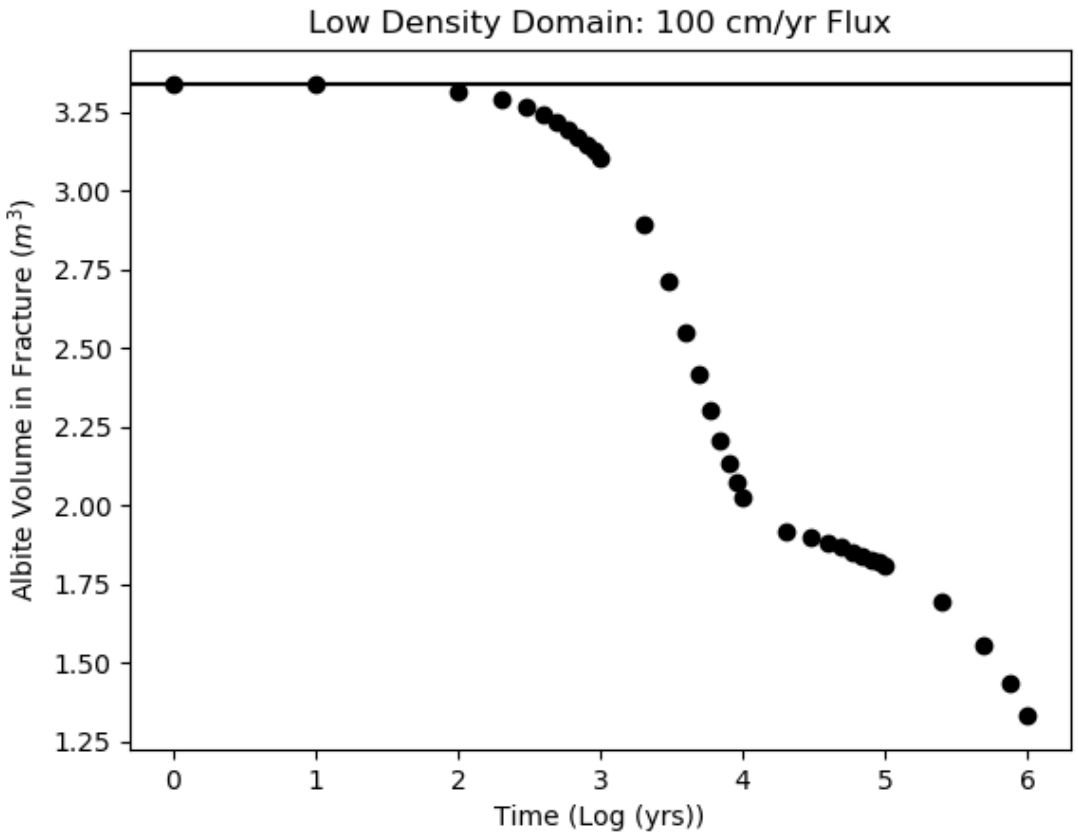
Low Density Domain: 100 cm/yr Flux
Albite Volume in Fracture (m^3)
3.25
3.00
2.75
2.50
2.25
2.00
1.75
1.50
1.25
0
1
2
3
4
5
6
Time (Log (yrs))

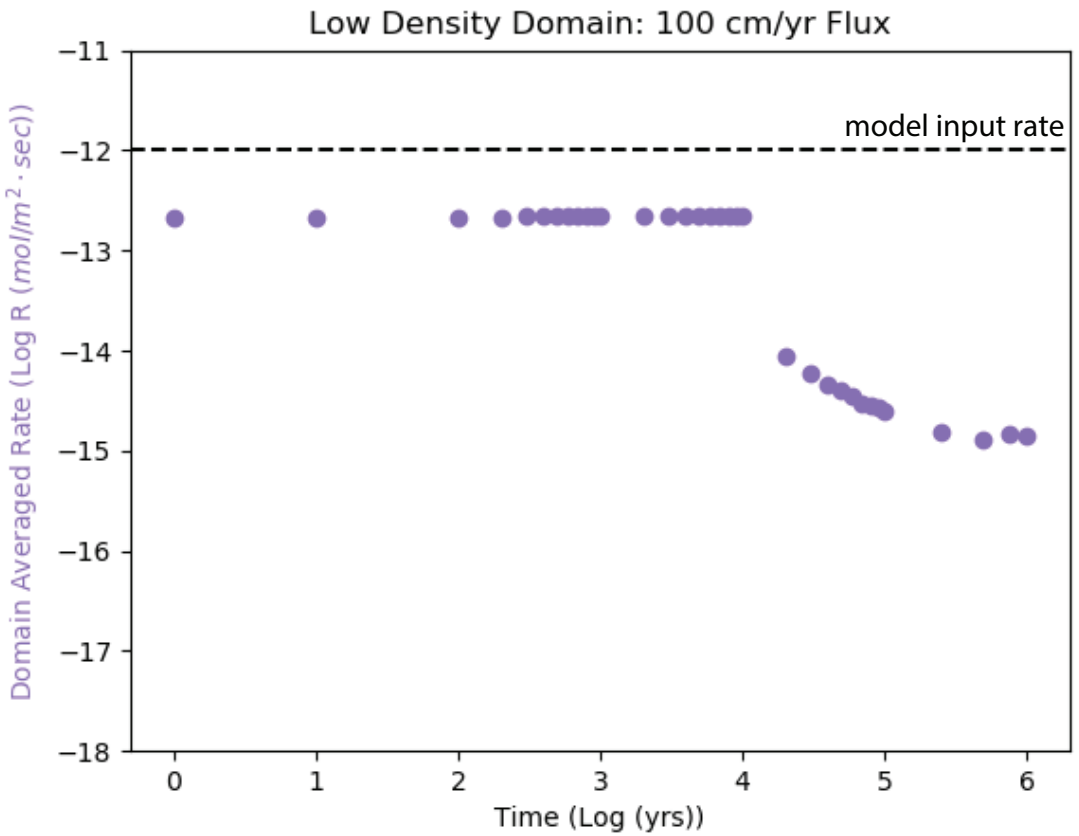
Low Density Domain: 100 cm/yr Flux
Domain Averaged Rate (Log R ($mol/m^2 \cdot sec$))
model input rate
−11
−12
−13
−14
−15
−16
−17
−18
0
1
2
3
4
5
6
Time (Log (yrs))

RESULTS: FAST WEATHERING IS DOMINATED BY REACTION IN FAST FLOWING FRACTURES

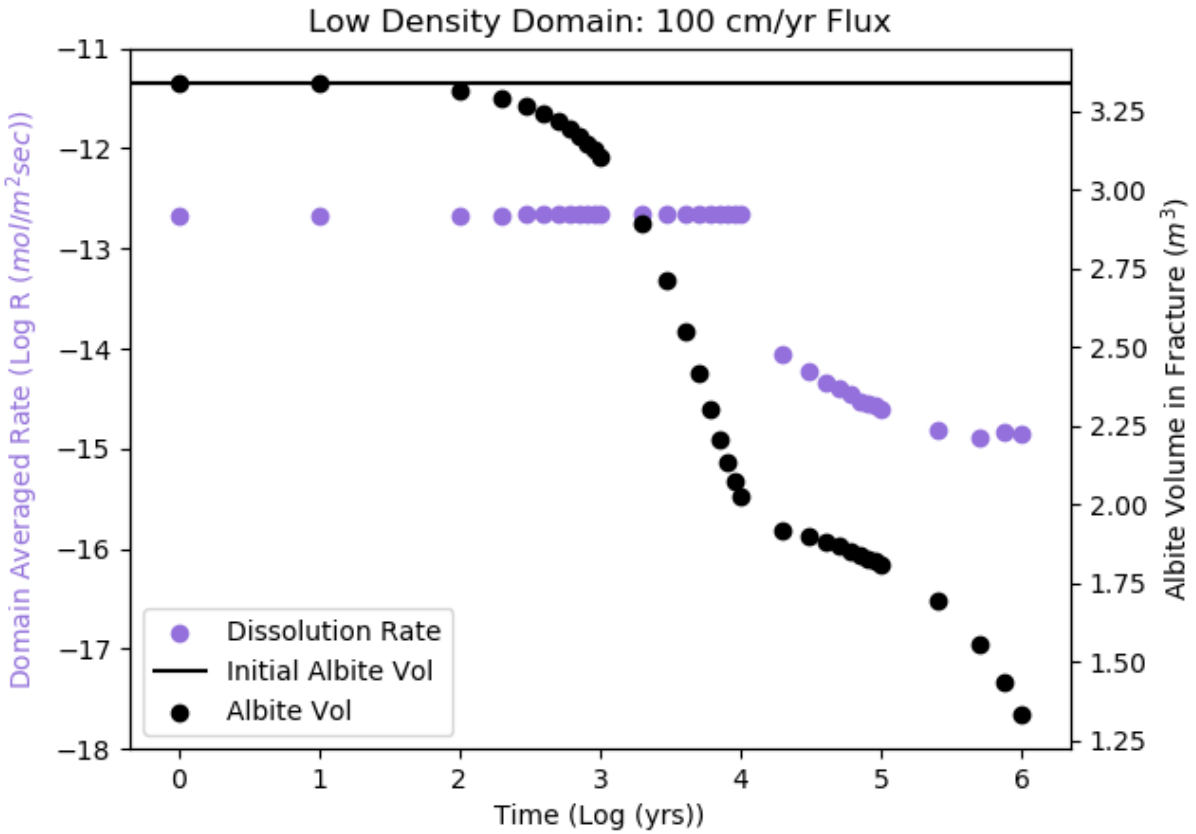

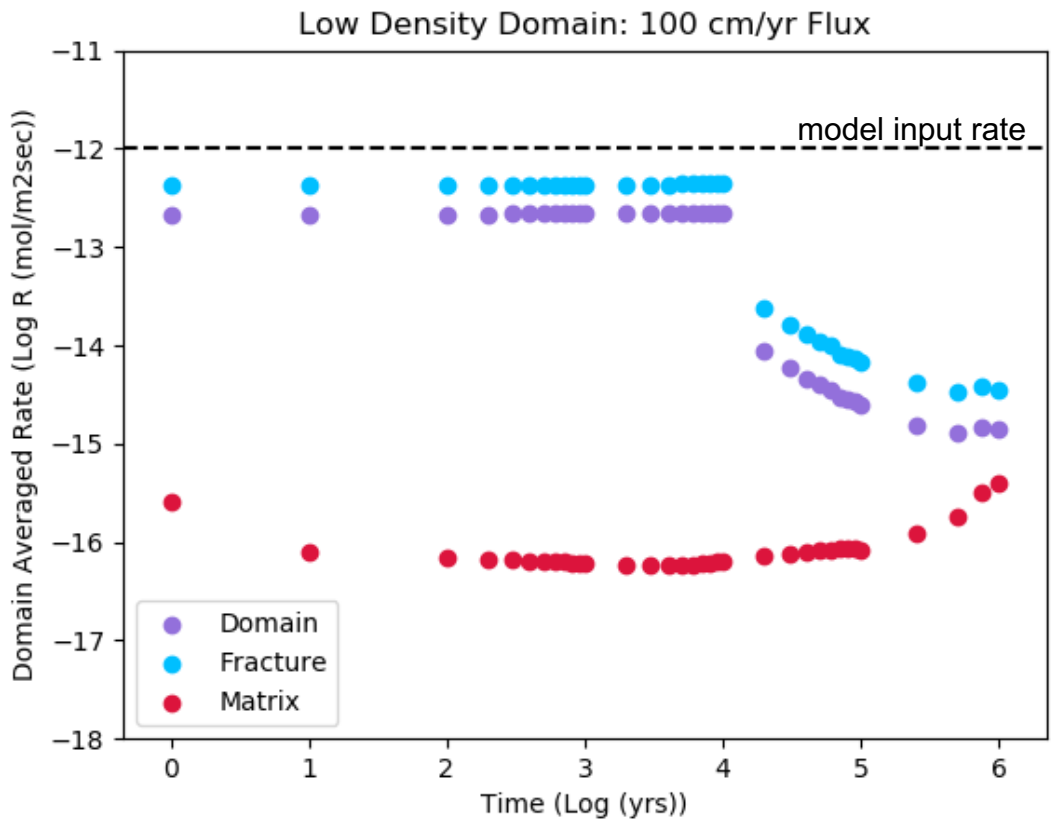

DISCUSSION

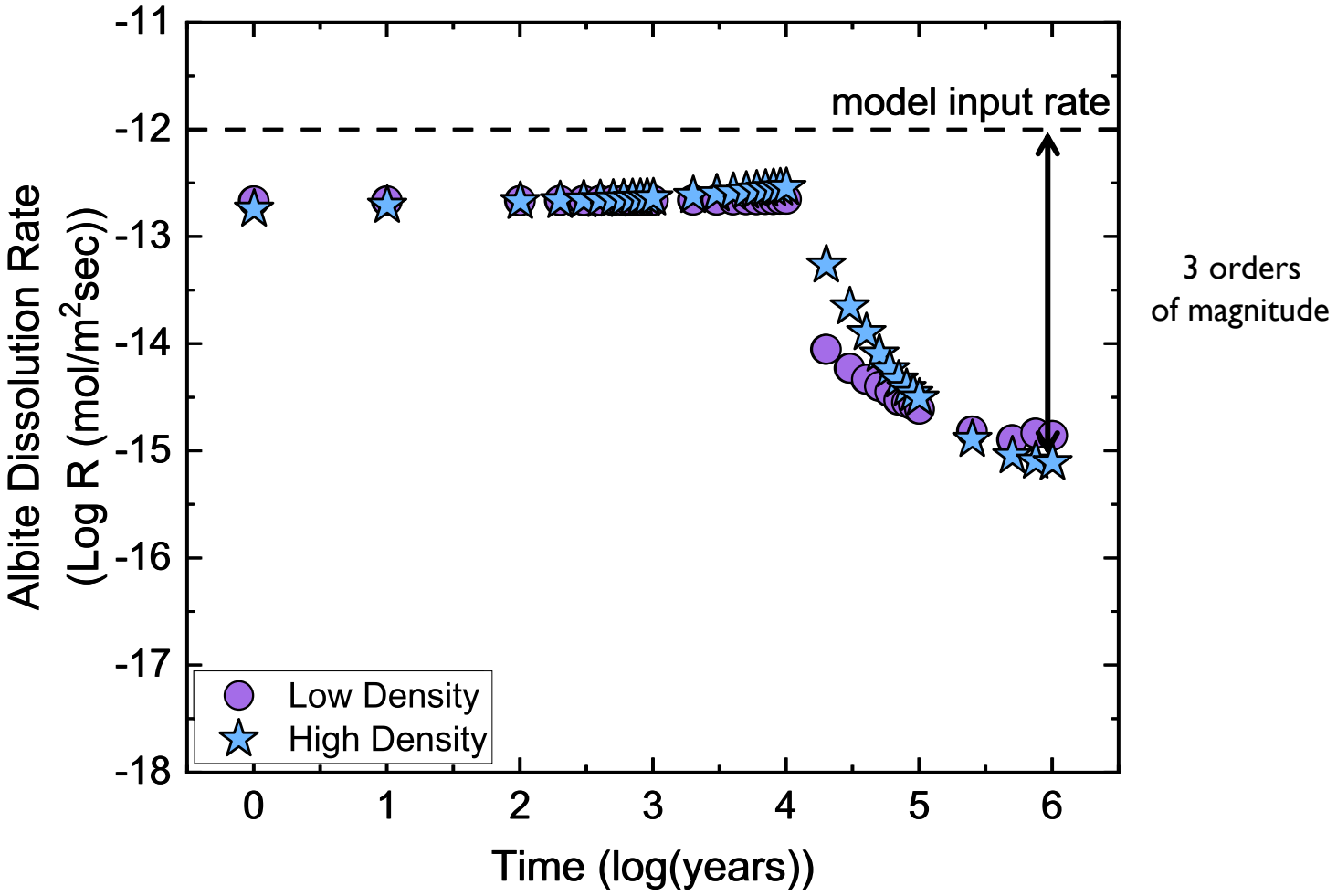

- At early times, no difference in rates between fracture density variations
- At late times, rate behavior varies
- After 100,000 years, the output weathering rate is 3 orders of magnitude smaller than the input rate
- The processes associated with flow through fractures could potentially explain the lab vs. field rate conundrum

THANKS! QUESTIONS?

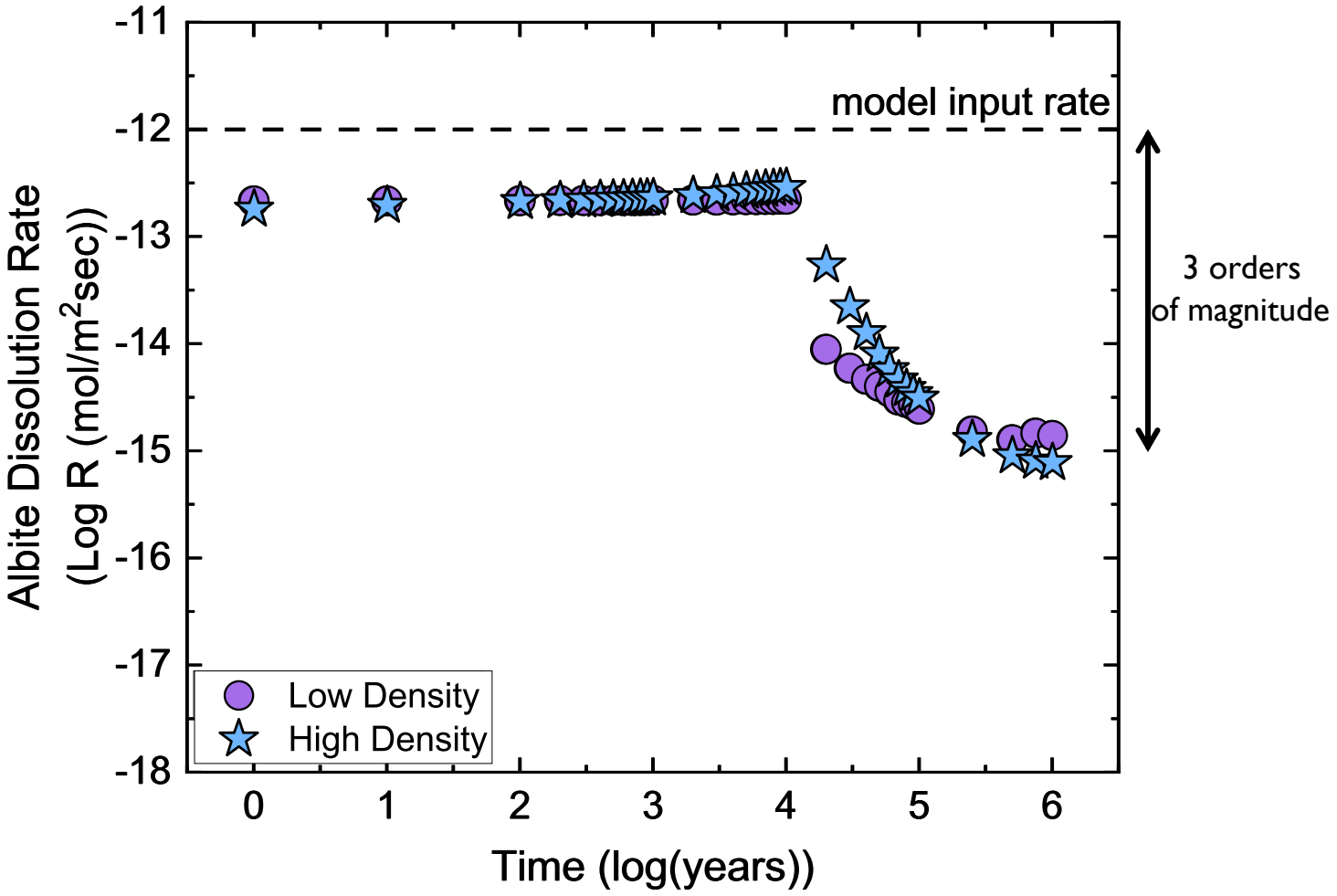

- At early times, no difference in rates between fracture density variations
- At late times, rate behavior varies
- After 100,000 years, the output weathering rate is 3 orders of magnitude smaller than the input rate
- The processes associated with flow through fractures could potentially explain the lab vs. field rate conundrum

de novo Assembly of a Reference Genome Sequence for *Pterophyllum*, spp.

•••

Jennifer A. Csicsery-Ronay
University of Houston
Theoretical Biology & Biophysics
Center for Nonlinear Studies
Mentor: William S. Hlavacek

Outline

- Specimen selection, Tissue Collection, and DNA Extraction
- Hybrid *de novo* assembly
- Quality Assessment of the Draft Genome
- Strategy for Evolutionary Analysis

Specimen Selection, Tissue Collection, & DNA Extraction

Black Lace Angelfish

Pterophyllum scalare

SEQUENCING RESULTS:

Sequencing Type	Library	Coverage	Sample
Illumina	800 bp	57x	3ME2
PacBio	long reads	70x	3ME1

Hybrid *de novo* Assembly

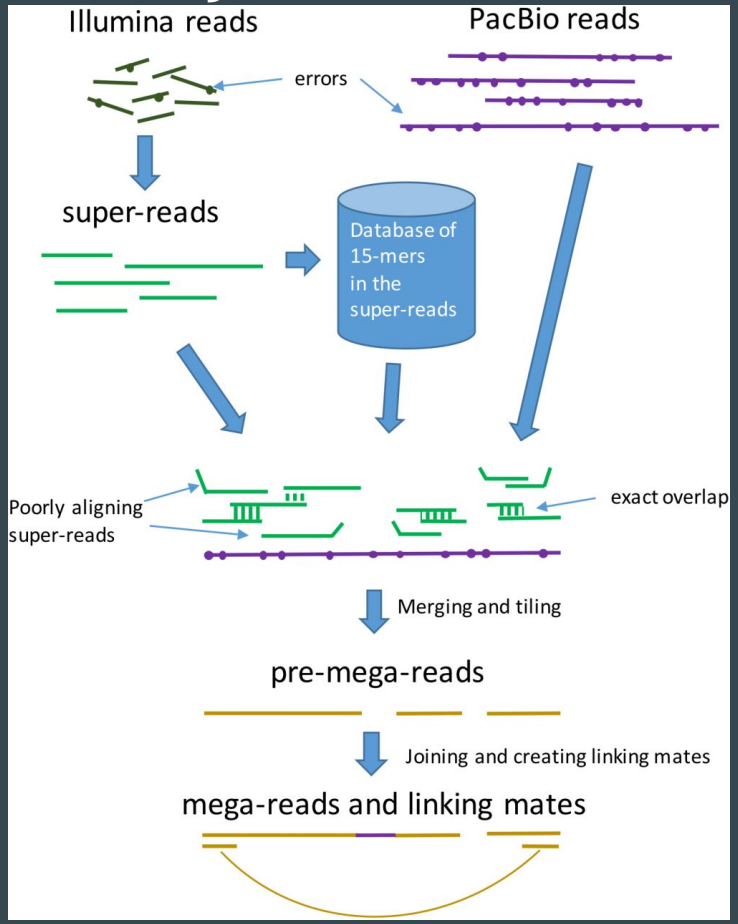

Zimin, Aleksey V. et al. “Hybrid assembly of the large and highly repetitive genome of Aegilops tauschii, a progenitor of bread wheat, with the MaSuRCA mega-reads algorithm.” *Genome research* 27 5 (2017): 787-792 .

Quality Assessment of the Draft Genome: BUSCO

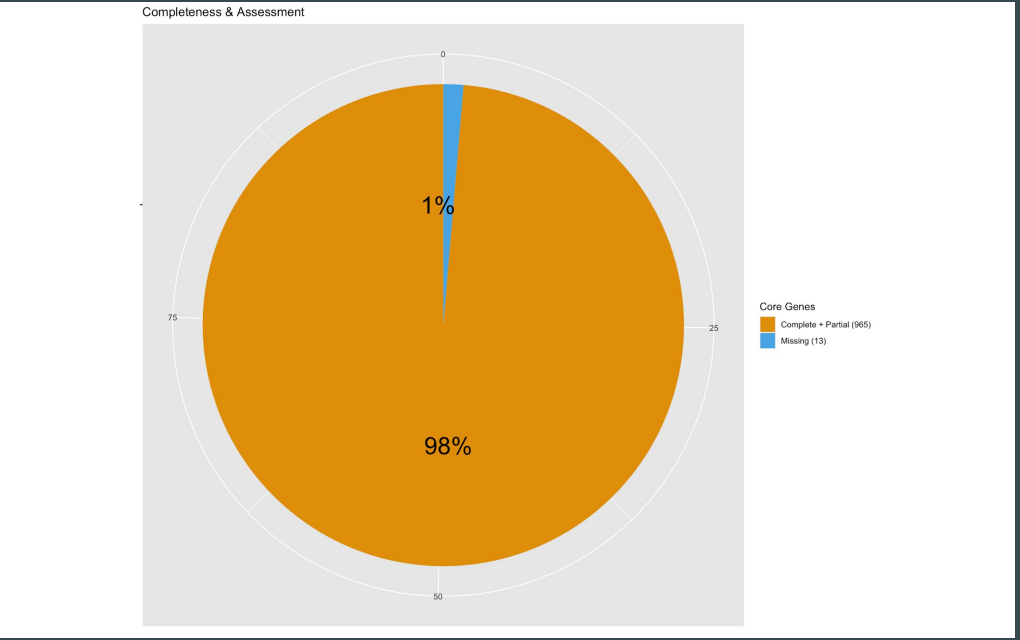

COMPLETENESS ASSESSMENT RESULTS:

Total number of core genes queried	978
Number of core genes detected	
Complete	959 (98.06%)
Complete + Partial	965 (98.67%)
Number of missing core genes	13 (1.33%)
Average number of orthologs per core genes	1.05
% of detected core genes that have more than 1 ortholog	4.59
Scores in BUSCO format	C:98.1%[S:93.6%,D:4.5%],F:0.6%,M:1.3%

Strategy for Evolutionary Analysis

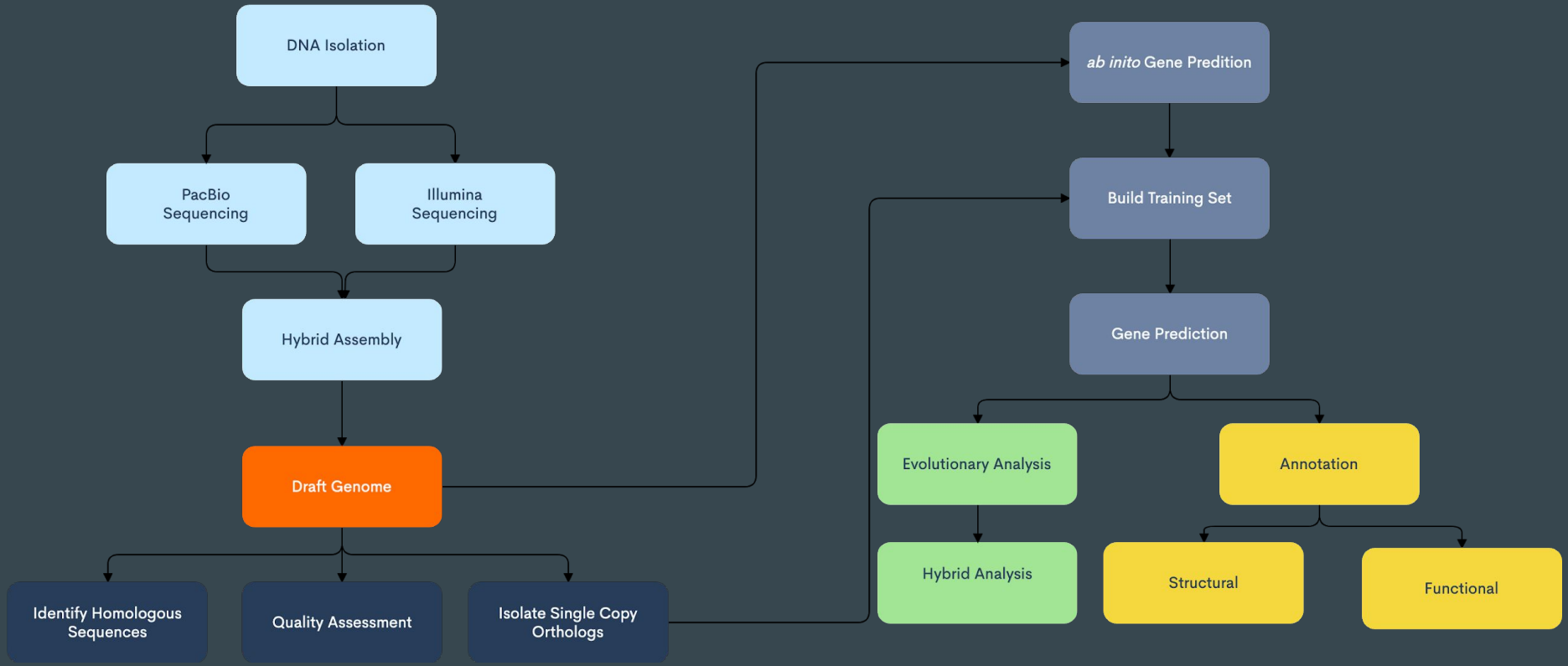

Next Steps

- Complete evolutionary analysis
- Deposit annotated reference sequence
- Re-sequence wild type individuals collected from geographically diverse locations
- Compare genomes to identify which wild types have contributed to the angelfish origin

Acknowledgments

Funding from CNLS

Mentoring:

William S. Hlavacek, T-6

Computational Search for Cancer Treatments

Los Alamos Theoretical Division T-6

Leah Darwin
Mentor: Chris Neale

Introduction

1

What is cancer?

- Cancer is a leading cause of death world wide
- Uncontrollable cell growth leads to the formation of tumors

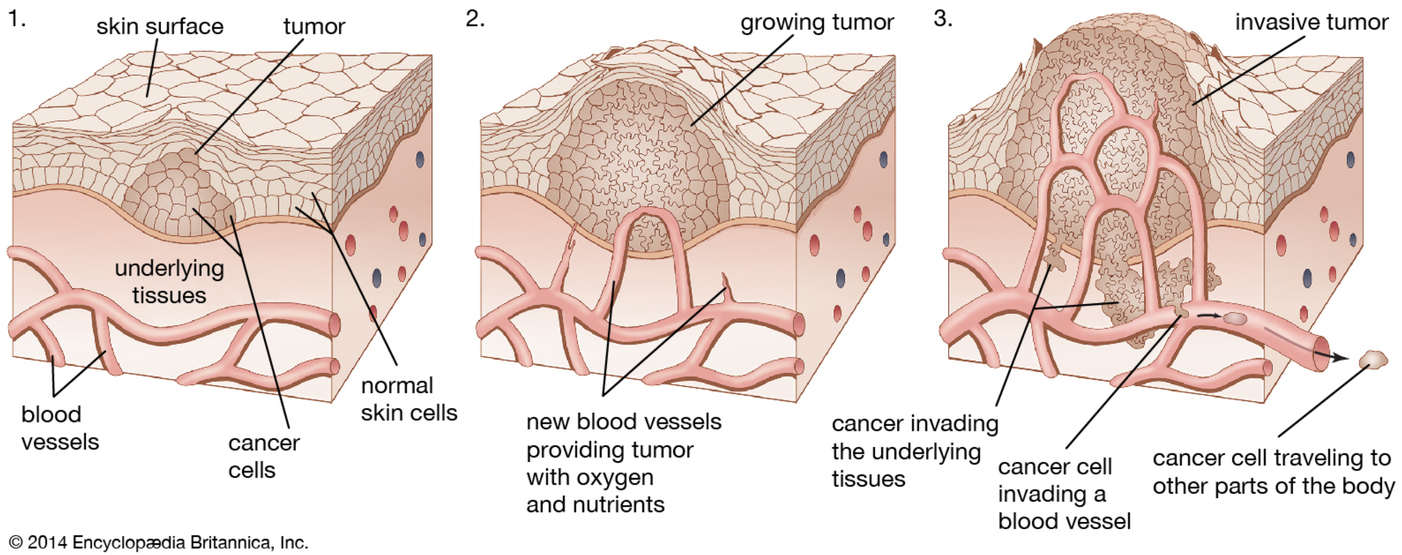

Introduction

Ras Mutations

- The Ras protein is involved in cell growth
- Ras works in a protein signaling pathway

"More cells"
or
"No more cells"

Normal Cell Growth

Introduction

Ras Mutations

- Mutations to Ras can eliminate the on-off function
- Ras becomes stuck in the on state

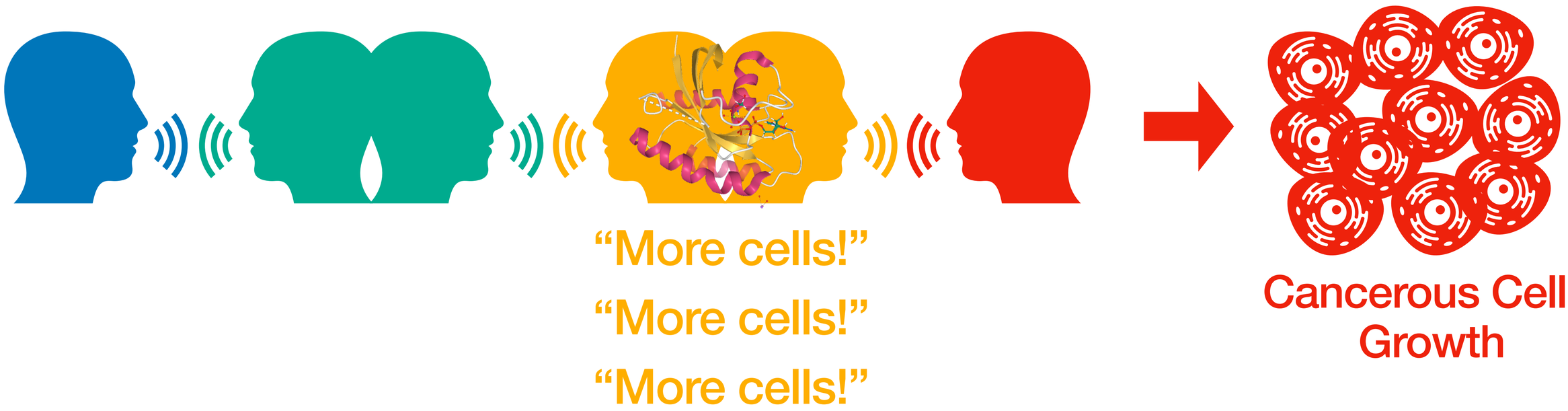

Goal: Find drug candidates that will restore the on-off mechanism of Ras

Methods

4

Molcular Dynamics (MD)

- Emulate the conditions of the human body through computer simulation
- The protein is able to interact with a chemical for a finite period of time
- Newton’s equations of motion determine trajectories

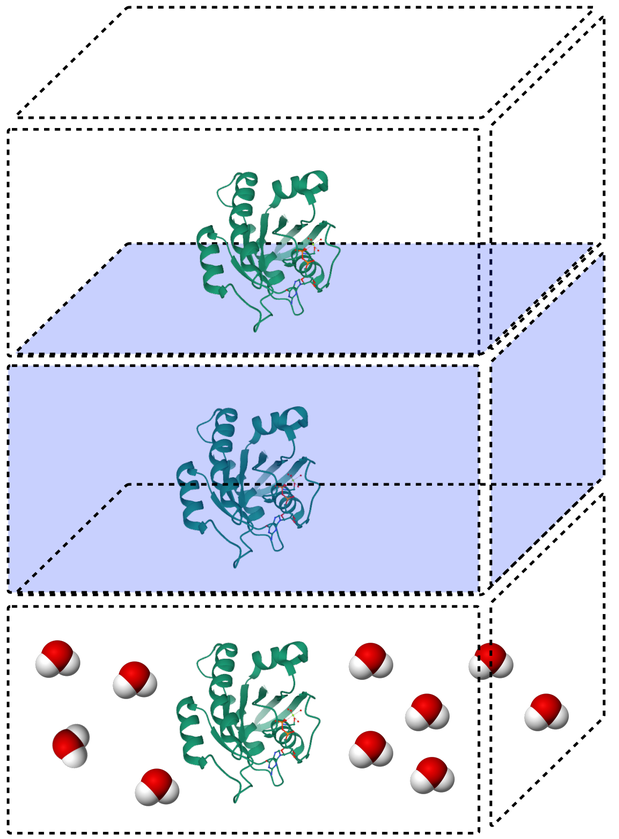

Methods

MD-Monte Carlo and T4 Lysozyme Model System

- T4 Lysozyme is used as a model system
- Three chemicals were used as they have well studied binding properties for T4 Lysozyme
- Monte Carlo moves allow chemicals to change into close structural relatives

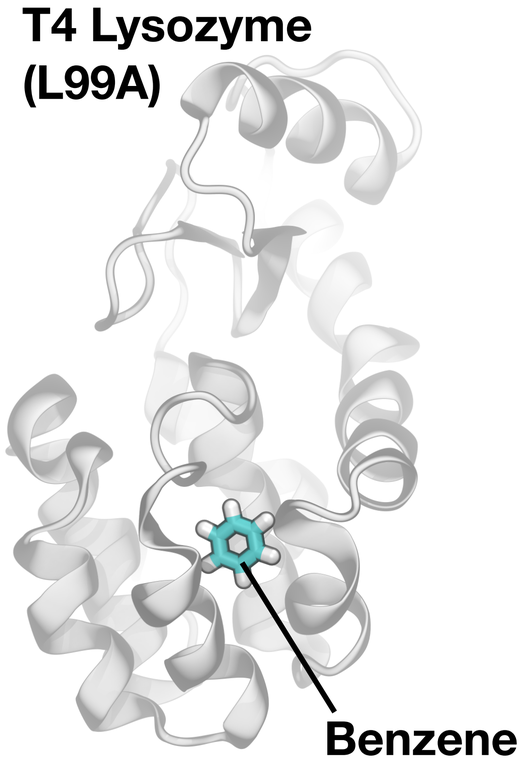

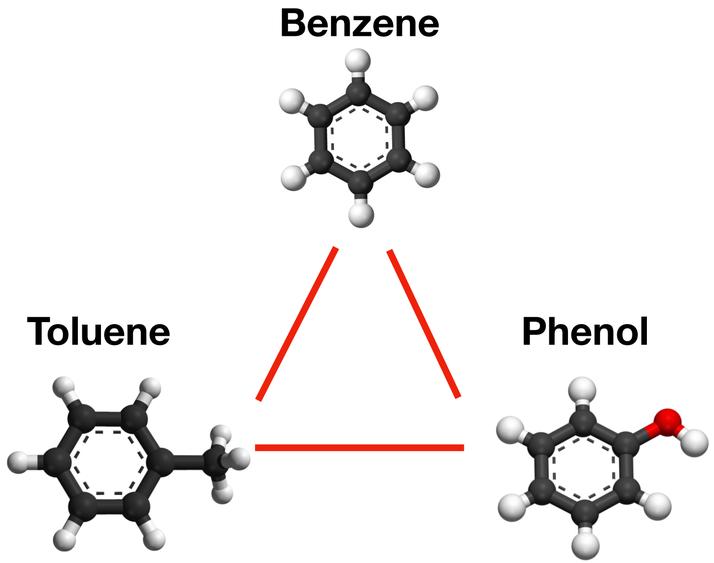

Methods

Alignment Algorithm Version 1

- First version of algorithm has issues with alignment
  - Wrong configuration
  - Placement of hydroxyl group is not random

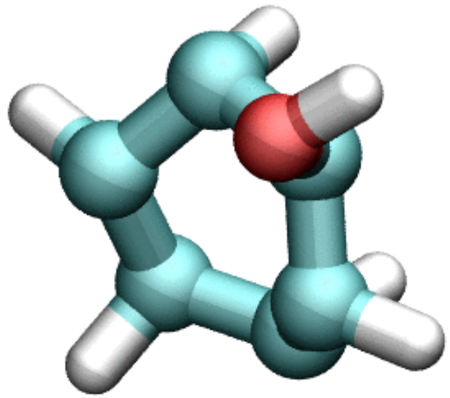

Image courtesy of: Lara A. Patel

Methods

Alignment Algorithm Version 2

- Updated version of alignment algorithm fixes major issues with the first version
  - Now in correct configuration
  - Random placement of hydroxyl group

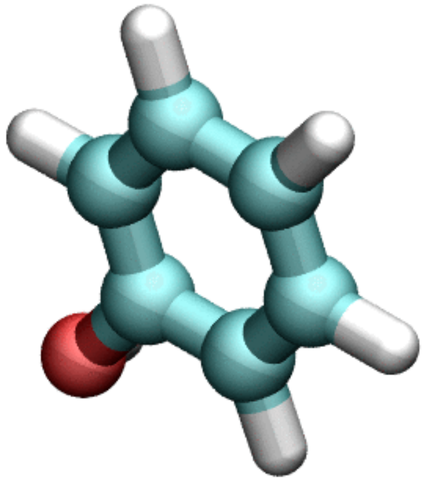

Image courtesy of: Lara A. Patel

Methods

Fixed Protein in Vacuum

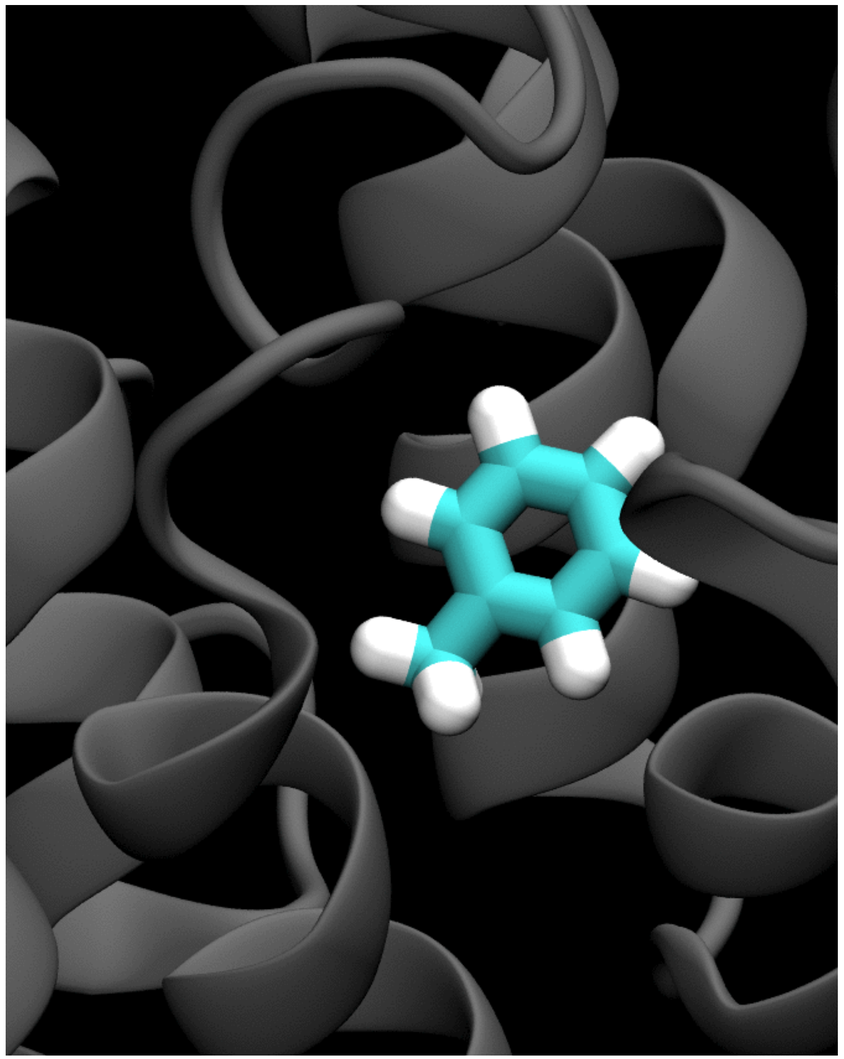

Parameter	Values
Environment	**Vacuum**, Implicit Solvent
Energy Minimization	ON, OFF
Alignment Algorithm	Version 1, Version 2

Results

Fixed Protein in Vacuum

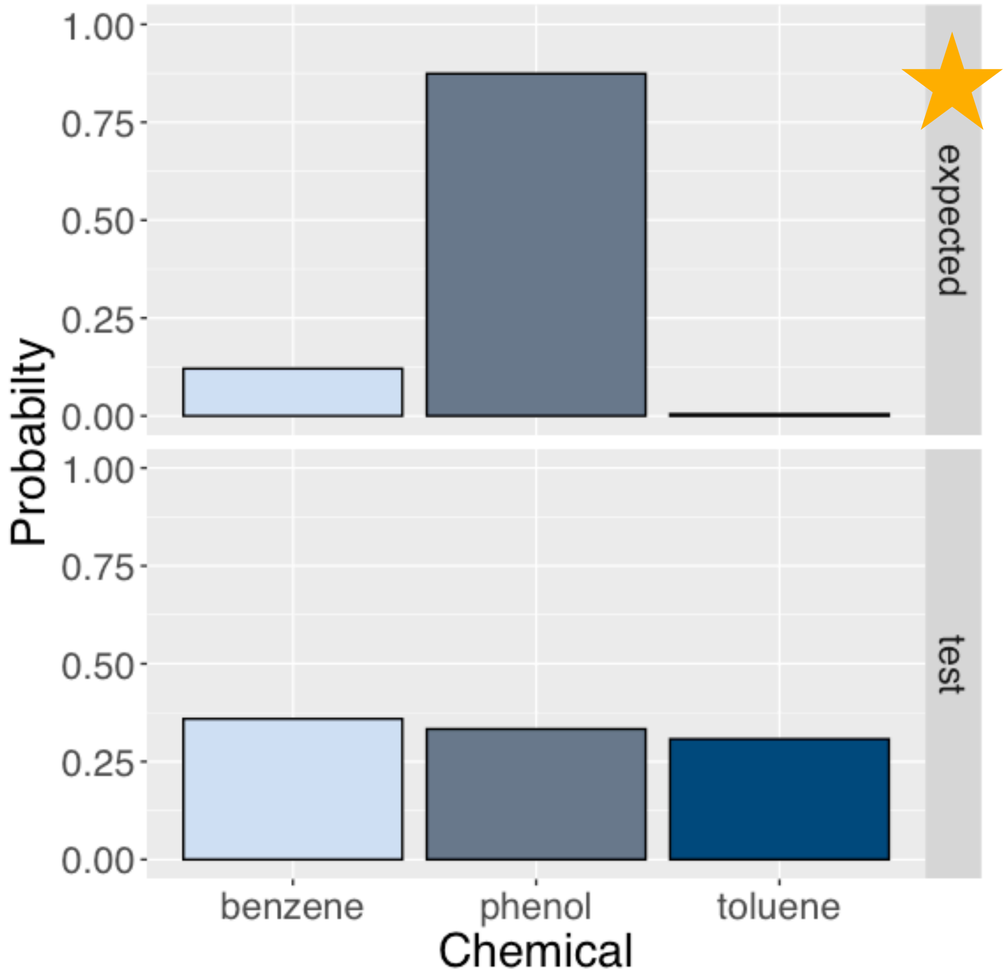

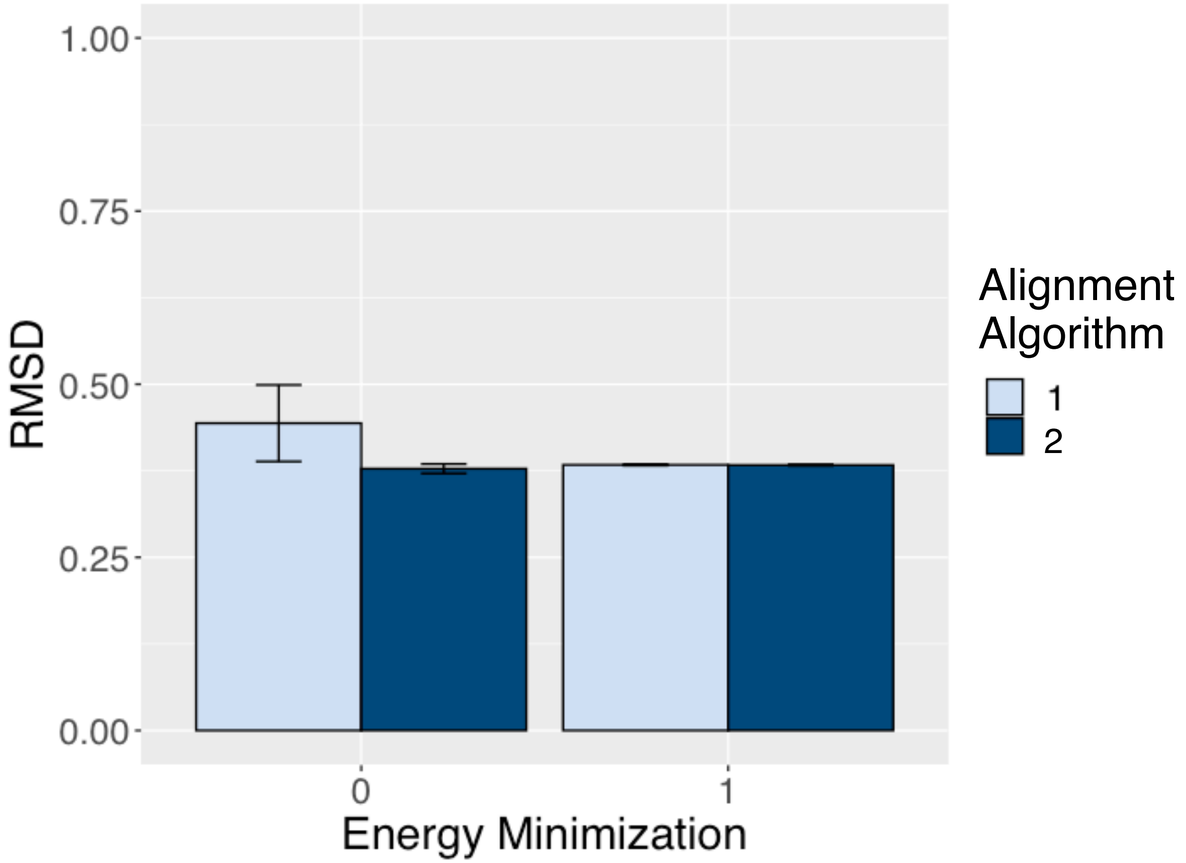

Methods

Dynamic Protein in Vacuum

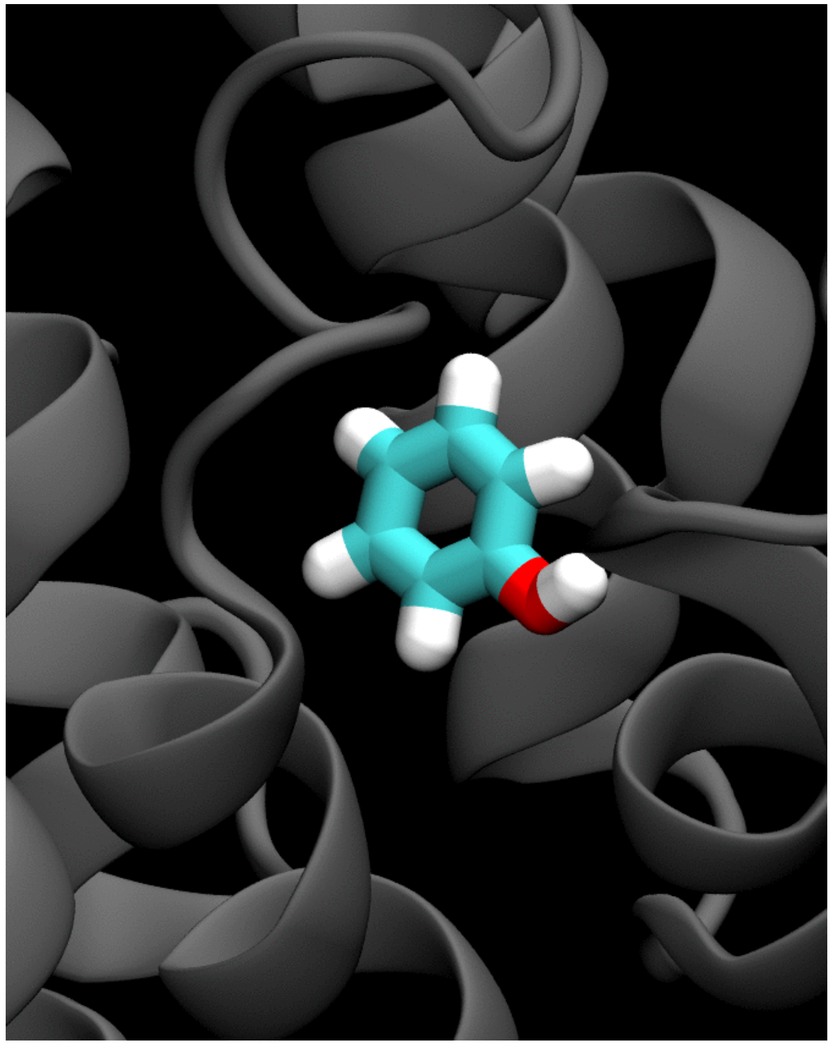

Parameter	Values
Environment	**Vacuum**, Implicit Solvent
Energy Minimization	ON, OFF
Alignment Algorithm	Version 1, Version 2

Results

Dynamic Protein in Vacuum

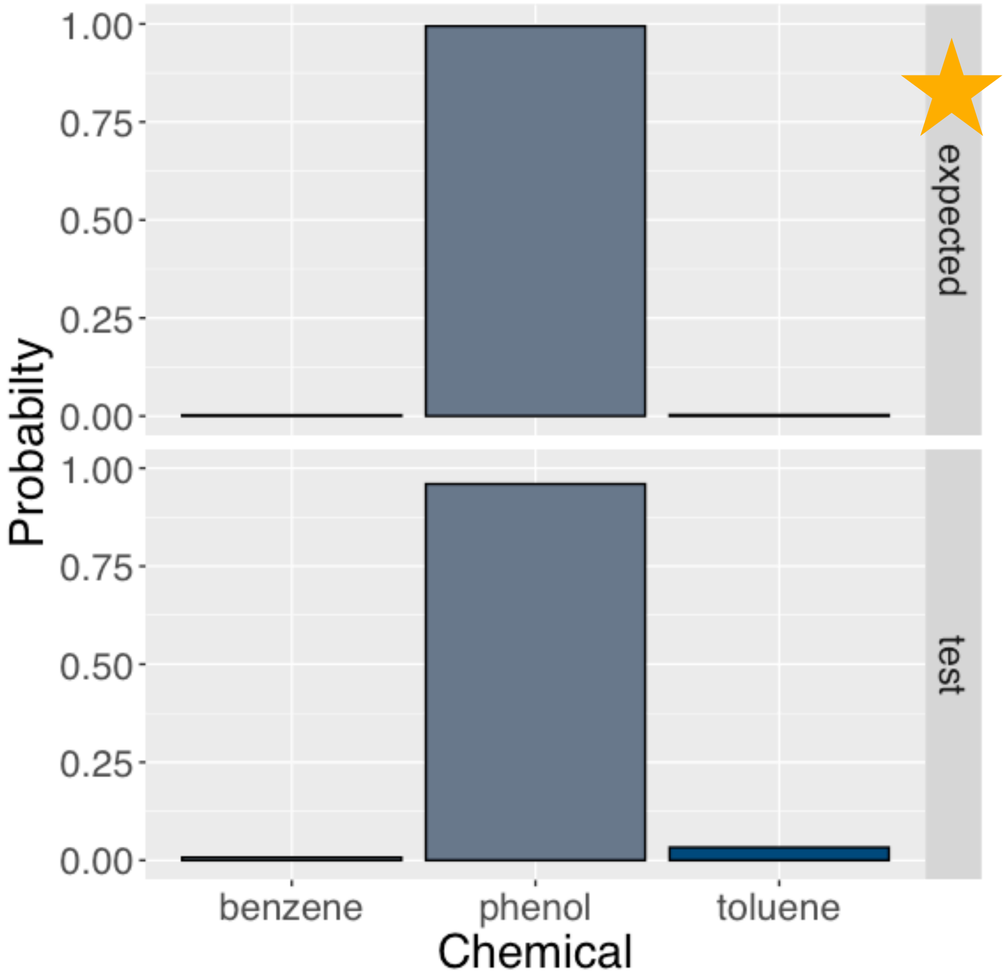

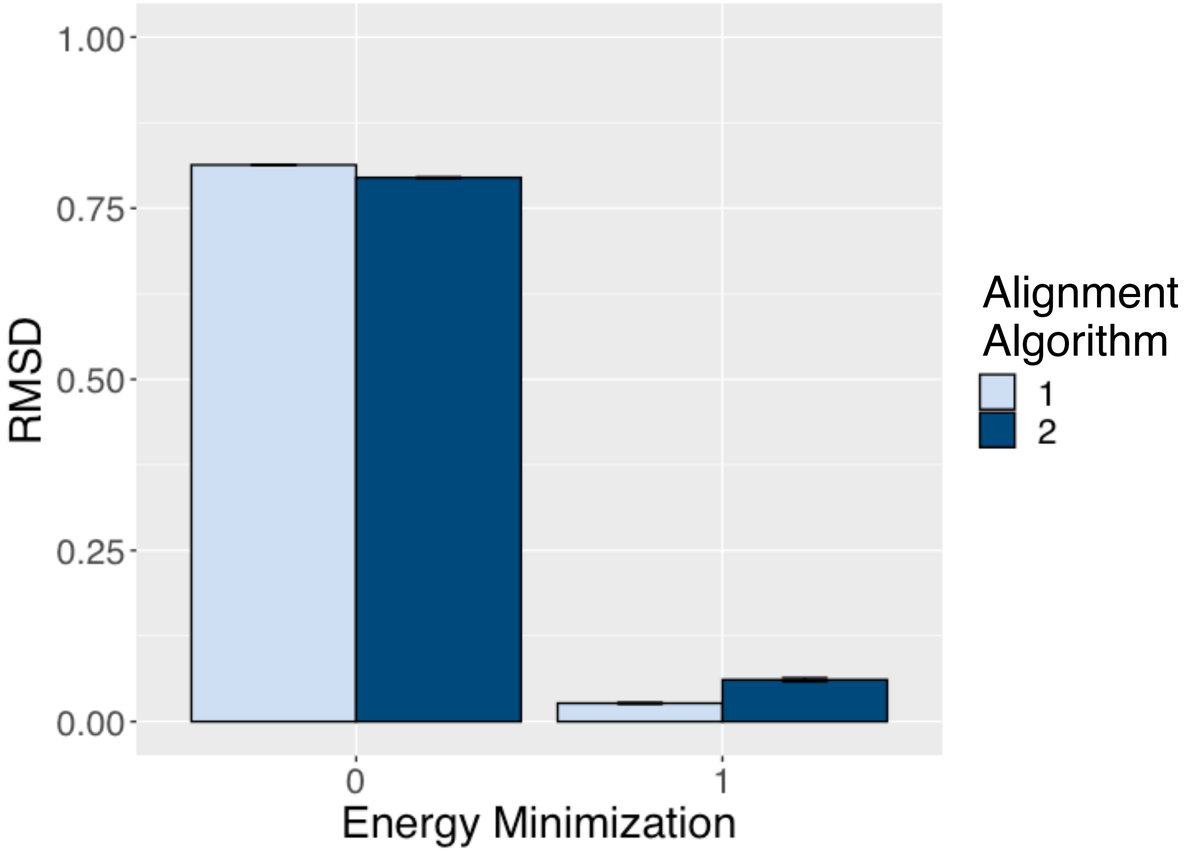

Results

Dynamic Protein in Vacuum

- Alignment algorithm 1 selected benzene 100% of the time
  - Didn’t explore any other chemical space
- Alignment algorithm 2 did slightly better because it was able to move away from benzene

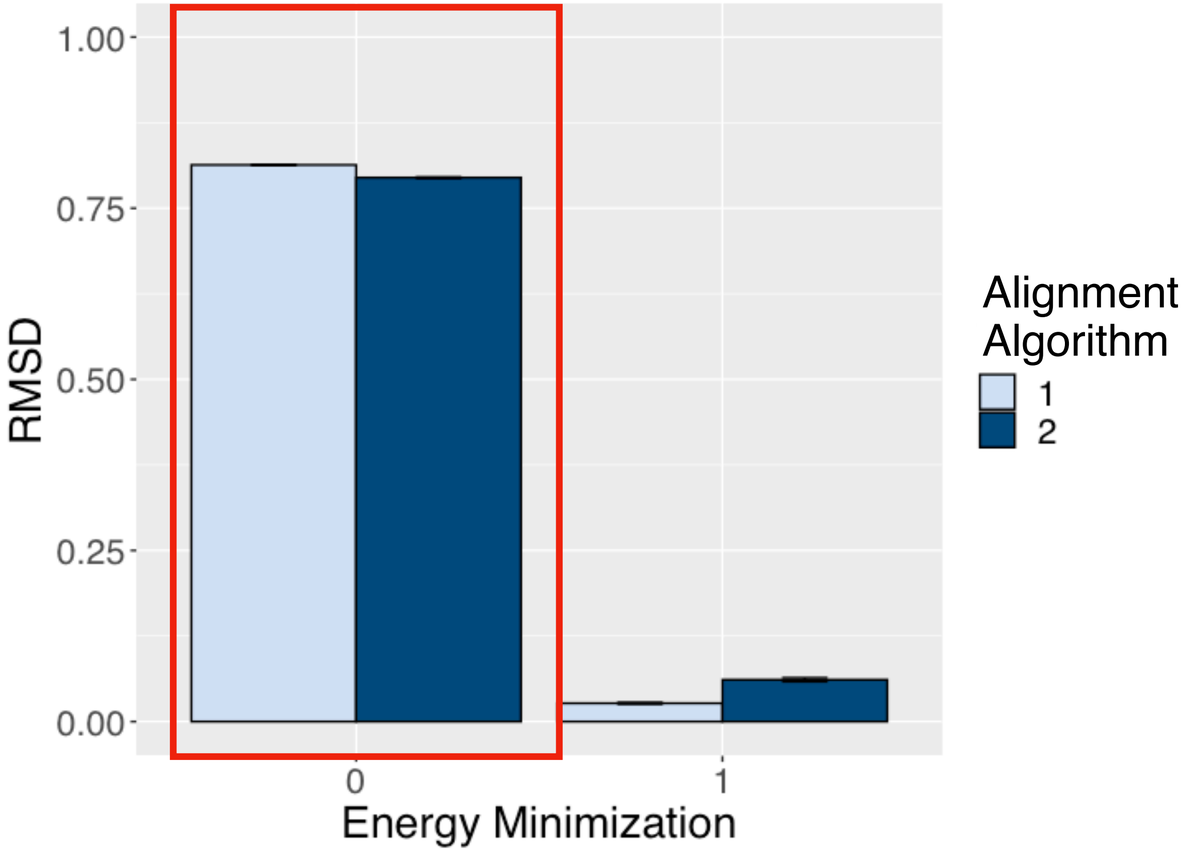

Conclusions

- Algorithm 1 and 2 showed very similar results under the same conditions
- However, algorithm 2 allows for more chemical space to be explored

Next Steps:

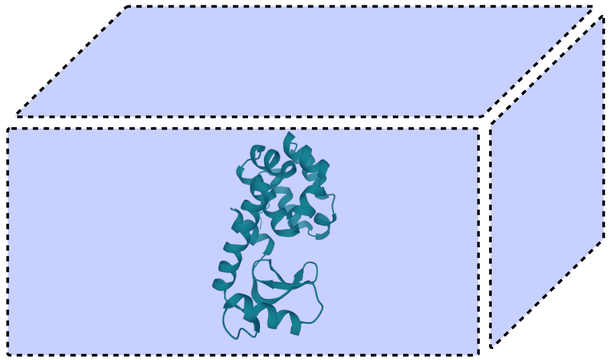

T4 Lysozyme
Implicit Solvent
Model

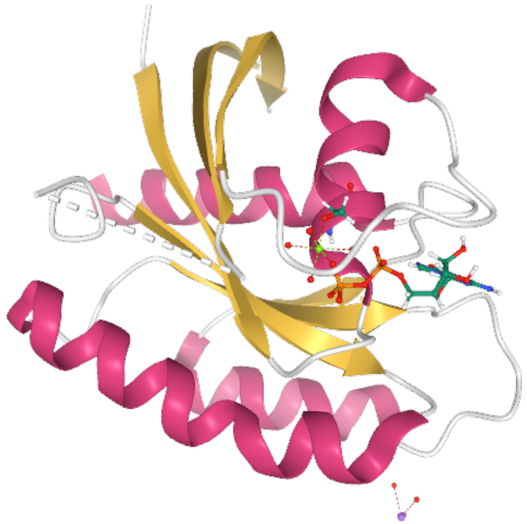

Apply software to find compatible drug candidates for RAS

Thank You!

Leah Darwin
Mentor: Chris Neale

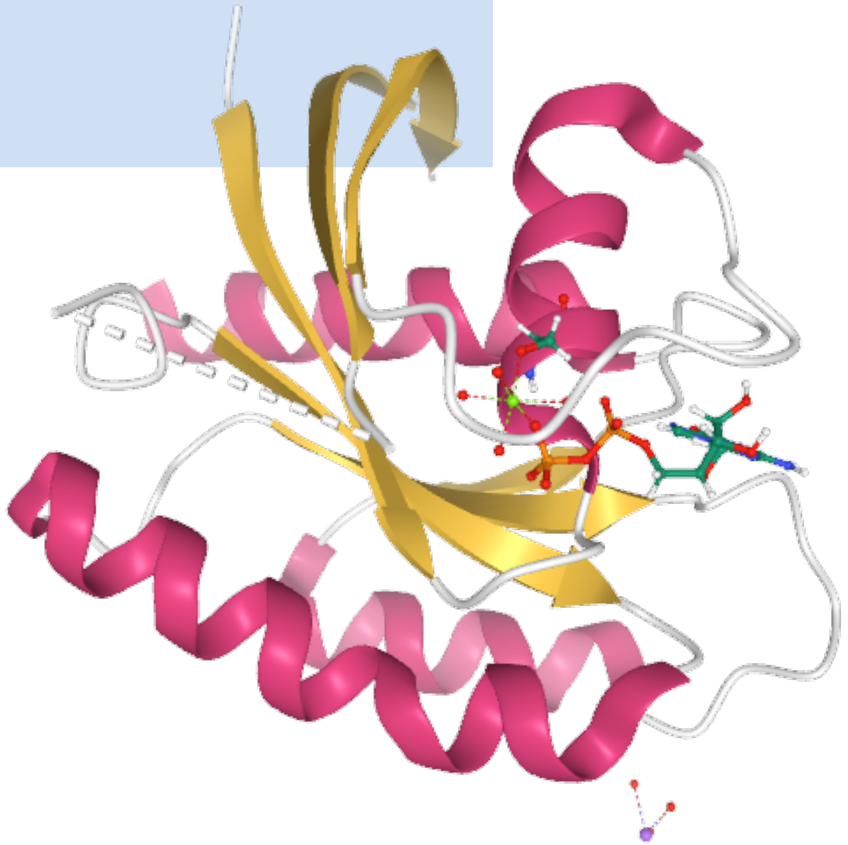

Machine learning parametrization of empirical and semiempirical methods for improving transition metal chemistry

Nikita Fedik

3rd year PhD student at Utah State University

GRA at T-1 division, LANL

Mentors: Benjamin Nebgen, Sergei Tretiak

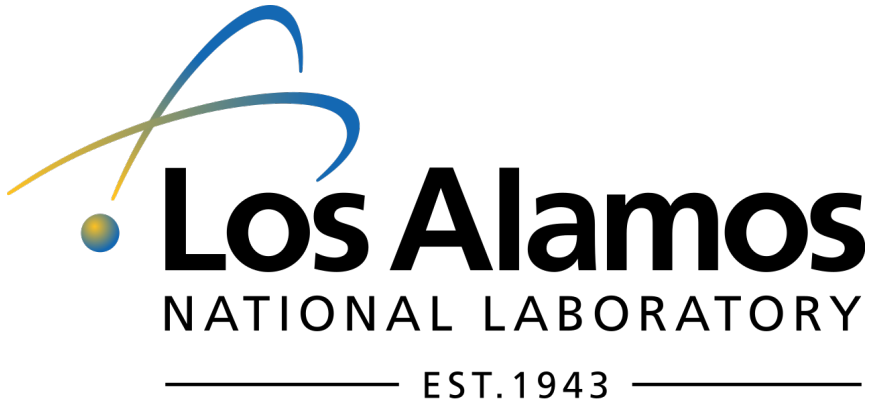

Transition metal chemistry

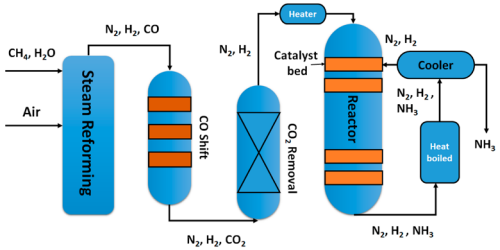

catalysis and industry

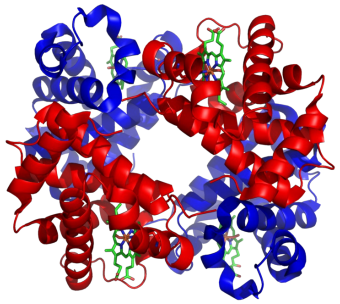

biochemistry

TM

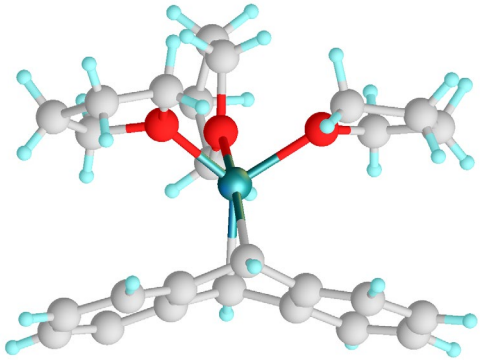

organometallics

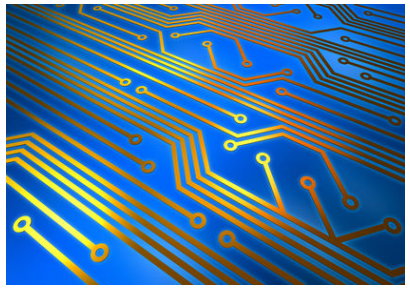

semiconductors

Simulation difficulties of TMs:

- large number of valence $\bar{e}$
- degeneracy of states
- complex wave functions (multireference)
- possible relativistic effects

Available methods

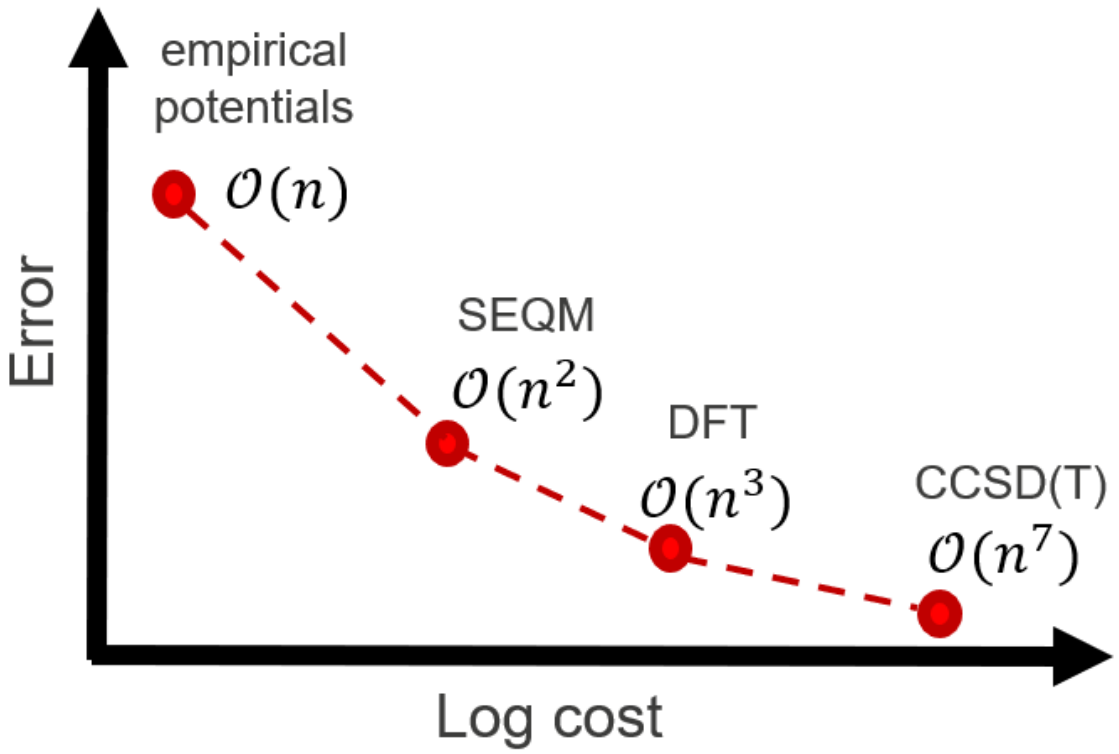

Empirical potentials usually do not have parameters for TMs at all.

Semiempirical QM are very inaccurate.

	MAD	RMSD
PM6	21.6	28.9
PM7	106.4	146.1
PM7-TS	68.2	141.9

THE JOURNAL OF PHYSICAL CHEMISTRY A
Article
Cite This: J. Phys. Chem. A 2019, 123, 3761−3781
pubs.acs.org/JPCA

Evaluating Transition Metal Barrier Heights with the Latest Density Functional Theory Exchange−Correlation Functionals: The MOBH35 Benchmark Database

Published as part of The Journal of Physical Chemistry virtual special issue "Leo Radom Festschrift".

Mark A. Iron*,† and Trevor Janes‡

Machine learning for dynamic parametrization

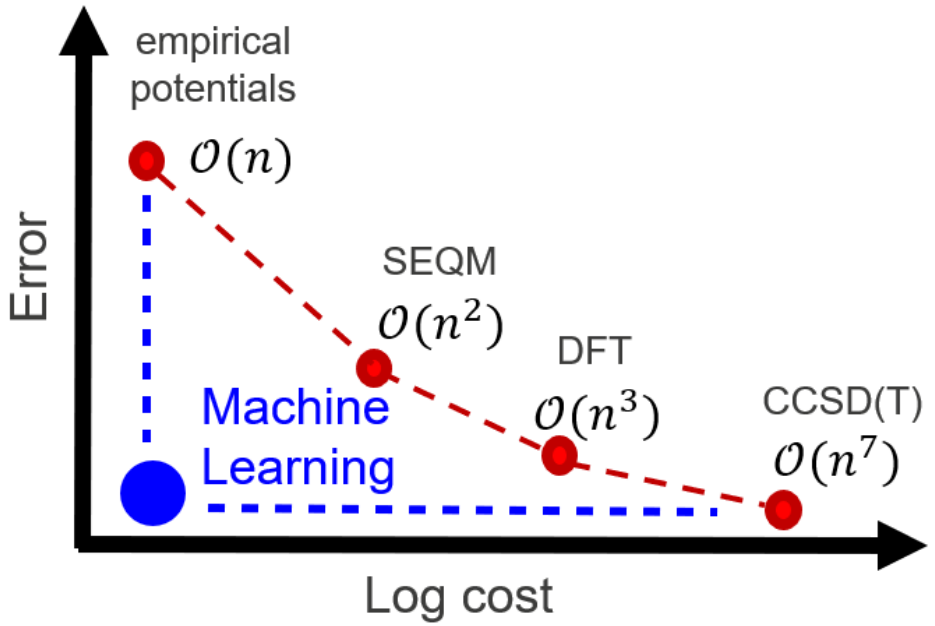

Neural Network potentials

- HIPNN architecture

THE JOURNAL OF CHEMICAL PHYSICS **148**, 241715 (2018)

Hierarchical modeling of molecular energies using a deep neural network

Nicholas Lubbers,[1,a] Justin S. Smith,[1,2] and Kipton Barros[1]
[1]*Theoretical Division and CNLS, Los Alamos National Laboratory, Los Alamos, New Mexico 87545, USA*
[2]*Department of Chemistry, University of Florida, Gainesville, Florida 32611, USA*

ML parametrized SEQM

- PYSEQM

JCTC Journal of Chemical Theory and Computation
pubs.acs.org/JCTC Article

Graphics Processing Unit-Accelerated Semiempirical Born Oppenheimer Molecular Dynamics Using PyTorch

Guoqing Zhou, Ben Nebgen,* Nicholas Lubbers, Walter Malone, Anders M. N. Niklasson, and Sergei Tretiak

HIP-NN: Hierarchically Interacting Particle Neural Network

1. Local atomic environment

$$E \approx \hat{E} = \sum_{i=1}^{N_{\text{atom}}} \hat{E}_i.$$

2. Hierarchical decomposition ansatz

$$\hat{E}_i = \sum_{n=0}^{N_{\text{interaction}}} \hat{E}_i^n.$$

3. Molecular representation

$$\{ R \} \longrightarrow \{ |r_i - r_j| \} \text{ if } r_{ij} < R_{\text{cutoff}}$$

invariant to rotations and translations

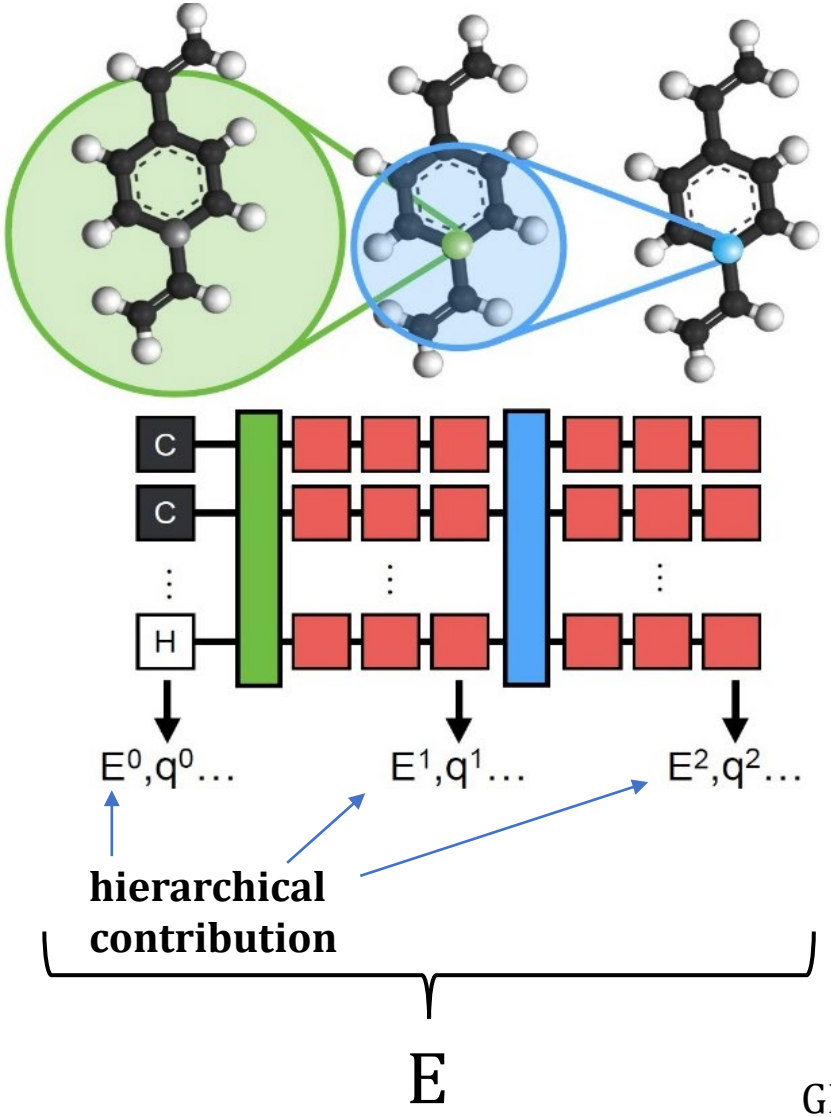

$$\hat{E}_i^n = \sum_{a=1}^{N_{\text{feature}}} w_a^n z_{i,a}^{\ell_n} + b^n,$$

learned parameters

GPU training > 100 times faster than CPU

We need a big and consistent dataset (10^3 – 10^6 entries)

Why pure TM clusters is a very a bad idea?

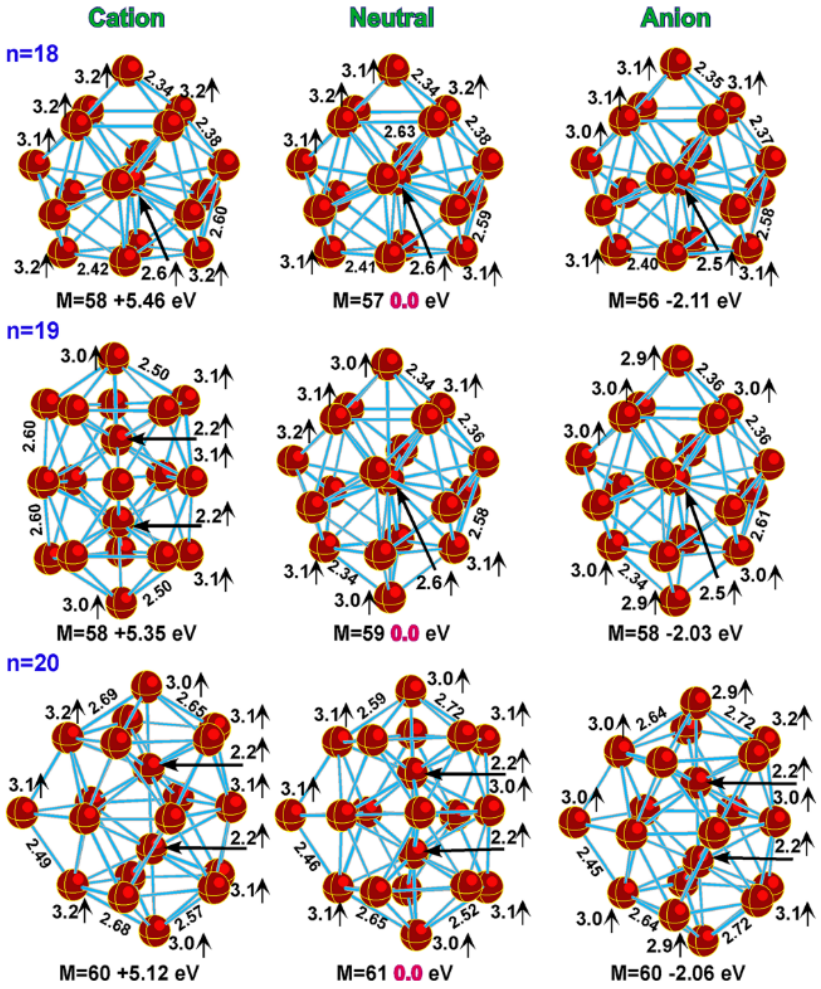

M = 2S+1 are in range **22 – 61!**

G. L. Gutsev et all. J. Phys. Chem. A 2012, 116, 10218−10228

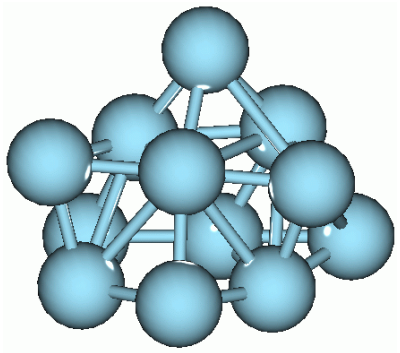

Pt_{12}, ^{7}**A** "cube"
-1430.881773 A.U.

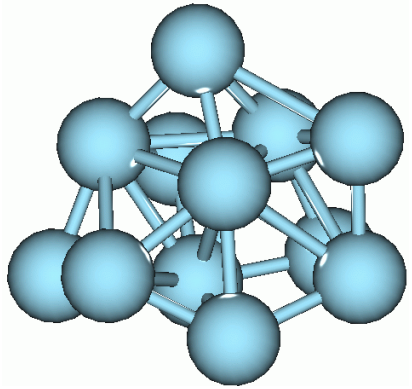

Pt_{12}, ^{5}**A** "cube"
-1430.875799 A.U.

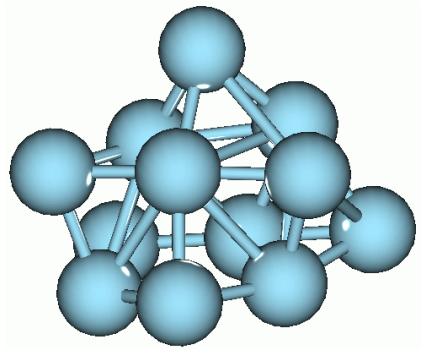

Pt_{12}, ^{1}**A** "cube" (from ^{7}A)
-1430.871506 A.U.

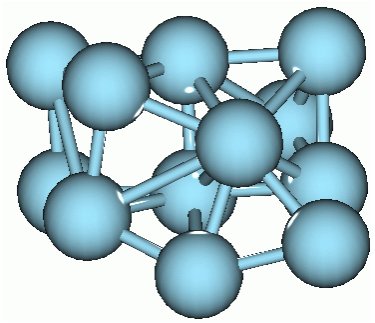

Pt_{12}, ^{11}**A** "cube"
-1430.864530 A.U.

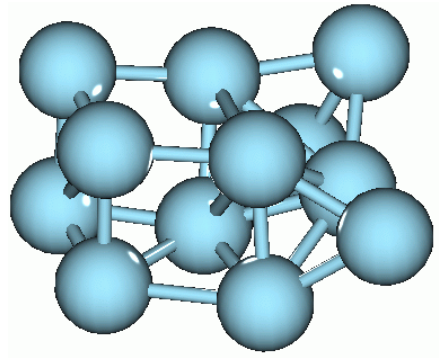

Pt_{12}, ^{9}**A** "cube"
-1430.866841 A.U.

New organometallic database

1. Organometallic (HCNO) complexes of Ti

   - closed shell singlets
   - only 4 *ve* ($3d^2 4s^2$)

2. Reference method – what to choose?

Comprehensive Thermochemical Benchmark Set of Realistic Closed-Shell Metal Organic Reactions

Sebastian Dohm,[†] Andreas Hansen,[*,†] Marc Steinmetz,[†,§] Stefan Grimme,[†] and Marek P. Checinski[*,‡]

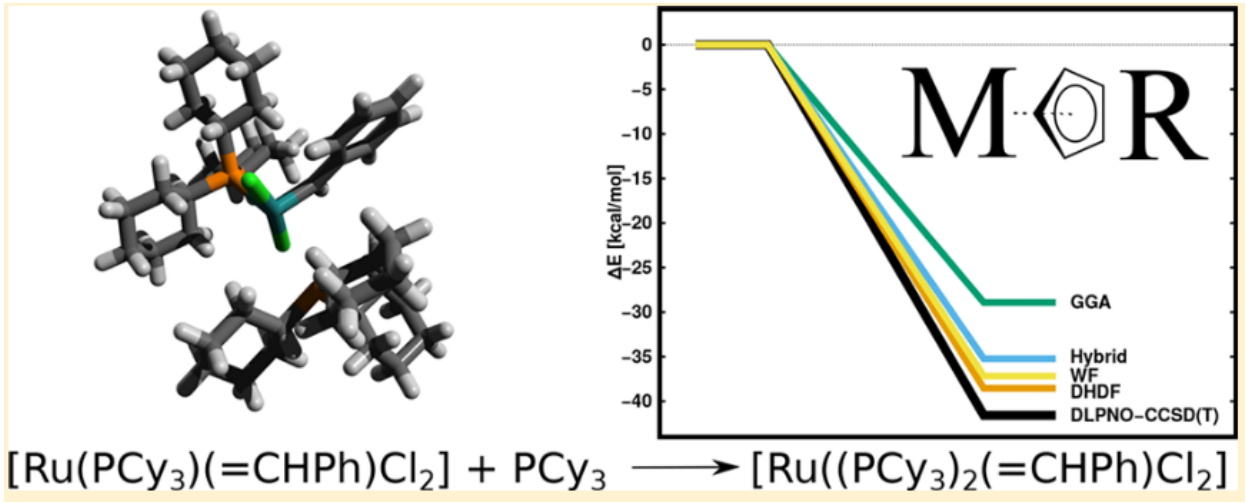

Evaluating Transition Metal Barrier Heights with the Latest Density Functional Theory Exchange–Correlation Functionals: The MOBH35 Benchmark Database

Published as part of The Journal of Physical Chemistry virtual special issue "Leo Radom Festschrift".

Mark A. Iron[*,†] and Trevor Janes[‡]

1. Hybrids are probably the best choice:
   - ωB97-D3BJ (MAD = 1.9 kcal/mol)

2. Dispersion correction is essential
   - Reduces error by 2-10 kcal/mol

3. Def2-TZVPP is very accurtae

PES sampling

1. **Coalescence Kick (CK)** https://github.com/averkiev75/Coalescence-Kick
   - only C_1 structures
   - allows orientation of predefined fragments
2. **AFFCK** https://github.com/hczhai/AFFCK
   - C_1 and symmetrical structures
3. **PyXtal** https://github.com/qzhu2017/PyXtal
   - Python library
   - C_1 and symmetrical structures

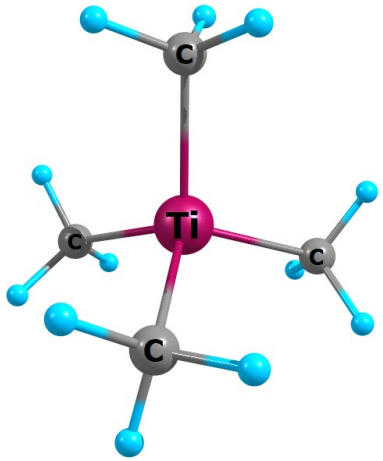

$Ti(Me)_4$ optimized structure

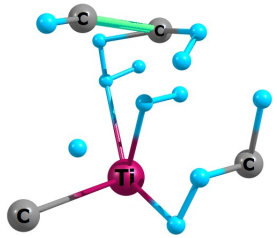

random C_1

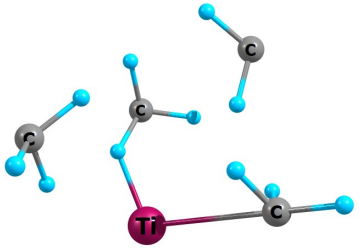

random C_1 (fixed Me fragments)

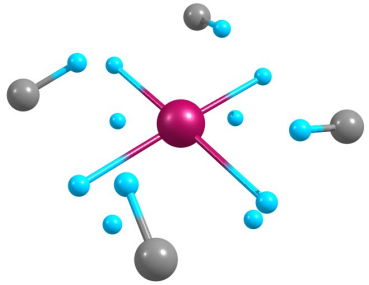

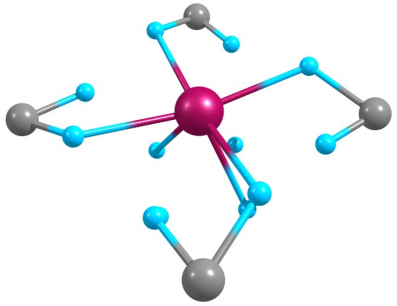

symmetrical guesses

unphysical structures: broken geometries and wave functions

PES sampling

4. MolSimplify http://hjkgrp.mit.edu/molSimplify-tutorials - designed for organometallics

- Different coordination numbers
- Different geometries of complex
- Specific spin state (e. g. closed-shell)
- Supports SMILES

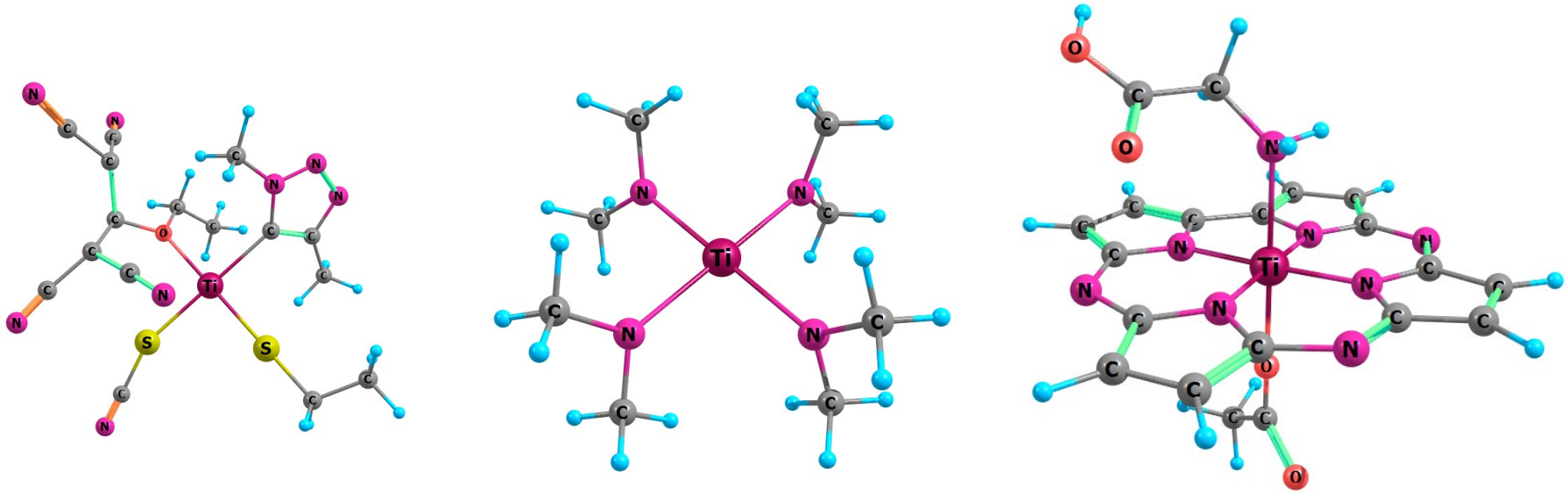

correct connectivity and valence angles

incorrect TM-L distance

Dataset generation

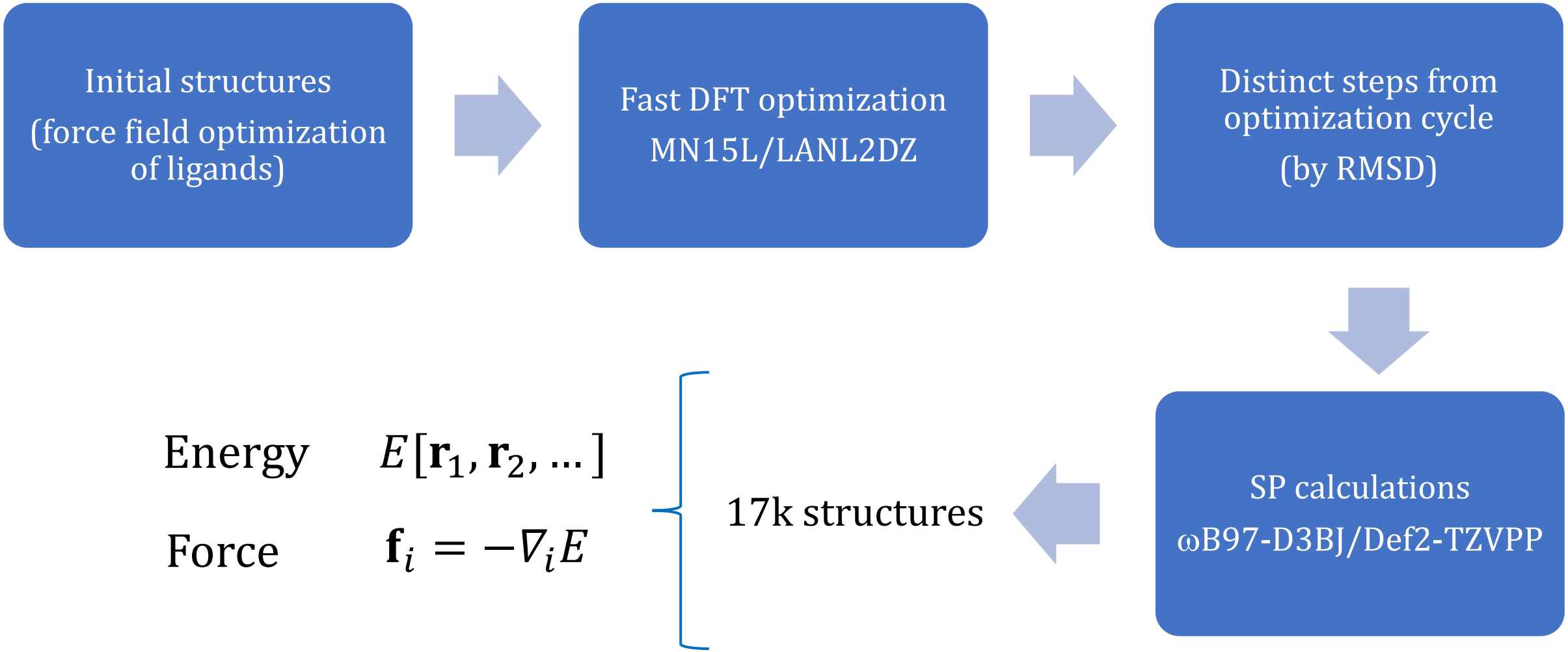

HIP-NN potential

	E, kcal/mol		
	train	**validation**	**test**
RMSE	2.23	13.62	14.59
MAE	1.36	4.60	4.50
MAE/atom	0.03	0.10	0.94

	MAE	RMSE
B97-3c	*a*	*a*
HF-3c	*a*	*a*
PBEh-3c	*a*	*a*
PM6	21.6	28.9
PM7	106.4	146.1
PM7-TS	68.2	141.9

Empirical potential with dynamic ML parametrization could outperform statically parametrized SEQM

Further work:

- Increase transferability
- Add forces to the model
- Parametrize SEQM on the same dataset

Chiroptical Properties Induced into a Lead-Halide Perovskite Cluster Through Surface Chemistry

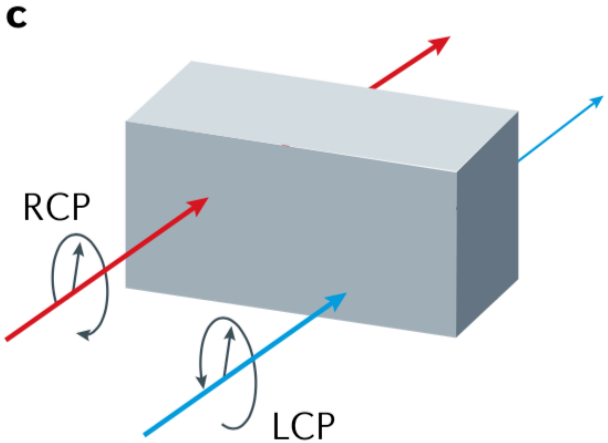

Aaron Forde (GRA)

North Dakota State University

LANL Lightning Talk – 8-27-2020

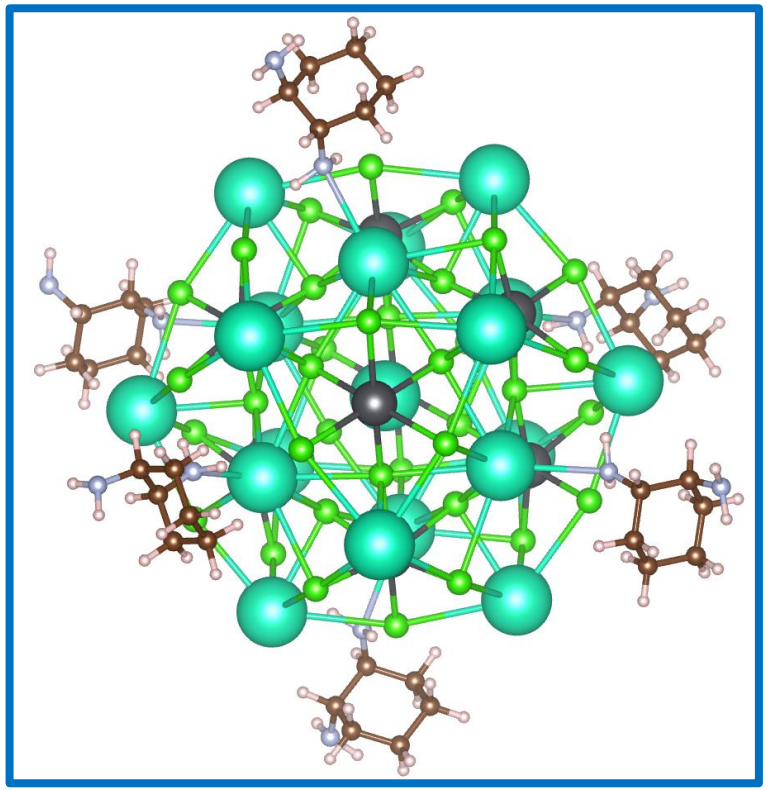

Light-Matter Interactions: Circular Dichroism

Classical Electromagnetic Field – Matter Interaction

$$\vec{\epsilon}\cdot\vec{d}_{ij}=\left\langle i\left|\exp\left(\frac{i\omega}{c}\vec{n}\cdot\vec{x}\right)\vec{\epsilon}\cdot\vec{p}\right|f\right\rangle\approx\underbrace{\langle i|\vec{\epsilon}\cdot\vec{p}|j\rangle}_{\text{Electric Dipole}}+\underbrace{\langle i|(\vec{n}\cdot\vec{x})(\vec{\epsilon}\cdot\vec{p})|j\rangle}_{\text{Magnetic Dipole and Electric Quadruple}}+\ \ldots$$

Rotatory Strength

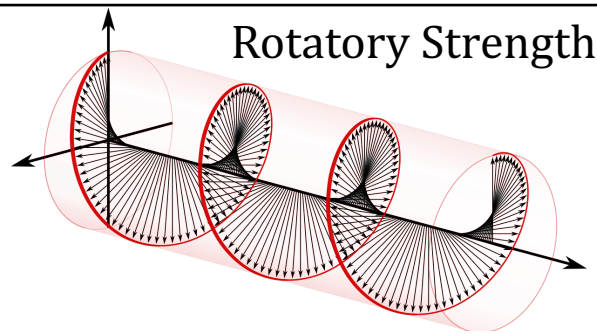

$$R_{0a}=\text{imag}(\langle\Psi_0|\underset{\sim}{\boldsymbol{\mu}}|\Psi_a\rangle\cdot\langle\Psi_a|\underset{\sim}{\mathbf{m}}|\Psi_0\rangle)$$

Electric Dipole Magnetic Dipole

Pure electronic absorbtion

Pure magnetic absorbtion

Optical activity!

Chiroptical Activity

Circular Dichroism

$$A_{RCP}\neq A_{LCP}$$

Difference in absorption of right-handed and left-handed circularly polarized light

Occurs in materials that do not have mirror symmetry

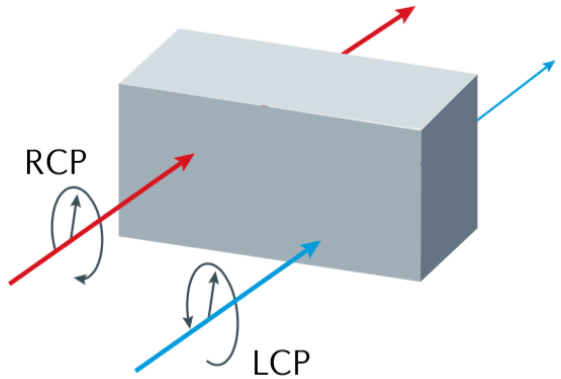

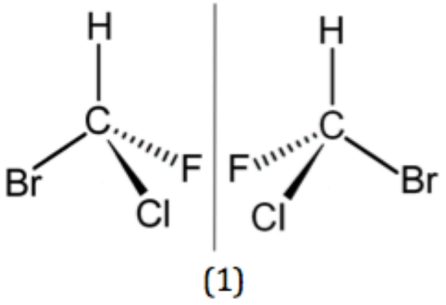

P. Ceroni (ed.), The Exploration of Supramolecular Systems and Nanostructures by Photochemical Techniques, Lecture Notes in Chemistry 78,

Long, G., Sabatini, R., Saidaminov, M.I. *et al.* Chiral-perovskite optoelectronics. *Nat Rev Mater* **5,** 423–439 (2020).

Chirality Induced into Lead-Halide Perovskite Semiconductors Through Surface Interactions

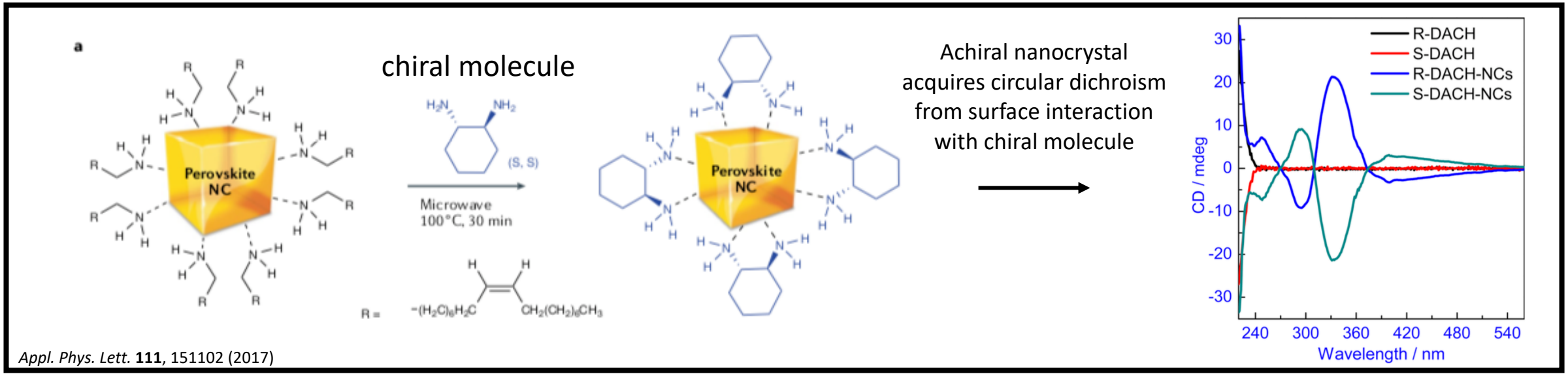

Appl. Phys. Lett. **111**, 151102 (2017)

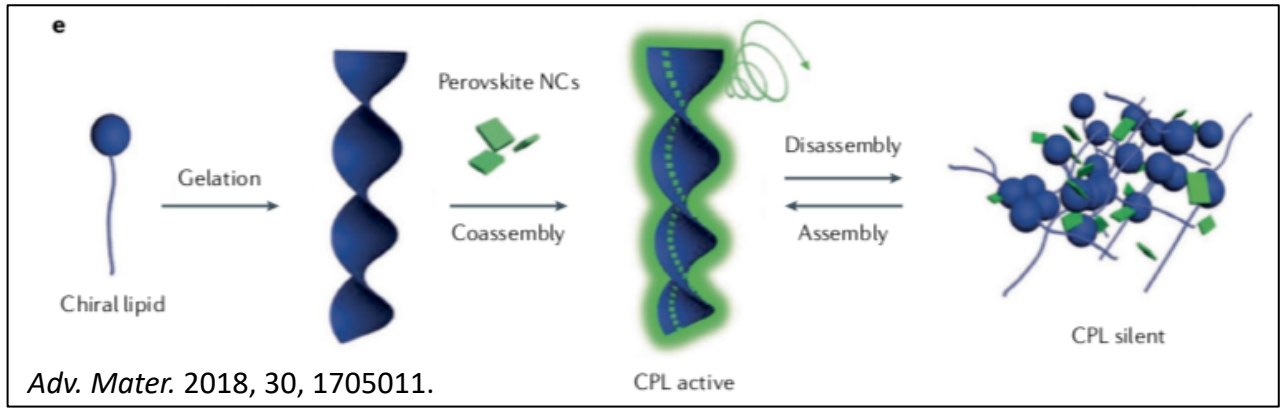

Adv. Mater. 2018, 30, 1705011.

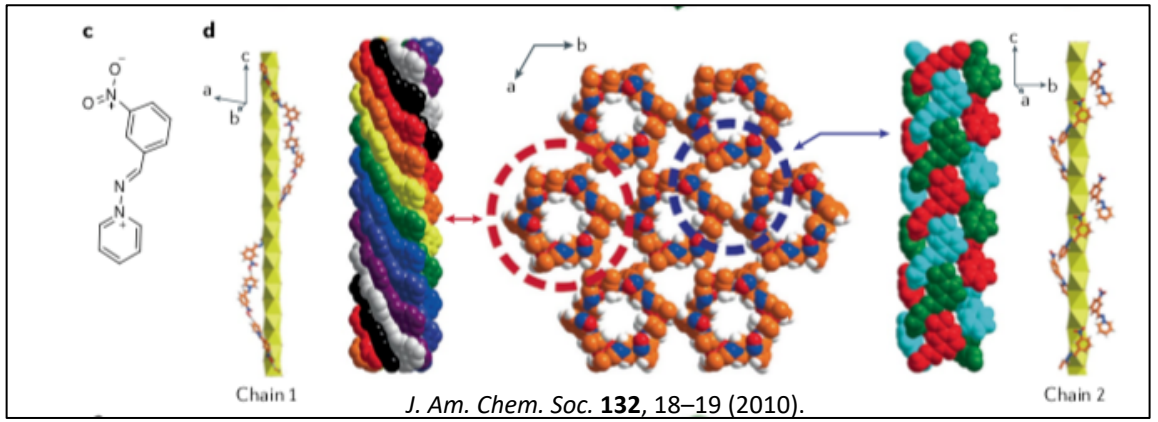

J. Am. Chem. Soc. **132**, 18–19 (2010).

What is the Photo-Physical Mechanism for Induced Chirality in Lead Halide Perovskite Nanocrystal?

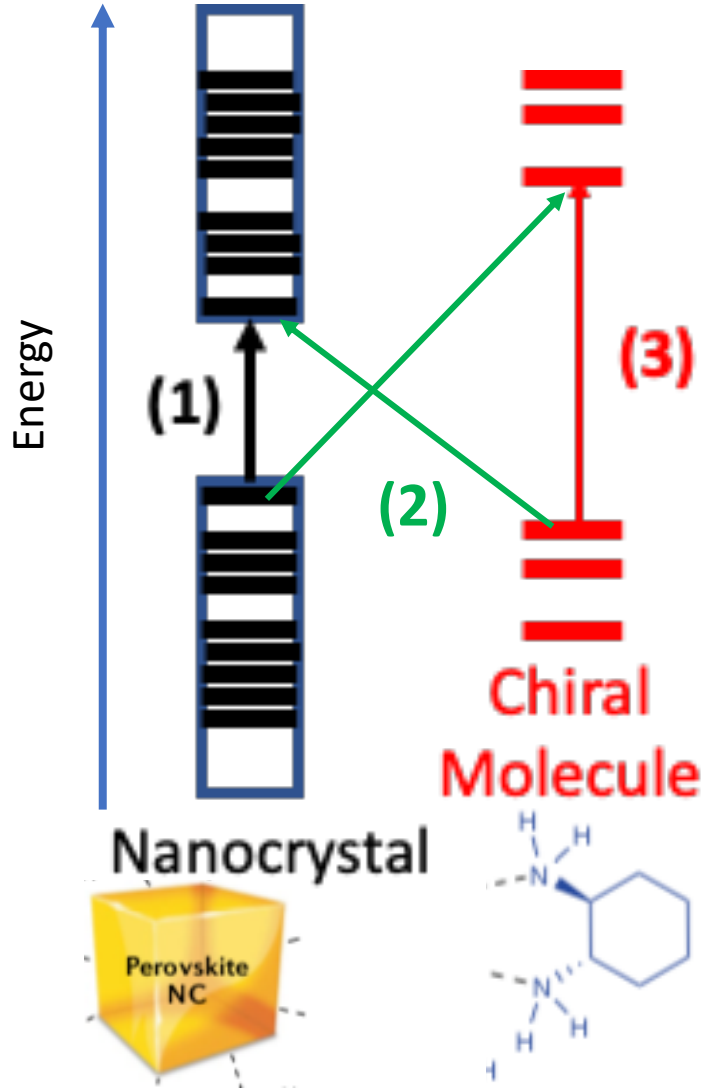

Possible Radiative Pathways

(1) Perovskite-to-Perovskite **(2) Charge-Transfer Excitations**

(3) Molecule-to-Molecule

(1) Chiral Templating

Chiral templating of the nanocrystal surface gives circular dichroism for perovskite-to-perovskite transitions

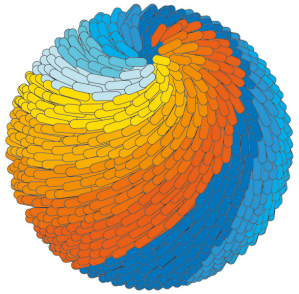

(2) Charge-Transfer Excitations

Electronic coupling between the nanocrystal and the chiral molecule give charge-transfer excitations that have chiral signatures.

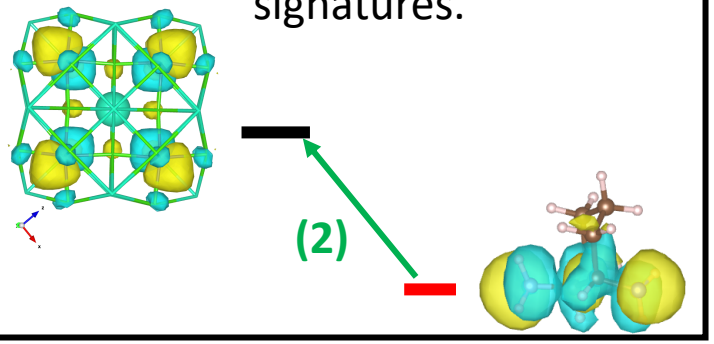

TD-DFT Investigation of Circular Dichroism in Chiral Capped Lead Halide Perovskite Cluster

Functional: CAM-B3LYP | Basis Set for Cluster: LANL2DZ | Basis Sets for Molecule: 6-311++g** | Solvent: Toluene

(i) Individual Components

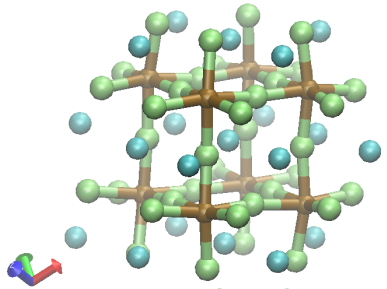

$Cs_{19}Pb_8Cl_{36}$

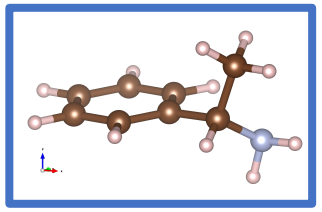

1R Methylbenzlamine

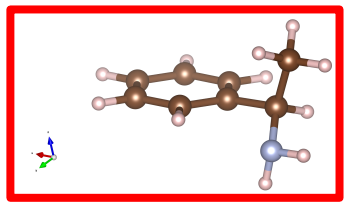

1S Methylbenzlamine

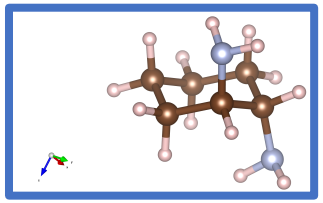

1R,2R Diaminocyclohexane

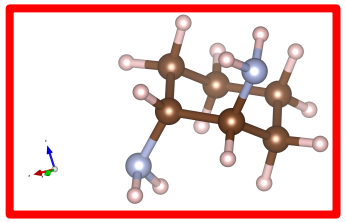

1S,2S Diaminocyclohexane

(ii) Single Molecule on Cluster Surface

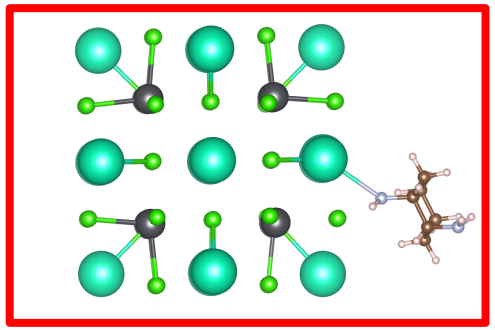

$Cs_{19}Pb_8Cl_{36}$ +1S,2S Diaminocyclohexane

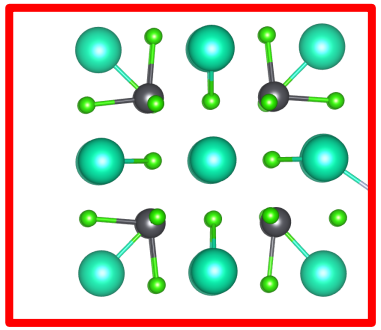

$Cs_{19}Pb_8Cl_{36}$

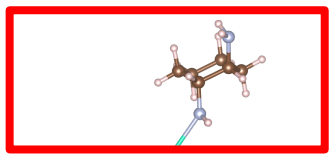

1S,2S Diaminocyclohexane

(iii) Multiple Molecules on Cluster Surface

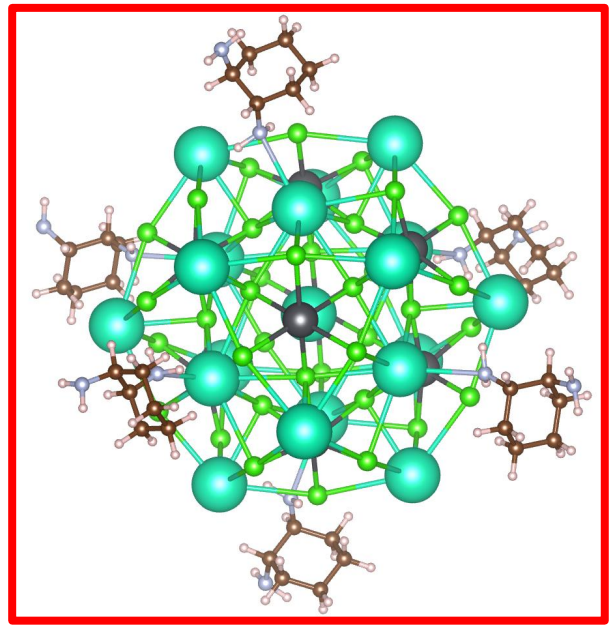

$Cs_{19}Pb_8Cl_{36}$ 1S,2S Diaminocyclohexane

(i) Circular Dichroism of Individual Components

Circular Dichroism of Perovskite Cluster

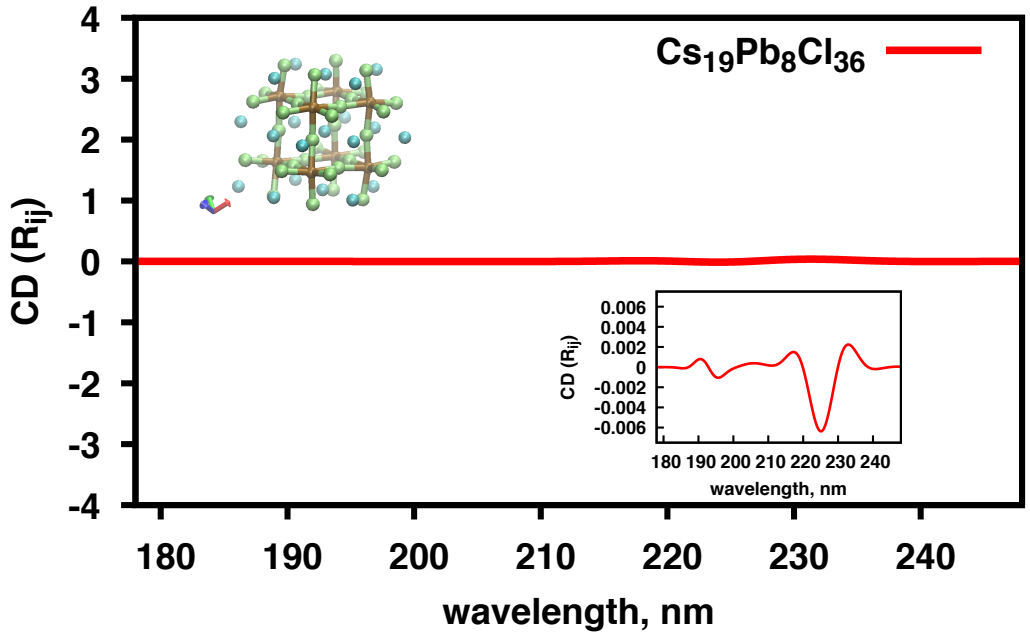

Cluster shows negligible chiroptical activity

$$CD(\omega_{ij}) = \sum_{ij} R_{ij}\delta(\hbar\omega - \hbar\omega_{ij})$$

$$R_{ij} \propto \mathrm{Im}\left(\left|\vec{\mu}_{ij}^{elec} \cdot \vec{\mu}_{ij}^{mag}\right|\right)$$

δ is broadened as a Gaussian with broadening parameter 0.01 eV

Circular Dichroism of Chiral Molecules

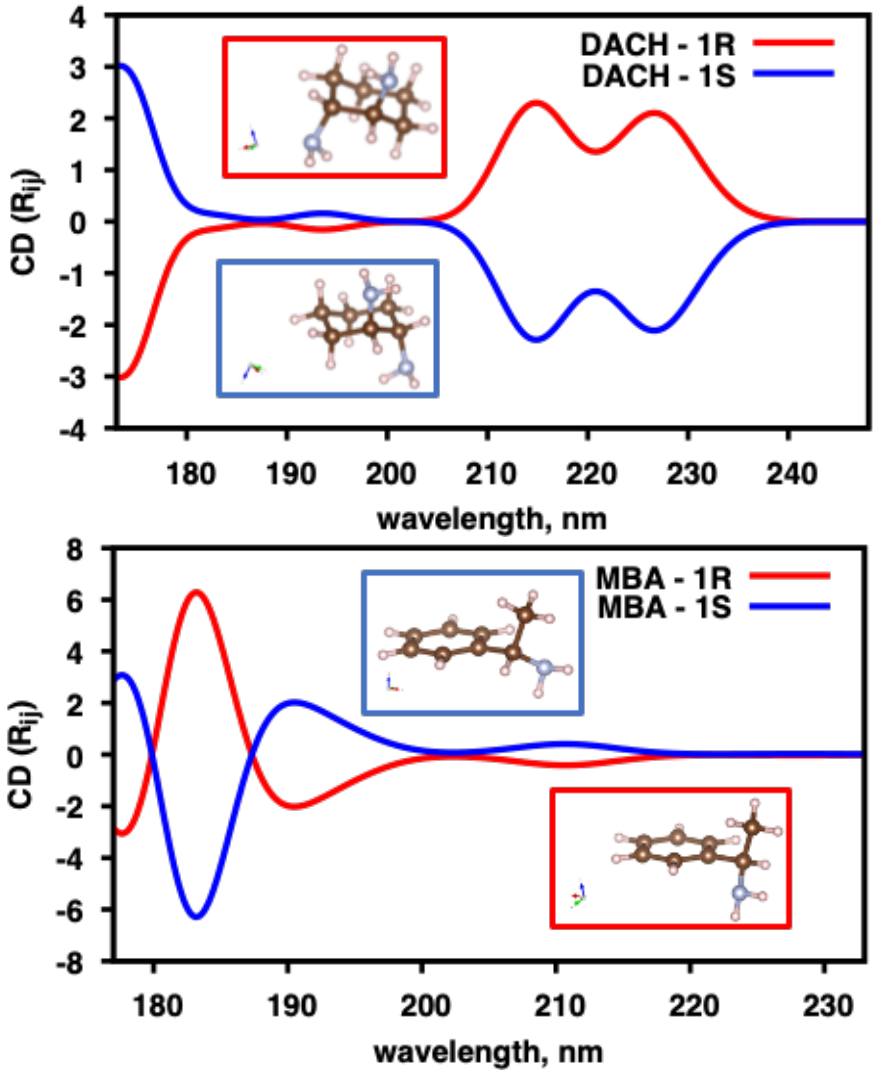

Enantiomers show expected mirrored CD spectra

(ii) Circular Dichroism with a Single Chiral Molecule on the Cluster Surface

$Cs_{19}Pb_8Cl_{36}$ 1R,2R Diaminocyclohexane

	binding [eV]
Configuration 1	-0.46
Configuration 2	-0.67
Configuration 3	-0.57
Configuration 4	-0.58

$Cs_{19}Pb_8Cl_{36}$ 1R Methylbenzlamine

	binding [eV]
Configuration 1	-0.45
Configuration 2	-0.53
Configuration 3	-0.44
Configuration 4	-0.48

$$E_{binding} = E(cluster + molecule) - [E(molecule) + E(Cluster)]$$

$$CD(\omega_{ij}) = \sum_{ij} R_{ij}\delta(\hbar\omega - \hbar\omega_{ij})$$

$$R_{ij} \propto \mathrm{Im}\left(\left|\vec{\mu}_{ij}^{elec} \cdot \vec{\mu}_{ij}^{mag}\right|\right)$$

δ is broadened as a Gaussian with broadening parameter 0.01 eV

Circular Dichroism of Joint System

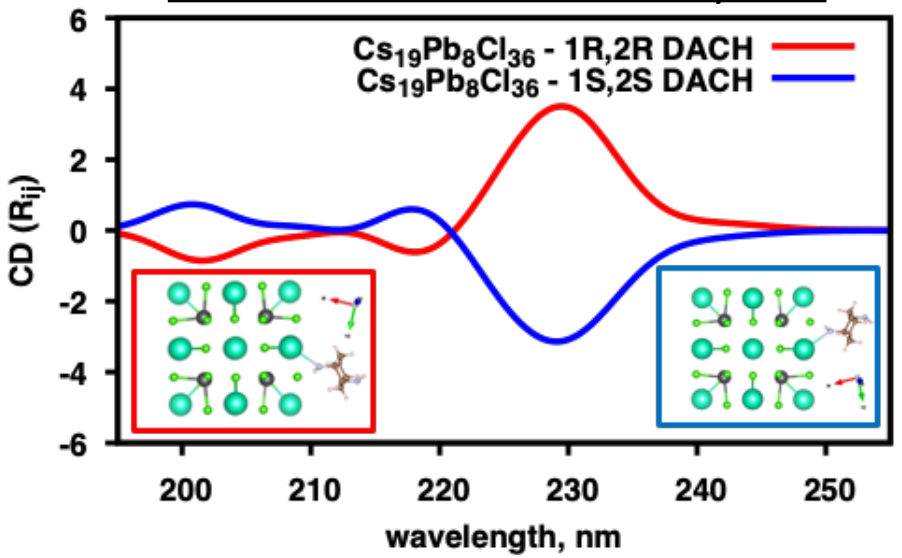

CD spectra for the joint system is distinct from individual contributions

'Decomposed' System:

$Cs_{19}Pb_8Cl_{36}$ 1S,2S DACH

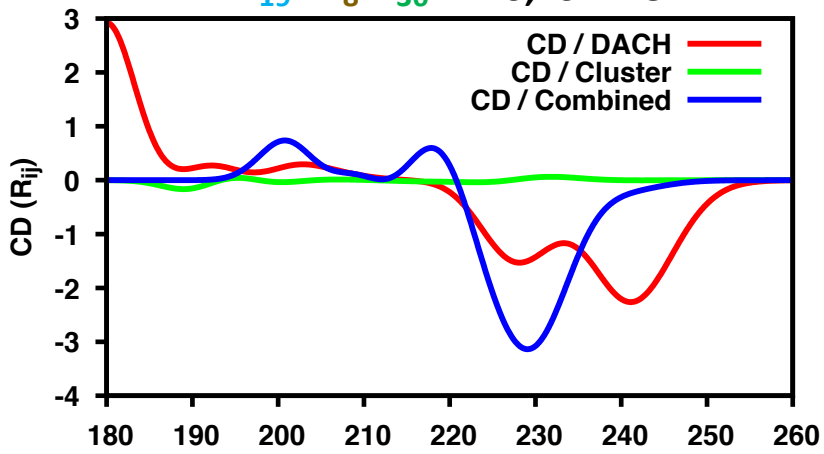

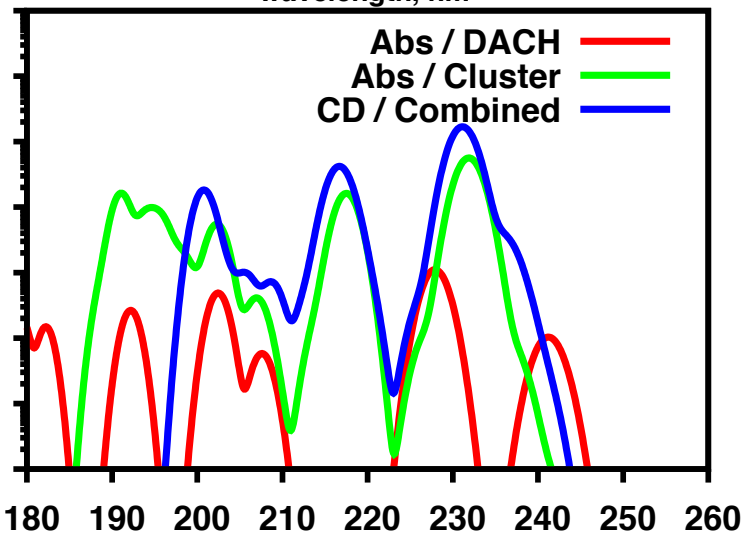

(iii) Circular Dichroism with Multiple Chiral Molecules on the Cluster Surface

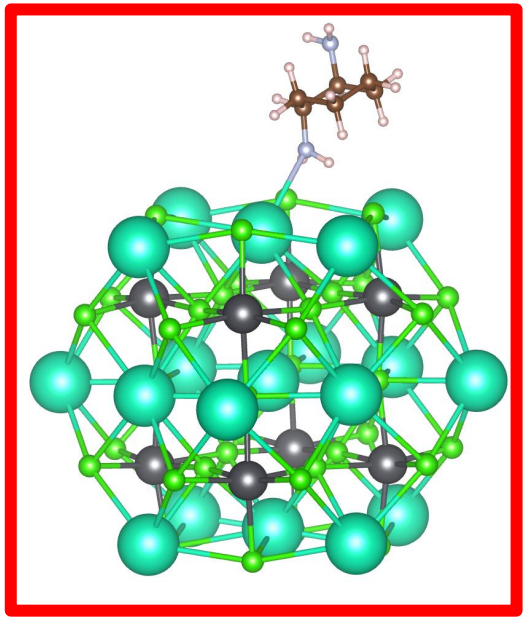

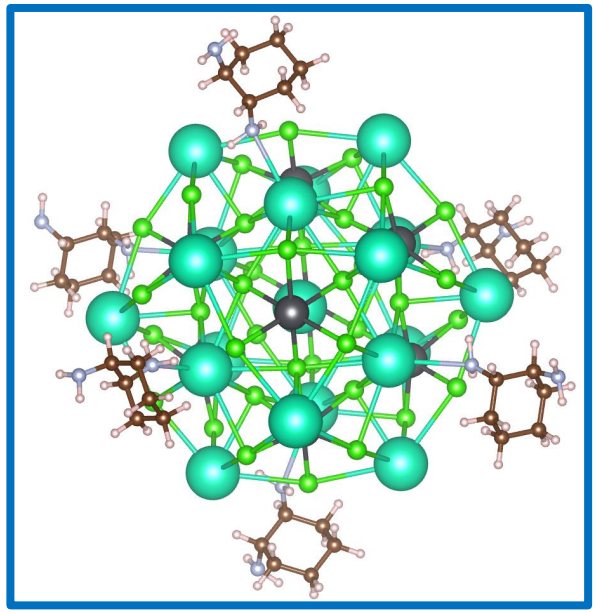

Circular Dichroism of With Chiral Molecules on the Surface

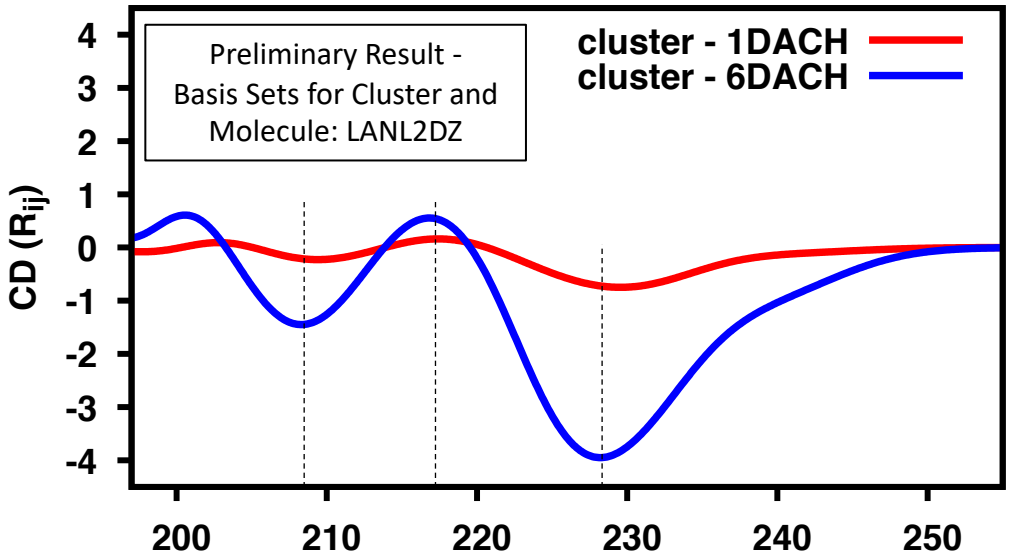

$$CD(\omega_{ij}) = \sum_{ij} R_{ij}\delta(\hbar\omega - \hbar\omega_{ij})$$

$$R_{ij} \propto \mathrm{Im}\left(\left|\vec{\mu}_{ij}^{elec} \cdot \vec{\mu}_{ij}^{mag}\right|\right)$$

δ is broadened as a Gaussian with broadening parameter 0.01 eV

Effect of having multiple chiral ligands on the surface is <u>additive</u> to the CD spectra

Contribution of Charge-Transfer Excitations Towards Circular Dichroism Spectra

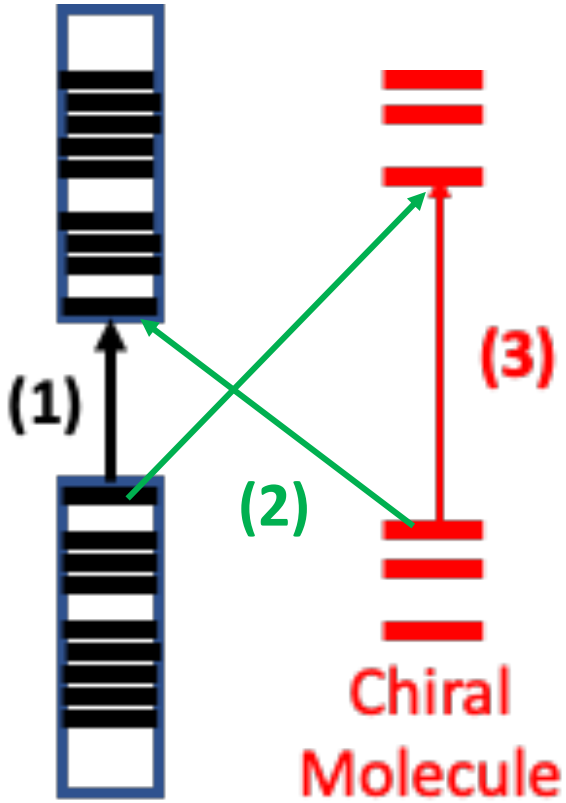

$$CD(\omega_{ij}) = \sum_{ij} R_{ij}\delta(\hbar\omega - \hbar\omega_{ij})$$

$$R_{ij} \propto \mathrm{Im}\left(\left|\vec{\mu}_{ij}^{elec} \cdot \vec{\mu}_{ij}^{mag}\right|\right)$$

δ is broadened as a Gaussian with broadening parameter 0.01 eV

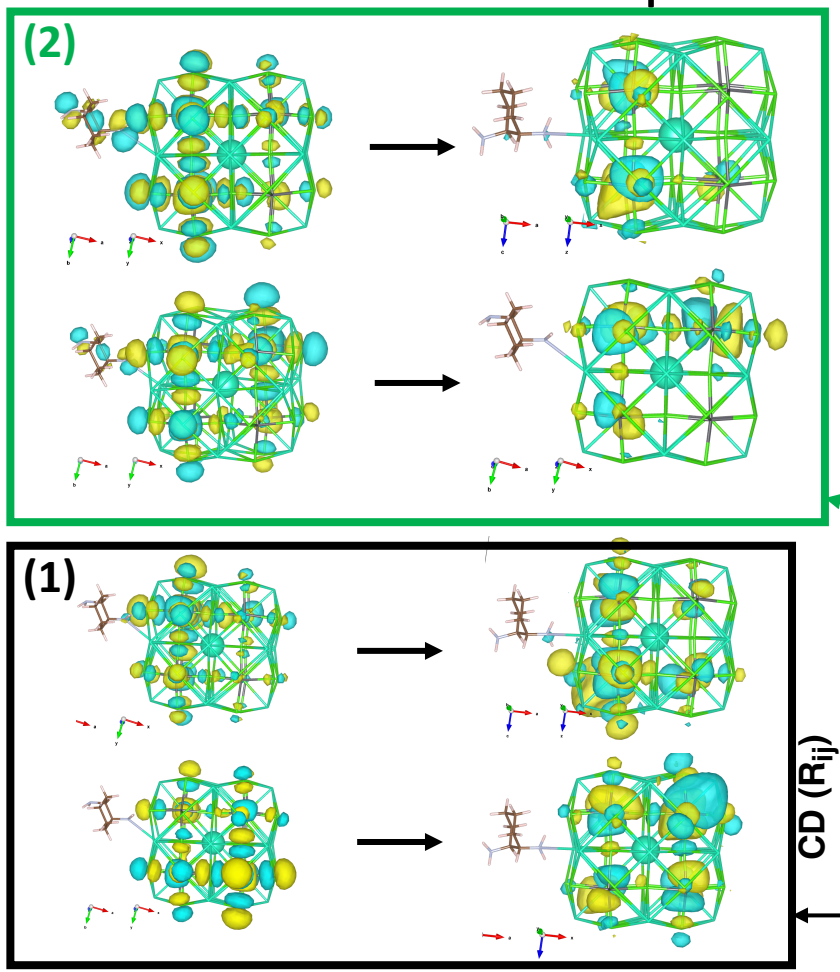

Additional features in CD spectra are not only attributable to **(2) Charge-Transfer Excitations**

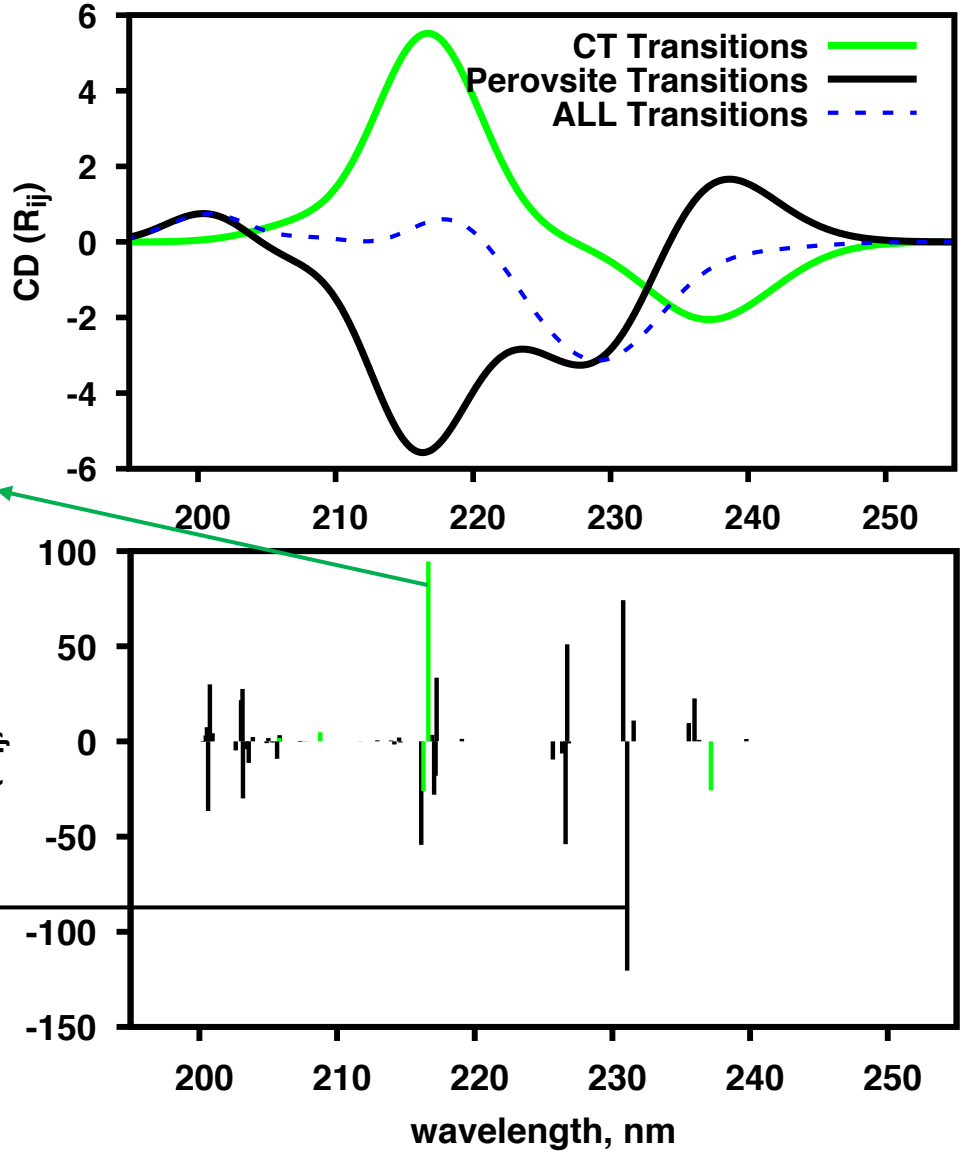

Key Findings:

(i) Circular Dichroism spectra for the joint system is distinct from individual contributions

- Total CD spectra is not sum of radiative pathways **(1) +** (2) + (3)

(ii) Effect of having multiple chiral ligands on the surface is additive to the CD spectra

(iii) Chemical interaction between the chiral molecule and achiral perovskite imprints chirality into **(1)** radiative pathways

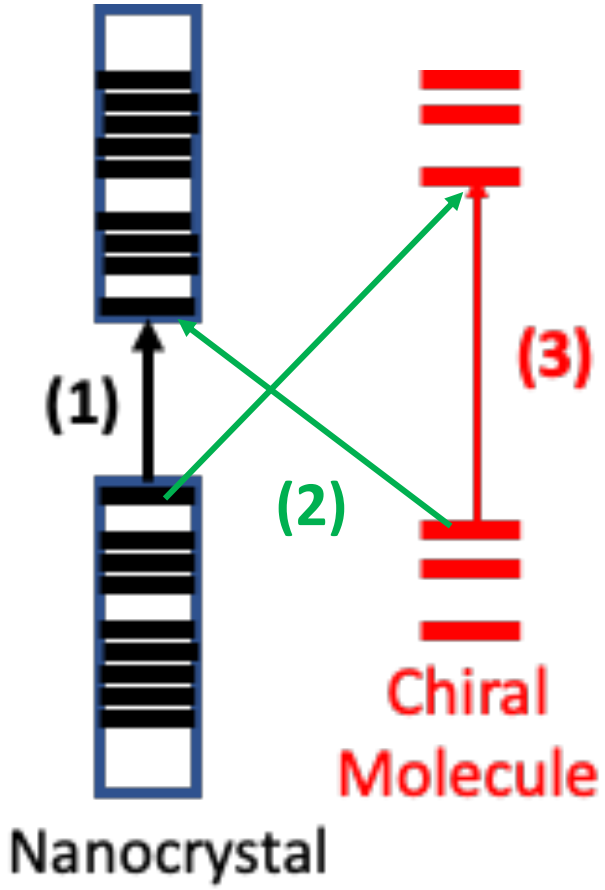

(1) Perovskite-to-Perovskite

(2) Charge-Transfer Excitations

(3) Molecule-to-Molecule

Acknowledgements

- LANL Mentors
  - Amanda Neukirch
  - Dibya Ghosh
  - Sergei Tretiak
- NDSU
  - Dmitri Kilin
  - Svetlana Kilina
  - Erik Hobbie

Supplemental

(a)

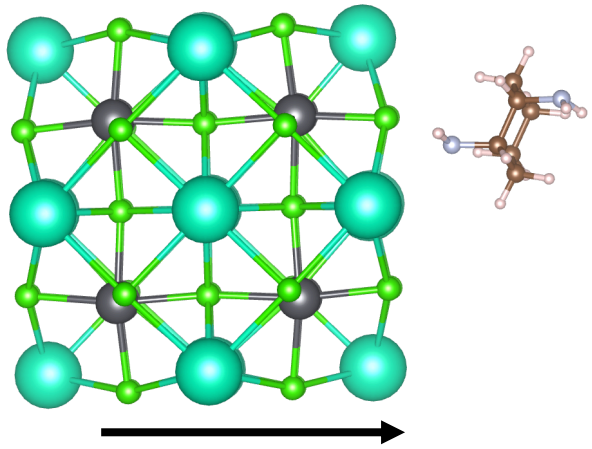

<100>
Configuration 1

(b)

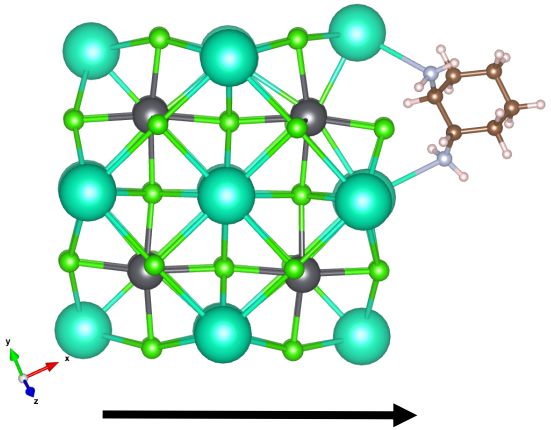

<100>
Configuration 2

(c)

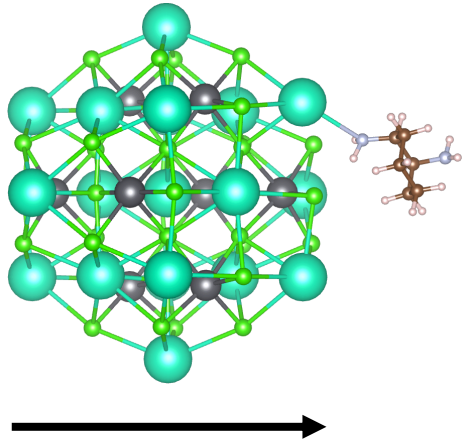

<111>
Configuration 3

(d)

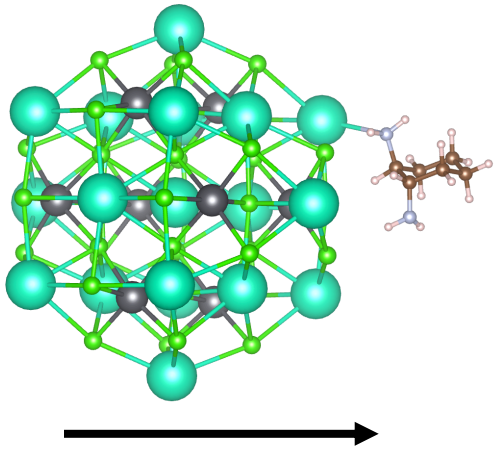

<111>
Configuration 4

(e)

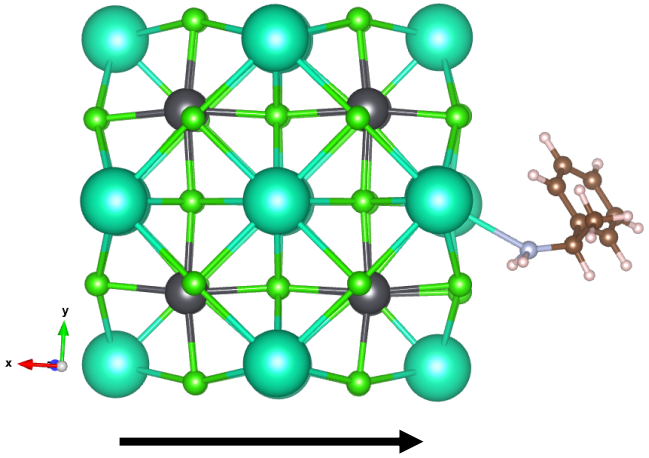

<100>
Configuration 1

(f)

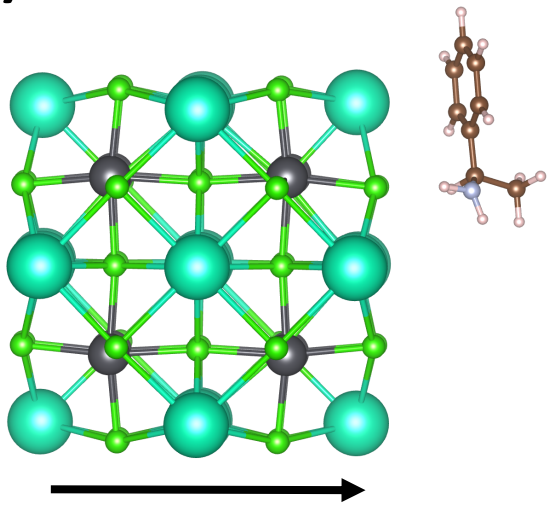

<100>
Configuration 2

(g)

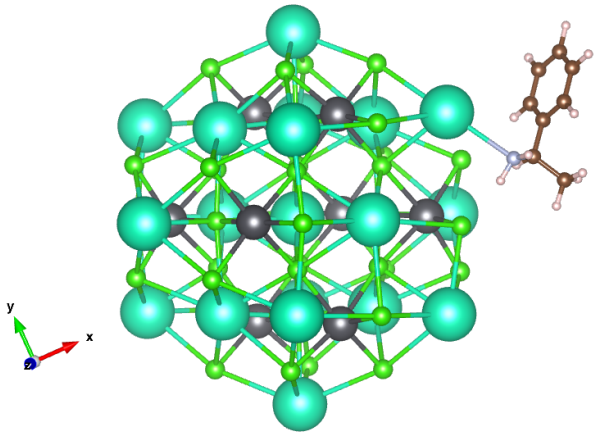

<111>
Configuration 3

(h)

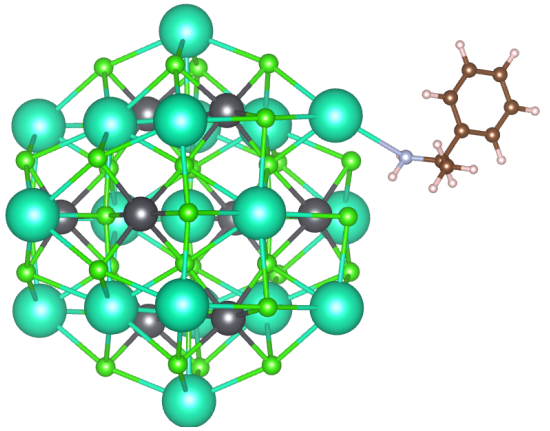

<111>
Configuration 4

Uncertainty quantification of atomic data for collisional-radiative modeling of fusion plasmas

Andrew George – Student intern at T-5 with Willem Kupets at T-1

Mentors: Nathan Garland (T-5) and Mark Zammit (T-1)

LA-UR-20-25815, Funding through ER Grant 20200356ER

The Tokamak

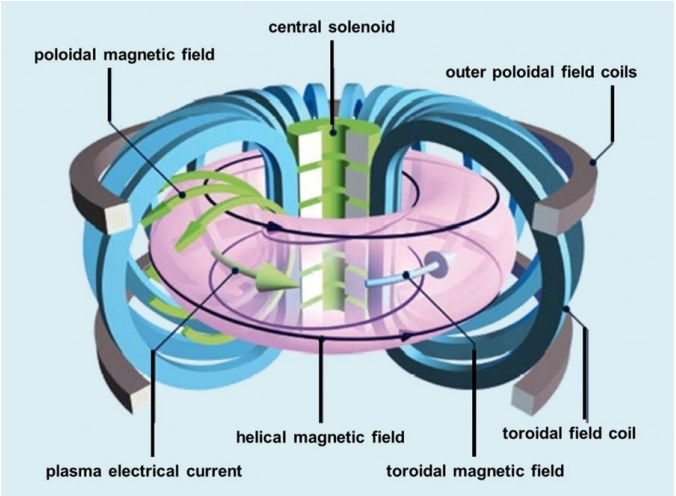

A tokamak is a magnetic confinement device that can confine plasma using counter propagating currents. It is a solenoid that uses the magnetic field that is generated by the electric field to pinch the plasma and confine it.
[1]

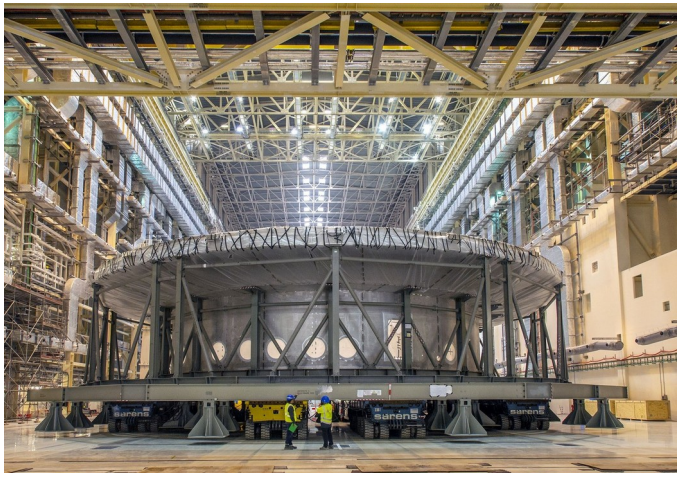

The tokamak that is related to our work is ITER. ITER is the international collaboration that is attempting to make self heating fusion.

Tokamak Disruption Problem

In a tokamak a factor that needs to be accounted for is the fact that a disruption can happen. A disruption is a plasma instability, and a possible scenario of a disruption are runaway electrons. The runaway electrons cause a beam that hits a part of the tokamak.

Our team at LANL is studying the underlying physics of disruptions in order to understand how they occur, in order to develop prevention or mitigation options.

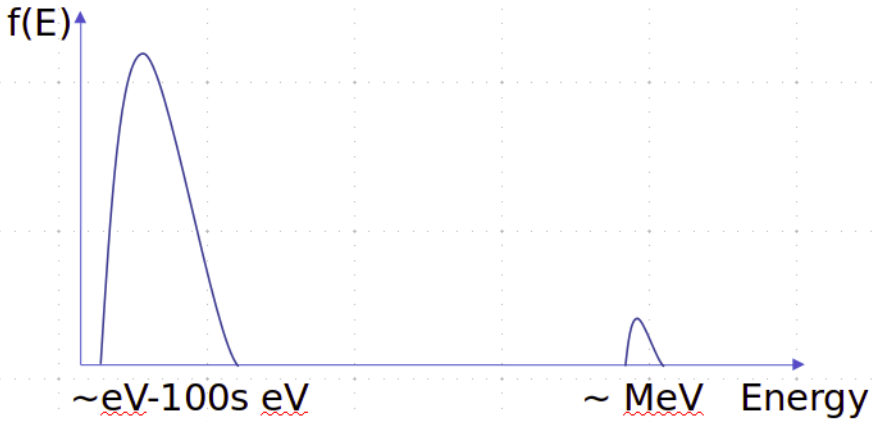

A Potential Solution?

In ITER the walls are mostly beryllium with a small area that is tungsten. Since electrons are highly relativistic and energetic, they need to be mitigated, in order to reduce potential destruction of the vessel.

A high z material such as argon or neon can be inserted to act as an energy sink for the runaway electrons. Therefore we need to understand the composition of ions in the plasma.

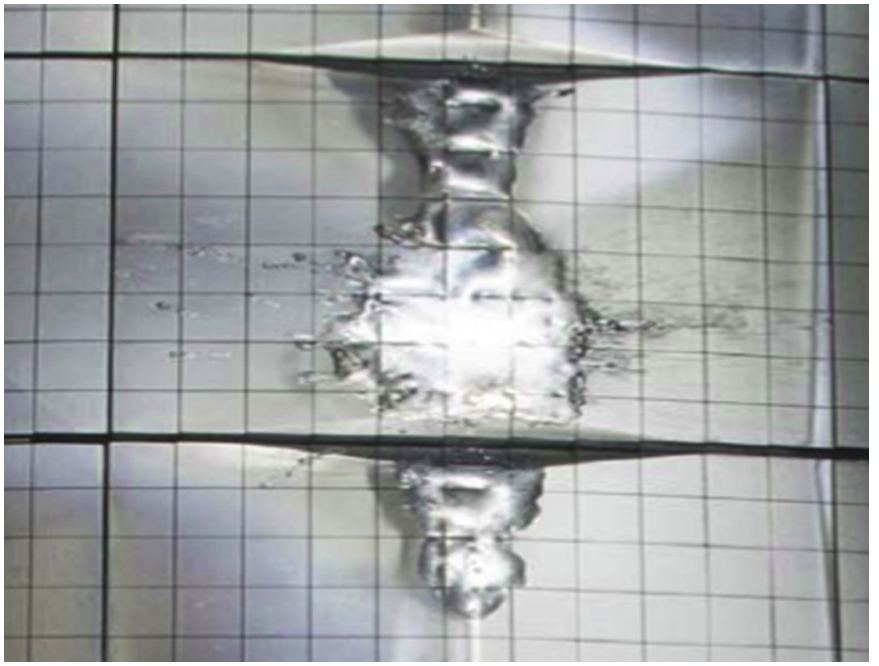

Damaged wall

Modeling the Plasma- CR Model

A collisional radiative model is a model that describes the collisional events and radiative processes(I.E. the up and down processes).

The collisional radiative model needs two things – state completeness and the appropriate rate matrix.

We are using a superconfiguration refinement which uses the principle quantum n for our states.

Quantum number	Name	What it labels	Possible values	Notes
n	principal	electron energy level or shell number	1, 2, 3, ...	Except for d-orbitals, the shell number matches the row of the periodic table.
ℓ	azimuthal	orbital type: s, p, d, f	0, 1, 2, ..., n-1	0 = s orbital 1 = p orbital 2 = d orbital 3 = f orbital
m_ℓ	magnetic	orbital sub-type	integers between and including $-\ell$ and $+\ell$: $-\ell, -\ell+1, \ldots \ell-1, \ell$	$\ell = 0$ (s): 2 e^- in one orbital $\ell = 1$ (p): 2 e^- in each of three sub orbitals (p_x, p_y, p_z) $\ell = 2$ (d): 2 e^- in each of 5 sub orbitals (d_{xy}, d_{xz}, d_{yz}, $d_{x^2-y^2}$, d_{z^2})
m_s	spin	electron spin	$\pm \frac{1}{2}$	Spins in any single sub-orbital must be paired.

$$\vec{J} = \vec{L} + \vec{S}$$

My Project – The Rate Matrix

The Rate matrix is the matrix that contains the collision and radiative transitions.

The rates coefficients are first found through the cross sections. The coefficients can then be used to create the rate matrix.

Using a code called FLYCHK and then an uncertainty quantification package called Dakota I'll be able to take an iterative approach to analyze the effect of uncertainty of the cross sections.

$$\frac{dn_i}{dt} = -n_i \sum_{j \neq i}^{N_L} W_{ij} + \sum_{j \neq i}^{N_L} n_j W_{ji} \qquad 1 \leq i \leq N_L$$

For upward transitions (i < j),

$$W_{ij} = B_{ij}\overline{J}_{ij} + n_e C_{ij} + \beta_{ij} + n_e \gamma_{ij} + \sigma_{ij} + I_{ij}$$

For downward transitions (j > i)

$$W_{ij} = A_{ji} + B_{ji}\overline{J}_{ji} + n_e D_{ji} + n_e \alpha_{ji}^{RR} + n_e \kappa_{ji}^{EC} + n_e^2 \delta_{ji}$$

where n_e is an electron density and $\overline{J}$ is a frequency-averaged mean intensity which is relevant to the transition. The subscript *ji* refers to a transition from level *j* to level *i*. The rate coefficients correspond to the following atomic processes:

A_{ij} spontaneous emission	α_{ji} radiative recombination
B_{ij} stimulated absorption (i < j) or emission (i > j)	β_{ij} photoionization plus stimulated recombination
C_{ij} collisional excitation	γ_{ij} collisional ionization
D_{ij} collisional deexcitation	δ_{ji} collisional recombination
I_{ij} beam and non-thermal electron collisions	κ_{ji} electron capture
	σ_{ij} autoionization

$$dn/dt = Rn$$

What is FLYCHK

- Upgrade from FLY which is a K-shell based code designed to study hot plasmas
- FLYCHK is a general purpose plasma code that applies to most laboratory plasmas(non-LTE, LTE, collisionally driven etc).
- Provides <Z> for fixed densities: ion, electron, mass
- Uses the principle quantum number n(superconfiguration) to describe ion energy levels[2]

Dakota UQ package

“At a high level, uncertainty quantification (UQ) or nondeterministic analysis is the process of (1) characterizing input uncertainties, (2) forward propagating these uncertainties through a computational model, and (3) performing statistical or interval assessments on the resulting responses.”[3]

Dakota also does sensitivity analysis. Sensitivity analysis goes hand in hand with the variance.

Uses Latin Hypercube Sampling(LHS) – Creates near random sample of parameter values from a multidimensional distribution. Dakota samples specifically from a Latin square which in arbitrary dimensions is a hypercube.

Our UQ approach

Inherit uncertainty exists in approximate formulas for cross-sections and rate input data.

We want to probe this uncertainty and its impact on our outputs.

We vary FLYCHK fundamental atomic data by 25%.

$$R^{UQ}_{emission} = x_{arat} A_{ij}$$

$$\sigma^{UQ}_{excitation} = x_{exc} \sigma_{exc}$$

$$\sigma^{UQ}_{ionization} = x_{ion} \sigma_{ion}$$

$$\sigma^{UQ}_{photon} = x_{pho} \sigma_{pho}$$

$$R^{UQ}_{autoion} = x_{ai} R_{ai}$$

$$0.75 \le x_i \le 1.25$$

Results: <Z>

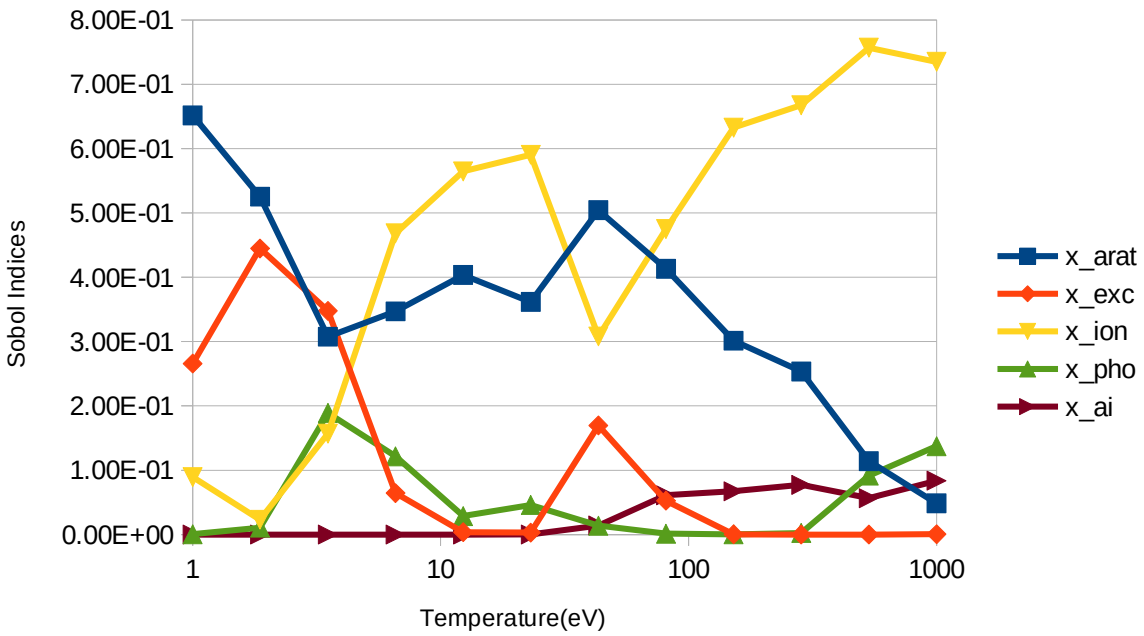

Surprisingly, excitation and spontaneous emission are the dominant processes at low temperatures,

At higher temperatures ionization becomes the dominant effect as one should expect,

Results: Zvar<σ_z^2>

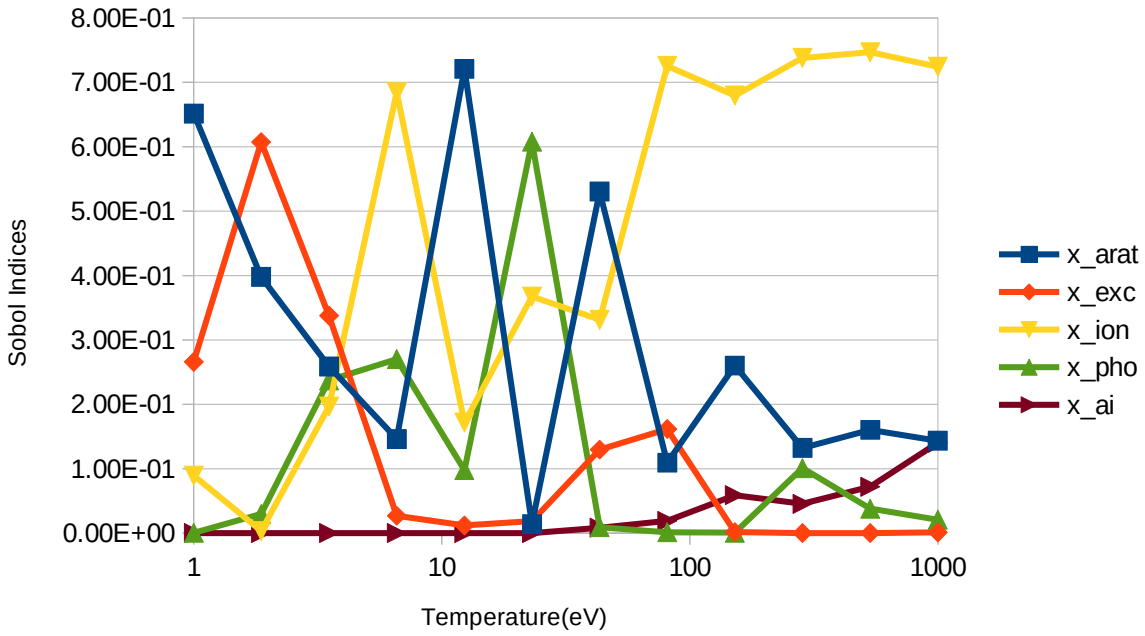

Below 10eV excitation, spontaneous emission and ionization have the biggest effect.

From 10eV to 100 eV, ionization has less of an effect. Spontaneous emission and photoionization are the dominant effects.

At high temperatures ionization is the dominant effect.

Results: RPL(Radiative Power Loss)

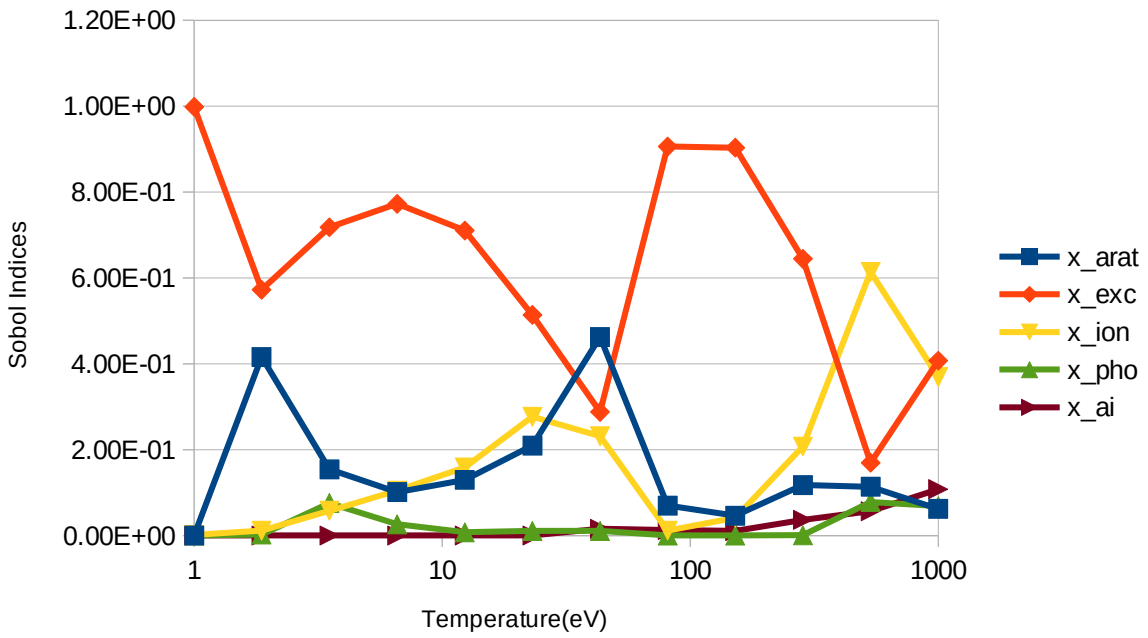

Excitation is the dominant effect at low temperatures.

At 100eV excitation is the dominant effect, but loses its impact as ionization begins to have more of an effect.

References

[1]Haupt, K. (2018, June 11). Fusion machines: Searching for the perfect shape. Retrieved July 02, 2020, from https://www.iter.org/newsline/-/3037

[2]Chung, H., Chen, M., Morgan, W., Ralchenko, Y., & Lee, R. (2005). FLYCHK: Generalized population kinetics and spectral model for rapid spectroscopic analysis for all elements. High Energy Density Physics, 1(1), 3-12. doi:10.1016/j.hedp.2005.07.001

[3]Adams, B.M., Bohnhoff, W.J., Dalbey, K.R., Ebeida, M.S., Eddy, J.P., Eldred, M.S., Geraci, G., Hooper, R.W., Hough, P.D., Hu, K.T., Jakeman, J.D., Khalil, M., Maupin, K.A., Monschke, J.A., Ridgway, E.M., Rushdi, A.A., Stephens, J.A., Swiler, L.P., Vigil, D.M., Wildey, T.M., and Winokur, J.G., "Dakota, A Multilevel Parallel Object-Oriented Framework for Design Optimization, Parameter Estimation, Uncertainty Quantification, and Sensitivity Analysis: Version 6.11 User's Manual," Sandia Technical Report SAND2014-4633, July 2014; updated November 2019.

Validating Experimental Results of toxins using Cheminformatics and Quantum Chemistry

Beauty Kolade
T-CNLS / B-11
08/14/2020

Mentor: Jacob Miner (B-11)
Co-Mentor / PI: Robert F. Williams (B-11)

LA-UR-20-25834

Plant-based toxins

- Derived from natural sources (i.e Foxglove plant)
- Treat heart failure and irregular heartbeats
- Binds to protein receptors

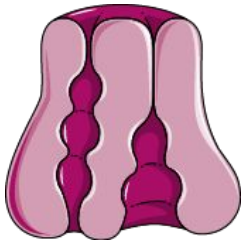

- Therapeutic range=10–40 nM

Structure →

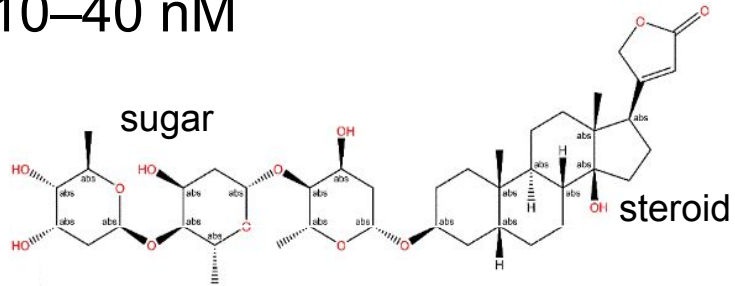

Digitoxin IM-MS spectrum

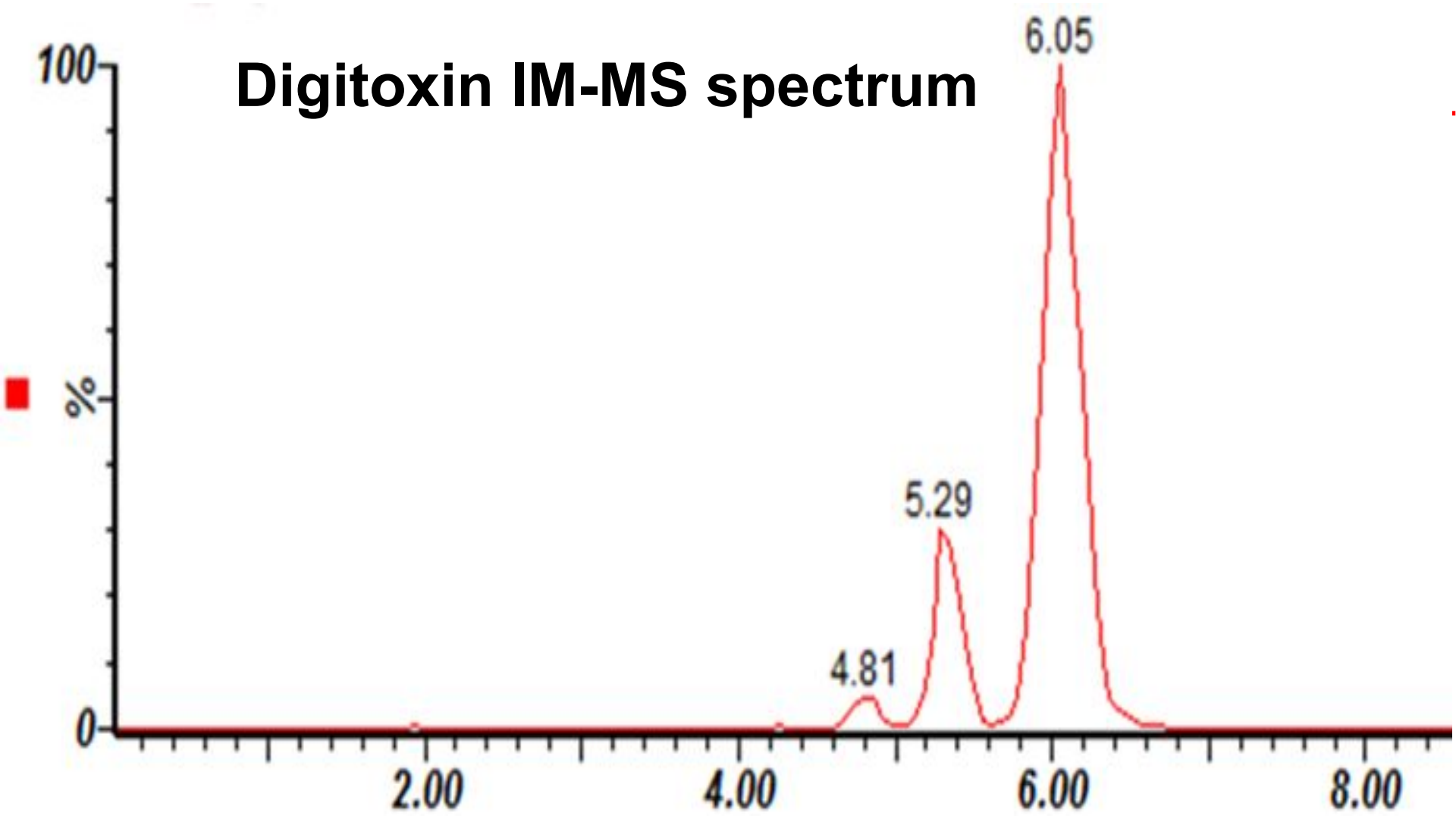

New procedure

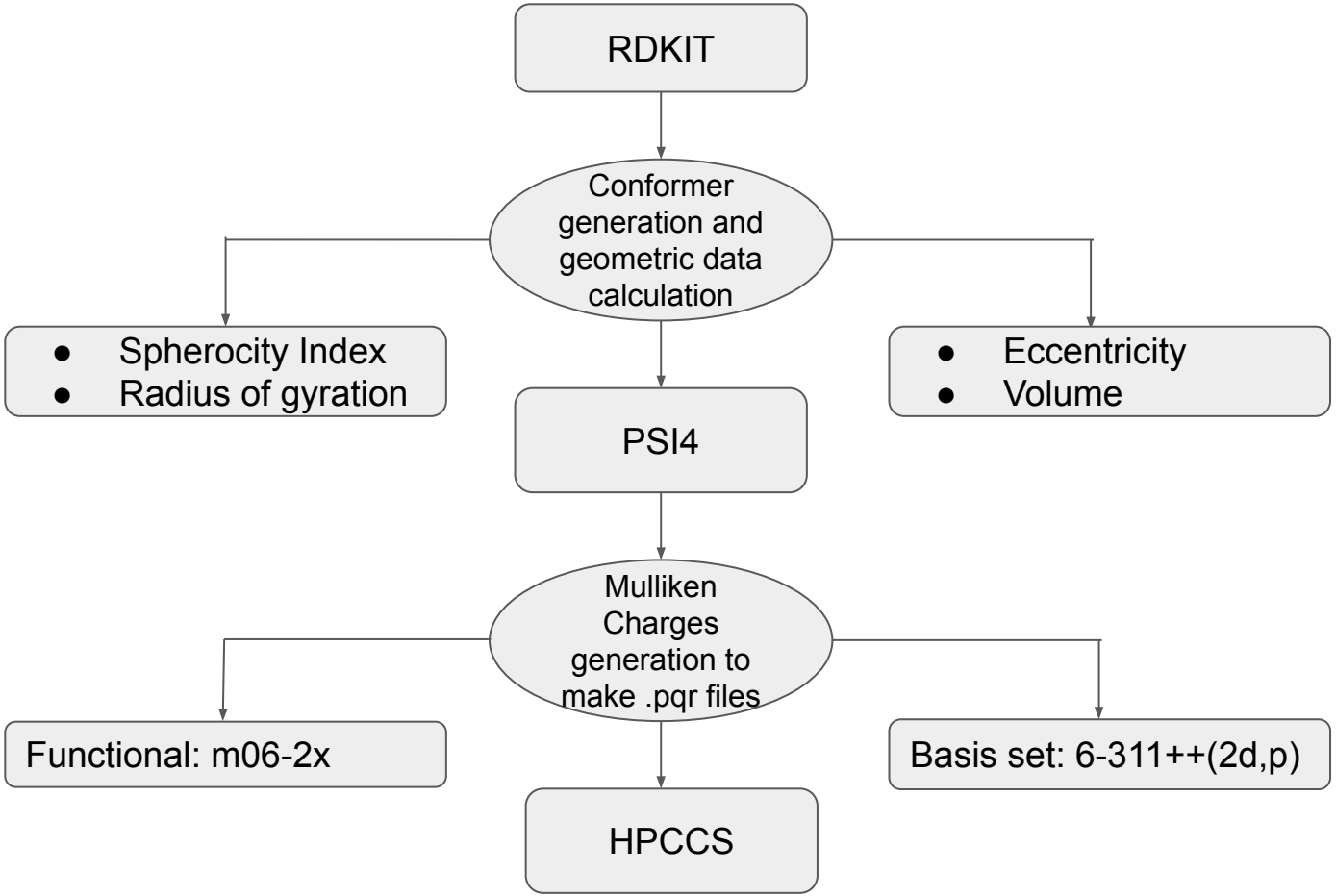

Goals

- Develop an approach for rapidly determining toxin molecule configurations to compare with experiment

➔ Create a library of ion-mobility-based data for cardiac glycosides

- Generate ensembles of molecular configurations without complex parameterization and intensive simulations through molecular dynamics

- Correlate geometric criteria of molecules with calculated CCS values

Systems

- Digitoxin- Complex structure
- Single-wall carbon nanotubes - oblong shape is similar to Digitoxin shape
- Buckyballs - used to calibrate the original mobility calculators ("like mobcal") and the IM-MS machines
- Single-wall carbon nanotubes and Buckyballs are simple structures
- Their geometric properties can be used as a standard to compare with the geometric properties of Digitoxin

Geometric data Results-Digitoxin

Molecule	End-to-end distance (Å)	Volume(Å^3)	Radius of gyration(Å)	Eccentricity	Spherocity Index
Digitoxin(RDKIT)	27.5	721±0.40	8.02±0.48	1.00± 0.009	0.11±0.03
Digitoxin(GROMACS)	23.6	708±3.00	6.85±1.21	0.98±0.02	0.19±0.08
3-3 Nanotubes	27.0	1121	8.38	1.00	0.09

Geometric data Results -Nanotubes

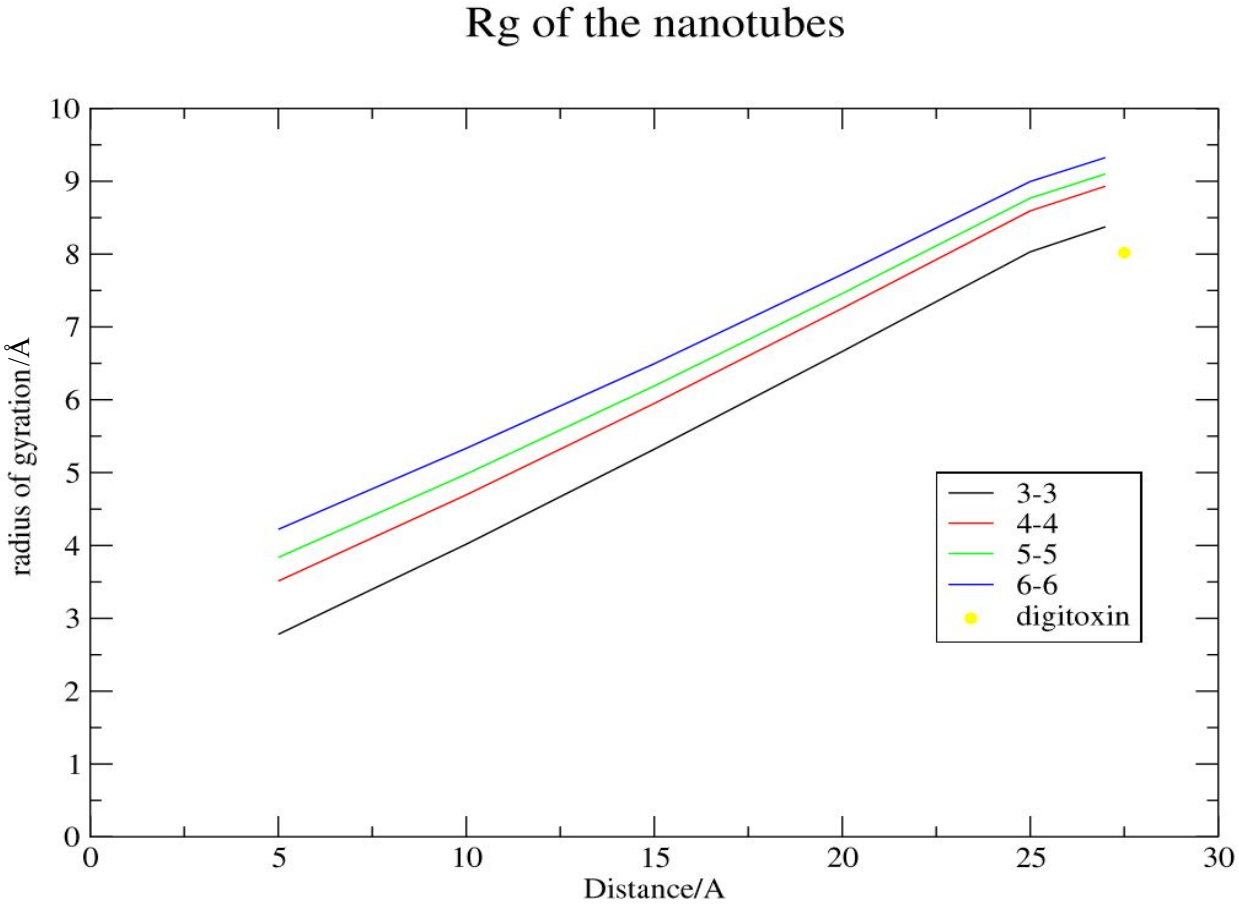

Geometric data Results -Nanotubes

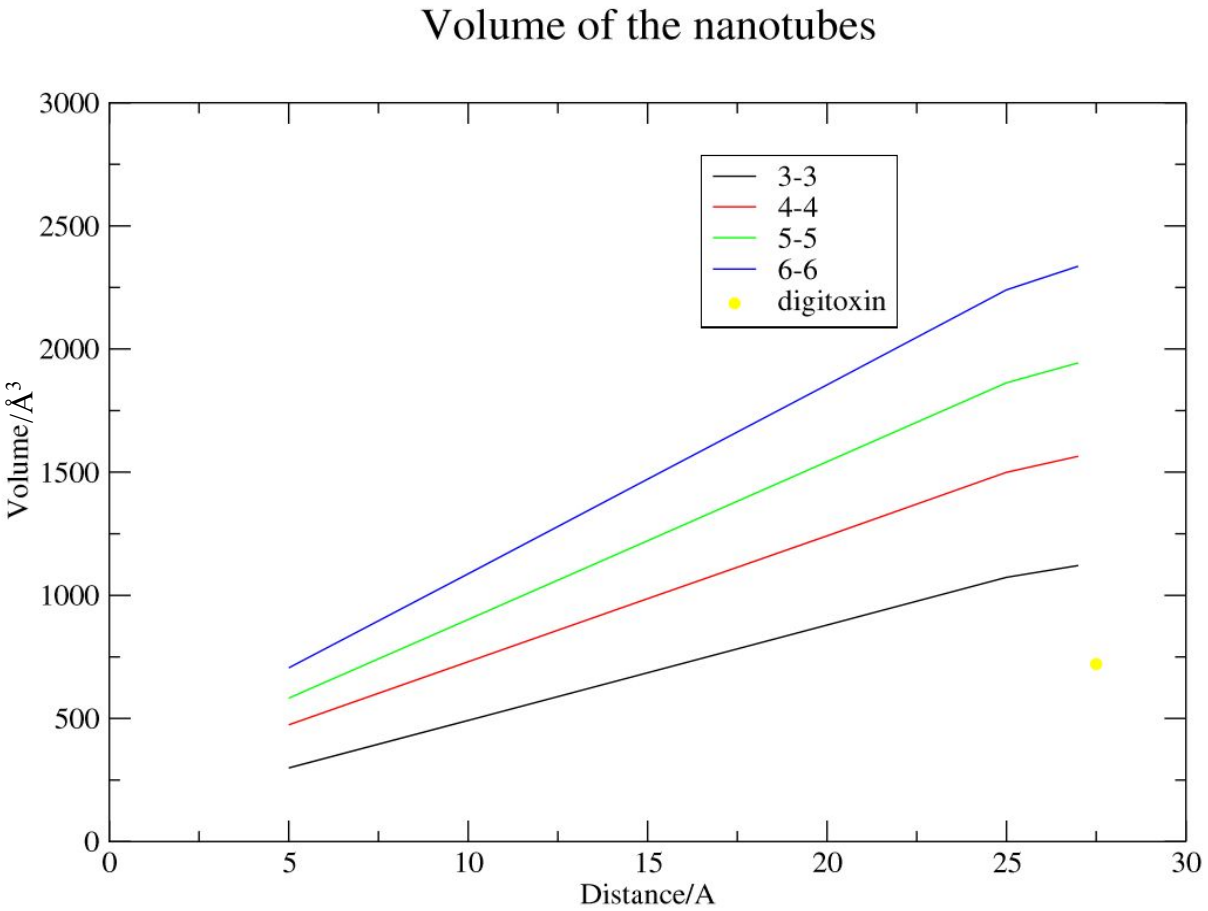

Next steps

- Calculate the CCS values of the most representative Digitoxin Configurations

- Apply clustering methods (i.e. k-means, principal component analysis) to identify the most salient geometric features that correlate with CCS in buckyballs and nanotubes

➔ Improve the pre-screening of CCS for biological molecules

- Compare with results of MD simulations (Amber, Ligpargen) to see if RDKit comes closer to predicting CCS.

Acknowledgement

CNLS:Angel Garcia

Mentors: Jacob Miner, Robert Williams

Funding: DHS funding

Thank you!

Diversification of ML Datasets via Bias Potential as Function of "Uncertainty"

Maksim Kulichenko

3rd year PhD, Utah State University

T-1 Division

Mentor: Justin Smith

Co-mentor: Sergei Tretiak

Collaborator: Kipton Barros

Make Dataset Better

Purpose: the ideal ratio between *Time, Size, Diversity*

- Capture as much conformational and configurational space as possible
- Dataset diversity increase
- Dataset preparation time decrease

Different Approaches to Space Sampling

- Random Sampling
- Normal modes descent

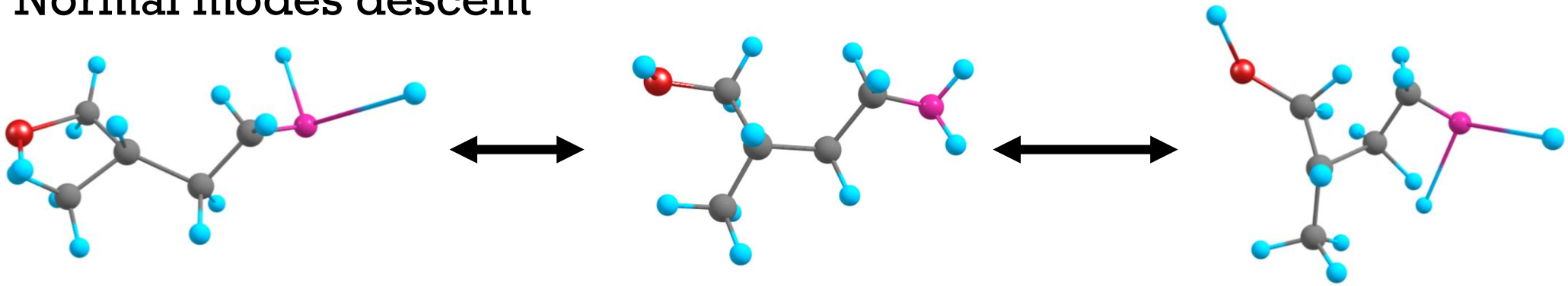

- Molecular Dynamics

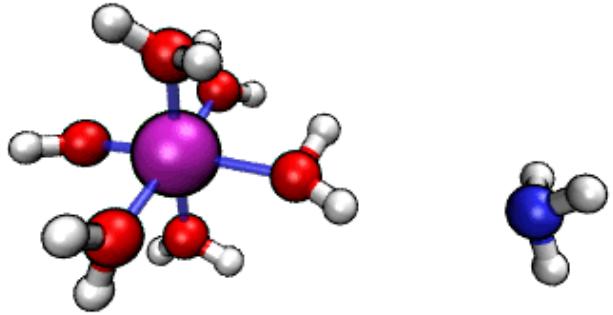

Active Learning MD Workflow

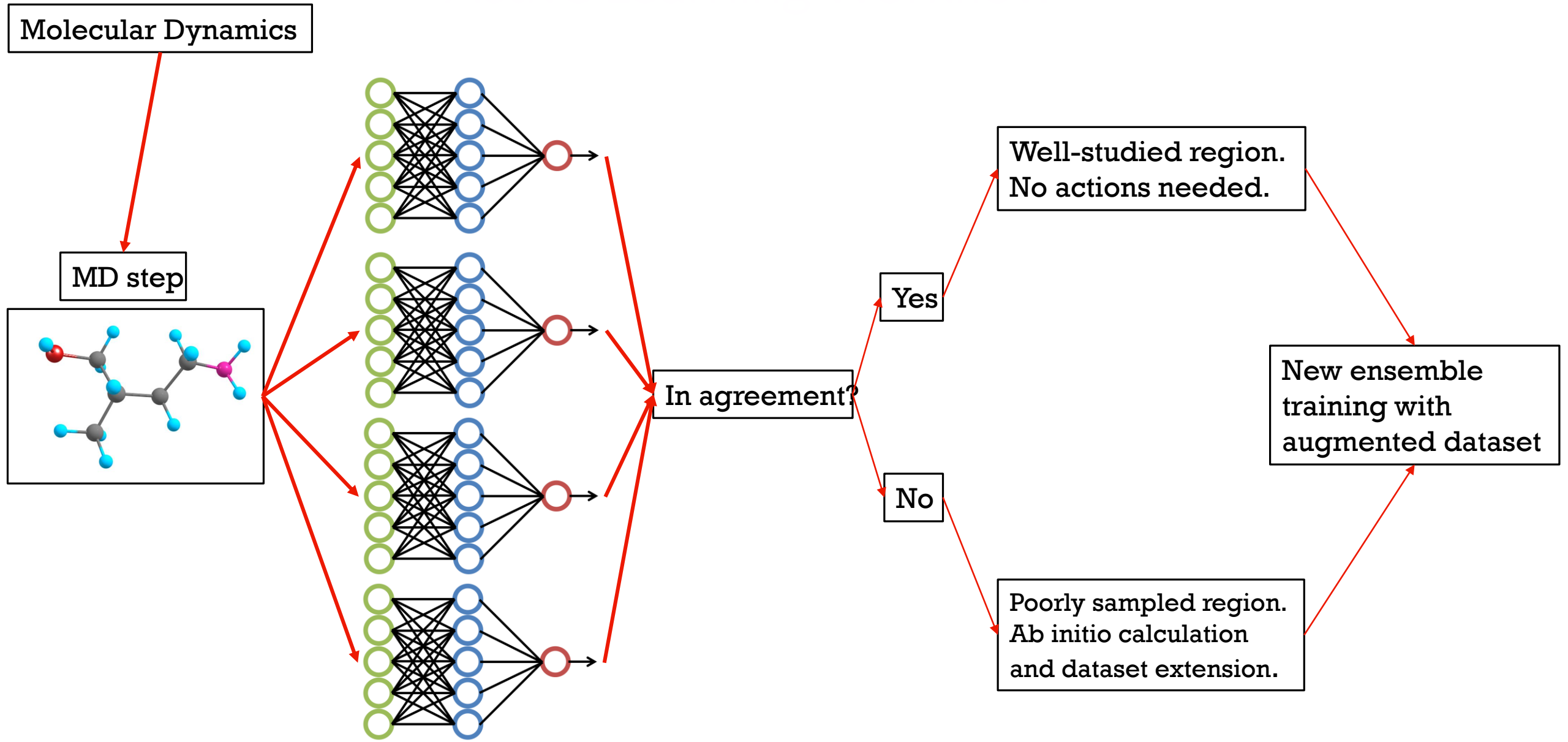

Moving towards Low Sampled Region

- Math of Energy uncertainty

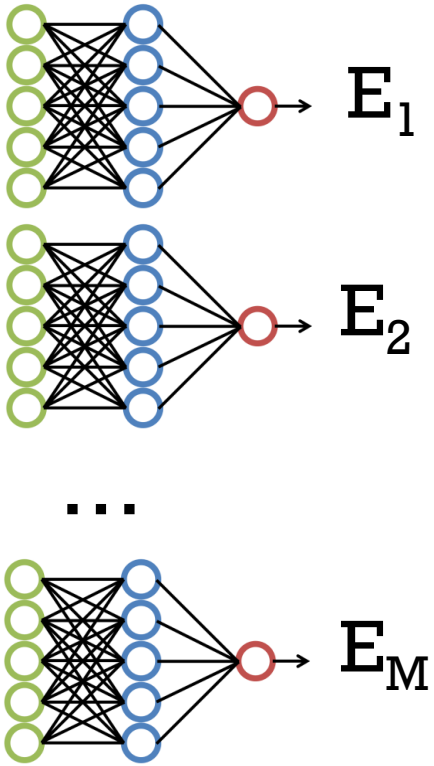

$$\bar{E} = \frac{1}{M}\sum_{m=1}^{M}\hat{E}_m$$

$$\sigma_E^2 = \frac{1}{M(M-1)}\sum_{m=1}^{M}\delta E_m{}^2,$$

$$\delta E_m = \hat{E}_m - \bar{E},$$

Energy as Function of Uncertainty

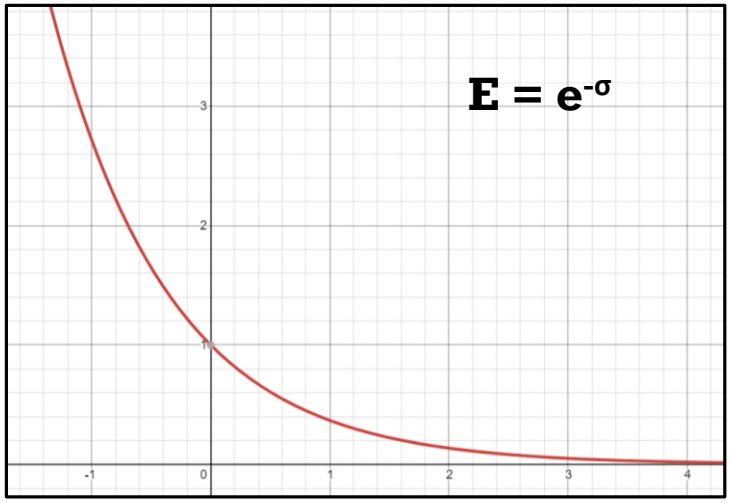

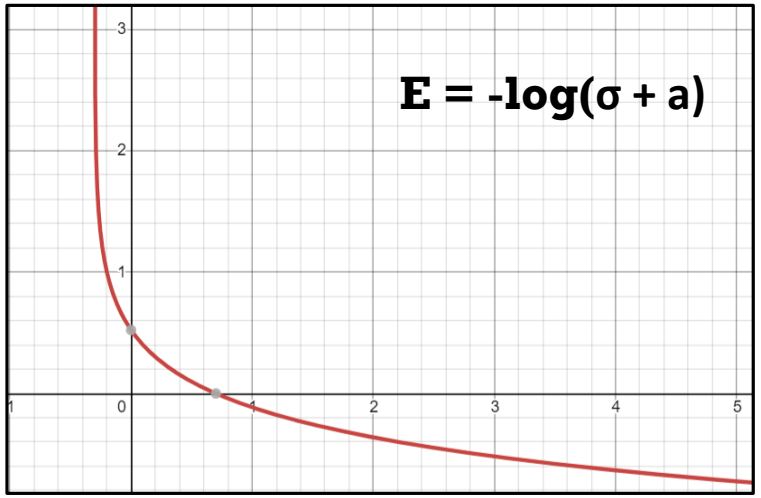

Driving Force of Uncertainty

$$-\nabla_i V(\sigma_{\mathbf{f}}^2) = -V'(\sigma_{\mathbf{f}}^2)\nabla_i \sigma_{\mathbf{f}}^2,$$

Energy uncertainty

$$\sigma_E^2 = \frac{1}{2}\sum_m (\hat{E}_m - \hat{E})^2,$$

where

$$\hat{E} = \frac{1}{N_{models}}\sum_m \hat{E}_m$$

Bias forces

$$\begin{aligned} -\frac{\partial}{\partial \mathbf{r}_i}\sigma_E^2 &= -\sum_m (\hat{E}_m - \bar{E})\frac{\partial}{\partial \mathbf{r}_i}(\hat{E}_m - \hat{E}) \\ &= \sum_m (\hat{E}_m - \bar{E})(\hat{\mathbf{f}}_m - \hat{\mathbf{f}}) \end{aligned}$$

UQ Test

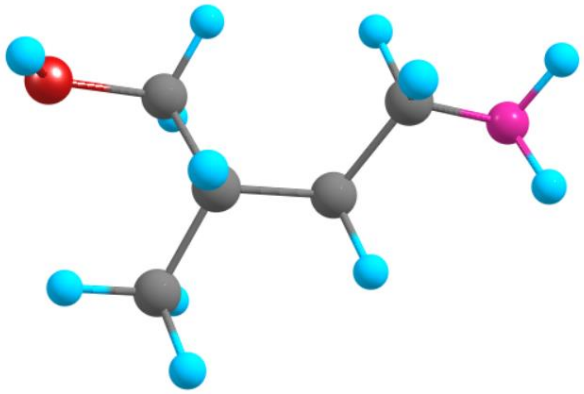

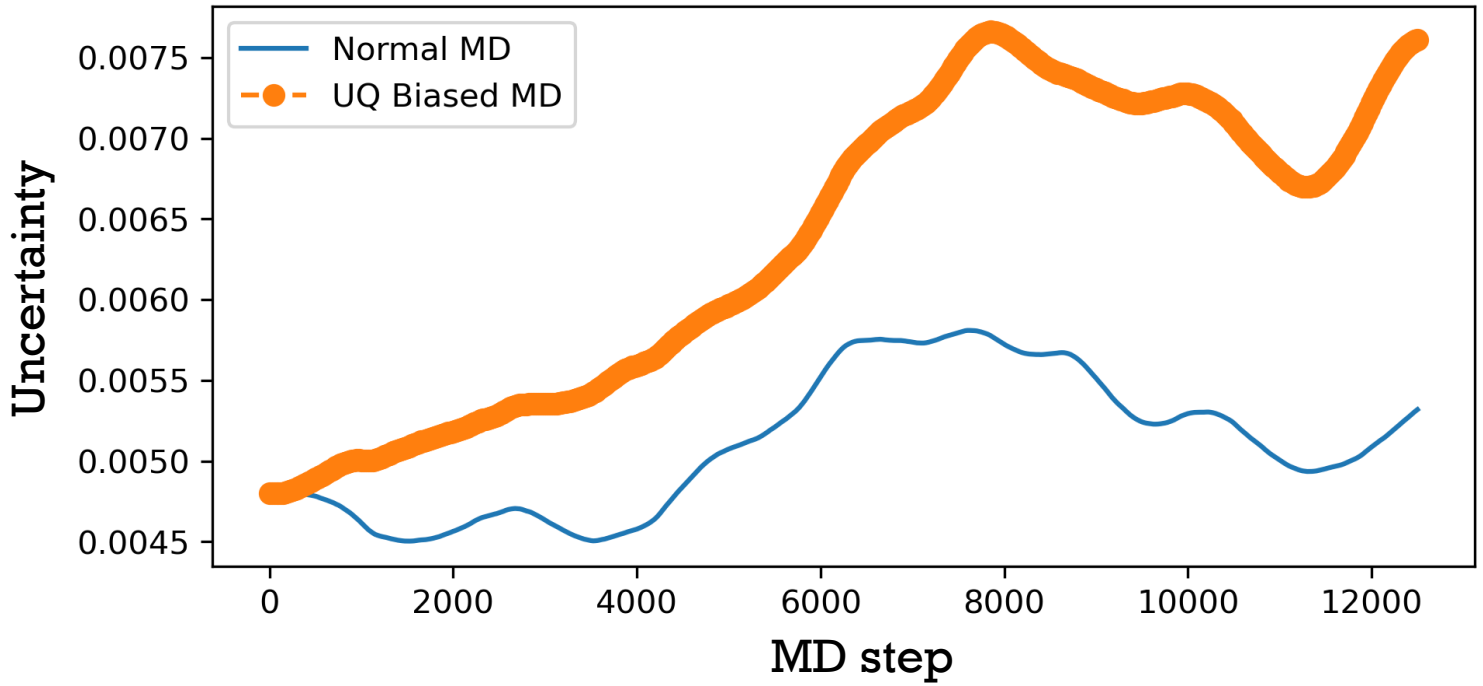
Normal MD
UQ Biased MD
Uncertainty
0.0075
0.0070
0.0065
0.0060
0.0055
0.0050
0.0045
0
2000
4000
6000
8000
10000
12000
MD step

t-SNE Latent Space

Plot biased and non-biased Active learning over lond scale MD (25 ns)

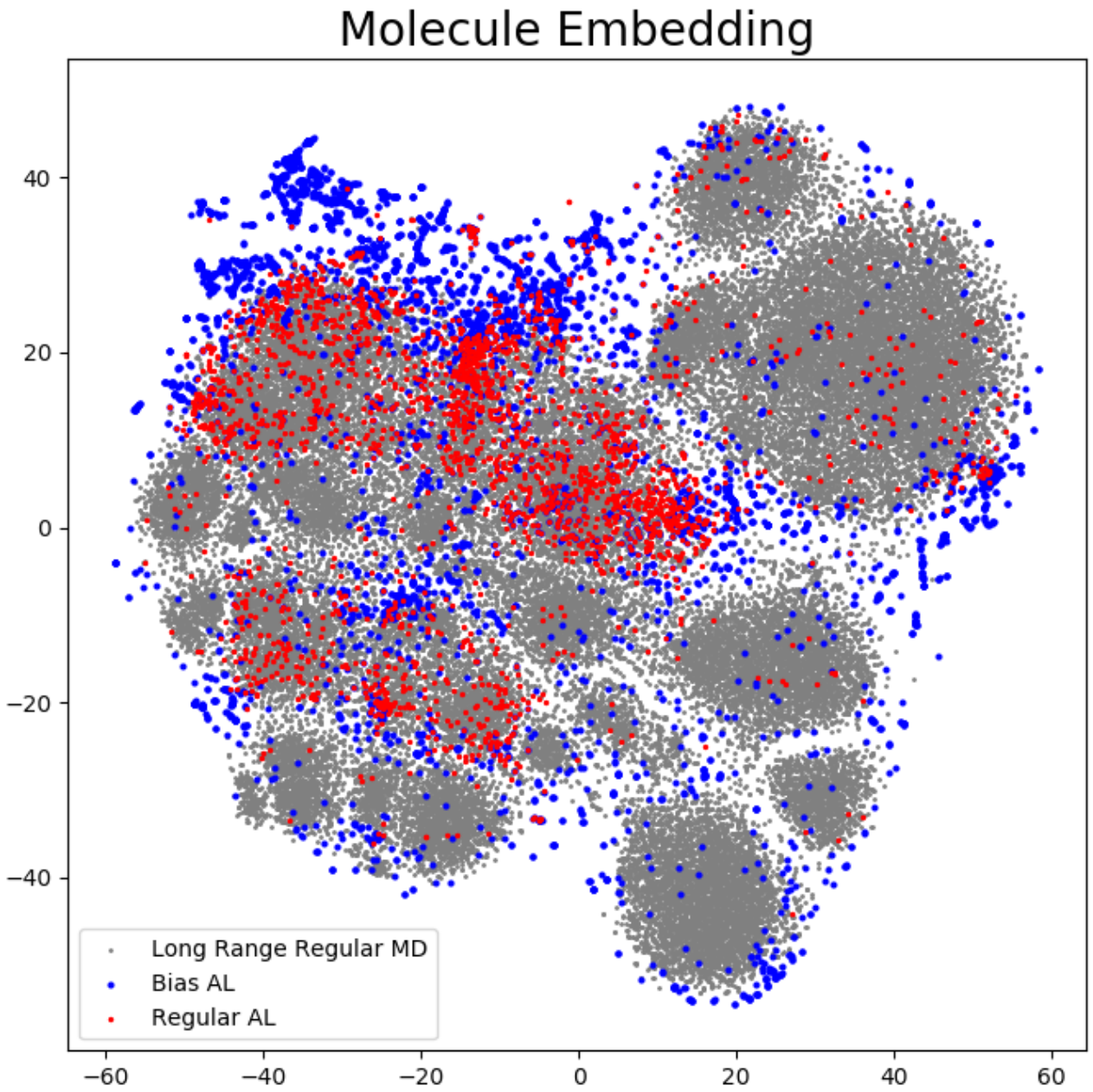

Feeding Long Range MD data to…

Model trained on non-biased AL data

Model trained on biased AL data

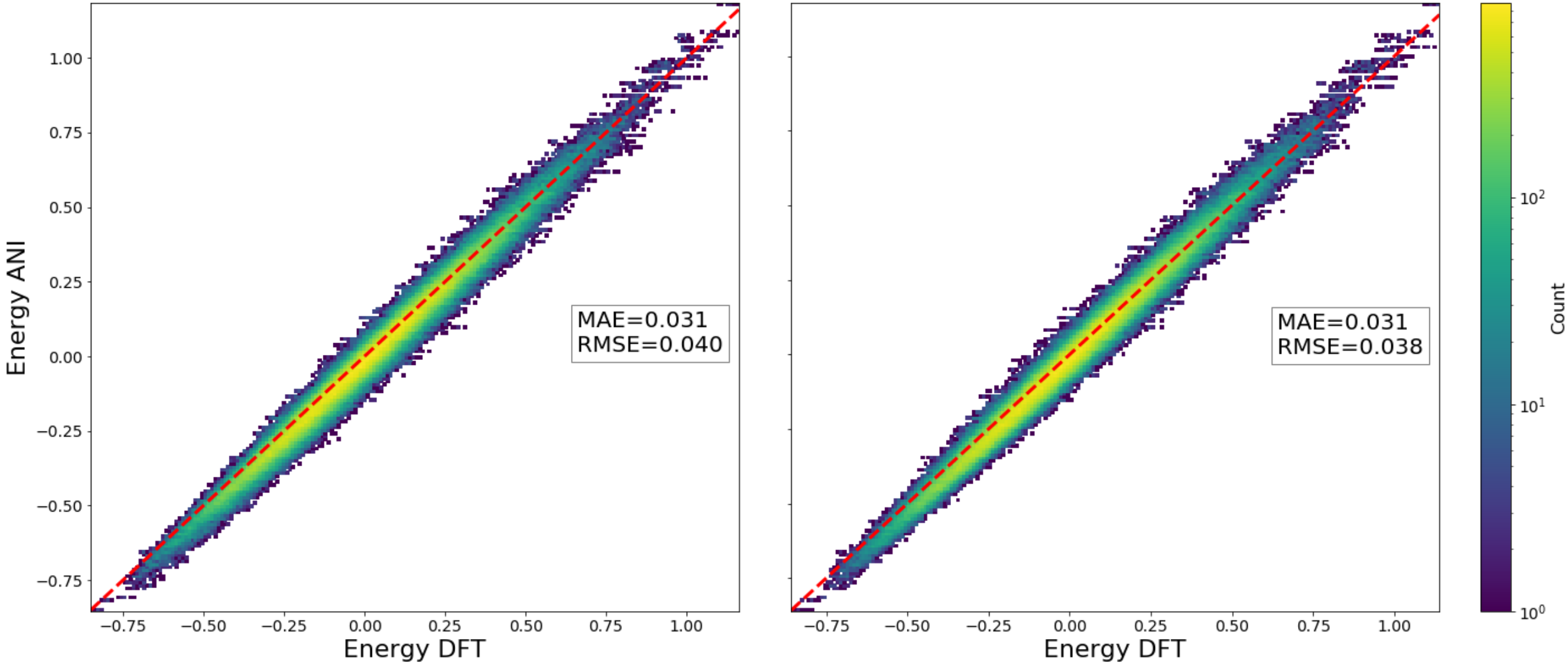

x1.5-2 faster

Further Development

- Application to larger systems and combinations of different systems
- Implementation of Hessian matrix
- Nano-reactors

Bayesian Uncertainty Quantification for COVID-19 Situational Awareness

Abhishek Mallela

Department of Mathematics

University of California, Davis

Mentor: William S. Hlavacek

Group: T-6 (Theoretical Biology and Biophysics)

Illustration of the populations and processes considered in a mechanistic compartmental model for the dynamics of COVID-19 transmission.

The model accounts for susceptible (S), exposed (E), asymptomatic (A), symptomatic (I), hospitalized (H), recovered (R), and deceased (D) populations. It also accounts for social distancing, which establishes mixing and protected subpopulations, quarantine driven by testing and contact tracing, and self-isolation spurred by symptom awareness. The incubation period is divided into 5 stages, which allows the model to reproduce an empirically determined Erlang distribution of waiting times for the onset of symptoms after infection. The exposed population (consisting of individuals incubating the virus) includes presymptomatic and asymptomatic individuals. The A-populations consist of true asymptomatic individuals in the immune clearance phase. The gray background indicates the populations that contribute to disease transmission. An auxiliary measurement model accounts for imperfect detection and reporting of new cases.

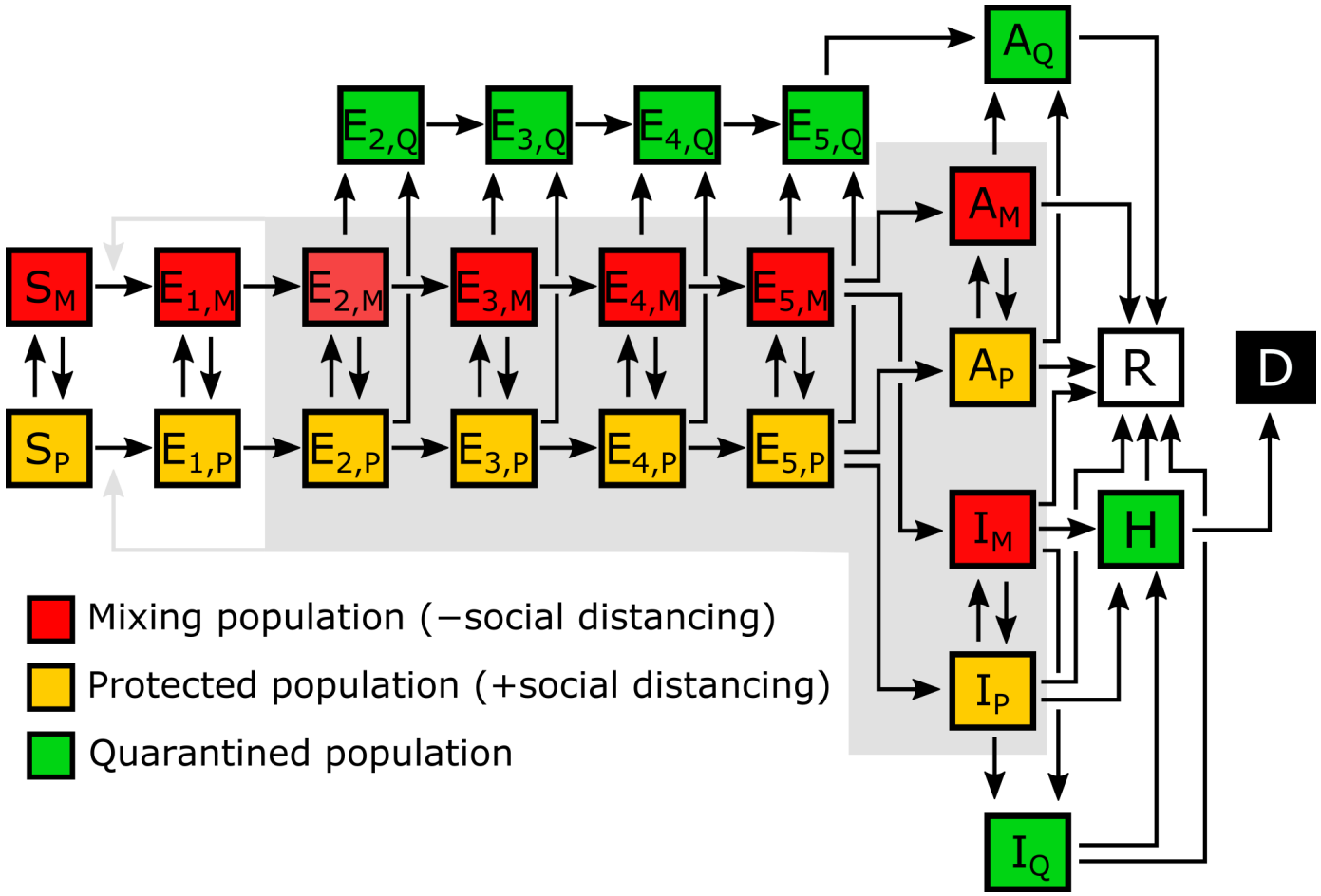

Illustration of Bayesian predictive inference.

We forecast future daily reports of new COVID-19 cases with rigorous uncertainty quantification (UQ) through online Bayesian learning of model parameters. Each day, using all daily case-reporting data available up to that point, we perform Markov chain Monte Carlo (MCMC) sampling of the posterior distribution for a set of adjustable parameters. Subsampling of the posterior samples then allows us to use the relevant model to generate trajectories of the epidemic curve that account for both parametric and observation uncertainty. The entire shaded region indicates the 95% credible interval for predictions of daily case reports. In other words, the central 95% of all predictions lie within the shaded region. The color-coded bands within the shaded region indicate other credible intervals, as indicated in the legend.

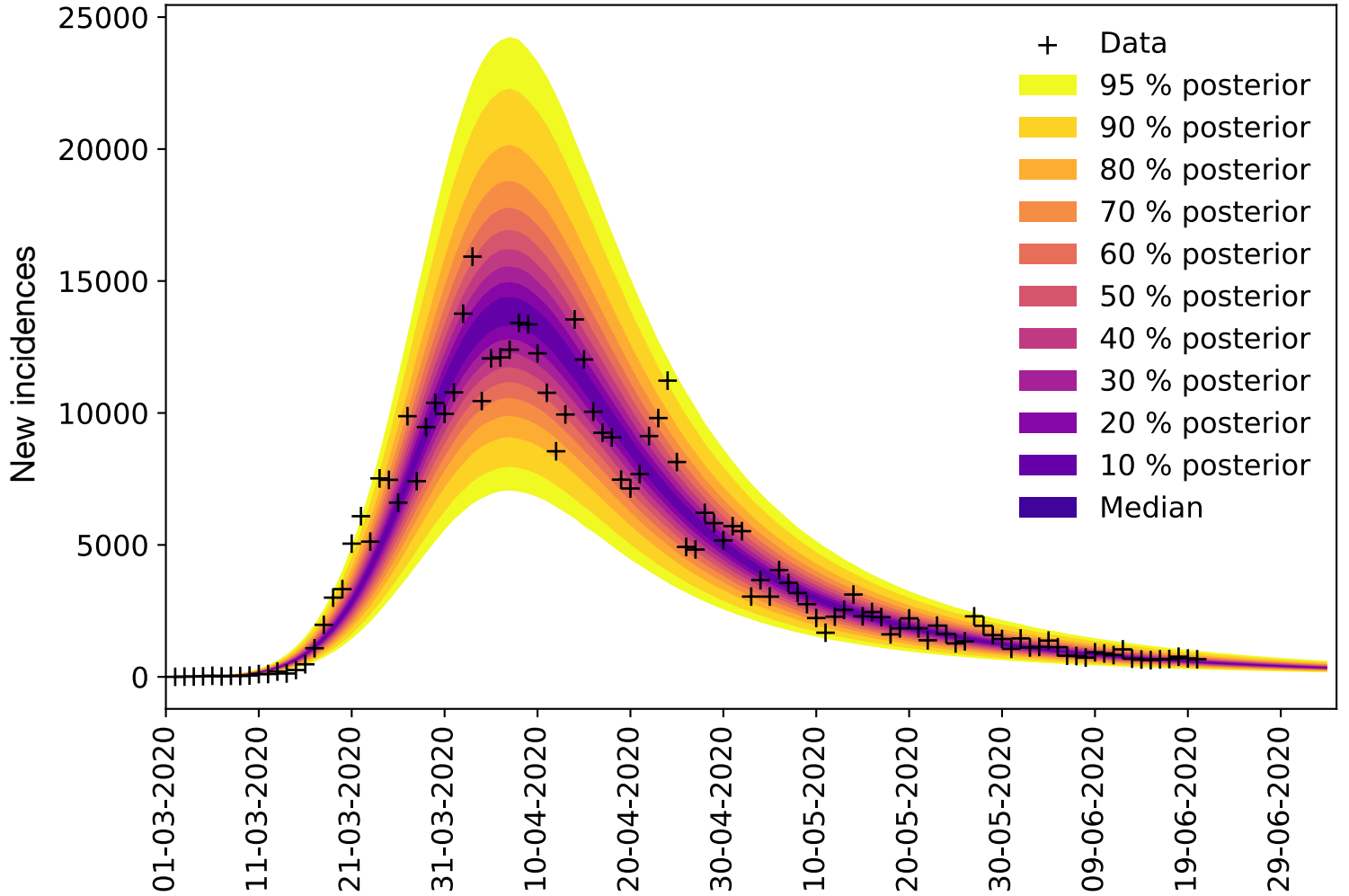

Top row: One phase; Bottom row: Two phases

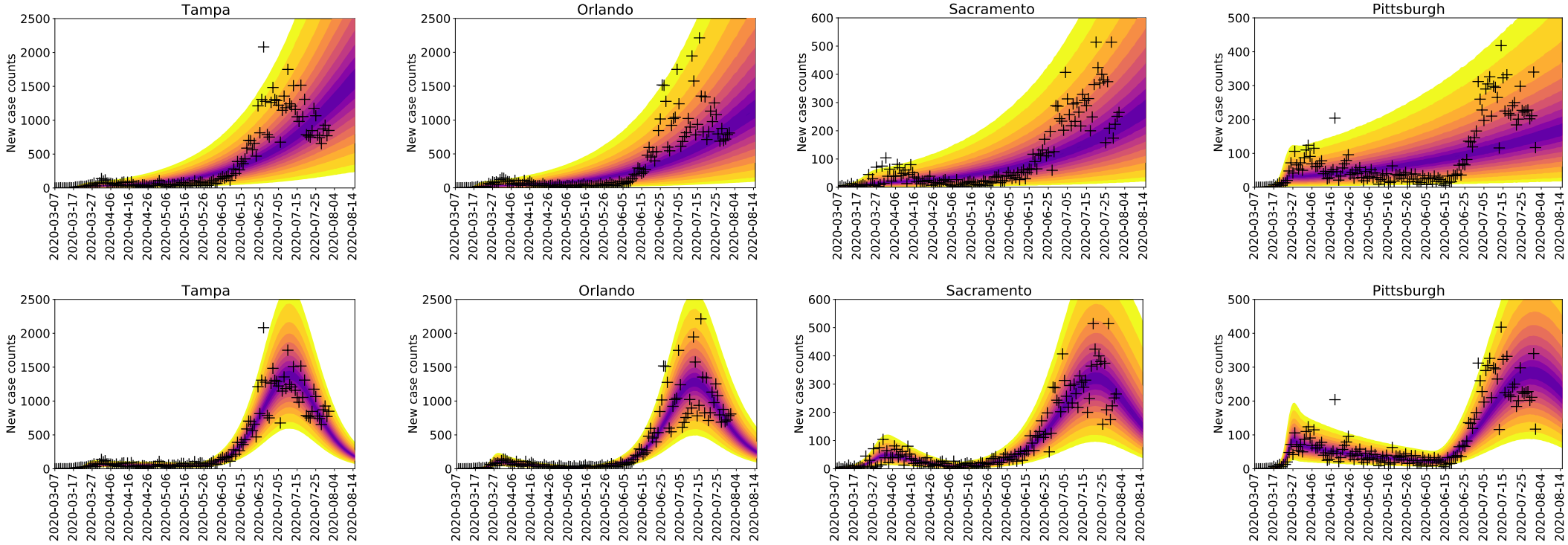

Summary

- In this work, we report the computational/statistical/mathematical modeling methodology we are using to make daily forecasts of new-case detection with rigorous quantification of uncertainty for each of the regional epidemics in the 15 most populous metropolitan areas in the United States.

- Our results
  - justify a modeling focus on cities
  - illustrate early detection of upward trends in new-case detection
  - explain rising-falling-rising epidemic curves because of distinct periods of adherence to social-distancing practices that reduce disease transmission

- Building on this work, I have shown that local COVID-19 epidemics are well-explained by a compartmental model with time-varying social-distancing parameters. The model can predict second-wave dynamics for any of the 384 metropolitan statistical areas in the United States.

References

Lin, Yen Ting, Jacob Neumann, Ely Miller, Richard G. Posner, **Abhishek Mallela**, Cosmin Safta, Jaideep Ray, Gautam Thakur, Supriya Chinthavali, and William S. Hlavacek. "Daily Forecasting of New Cases for Regional Epidemics of Coronavirus Disease 2019 with Bayesian Uncertainty Quantification." In submission, a*Rχiv preprint: arXiv:2007.12523* (2020).

USC University of Southern California

TDDFT Characterization of $CsPbBr_3$ Clusters Optical Properties

CARLOS MORA PEREZ, AMANDA NEUKIRCH, DIBYAJYOTI GHOSH, SERGEI TRETIAK

USC Dornsife
Dana and David Dornsife College of Letters, Arts and Sciences

Motivation

Perovskites most abundant mineral on earth!!

Halide perovskites (ABX_3) for optoelectronic devices

- Hybrid
- All-inorganic

Optoelectronic applications

- Electroluminescence (EL)
- Photoluminescence (PL)
- X-ray
- LEDs

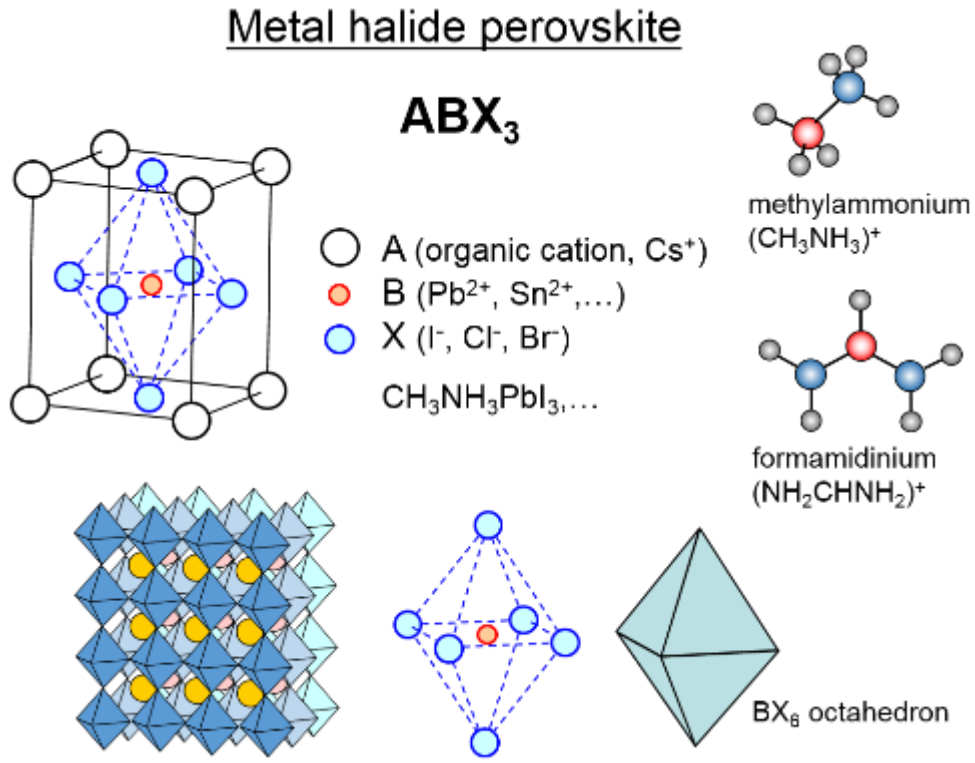

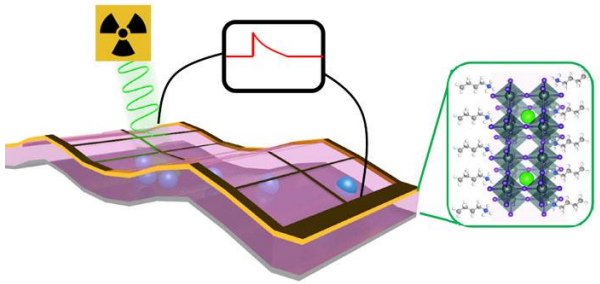

SCIENCE **2017**, *358*, 732-733.
HTTPS://WWW.HELMHOLTZ-BERLIN.DE/FORSCHUNG/OE/EE/SI-PV/ARBEITSGEBIETE/PEROWSKITE/INDEX_EN.HTML
HIGHLY SENSITIVE, SELF-POWERED THIN FILM X-RAY DETECTOR USING 2D LAYERED PEROVSKITE DIODES, SCIENCE ADVANCES, DOI TBD

Why perovskites?

1. Direct gap semiconductor
    1. Easily tunable
    2. Cover Whole visible light range
    3. High PL quantum yield
2. High defect tolerance
3. Cheaper raw materials and equipment
4. Ambipolar Charge Transfer
    1. Can transport both holes and electrons
    2. Better than OLEDs
5. Facile Synthesis
    1. Solution-based methods at low temperature.
    2. VS. all-vacuum thermal evaporation method in OLEDs

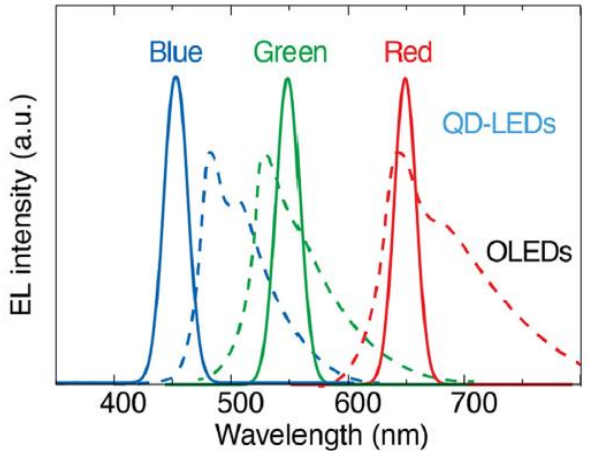

J. PHYS. CHEM. LETT. **2019**, *10*, 3035-3042.
NATURE **2018**, *562*, 245-248.
NATURE **2018**, *562*, 249-253.

$CsPbBr_3$ Cluster

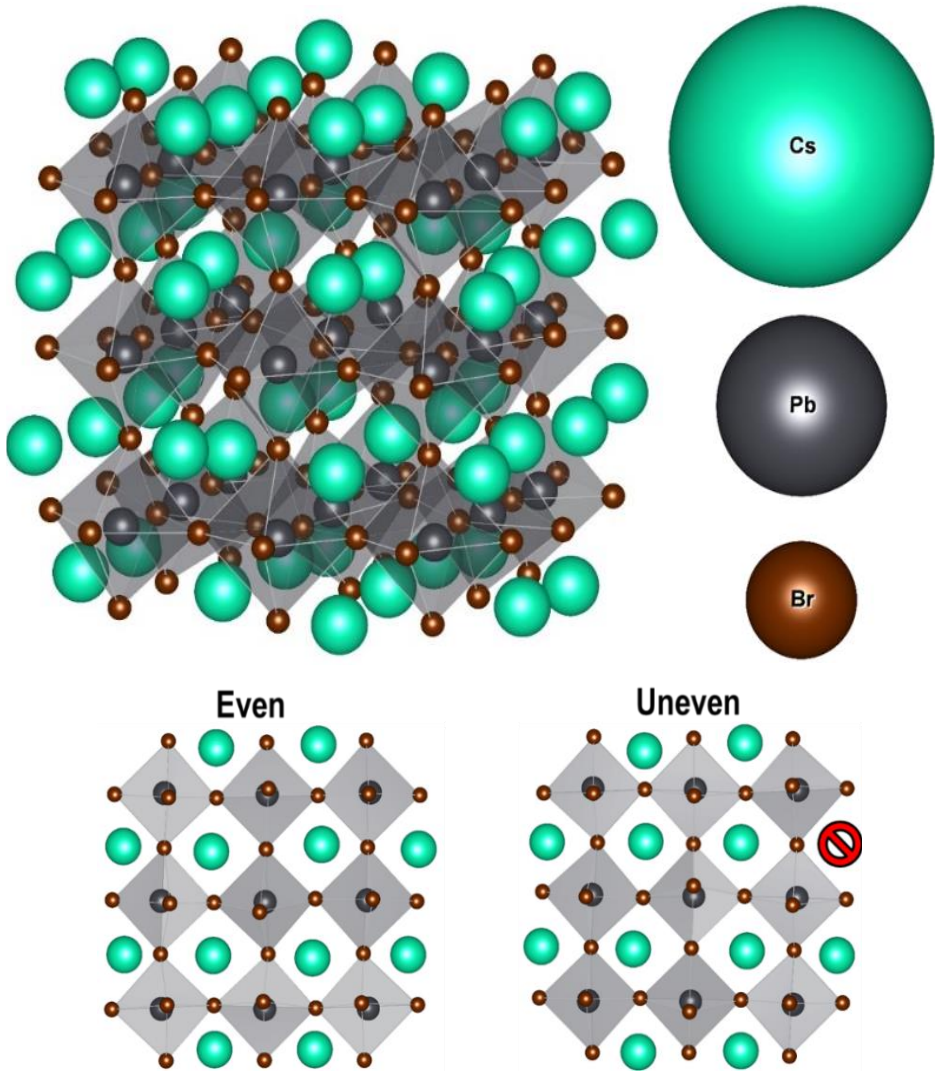

Pristine System

- 189 Atoms
  - $Cs_{54}Pb_{27}Br_{108}$
- Dimension
  - 1.8x1.8 nm
- Unique Surfaces
  - Even
  - Uneven

Computational Methods

- Software: Gaussian16
  - Optimization
  - TDDFT Calculations
- Functional: CAM-B3LYP
- Basis Set: LANL2DZ
- Solvent: Water

Point Defects (low formation energy)

- Br^{-1}
- Pb^{+2}
- Cs^{+1}
- Positive: $[CsPbBr_3]^{+1}$
- Negative:$[CsPbBr_3]^{-1}$

UV-Vis Profile

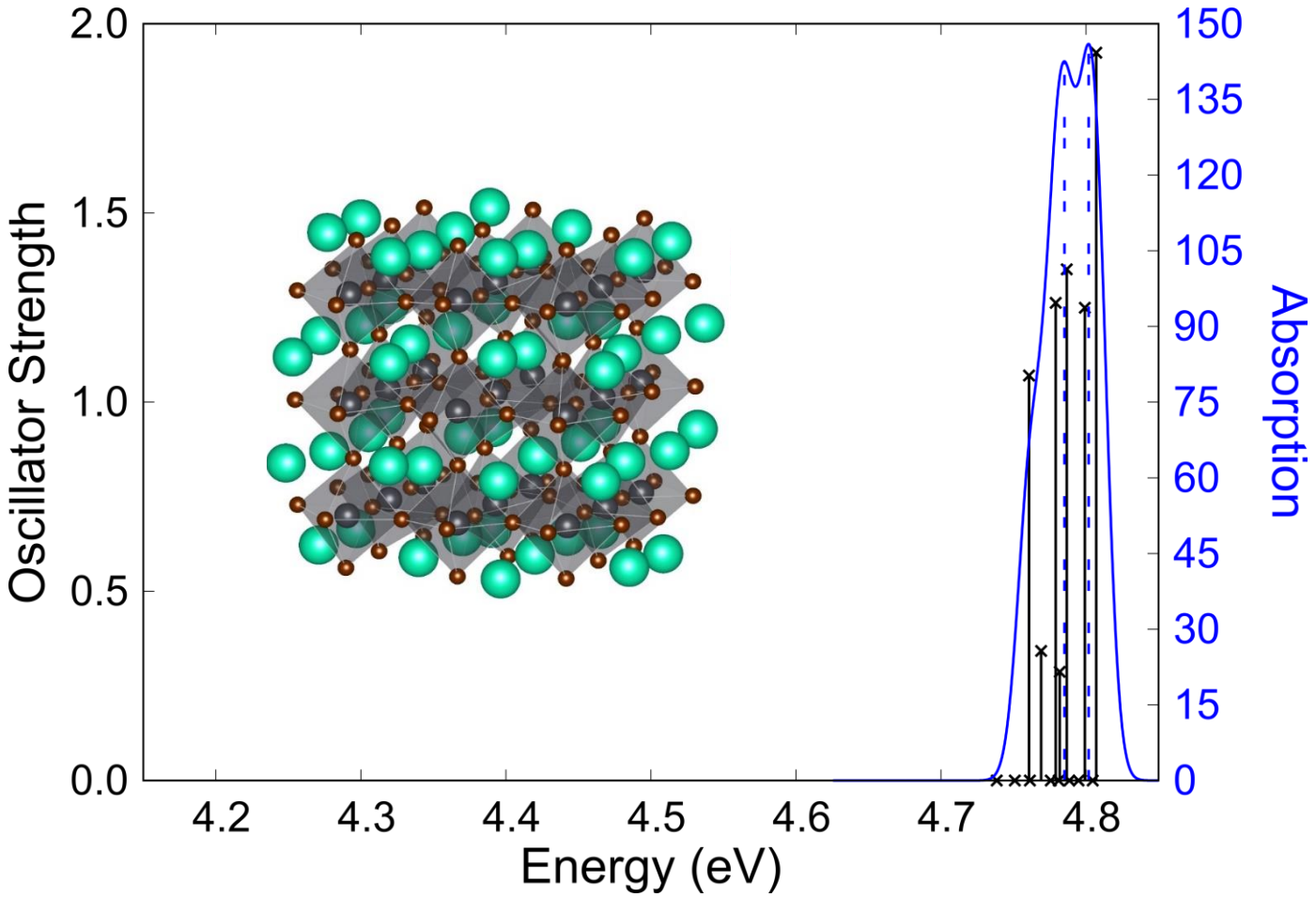

High energy due to small size of cluster

Band peaks at 4.78 and 4.80 eV

Vacancies introduces defects states which lowers energy gap

- ~4.2 eV band peak
- ~0.5 eV red shift

UV-Vis Profile

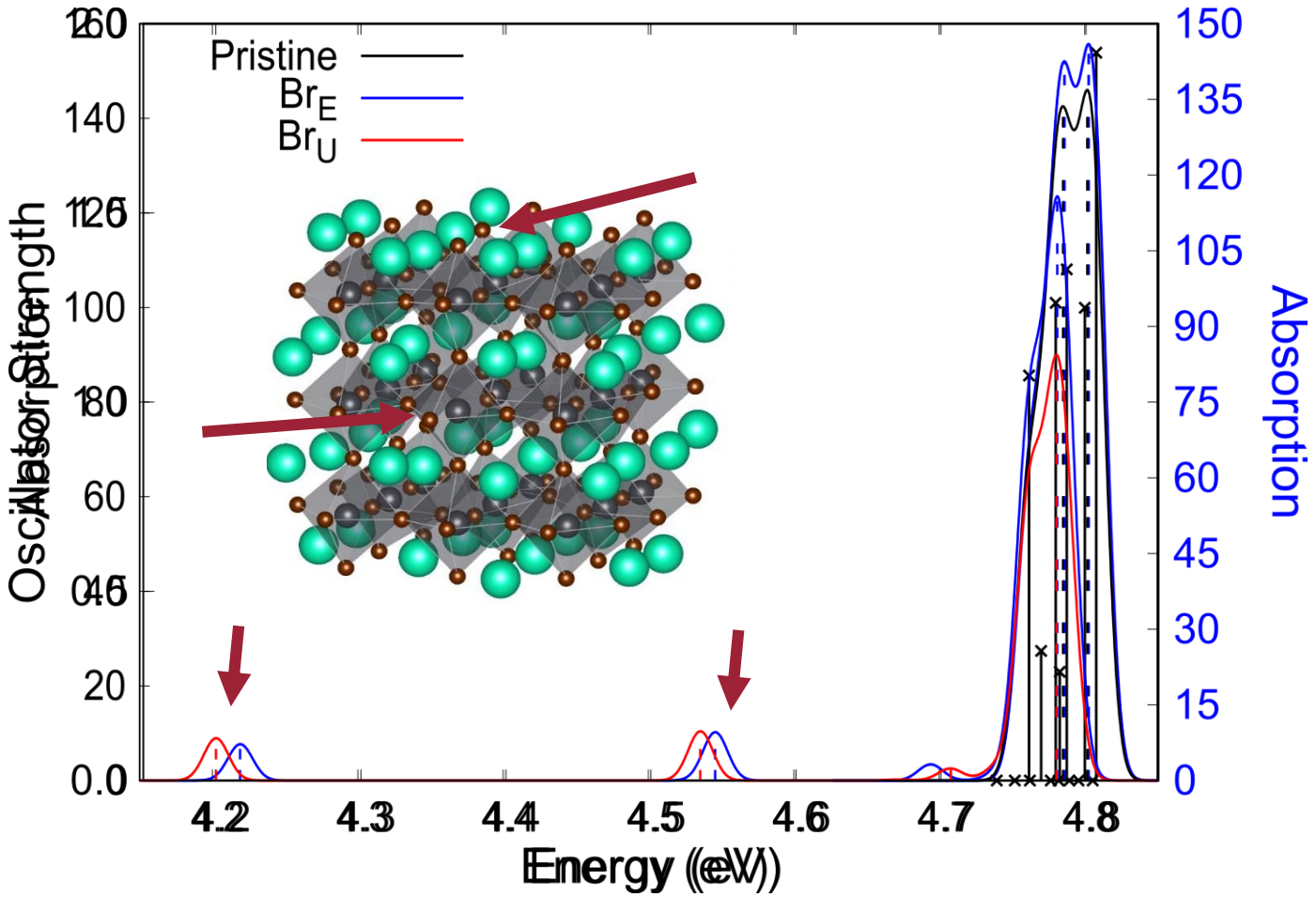

High energy due to small size of cluster

Band peaks at 4.78 and 4.80 eV

Vacancies introduces defects states which lowers energy gap

- ~4.2 eV band peak
- ~0.5 eV red shift

Summary

Vacancies introduce defect states which lowers bandgap

- Leads to lower absorption
- Lower performance devices

Mitigate defects to gain performance

- Halide rich/Cs poor environment
- Surface passivation
  - Ligands
  - Oxygen

Physics based machine learning report card

CONJUGATED HYDROCARBONS

Yamilée Morency
Mentor: Justin Smith

Managed by Triad National Security, LLC for the U.S. Department of Energy's NNSA

BACKGROUND

- Molecular potential energy surfaces are essential to solving problems in physics, chemistry and biology
- Theoretical ab initio methods are not tractable for very large systems
- Machine Learning Potentials (MLPs) provide a faster alternative with little to no loss in accuracy
- MLPs depend on chemical feature representation, quality of the data & ML algorithms
- MLPs have no physical basis
- How well do these models reproduce complex physical phenomena?

Conjugated Hydrocarbons

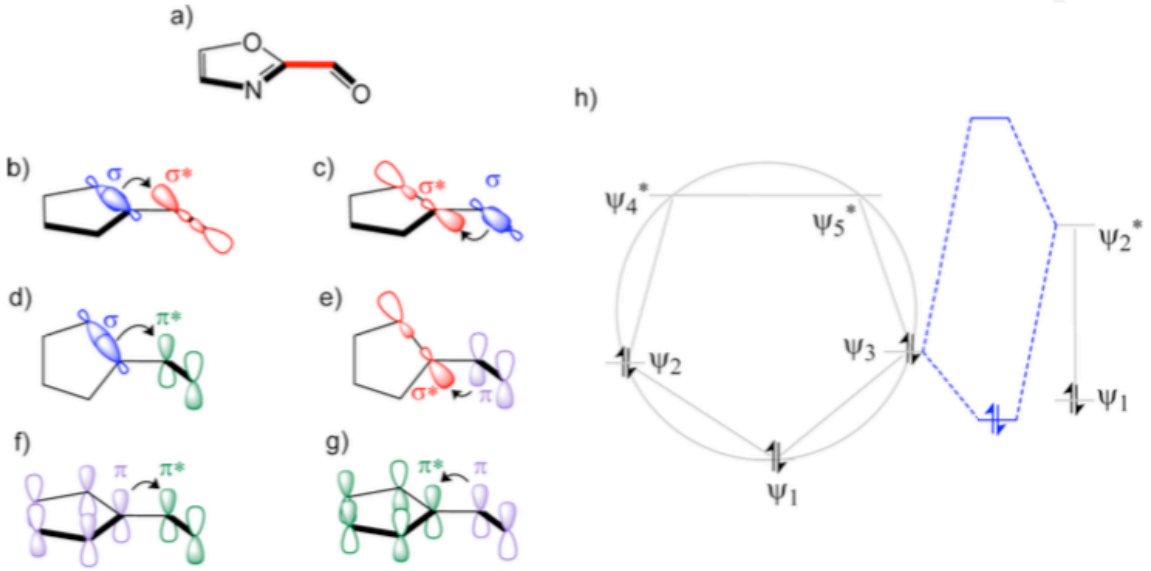

Wei, W., Champion, C., Barigye, S. J., Liu, Z., Labute, P., & Moitessier, N. (2020). Use of Extended-Hückel Descriptors for Rapid and Accurate Predictions of Conjugated Torsional Energy Barriers. *Journal of Chemical Information and Modeling,60*(7), 3534-3545. doi:10.1021/acs.jcim.0c00440

Models & Training data

Data

- All hydrocarbons from GDB13 & GDB17
- All PubChem hydrocarbons w/ up to 20 carbons
- Total 122k hydrocarbons
- Coordinates for molecules in training generated from rdkit & MMFF94 optimized

Model 1 (no Active Learning)

- ANI-1 type model
- Trained with 3.5 k conjugated molecules selected at random from the 122k

Model 2 (Active Learning):

- Active learning sampled from 122k molecules

ANI Functional Form

$$E_T \sum_{i=1}^{\text{Natom}} E_i$$

Heavily modified Behler Parrinello symmetry functions (BPSFs)
BPSFs compute atomic environment vector (AEV)
Each element in an AEV

$$G_m^{A_{\text{mod}}} = 2^{1-\xi} \sum_{i \neq j,k}^{\text{Natom}} \left(1 + \cos\left(\theta_{ijk} - \theta_s\right)\right)^{\xi} e^{-v\left(R_{ij}+R_{ik}+R_s\right)} \text{fc}\left(R_{ij}\right) * f\left(R_{ik}\right)$$

The local AE is achieved with this piecewise cutoff function:

$$f_c(R) = \begin{cases} 0.5 \cos\left(\frac{\pi R_{ij}}{R_c}\right) + 0.5 & \text{for } R_{ij} \leq R_c \\ 0 & \text{for } R_{ij} > R_c \end{cases}$$

The AE cuts off at :
4.6 A for radial symmetry functions
3.1 A for angular symmetry functions

Conjugated Hydrocarbons

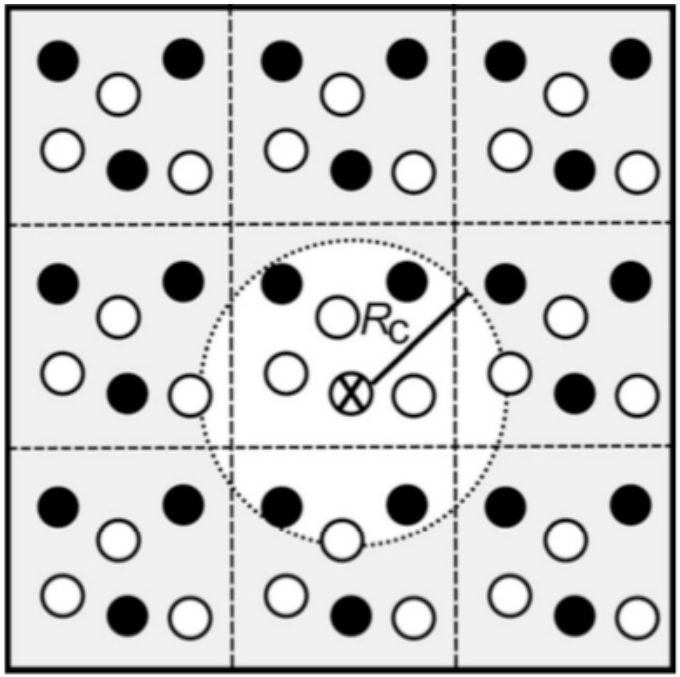

Behler, J. (2015). Constructing high-dimensional neural network potentials: A tutorial review. *International Journal of Quantum Chemistry,115*(16), 1032-1050. doi:10.1002/qua.24890

Conjugated Hydrocarbons

- Alkanes & Alkenes
  - Generated with rdkit from SMILES strings
  - 2 to 32 carbons
  - MMFF94 Optimized
  - Torsion angles frozen at 180°
- Alkynes
  - Generated with rdkit from SMILES strings
  - 2 to 32 carbons
  - MMFF94 Optimized
- Annulenes
  - Generated with rdkit from SMILES strings
  - Up to 20 carbons
  - MMFF94 Optimized
- Conjugation Length
  - Linear Hydrocarbons
  - Increasing conjugation
  - All molecules have 32 Carbons
  - Generated with rdkit from SMILES strings
  - MMFF94 Optimized
  - All molecules have 32 Carbons

Plot information

- Individual Error: difference between predicted and calculated energy
- Individual Error / Sq(N): Individual error divided by the square root of the number of atoms in molecule
- Conjugation Length: Longest length of uninterrupted pi bonds (2 or more)
- Total Conjugation: Sum of all the length of uninterrupted pi bonds

Alkanes

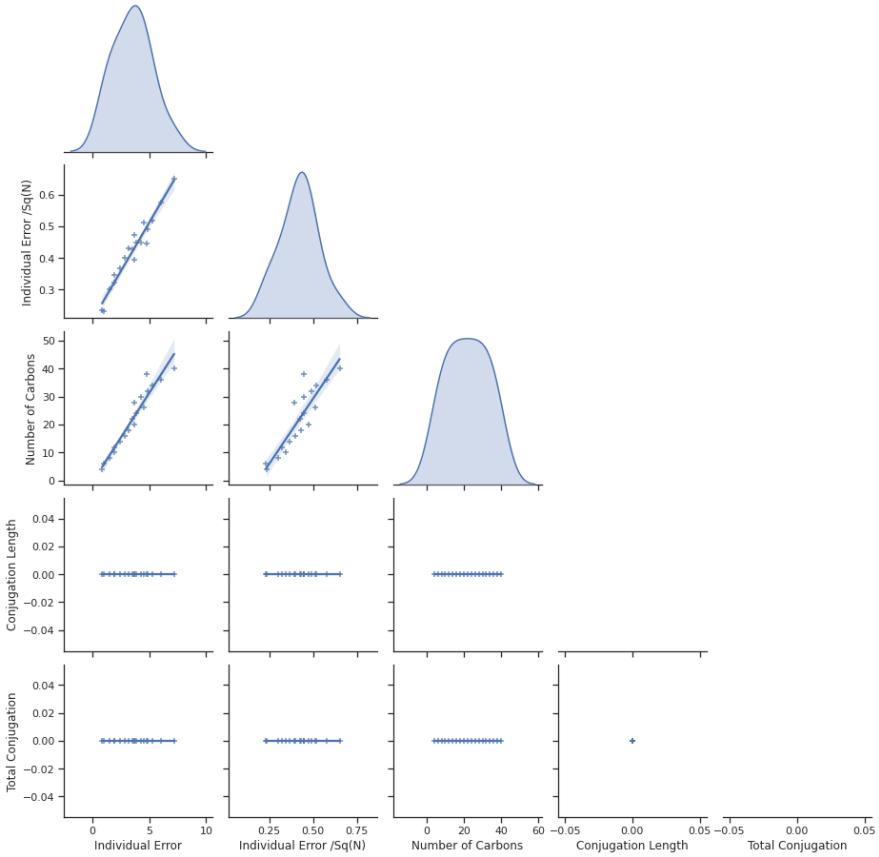
Individual Error /Sq(N)
Number of Carbons
Conjugation Length
Total Conjugation
Individual Error
Individual Error /Sq(N)
Number of Carbons
Conjugation Length
Total Conjugation

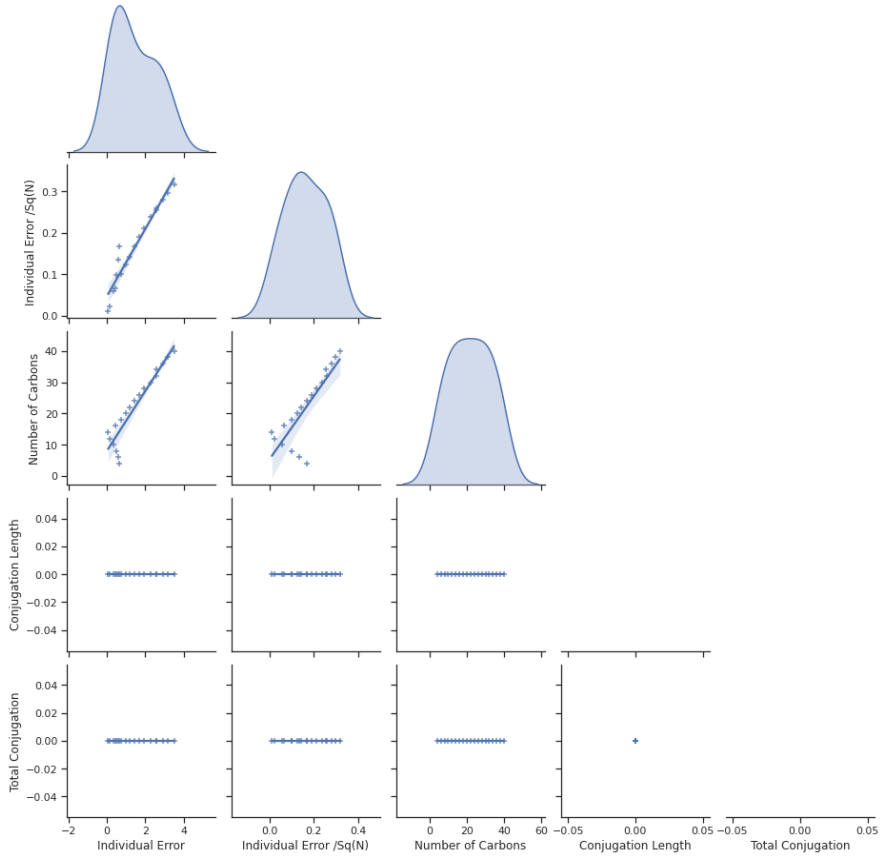
Individual Error /Sq(N)
Number of Carbons
Conjugation Length
Total Conjugation
Individual Error
Individual Error /Sq(N)
Number of Carbons
Conjugation Length
Total Conjugation

Alkenes

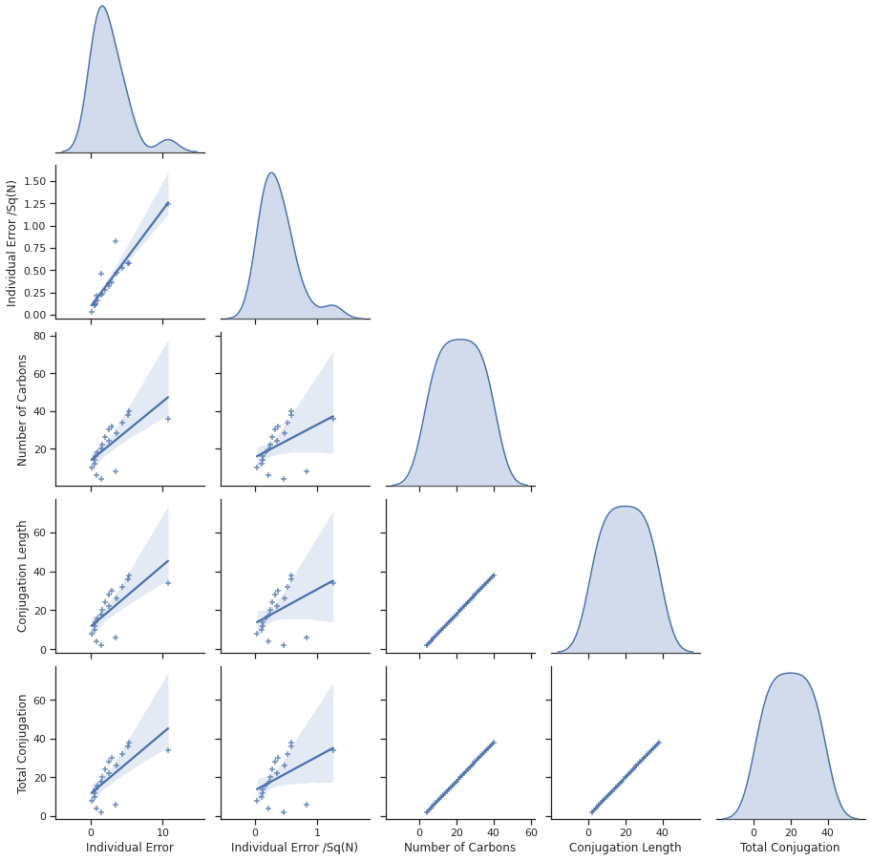
Individual Error /Sq(N)
Number of Carbons
Conjugation Length
Total Conjugation
Individual Error
Individual Error /Sq(N)
Number of Carbons
Conjugation Length
Total Conjugation

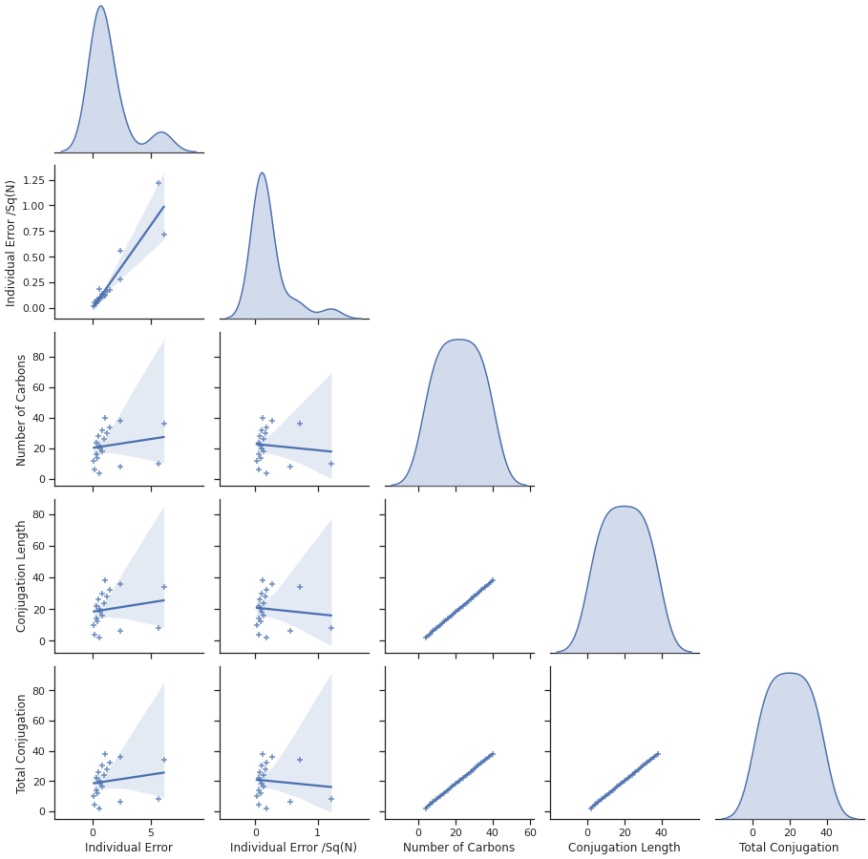
Individual Error /Sq(N)
Number of Carbons
Conjugation Length
Total Conjugation
Individual Error
Individual Error /Sq(N)
Number of Carbons
Conjugation Length
Total Conjugation

Alkynes

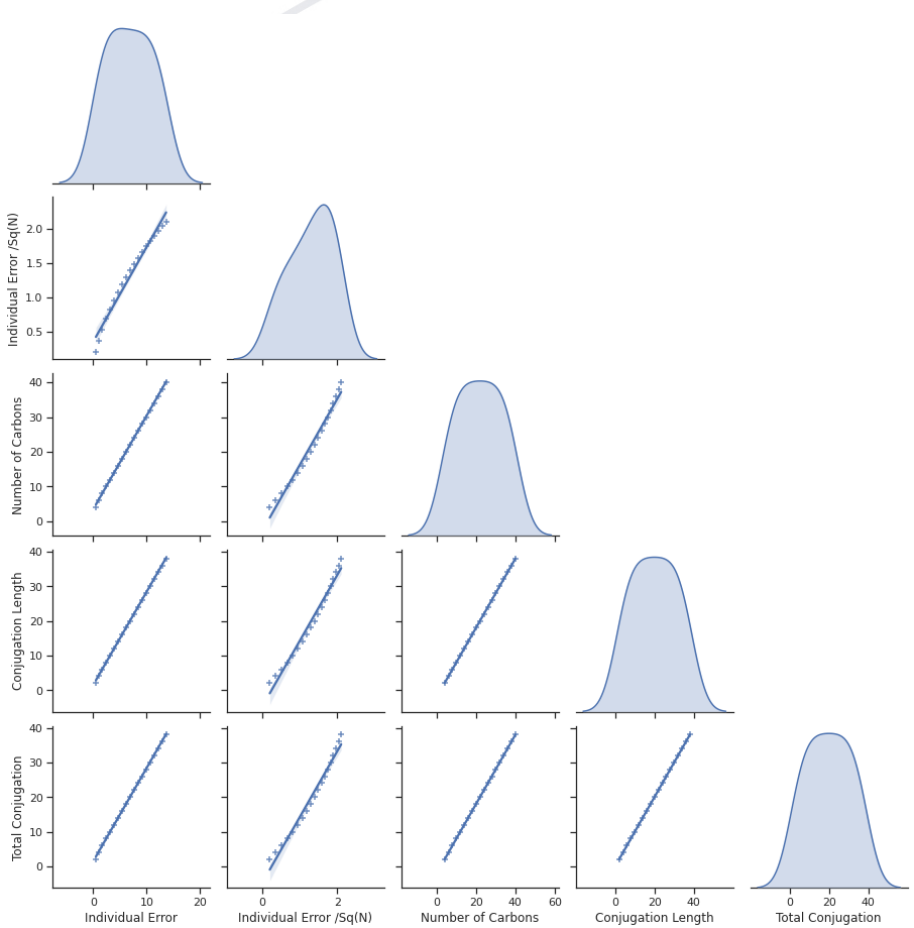
Individual Error /Sq(N)
Number of Carbons
Conjugation Length
Total Conjugation
Individual Error
Individual Error /Sq(N)
Number of Carbons
Conjugation Length
Total Conjugation

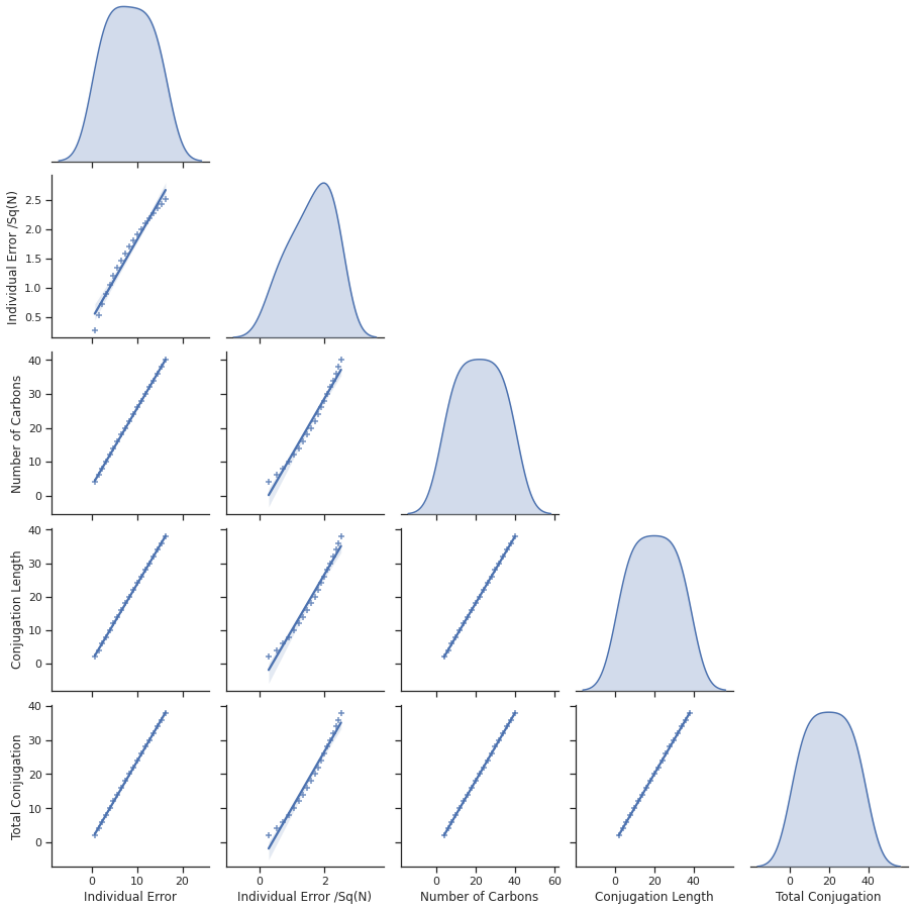
Individual Error /Sq(N)
Number of Carbons
Conjugation Length
Total Conjugation
Individual Error
Individual Error /Sq(N)
Number of Carbons
Conjugation Length
Total Conjugation

Annulenes

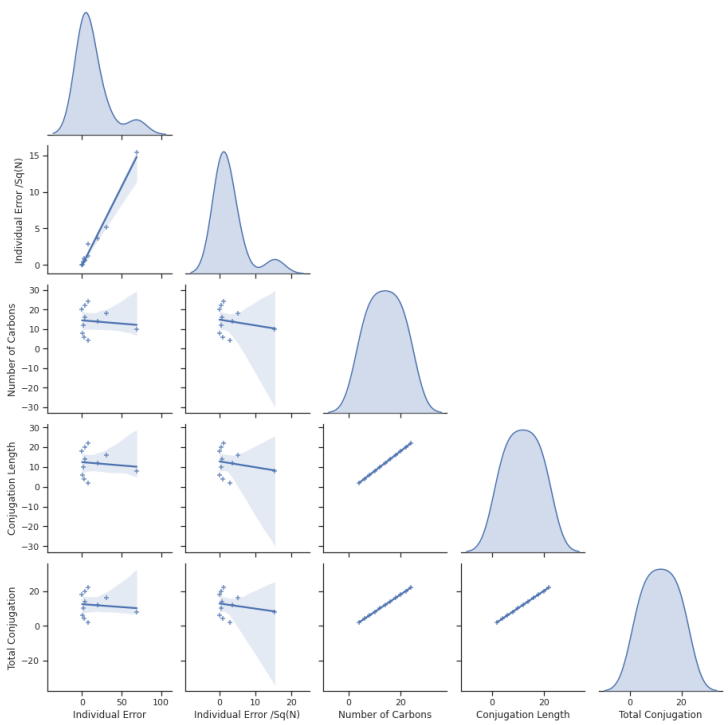
Individual Error /Sq(N)
Number of Carbons
Conjugation Length
Total Conjugation
Individual Error
Individual Error /Sq(N)
Number of Carbons
Conjugation Length
Total Conjugation

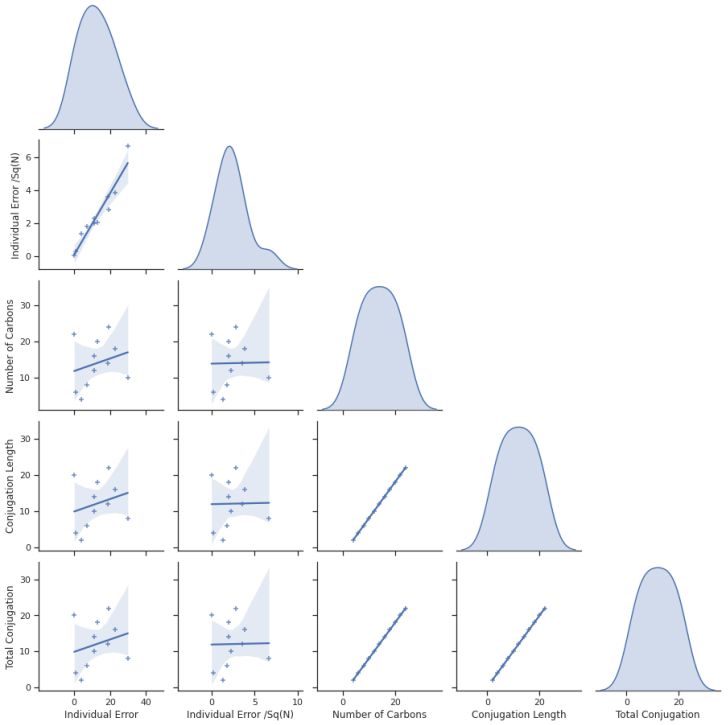
Individual Error /Sq(N)
Number of Carbons
Conjugation Length
Total Conjugation
Individual Error
Individual Error /Sq(N)
Number of Carbons
Conjugation Length
Total Conjugation

Conjugation Length

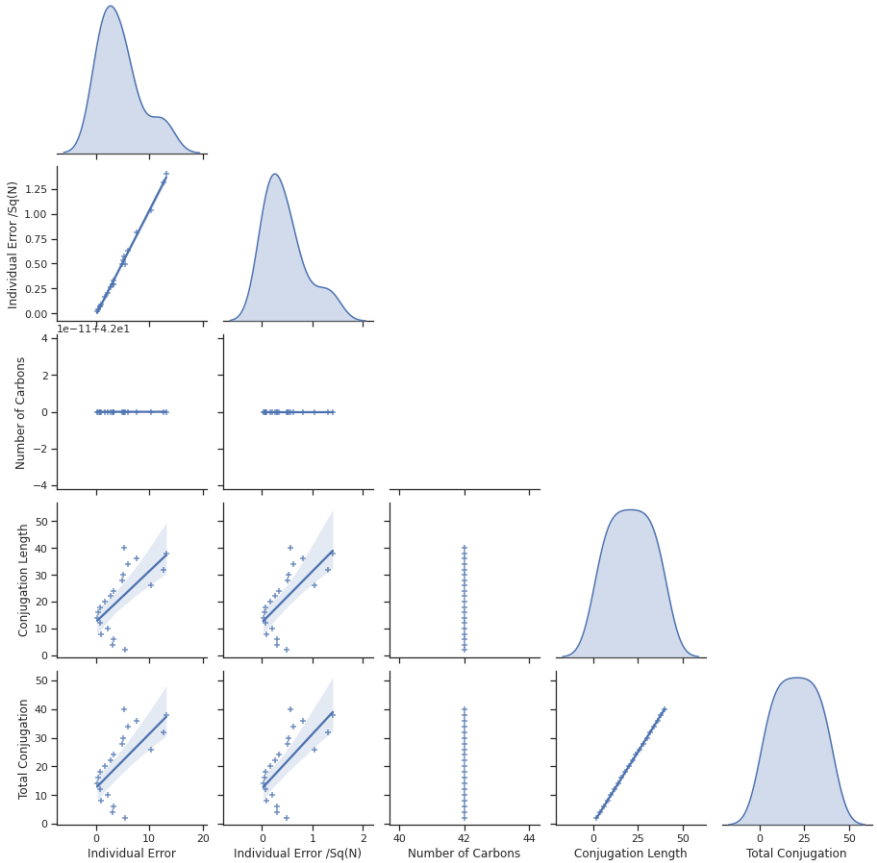

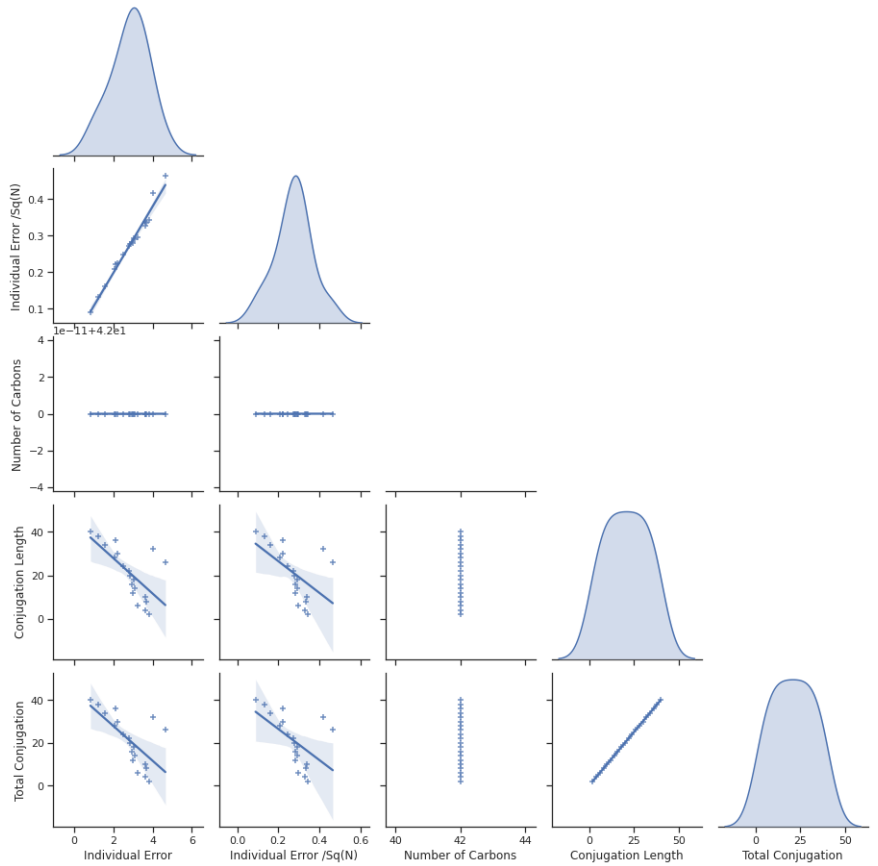

Model 1 vs Model 2

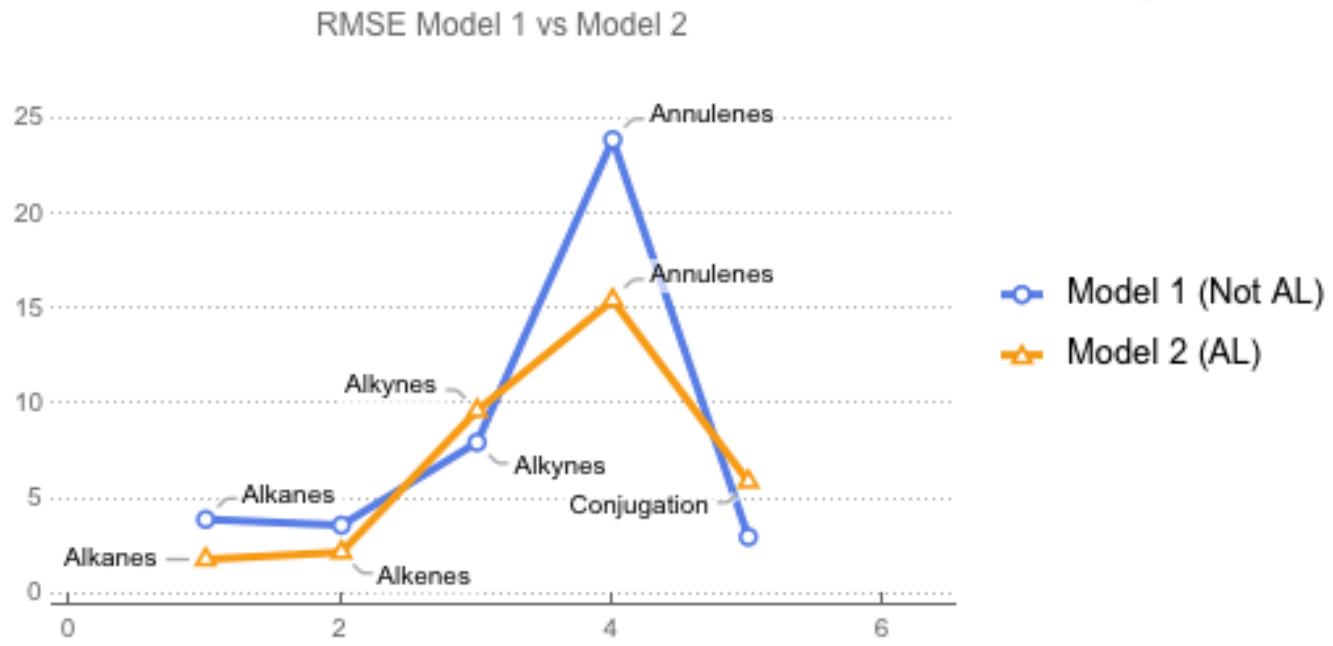

Moving forward

- Add more tests to conjugated hydrocarbons
- Increase training set to improve model
- Active learning to improve model
- Qualitative test

Lightning Talks

Nonparametric estimation in a generalized SEIR model

Amanda Patrick, MS

Mentors: Nick Hengartner, PhD and Imelda Trejo, PhD

August 4, 2020

Theoretical Biology and Biophysics

Los Alamos NATIONAL LABORATORY EST. 1943

Compartmental Modeling for Infectious Diseases

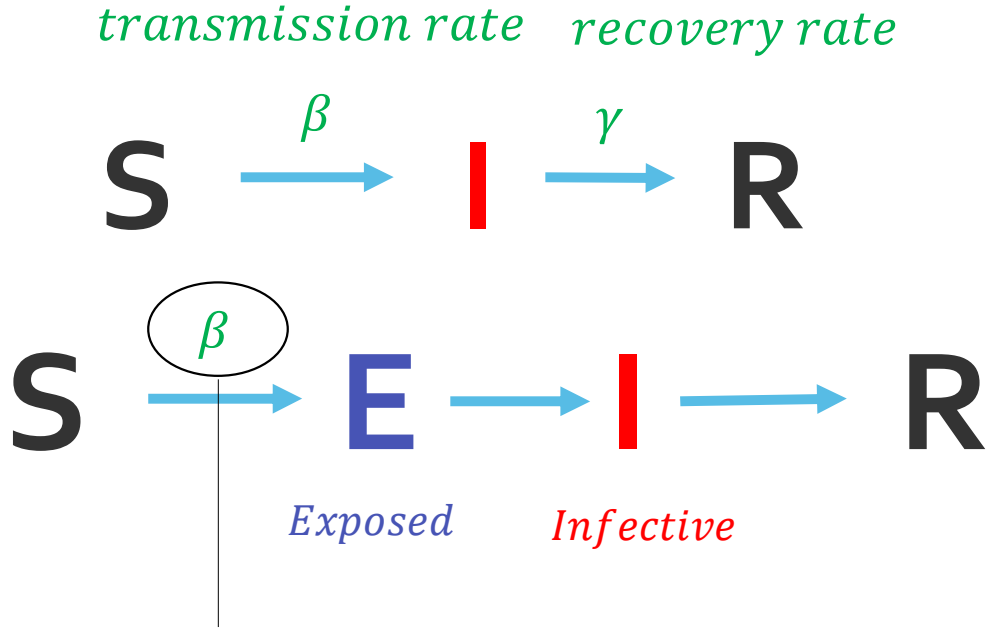

Force of infection: *Per person rate a which a susceptible person will contract the disease*

$$\frac{dS}{\mathrm{dt}} = -\beta IS$$

$$Force\ of\ infection\ = \beta I$$

Explanation

Random Variables:

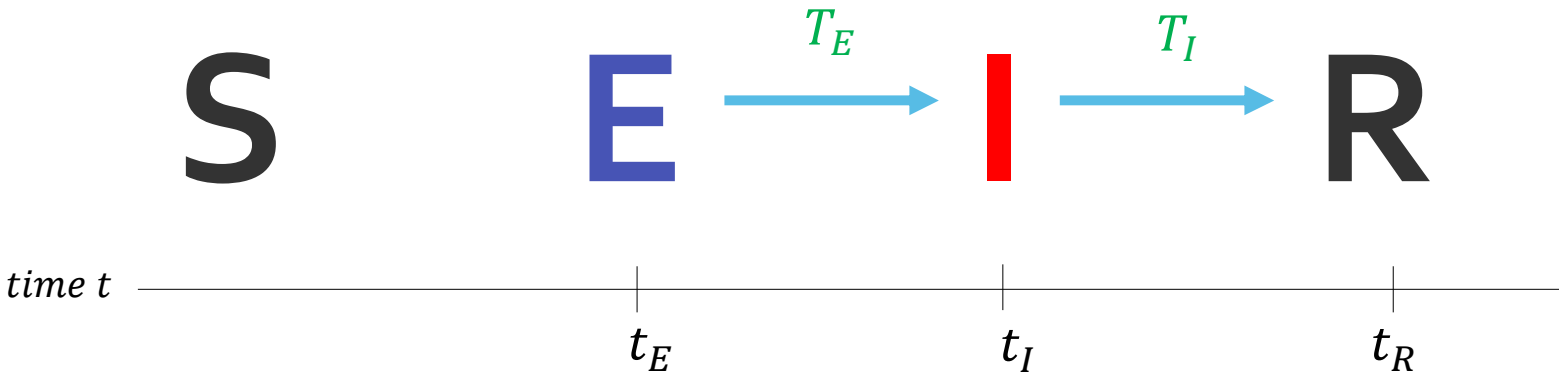

Incoming Infected per time $-S'(t) = \boldsymbol{\rho}(\boldsymbol{t})I(t)$

$\rho(t)$: *per capita rate at which an infective will transmit the disease*

Generalized SEIR Model

Set of integral-differential equations

$$S'(t) = -\boldsymbol{\rho(t)} I(t)$$

$$E(t) = \int_0^t -S'(w)\big(1 - G(t-w)\big)dw + \big(1 - G(t)\big)E_0$$

$$I(t) = \int_0^t \nu(w)\big(1 - F(t-w)\big)dw + \big(1 - F(t)\big)I_0 + G(t)E_0$$

$$R(t) = \int_0^t \nu(w)\, F(t-w)dw + R_0 + F(t)I_0$$

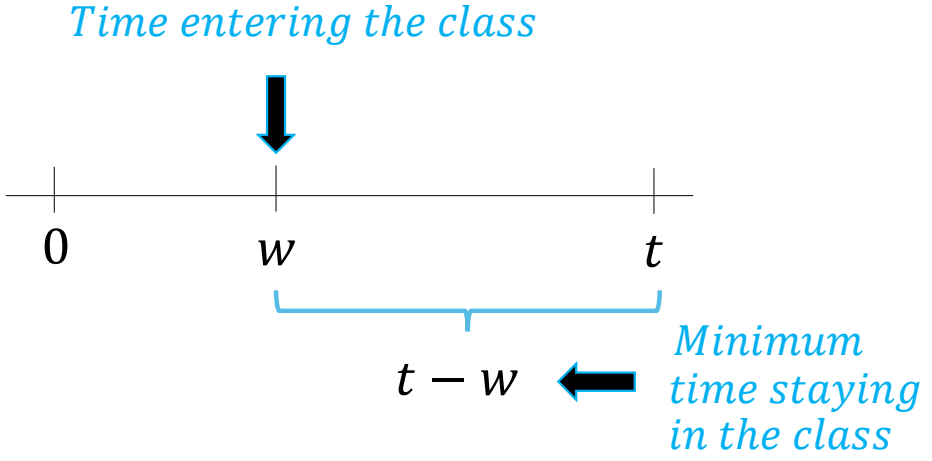

$G(t)$: CDF of Exposure time

$F(t)$: CDF of time spent in I Class

$$\nu(t) = \int_0^t -S'(w)g(t-w)dw: \ \textit{Incoming Infective per time}$$

Two Equations for the Infective Class

Rate coming into the I class

$$I(t) = \int_0^t \nu(w)\big(1 - F(t-w)\big)dw + \big(1 - F(t)\big)I_0 + G(t)E_0$$

$P(T_I > t - w)$

From Model

Rate coming into the E class

$$= \int_0^t -S'(w)\psi(t-w)dw + \big(1 - F(t)\big)I_0 + G(t)E_0,$$

$P(T_E + T_I > t - w)$

Another Interpretation

$$= \int_0^t \rho(w)I(w)\psi(t-w)dw + \big(1 - F(t)\big)I_0 + G(t)E_0$$

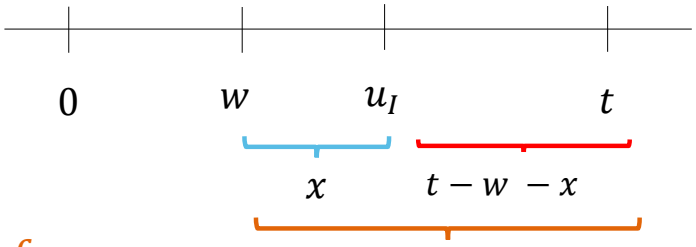

$$\psi(t) = \int_0^t \big(1 - F(t-v)\big)g(v)dv$$

Minimum time for total time in E and I class ➡ $t - w$

Two Equations for the Infective Class

$$I(t) = \int_0^t \boldsymbol{\nu(w)}\big(\mathbf{1} - \boldsymbol{F(t-w)}\big)dw \; + \big(1 - F(t)\big)I_0 \; + G(t)E_0$$

⬅ **Can be used to get estimation for I(t)**

$$I(t) = \int_0^t \boldsymbol{\rho(w)I(w)\psi(t-w)}dw \; + \big(1 - F(t)\big)I_0 \; + G(t)E_0$$

⬅ ***Volterra equation of the second type***

Use to estimate $\boldsymbol{\rho(t)}$

Using 1st interpretation of I(t)

Rate coming into the I class

$$I(t) = \int_0^t \boldsymbol{\nu(w)}\big(\mathbf{1} - \boldsymbol{F(t-w)}\big)dw \; + \big(1 - F(t)\big)I_0 \; + G(t)E_0$$

⬅ **Can be used to get estimation for I(t)**

$\{\boldsymbol{Y_k}\}_{\boldsymbol{k}}$: *Cumulative number of individuals entering the I class on the interval* $(t_{k-1}, t_k]$

$\boldsymbol{E[Y_k]} = \int_{t_{k-1}}^{t_k} \boldsymbol{\nu(w)dw}$: *Expected number of people per time entering the the I class on the interval* $(t_{k-1}, t_k]$

Let $s_\tau \in (t_{k-1}, t_k]$

Estimation for I(t): $$\hat{\boldsymbol{I}}(\boldsymbol{s_\tau}) = \sum_{\boldsymbol{j}:\boldsymbol{t_j} \le \boldsymbol{s_\tau}} \frac{\boldsymbol{Y_j}}{\boldsymbol{t_j - t_{j-1}}} \int_{\boldsymbol{t_{j-1}}}^{\boldsymbol{t_j}} \big(\mathbf{1} - \boldsymbol{F(t-w)}\big)\boldsymbol{dw} + \frac{\boldsymbol{Y_k}}{\boldsymbol{t_k - t_{k-1}}} \int_{\boldsymbol{t_{k-1}}}^{\boldsymbol{s_\tau}} \big(\mathbf{1} - \boldsymbol{F(t-w)}\big)\boldsymbol{dw}$$

Using 2nd Interpretation of I(t)

$$I(t) = \int_0^t \boldsymbol{\rho(w)I(w)\psi(t-w)}dw \; + \big(1 - F(t)\big)I_0 \; + G(t)E_0$$

Volterra equation of the second type

Trapezoidal Method

$$I(s_k) = \frac{\delta}{2}\left[I(0)\rho(0)\psi(s_k) + 2\sum_{j=1}^{k-1} I(s_j)\rho(s_j)\psi(s_k - s_j) + I(s_k)\rho(s_k)\psi(s_0)\right] + \big(1 - F(t_k)\big)I_0 \; + G(t_k)E_0$$

Linear in elements of ρ

$$\delta = s_j - s_{j-1}$$

$$\vec{I} = H\vec{\rho} \; + \vec{v}, \qquad \vec{v} = \overrightarrow{1 - F}\, I_0 + \vec{G}\, E_0$$

Constraints

Use estimation for I: $\hat{I}$

$$\hat{\boldsymbol{I}} = H\vec{\rho} + \vec{v}, \qquad \vec{v} = \overrightarrow{1 - F}\, I_0 + \vec{G}\, E_0$$

$$\begin{aligned} H_{i0} &= \frac{\delta}{2}\hat{\boldsymbol{I}}(s_0)\psi(s_i) \\ H_{ij} &= \delta\hat{\boldsymbol{I}}(s_j)\psi(s_i - s_j), \qquad j < i \\ H_{ii} &= \frac{\delta}{2}\hat{\boldsymbol{I}}(s_i)\psi(s_0) \\ H_{ij} &= 0, \qquad j \geq i \end{aligned}$$

Another Linear Relationship

$\boldsymbol{E[Y_k] = \int_{t_{k-1}}^{t_k} \nu(w)dw}$:

Expected number of people per time entering the I class on the interval $(t_{k-1}, t_k]$

$$= \int_{t_{k-1}}^{t_k} \nu(w)dw$$

$$= \int_{t_{k-1}}^{t_k} \int_{t_0}^{w} S'(u)g(w-u)du\ dw$$

$$= \int_{t_{k-1}}^{t_k} \rho(u)I(u) \int_{\max(u,t_{k-1})}^{t_k} g(w-u)du\ dw\,, \qquad \forall u \in [0, t_k]$$

$$R_k(u) = G(t_k - u) - G(\max(t_{k-1}, u) - u)$$

Trapezoidal Method

$$E[Y_k] = \frac{\delta}{2}\left[\rho(0)I(0)R_k(0) + 2\sum_{i=1}^{\frac{k}{\delta}-\delta} \rho(s_i)I(s_i)R_k(s_i) + \rho\left(\tfrac{s_k}{\delta}\right)I\left(\tfrac{s_k}{\delta}\right)R_k\left(\tfrac{s_k}{\delta}\right)\right]$$

$$\vec{Y} = M\,\vec{\rho}$$

Optimization Problem

$$\vec{Y} = M\,\vec{\rho}$$

Regularization with the 2nd difference matrix to control smoothness

$$D_{ij} = \begin{cases} 1 & |\,i-j| = 1 \\ -2 & i = j \\ 0 & otherwise \end{cases}$$

$$\hat{\boldsymbol{I}} = H\vec{\rho} + \vec{v}, \qquad \vec{v} = \overrightarrow{1-F}\,I_0 + \vec{G}\,E_0$$

Questions?

Comparing RDX and HMX reduced chemistry models applied to 1-D hot spot simulations

Michael N. Sakano*, Alejandro Strachan*, Edward M. Kober†
*School of Materials Engineering and Birck Nanotechnology Center, Purdue University
†T-1 Division, Los Alamos National Laboratory

Funding provided by High Explosives Grand Challenge
08/19/2020

Complex chemical initiation coupled across scales

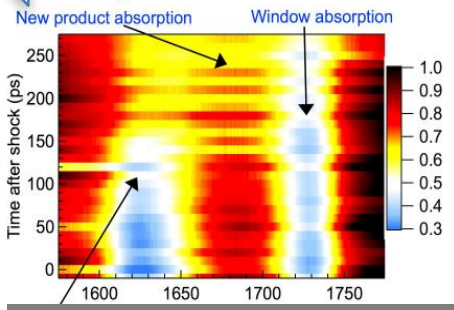

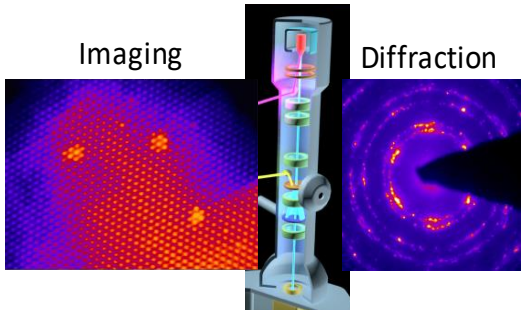

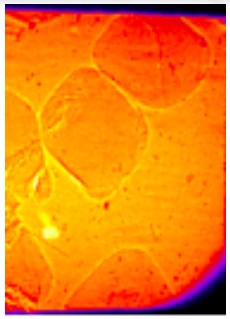

Laser shocks | Laser heating | Vibrations | Kolsky bar | Gas gun

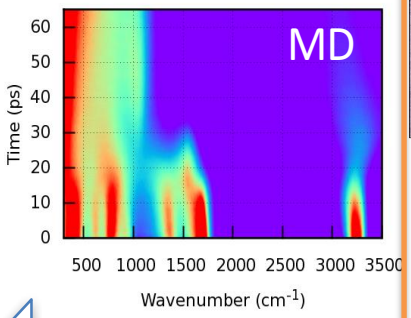

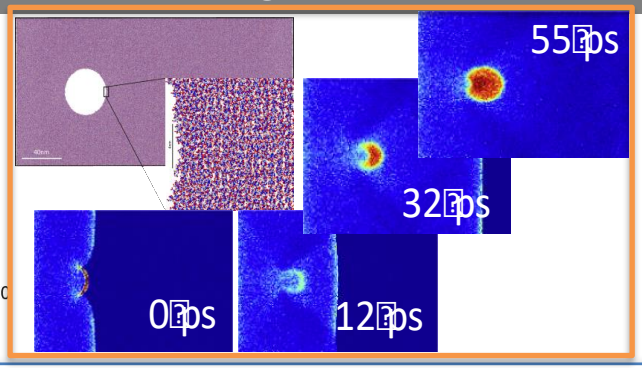

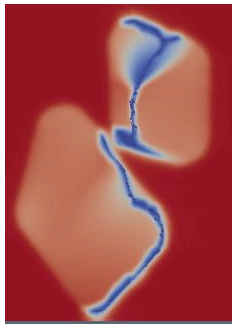

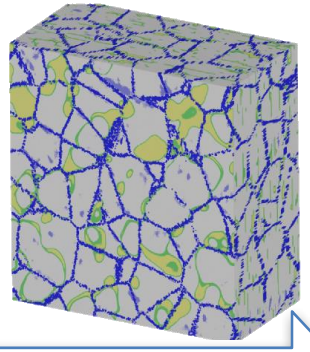

ONR MURI Topic 21 – Purdue, Stanford, LANL – PI: Strachan
PCP@Xtreme - Predictive Chemistry & Physics at Extreme Temperature and Pressure

Discrepancies in initiating single crystal HMX

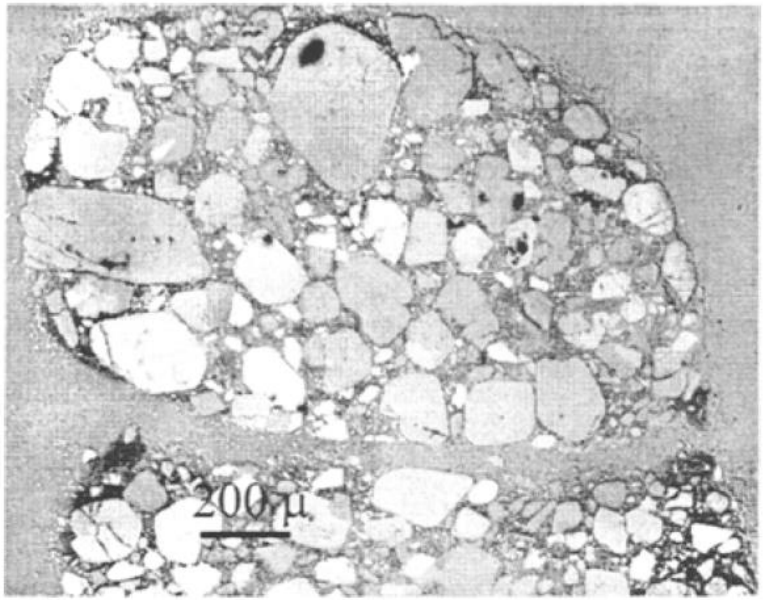

PBX 9501 Molding Powder

Flyer plate

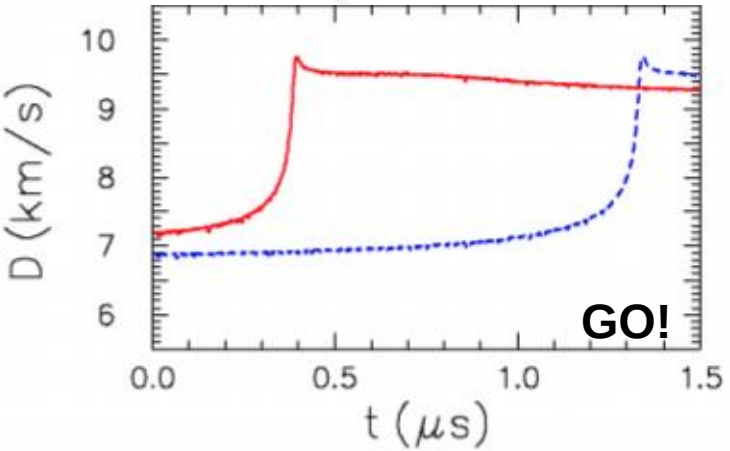

PBX 9404 detonation wave

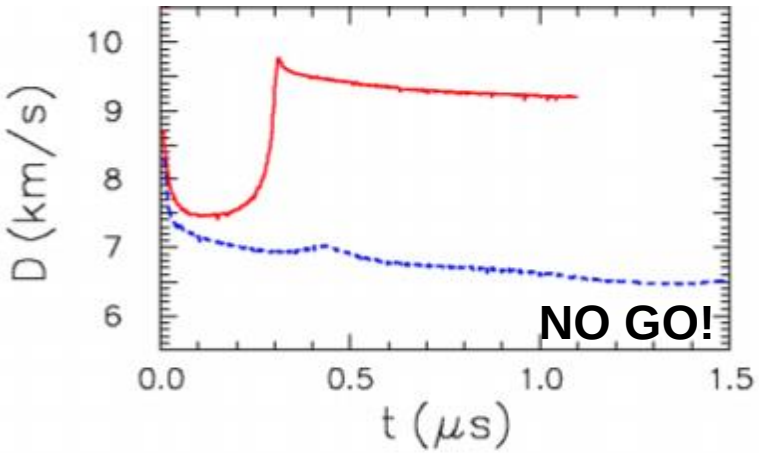

Skidmore, C. B.; Phillips, D. S.; Son, S. F.; Asay, B. W. Characterization of HMX Particles in PBX 9501. *AIP Conf. Proc.* **1998**, *429* (1), 579–582. https://doi.org/10.1063/1.55666.
Menikoff, R. Micro-gap Experiments and Insensitive Explosives. *AIP Conf. Proc.* **2007**, *955* (1), 967–970. https://doi.org/10.1063/1.2833290.

Gaps/voids/pores can increase sensitivity of PBXs

Jetting leads to critical hot spots

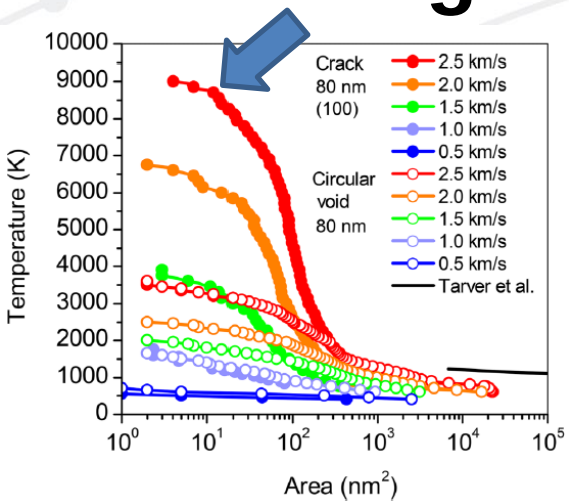

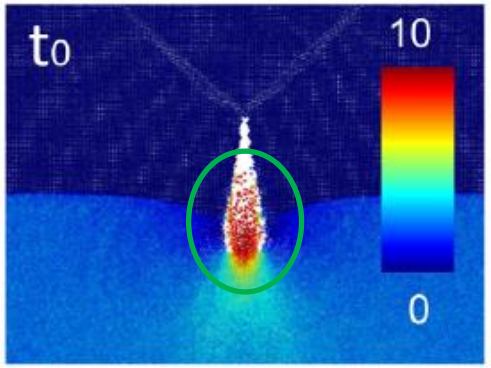

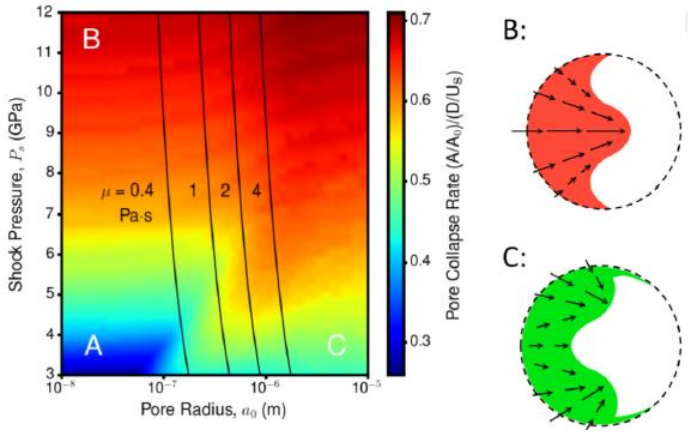

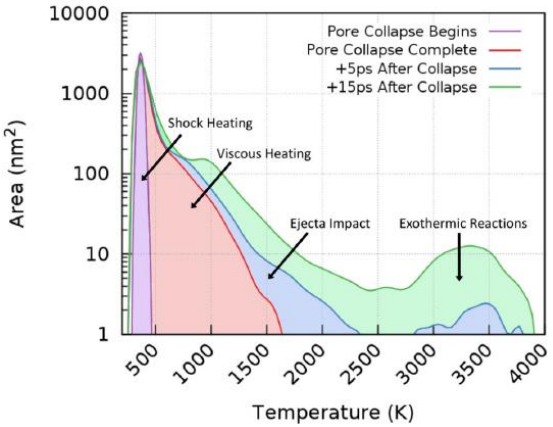

Li, C.; Hamilton, B. W.; Strachan, A. Hotspot Formation Due to Shock-Induced Pore Collapse in 1,3,5,7-Tetranitro-1,3,5,7-Tetrazoctane (HMX): Role of Pore Shape and Shock Strength in Collapse Mechanism and Temperature. *J. Appl. Phys.* **2020**, *127* (17), 175902. https://doi.org/10.1063/5.0005872.

Wood, M. A.; Kittell, D. E.; Yarrington, C. D.; Thompson, A. P. Multiscale Modeling of Shock Wave Localization in Porous Energetic Material. *Phys. Rev. B* **2018**, *97* (1), 014109. https://doi.org/10.1103/PhysRevB.97.014109.

Hot spot model of detonation

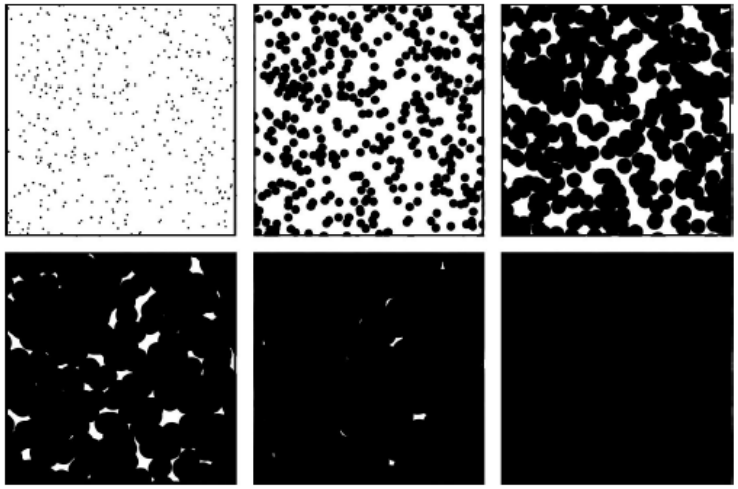

FIGURE 1. 2D rendering of the standard SHSM.

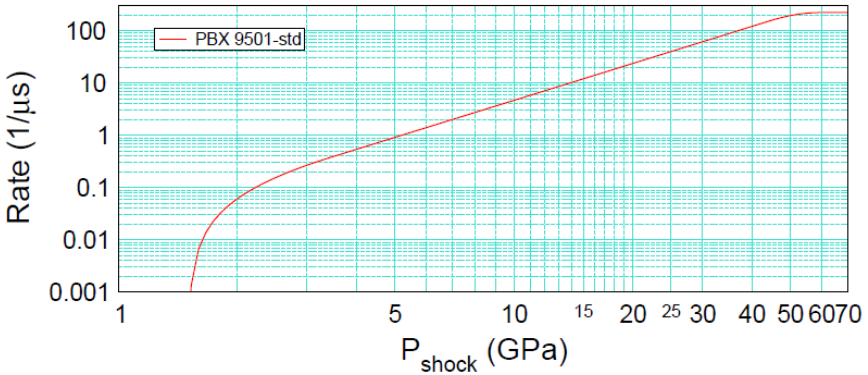

Figure 3: SURF burn rate for PBX 9501.

SURF parameters

p_{scale}	1 GPa
t_{scale}	1 μs
P_0	1.5
P_{low}	3.5
P_1	45.
P_{hi}	60.
C	0.0208
f_n	2.35
n	1.0
n_{hi}	0.0
P_{burn}	35.

Critical parameters:

1) Number, size and distribution of initial hot spots
2) Growth (deflagration) rate of hot spots vs local conditions

Hill, L. G. The Shock-Triggered Statistical Hot Spot Model. *AIP Conf. Proc.* **2012**, *1426* (1), 307–310. https://doi.org/10.1063/1.3686280.

Menikoff, R. Effect of Heterogeneities on the Reaction-zone Profile of a Propagating Detonation Wave. *LA-UR-20-24842.* **2020**.

Focus on deflagration rate versus temperature and pressure

Experimental measurements of deflagration rates

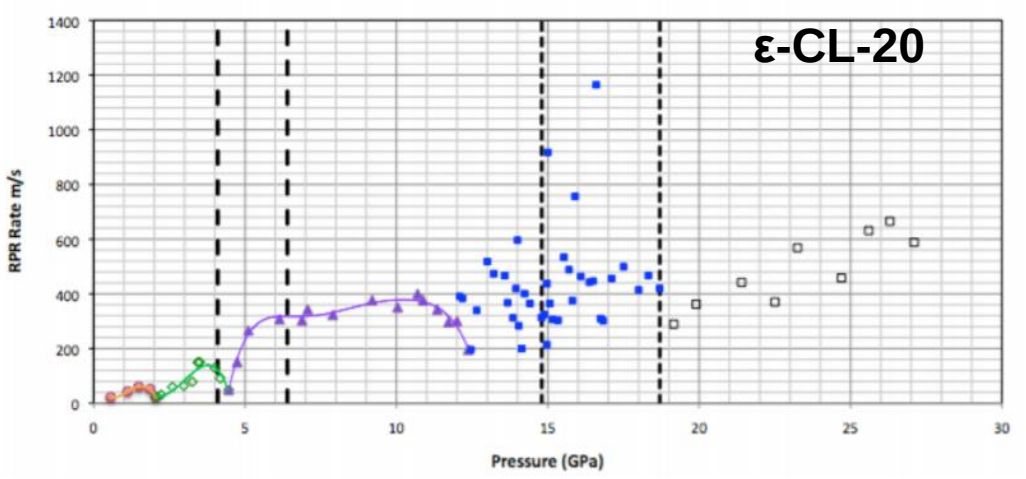

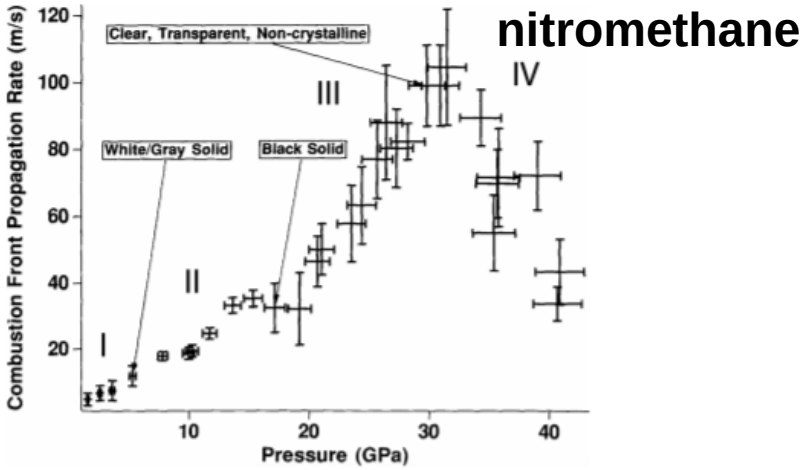

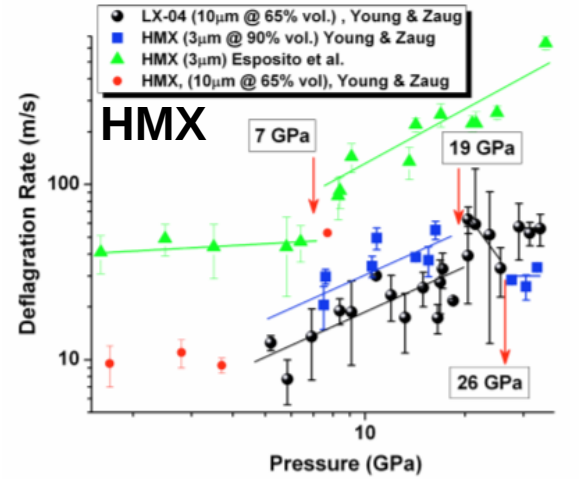

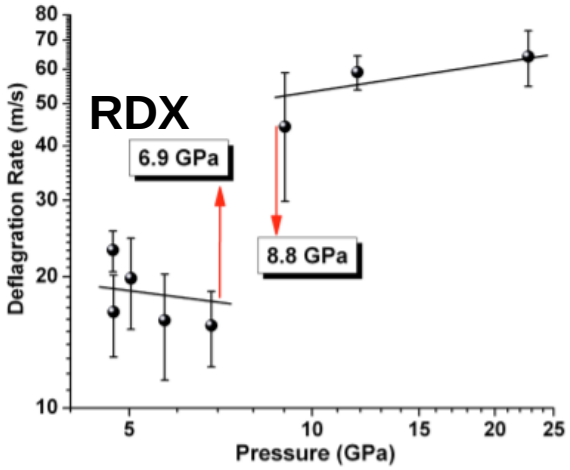

Zaug, J. M.; Young, C. E.; Long, G. T.; Maienschein, J. L.; Glascoe, E. A.; Hansen, D. W.; Wardell, J. F.; Black, C. K.; Sykora, G. B. Deflagration Rates of Secondary Explosives under Static Mpa—Gpa Pressure. *AIP Conf. Proc.* **2009**, *1195* (1), 420–423. https://doi.org/10.1063/1.3295162.

Zaug, J. M.; Foltz, M. F.; Hart, E. *Deflagration Rates and Molecular Bonding Trends of Statically Compressed Secondary Explosives*; LLNL-PROC-425270; **2010**.

Difficult to determine reaction deflagration rate from experiments

Deflagration wave from hot spot

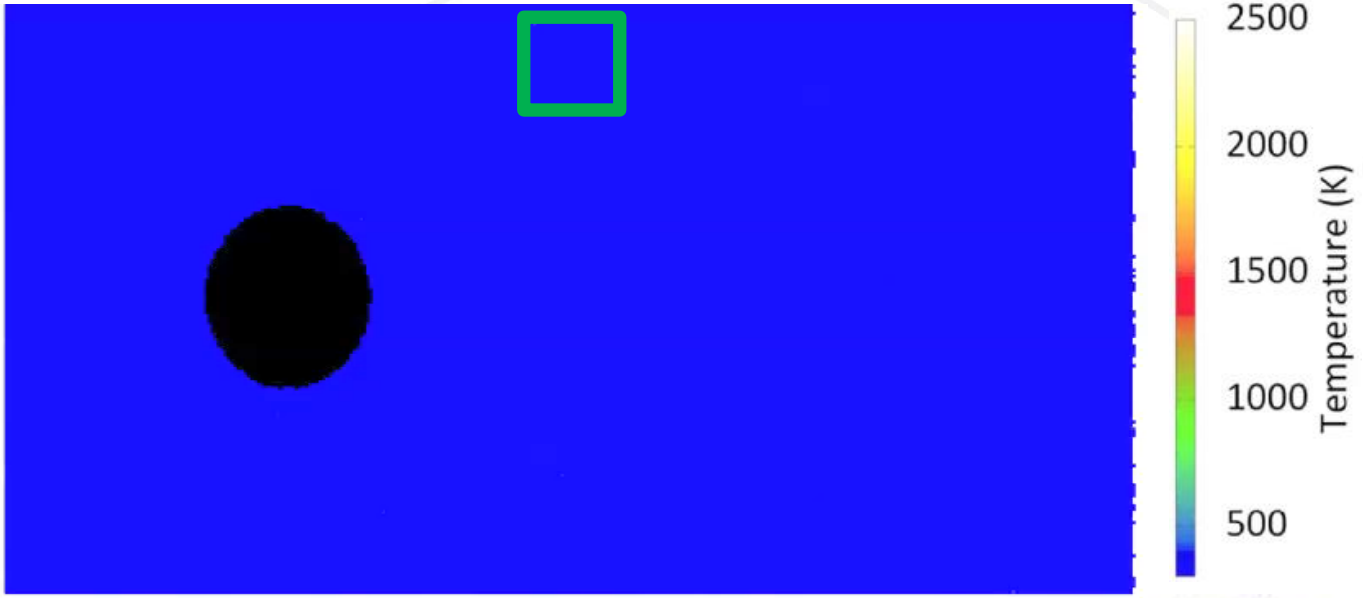

Wood, M. A.; Cherukara, M. J.; Kober, E. M.; Strachan, A. Ultrafast Chemistry under Nonequilibrium Conditions and the Shock to Deflagration Transition at the Nanoscale. *J. Phys. Chem. C* **2015**, 119 (38), 22008–22015.

Shan, T.-R.; Thompson, A. P. Shock-Induced Hotspot Formation and Chemical Reaction Initiation in PETN Containing a Spherical Void. *J. Phys. Conf. Ser.* **2014**, 500 (17), 172009.

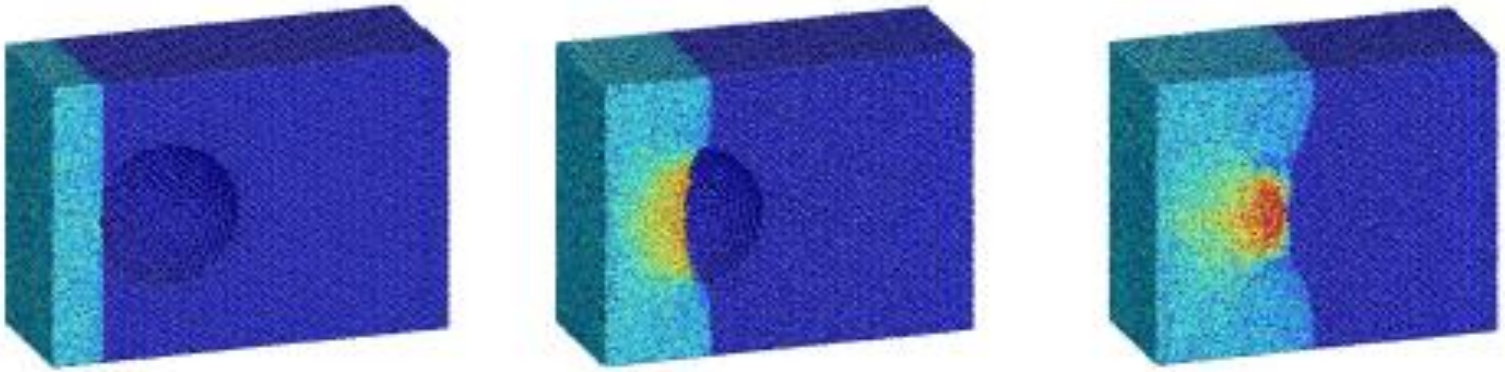

Need to model the chemistry as a function of T and P

Molecular Dynamics

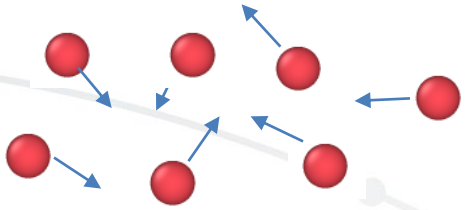

Initial atomic positions $\vec{R}_i$ and velocities $\vec{V}_i$

Compute forces on atoms $\vec{F}_i = -\vec{\nabla}_{R_i} V\left(\{R_j\}\right)$

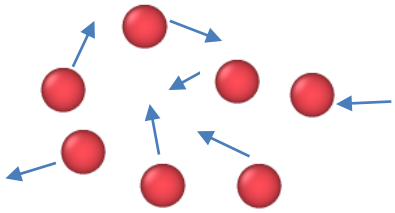

Solve Newton's Second Law $\dot{\vec{V}}_i = \frac{\vec{F}_i}{M_i} \quad \dot{\vec{R}}_i = \vec{V}_i$

Integrate classical equations of motion

Bond order reactive potential

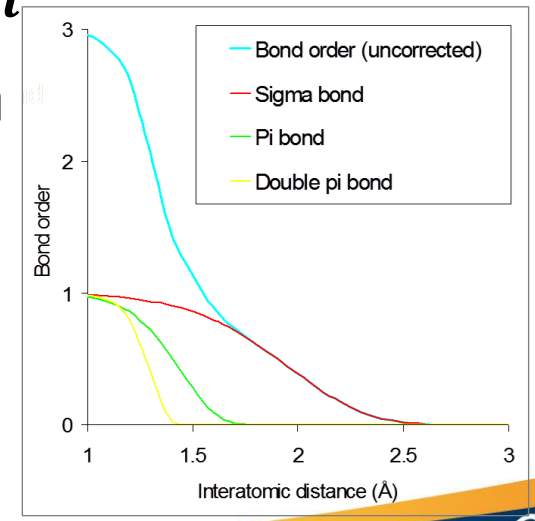

[1] Senftle, T. P. et al. *npj Comp. Mat.* **2**, (2016)

What is a good potential to use?

ReaxFF / ReaxFF-lg

Unimolecular Decomposition …*comparison between ReaxFF and B3LYP/6-31G***

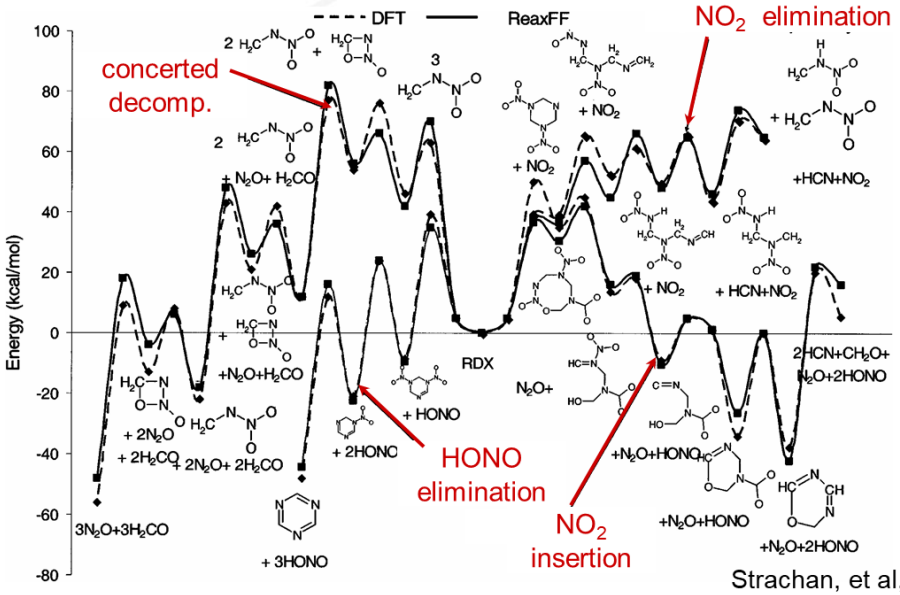

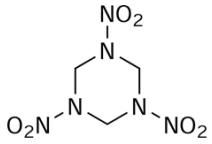

RDX

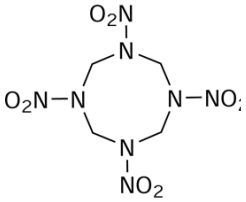

HMX

Strachan, et al, *JCP*, 122, 054502 ('05).

L. Lui et al., *J Phys. Chem. A*, 2011, **115**, 11016

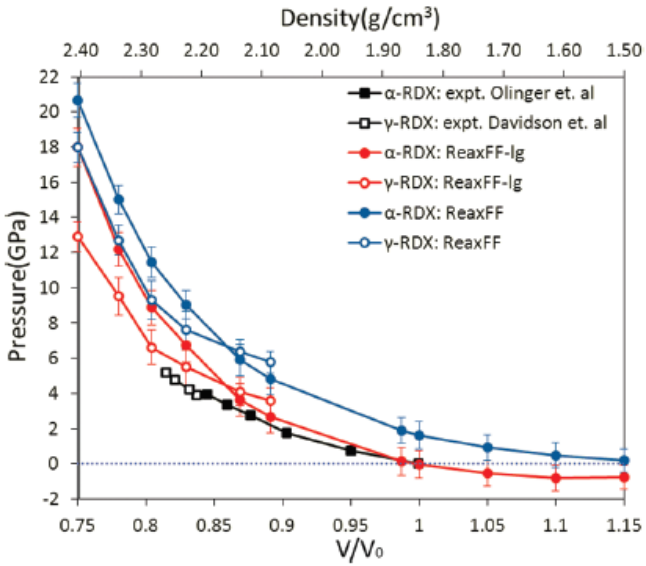

Lack of bi-molecular reaction schemes
Low gradient vdw term: improved solids' densities
Calibrated to ground state and transition state geometries

Sample Preparation

- **2** systems
  - RDX and HMX
- **10** densities
  - $V/V_0 = 0.65 – 1.50$
- **7** temperatures (NVT)
  - 1200 - 3000 K

RDX

- 4x4x3 unit cells
- 8064 atoms
  - 384 molecules
- V = 76.25 nm³

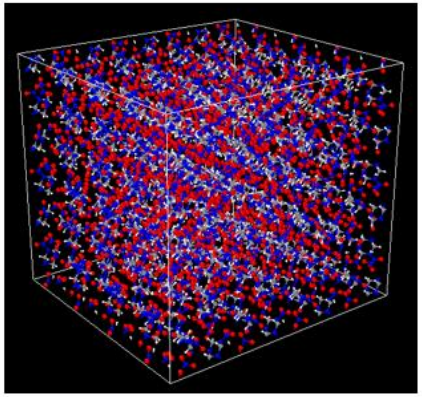

HMX

- 6x5x4 unit cells
- 6720 atoms
  - 240 molecules
- V = 75.45 nm³

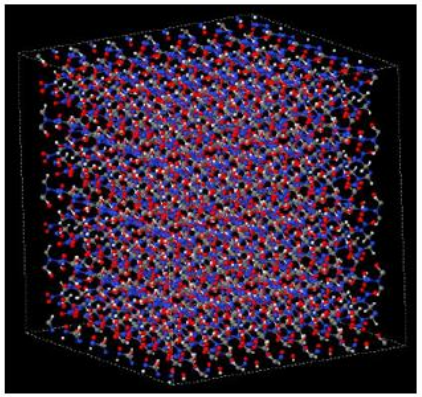

Coordination Geometry Analysis

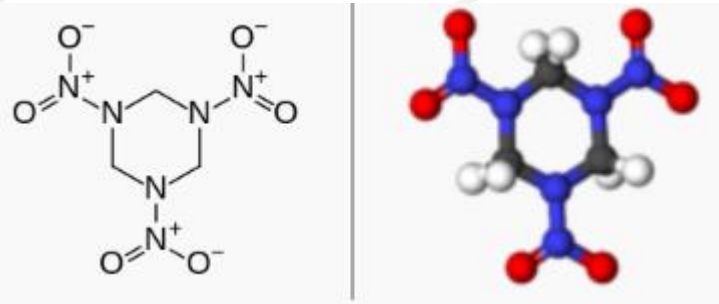

https://ipfs.io/ipfs/QmXoypizjW3WknFiJnKLwHCnL72vedxjQkDDP1mXWo6uco/wiki/RDX.html

- Assume all atoms have a maximum of four bonds
- 280 different geometry configurations for *HCNO* atom types
- Based on group additivity approach of Benson et al.

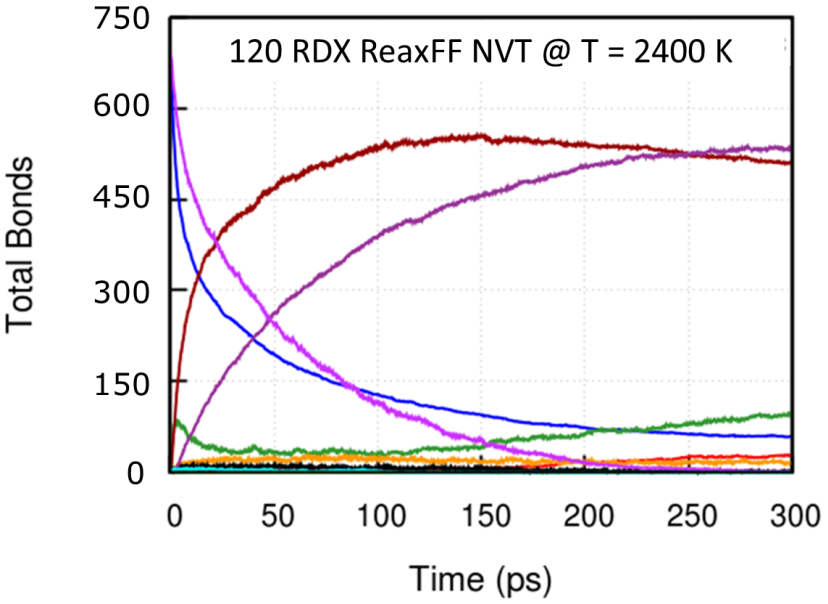

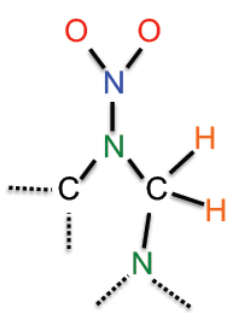

Nitro group dissociation

N[NOO] → N[OO]

N[NCC] → N[CC]

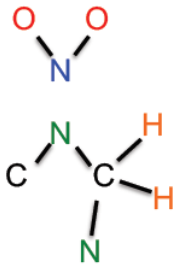

Cohen, N.; Benson, S. W. Estimation of Heats of Formation of Organic Compounds by Additivity Methods. *Chem. Rev.* **1993**, *93* (7), 2419–2438. https://doi.org/10.1021/cr00023a005.

Dimensionality Reduction – Non-negative matrix factorization

BONDS

Time (ps)

	H-H	H-C	H-N	⋯	O-O
	0	720	0	⋯	0
	0	694	0	⋯	0
	0	688	0	⋯	0
	2	680	6	⋯	0
	⋮	⋮	⋮	⋯	⋮
	10	60	118	⋯	16

≈

Example:
Decomposition of
120 RDX molecules

http://scikit-learn.org/stable/modules/generated/sklearn.decomposition.NMF.html

Components (N)

Time (ps)

0.0	0.0	1.0	0.0
0.0	0.0	1.0	0.0
0.0	0.0	1.0	0.0
0.0	0.0	0.9	0.1
⋮	⋮	⋮	⋮
0.9	0.1	0.0	0.0

(Concentration)

•

BONDS

H-H	H-C	H-N		O-O
0	0	0	⋯	12
0	0	0	⋯	10
0	680	0	⋯	0
10	0	0	⋯	0

(Composition)

Components (N)

E. M. Kober, personal communication & manuscript in preparation

Application of NMF - RDX

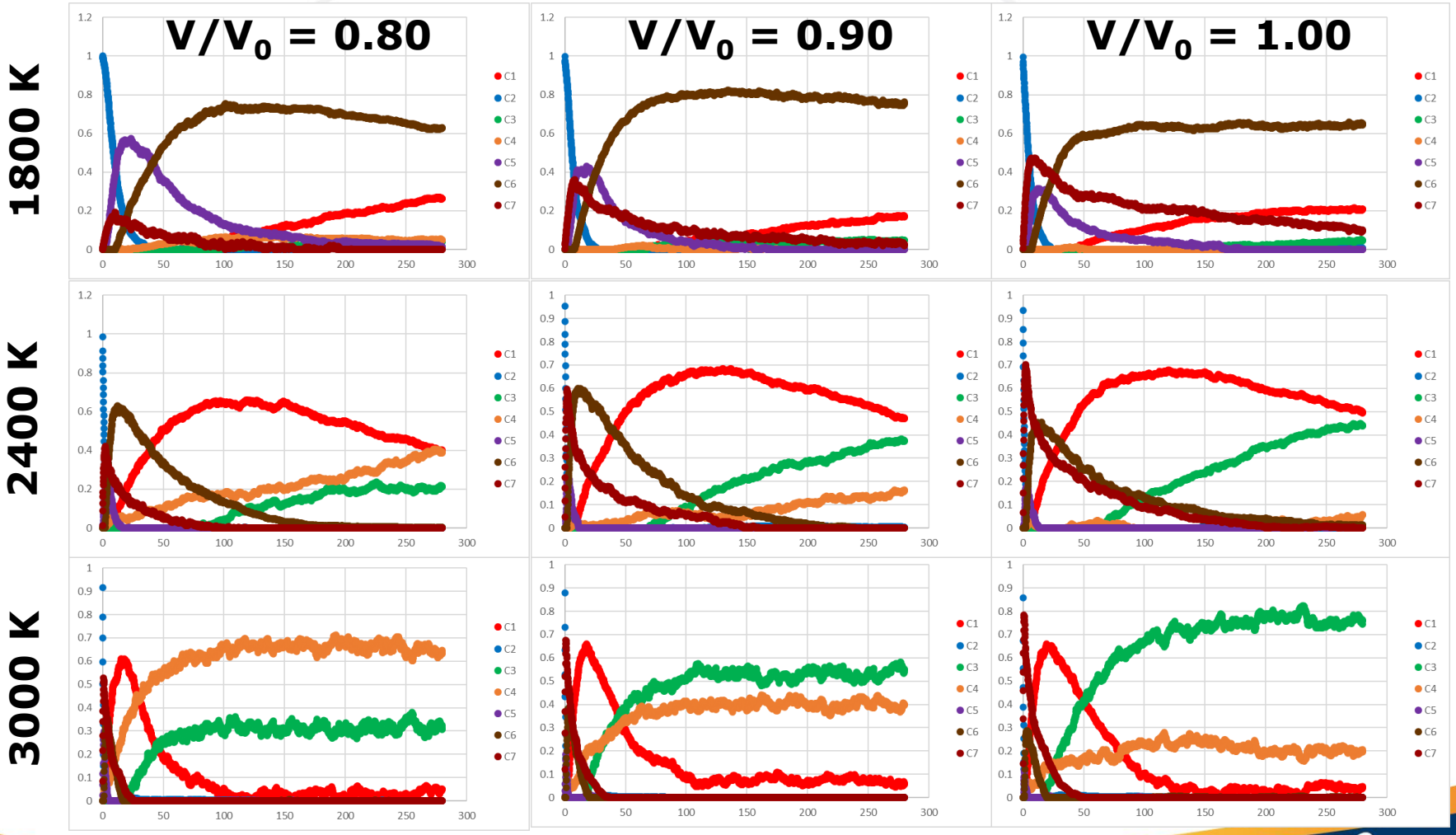

Concentrations as a function of T and P

Comparison of 7-Compoent reduced models

$V/V_0 = 0.65 – 1.50$

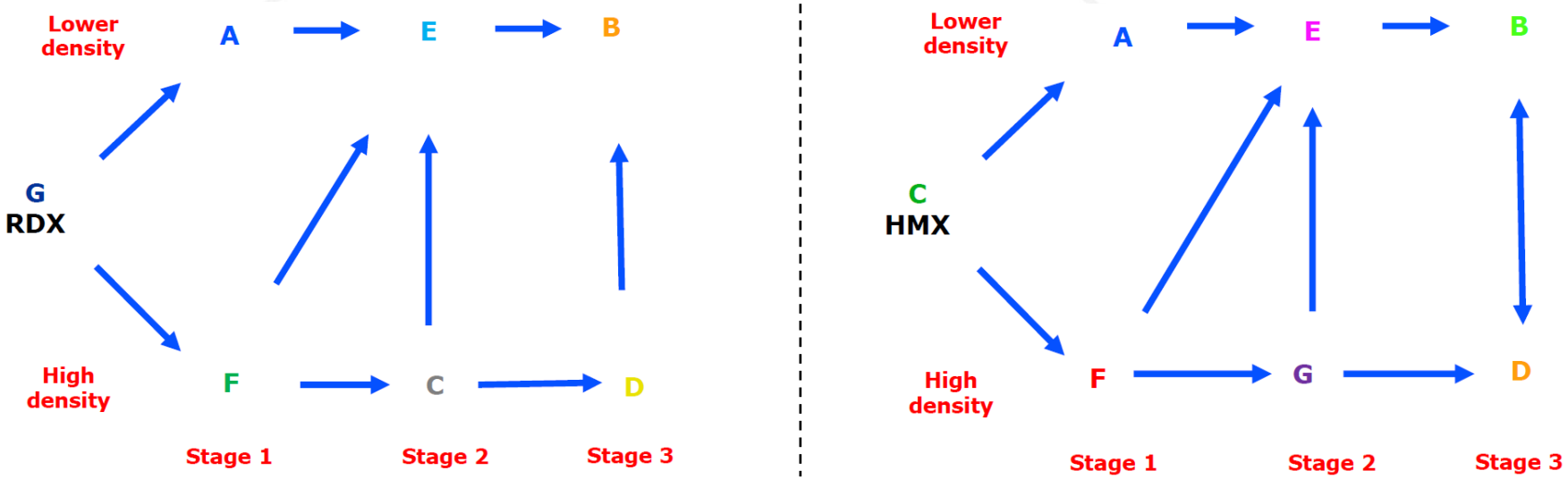

Similarity in pathways but differences in chemistry:

Lower density path: 1) NO_2 dissociation and ring break-up; 2) N_2 and H_2O production; 3) Carbon oxidation

Higher density path: 1) Associative reaction to form NO_3, ring stays intact, RDX forms triazine (stable intermediate); 2) RDX forms N_2 and H_2O, while HMX oxidizes carbon in the ring; 3) RDX oxidizes the triazine, while HMX produces N_2 and H_2O

Extracting rate constants from these schemes assuming Arrhenius kinetics

1-D Deflagration Simulations on HPC resources

- Typical simulation: 5 x 5 x 200 nm ~ 1M atoms (20-100 nodes, 20-100 hours)
- Thermalize selected region for ignition: 10-50 nm, 1500-2500 K
- Downstream conditions: ambient, 600K 0.8 GPa
- Deflagration wave speed = F(rates, conductivity, initial conditions)
- Local velocity

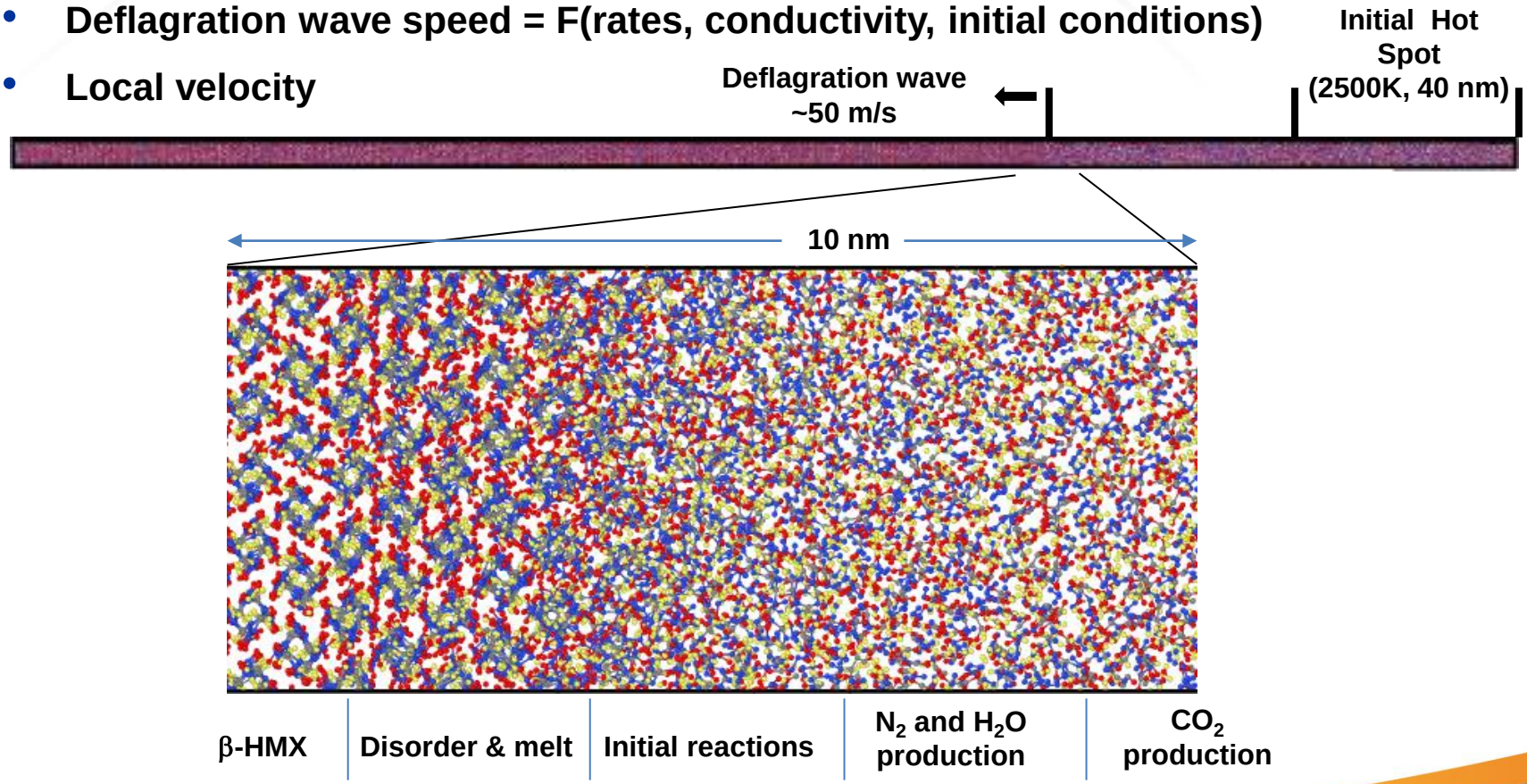

1-D Thermal Sticks, 40 nm @ 2500 K

- **Fixed wall on both ends**
- **Projection onto 7 component cook-off model**

RDX

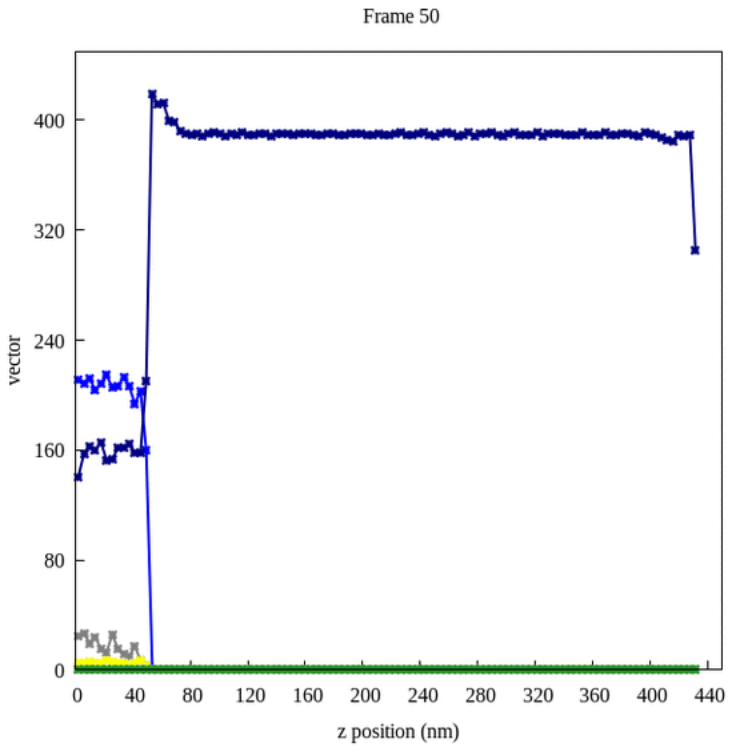

HMX

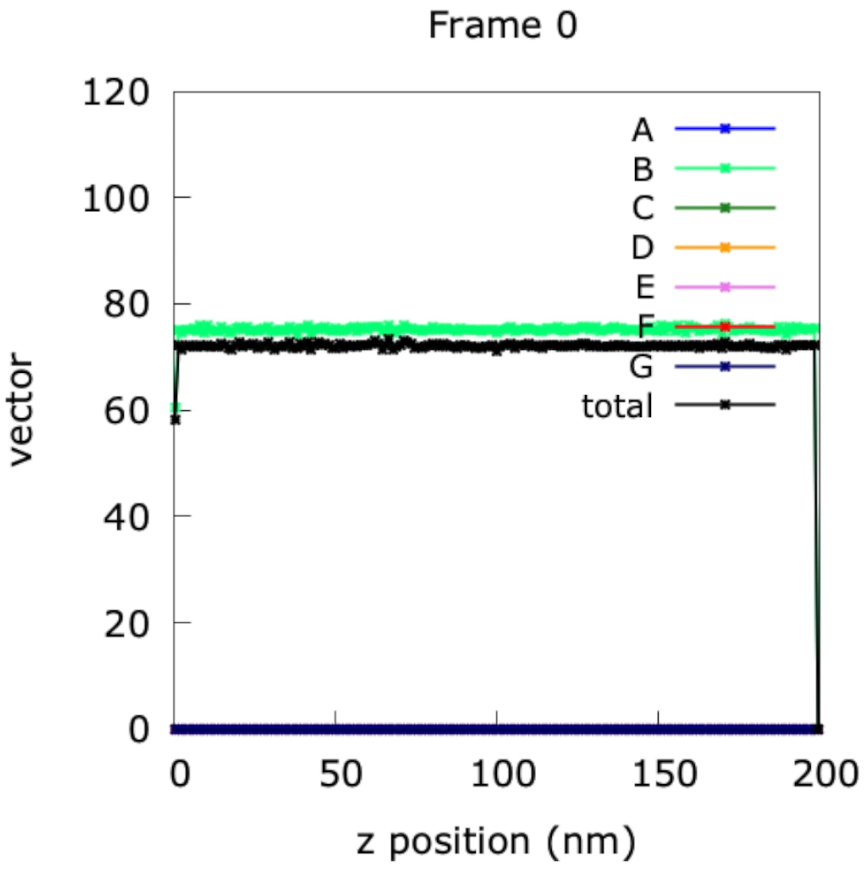

Apparent differences in local chemistry

1-D Thermal Sticks, 40 nm @ 2500 K for HMX

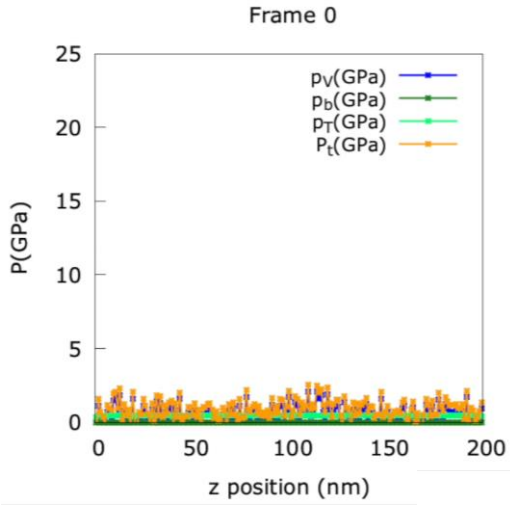

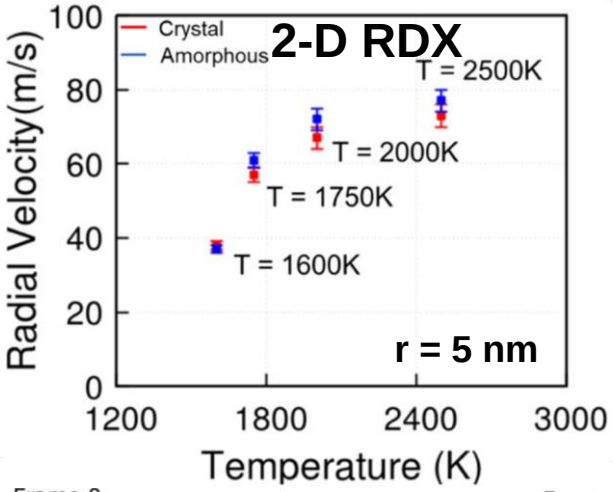

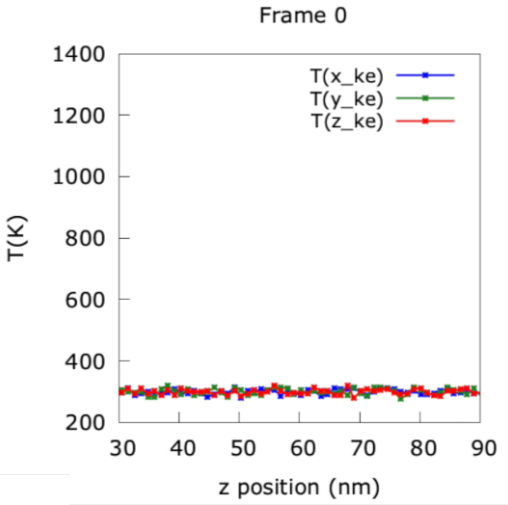

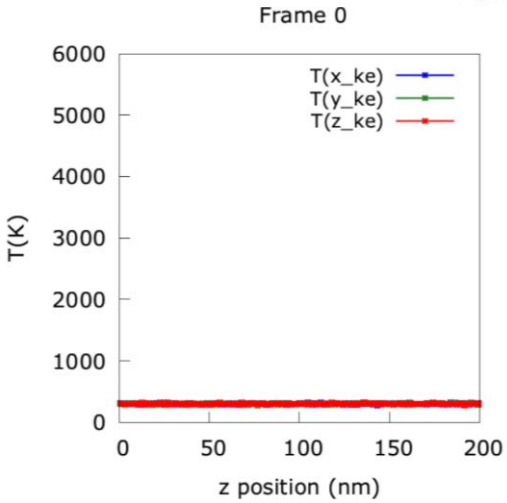

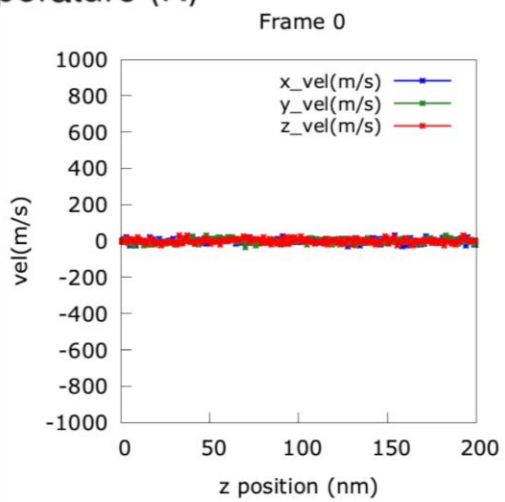

Sakano, M.; Hamilton, B.; Islam, M. M.; Strachan, A. Role of Molecular Disorder on the Reactivity of RDX. *J. Phys. Chem. C* **2018**, *122* (47), 27032–27043. https://doi.org/10.1021/acs.jpcc.8b06509.

Measure reaction front velocity vs temperature and size

Summary

- Refining reduced-order chemistry model for RDX and HMX (Arrhenius fits, EOS)
- Map small-scale cook-off simulations to HPC runs of 1-D thermal stick variations
- Extracting deflagration wave speeds

- Will map to 1-D gaps (voids) for various sizes and shock speeds: common chemistry to deflagration?
- Improve modeling of chemistry by implementing Quantum Thermal Bath (redistributes energies)

Reducing Complexity of Variational Quantum Eigensolvers for Quantum Chemistry

July 14th, 2020

James Sud (Post-Bachelor)

University of California, Berkeley Quantum Computing Summer School

Nikolay Tkachenko (2nd year Ph.D student)

Utah State University

20200056DR Quantum Chemistry with Quantum Computers

Mentors: Lukasz Cincio (T-4), Yu Zhang (T-1), Pavel Dub (C-IIAC)

Agenda

July 14, 2020

- Intro to quantum chemistry and computing
- Quantum chemistry simulations on quantum computers
- The Variational Quantum Eigensolver (VQE)
- ROSALIN optimizer for reducing measurement counts
- Choosing an ansatz
- Qubit permutations for reducing circuit depth and measurement counts
- Preliminary Results

Introduction

DOE pushes for quantum computing (2018): Quantum chemistry is immediate applications of quantum computing directly impacting LANL present and future missions

Goal: Find the electronic ground state of chemical systems

Motivation: drug discovery, catalysis, materials design, etc.

Challenge: The **exact** simulation of the Caffeine molecule in sto-3g basis is a daunting task for any existing supercomputer (Diagonalizing and storing a matrix of size 6×10^{43})

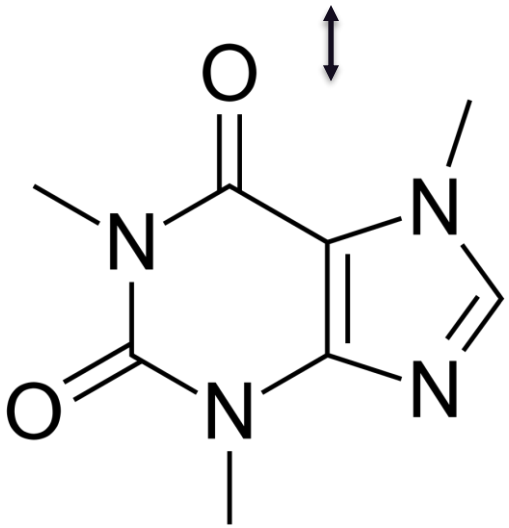

https://en.wikipedia.org/wiki/Caffeine#/media/File:Caffeine_structure.svg

Introduction

Solution: Use quantum computers – each one-electron spin-orbital is encoded in one qubit

Example: LiH, 4 electrons, 495 possible configurations (sto-3g basis)

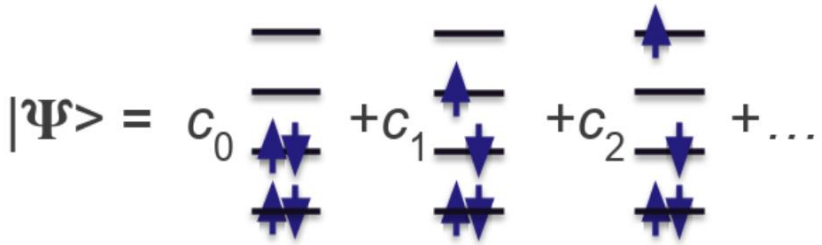

$$|\Psi\rangle = c_0 + c_1 + c_2 + \ldots$$

$$|\Psi\rangle = c_0|111100\ldots0\rangle + c_1|111010\ldots0\rangle$$

CPU/GPU

scales exponentially

$$\hat{H}|\Psi\rangle = E|\Psi\rangle$$

scales polynomially

QPU

Quantum Chemistry on Quantum Computers

Start with Molecular Coordinates

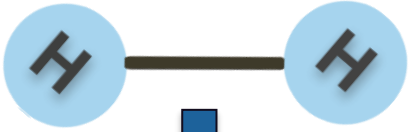

OpenFermion Qiskit

Convert to qubit Hamiltonian

```
-0.09064961228803427 [] +
0.04523355281799211 [X0 Z1 X2] +
0.04523355281799211 [X0 Z1 X2 Z3] +
0.04523355281799211 [Y0 Z1 Y2] +
0.04523355281799211 [Y0 Z1 Y2 Z3] +
0.17217557977330947 [Z0] +
0.17217557977330947 [Z0 Z1] +
0.16614307978715506 [Z0 Z1 Z2] +
0.16614307978715506 [Z0 Z1 Z2 Z3] +
0.12090952696916293 [Z0 Z2] +
0.12090952696916293 [Z0 Z2 Z3] +
0.16892496212247482 [Z1] +
-0.22572827882218005 [Z1 Z2 Z3] +
0.17464093706423592 [Z1 Z3] +
-0.22572827882218005 [Z2]
```

Prepare quantum circuit and measure with respect to qubit Hamiltonian

H2 molecule in sto-3g basis

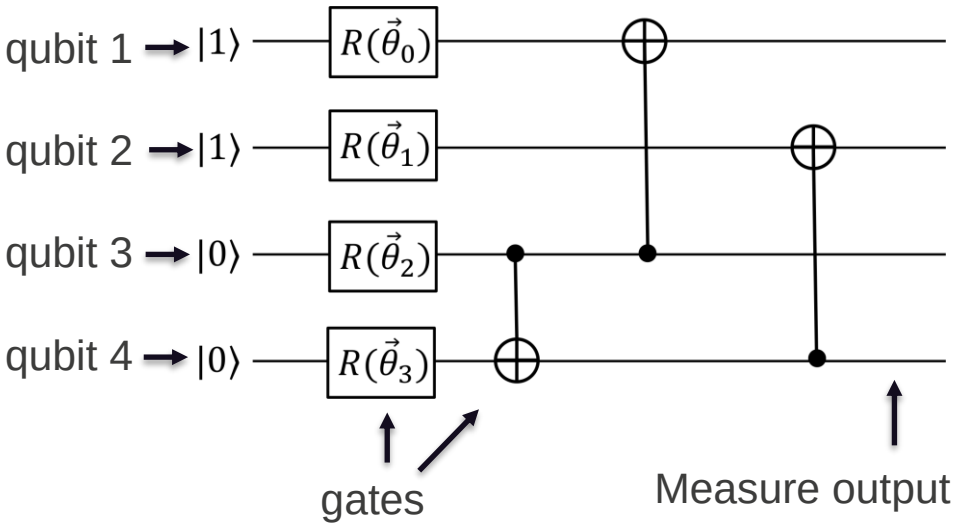

https://github.com/quantumlib/OpenFermion
https://ai.googleblog.com/2016/07/towards-exact-quantum-description-of.html
https://www.eagleresearchllc.com/products/uncategorized/h2-true-molecular-hydrogen/
https://user-images.githubusercontent.com/50955024/69568348-ac558780-0f78-11ea-9242-7ac8e8ba450a.png

ROSALIN Optimizer Designed for Chemistry Hamiltonians

Variational Quantum Eigensolver (VQE)

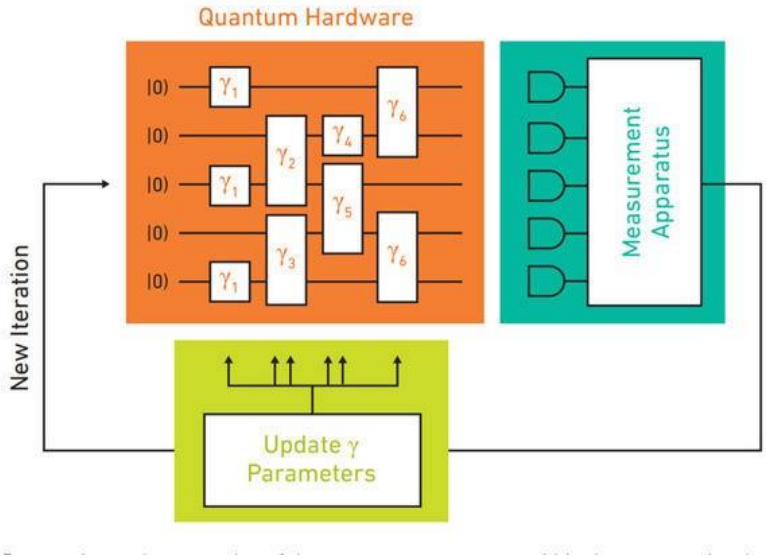

Rosalin Optimizer for VQE (Developed at LANL in this DR project)*

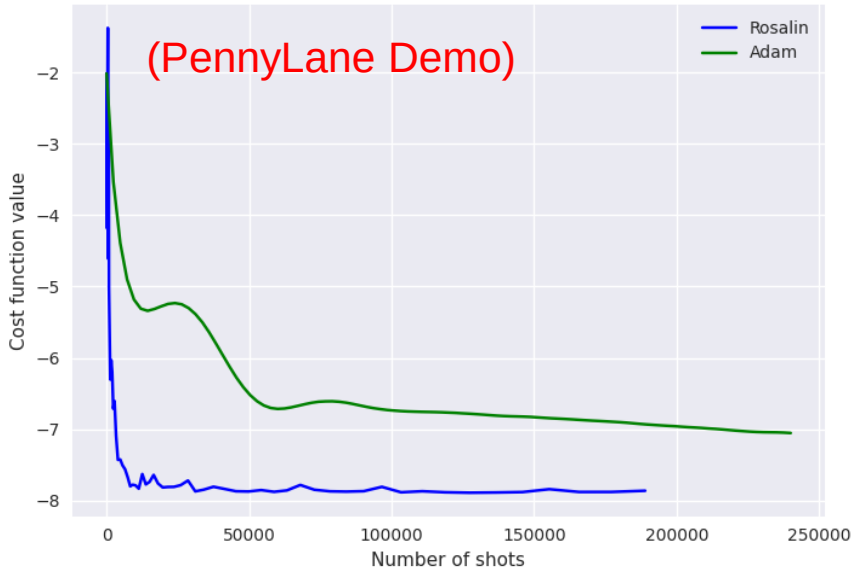

Classical VQE (2014): Full sampling. Requires many measurements

ROSALIN optimizer: Random sampling from the Hamiltonian. Reduces number of measurements.

Implemented in Open-source PennyLane software package

* Arrasmith et. al. https://arxiv.org/pdf/2004.06252.pdf
**https://medium.com/@lana.bozanic/the-variational-quantum-eigensolver-efb8fab14c85
https://pennylane.ai/qml/demos/tutorial_rosalin.html

Creating a Variational Ansatz (Trial Wavefunction)

H2 molecule in sto-3g basis

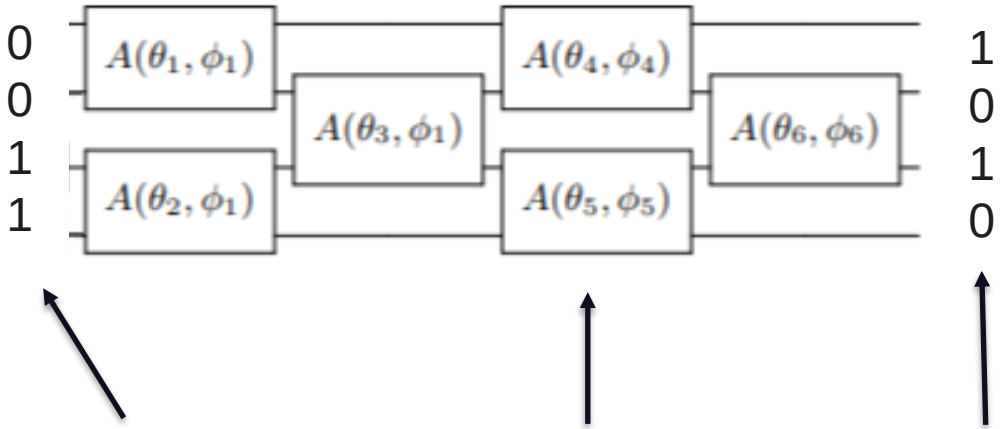

Start with 2 electrons

Choose any parameters

End with 2 electrons

Electron number preserving gates: Ensures that our guess has the correct number of electrons. Constrains search to subspace of 2^4 Hilbert Space

Advantage: Sweet spot between circuit depth and number of parameters.

Reduces measurement count from $>10^8$ to 10^5 for Hydrogen molecule

https://arxiv.org/pdf/1904.10910.pdf

Permutations of Hamiltonian

- **Idea:** to place more ***entangled*** qubits close to each other to reduce the required depth of the circuit and increase the accuracy of the final energy.

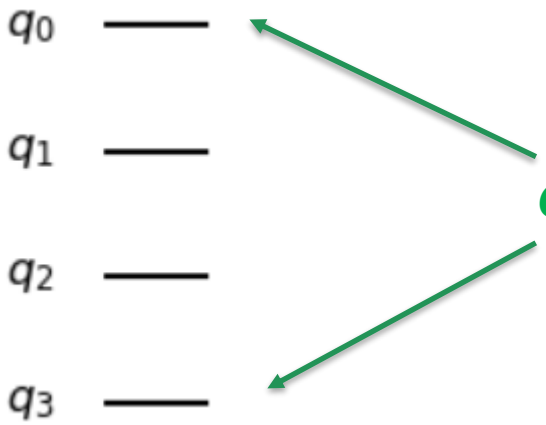

Qubit 0 is entangled with qubit 3

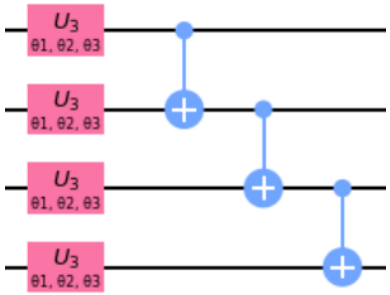

Ansatz layer that corresponds to qubit chain architecture.

Permutations of Hamiltonian

- **Idea:** to place more ***entangled*** qubits close to each other to reduce the required depth of the circuit and increase the accuracy of the final energy.

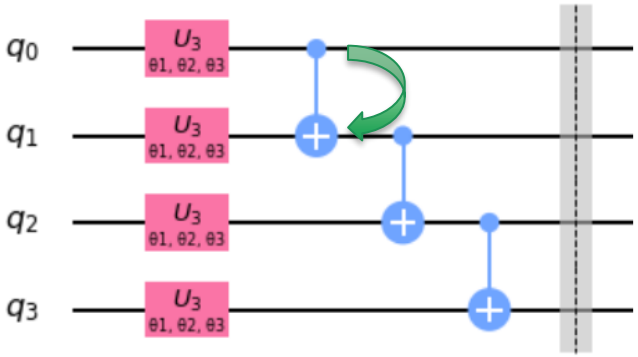

3 layers are required to model the system

Let us swap qubit 1 and qubit 3

Permutations of Hamiltonian

- **Idea:** to place more ***entangled*** qubits close to each other to reduce the required depth of the circuit and increase the accuracy of the final energy.

Now qubit 0 and 3 are close to each other

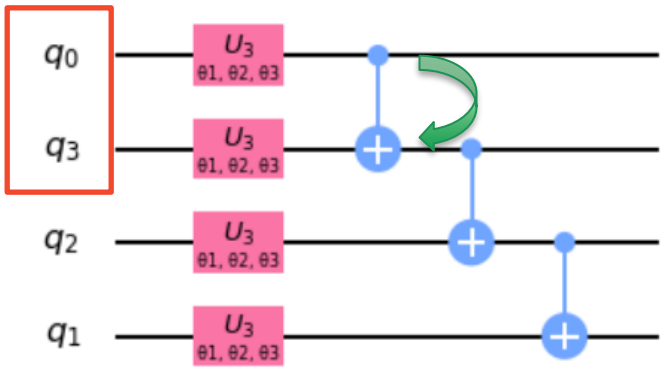

After the permutation only 1 layer is required

Examples

- **System:** H_3^+
- **Basis:** STO-3G
- **Geometry:**

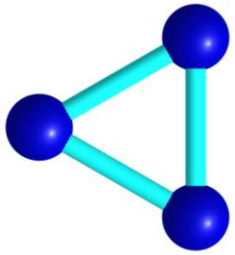

Number of qubits: 6
Exact energy: -1.35076 (need to match this energy by quantum computer)

Before

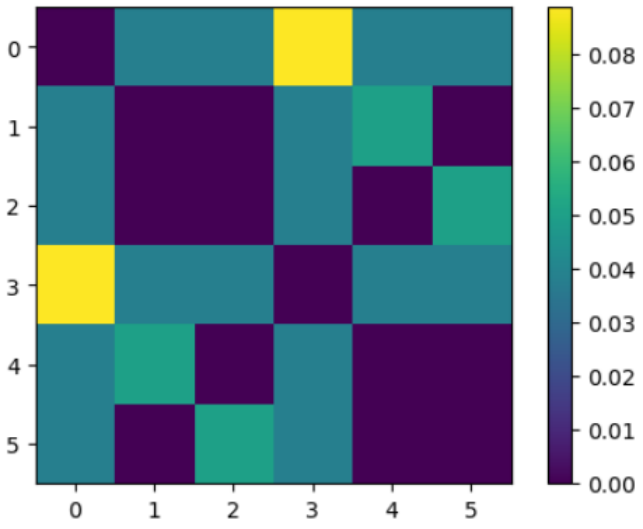

After

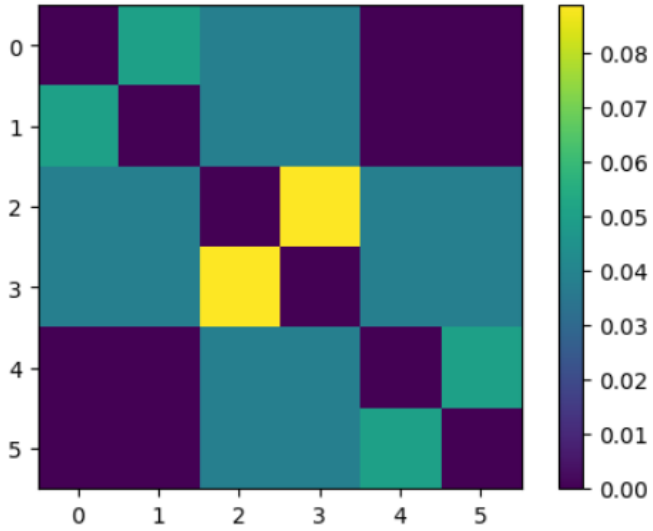

	Not permuted	Permuted
Final optimized energy for ansatz with a fixed depth = 5	-1.33158301 Hartree	**-1.35070986 Hartree**
Optimized energy - Exact energy	12 kcal/mol	**0.03 kcal/mol**

Conclusions

- U1 symmetric ansatz was encoded in LANL made Rosalin optimizer and reduces measurement counts by multiple orders of magnitude
- The algorithm to implement the permutations of Hamiltonian to ensure better entanglement between spin orbitals has been developed.
- Permuted Hamiltonian was found to be more efficient based on the several examples of molecules/encodings.

Future plans

Take into account the topology of actual devices and run calculations on actual hardware (IBMQ, Rigetti).

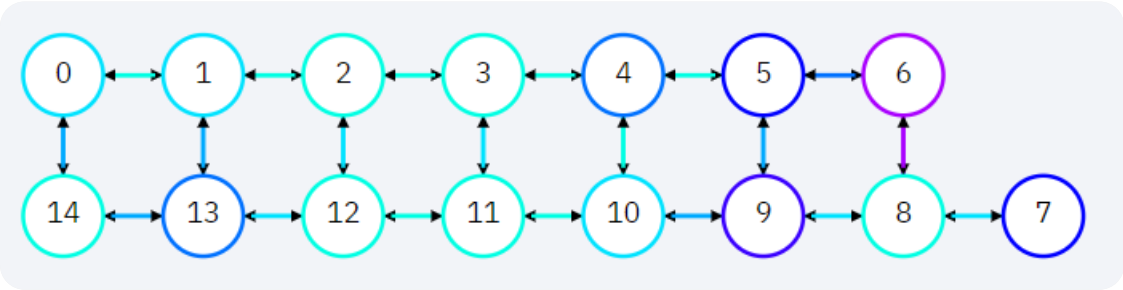

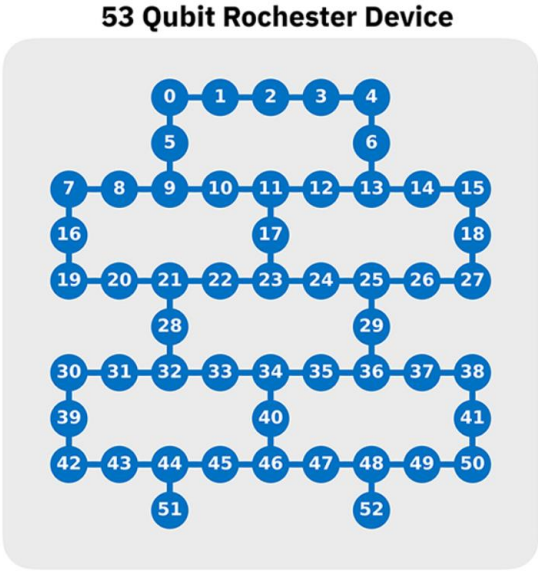

Thank you for your attention!

Acknowledgments

– LANL LDRD 20200056DR “Quantum Chemistry using Quantum Computers”

– LANL Quantum Summer School 2020

Permutations of Hamiltonian

- **Idea:** to place more ***entangled*** qubits close to each other to reduce the required depth of the circuit and increase the accuracy of the final energy.

- **Entanglement measurement:**

  Von Neumann entropy for the reduced system

$$S = -\sum_{\alpha} \omega_\alpha \ln(\omega_\alpha)$$

ω_α is the eigenvalue of the reduced density matrix

S_i - single orbital entropy (ρ contains only one qubit)
S_{ij} - two - orbital entropy (ρ contains two qubits)

Mutual information: $I_{ij} = (S_i + S_j - S_{ij})(1 - \delta_{ij})$

Fiedler Vector

Cost function: $\mathrm{f} = \sum_{i<j} I_{ij}(i-j)^2$

We know that Fiedler vector can minimize the following function:

$$\mathrm{F(x)} = x^{+}Lx = \sum_{i<j} I_{ij}\left|x_i - x_j\right|^2$$

Where L is a graph Laplacian: $\mathbf{L} = \mathbf{D} - \mathbf{I}$, with $\mathbf{D_{ii}} = \sum_j \boldsymbol{I_{ij}}$

Examples

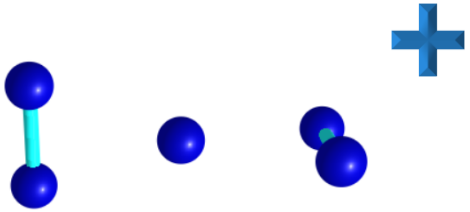

Before

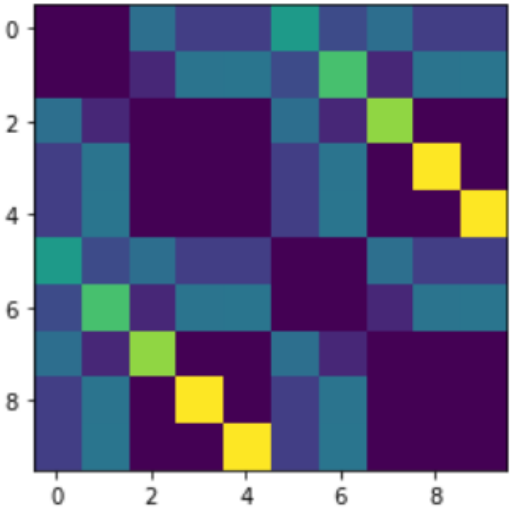

After

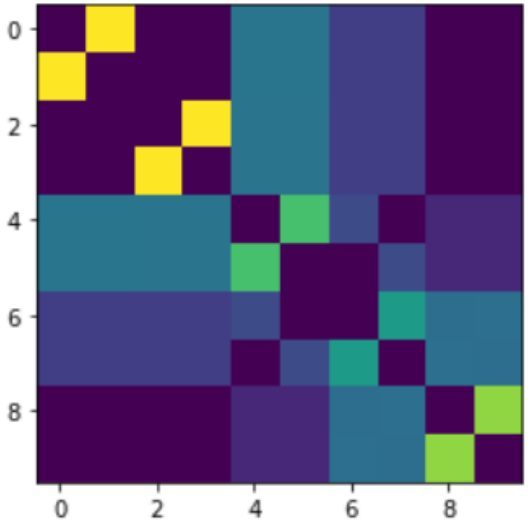

Examples

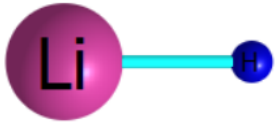

Before

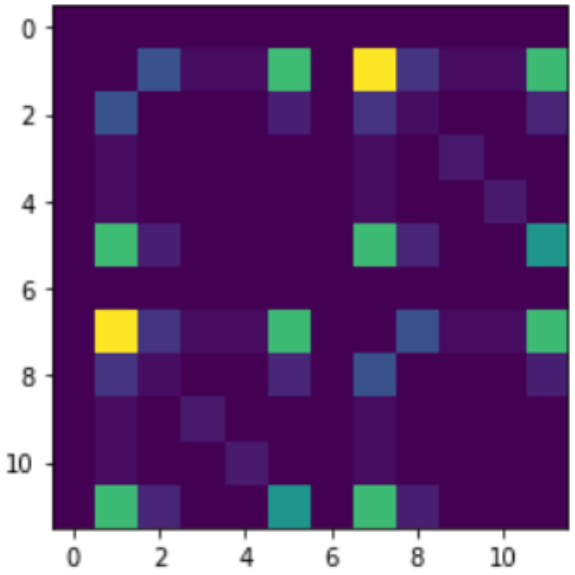

After

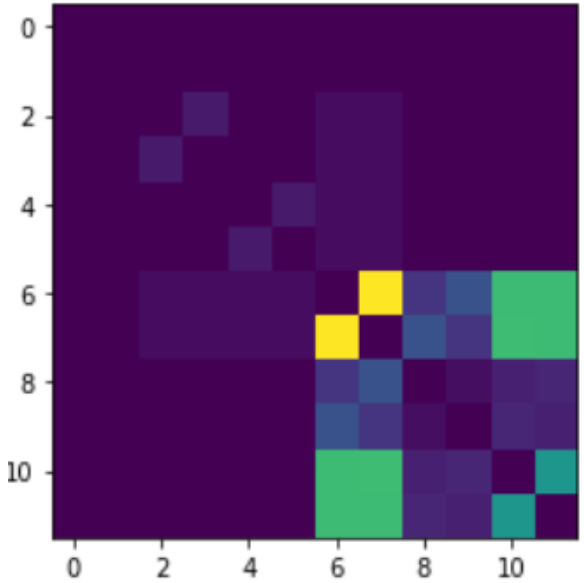

Preliminary Results

- **System:** H_3^+
- **Optimizer:** COBYLA
- **Exact energy:** -1.3507306 (need to match this energy by quantum computer)
- **Ansatz depth:** 5

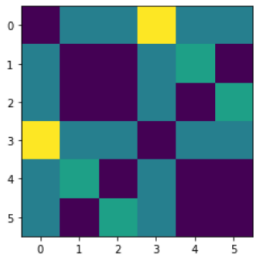

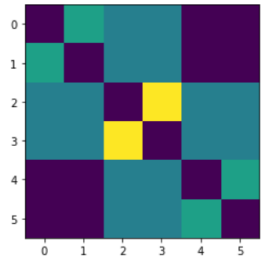

	Not permuted	Permuted
Energy	-1.33158301	**-1.35070986**
Num_evaluations	100000	100000

Nonadiabatic molecular dynamics analysis of Hybrid Dion-Jacobson 2D Lead Iodide Perovskites

Ying Wang
Mentor: Dr. Amanda Neukirch
Co-mentor: Dr. Dibyajyoti Ghosh

08/13/2020

Introduction to Solar Cells

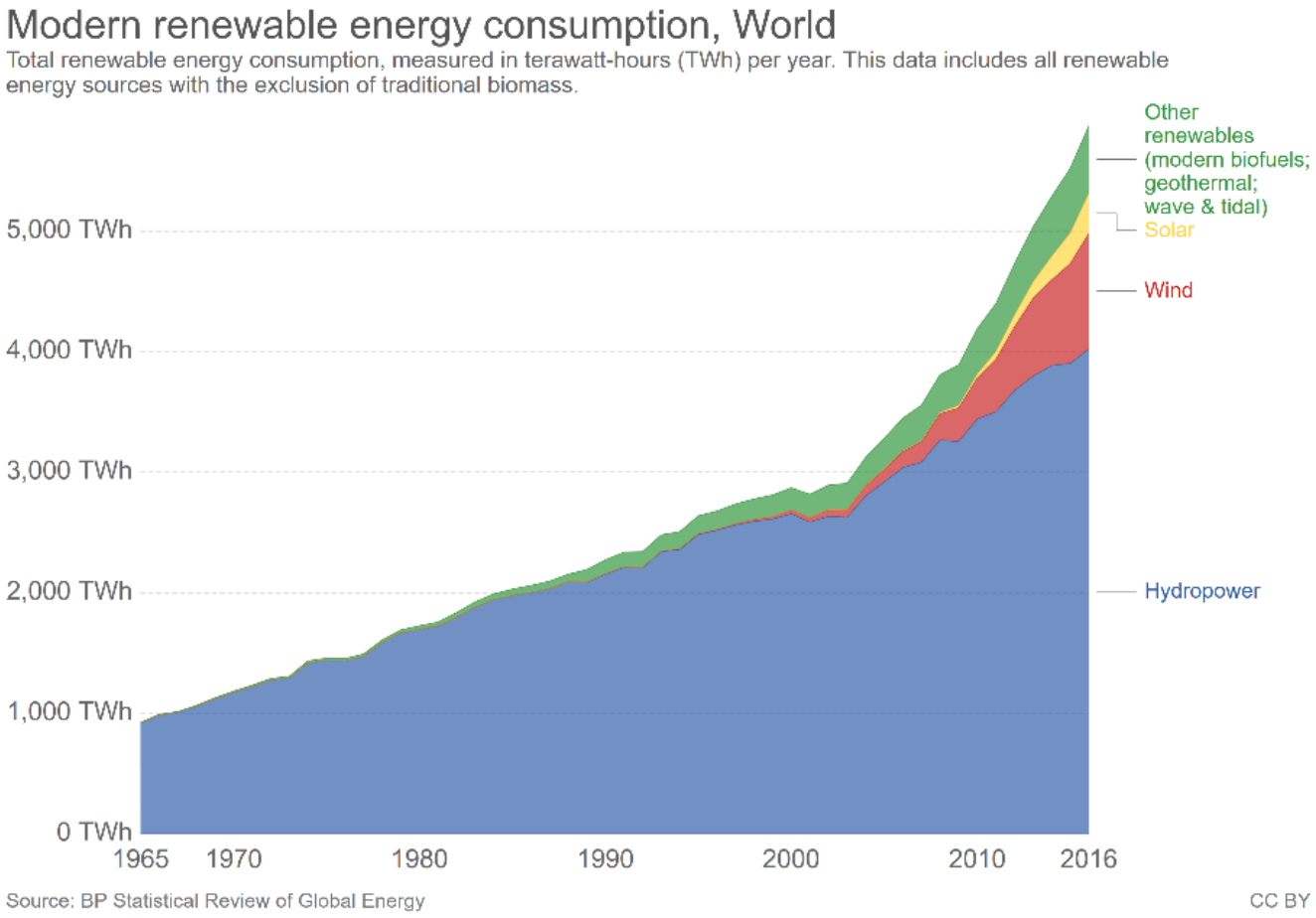

crystalline silicon:

- Manufacturing is relatively expensive
- Improvement of efficiency is almost saturated.

Hybrid Organic-Inorganic Lead Halide Perovskites: Promising Materials as Solar Cells

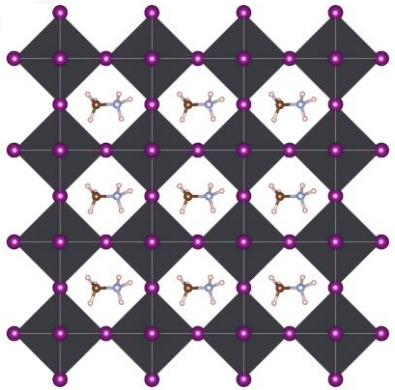

3D hybrid organic-inorganic lead halide perovskites

Pros:

- **Solution-processed, low cost**
- **Direct bandgap**
- **Strong light absorption**
- **High carrier mobility**

Cons:

- **Instability against moisture, light and heat**

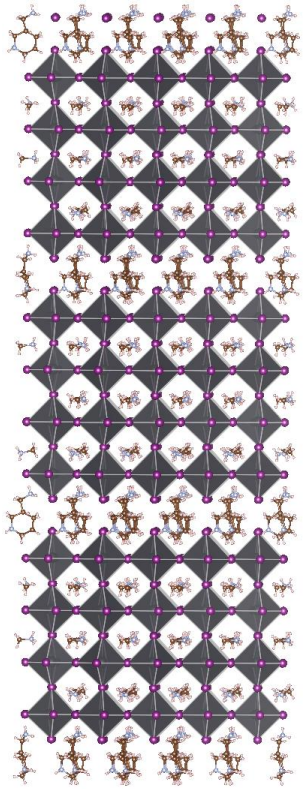

hybrid Dion-Jacobson 2D lead iodide perovskites

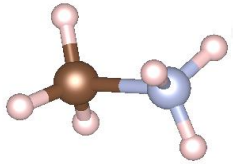

methylammonium

Interlayer cations

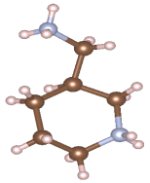

3AMP
3-(aminomethyl)piperidinium

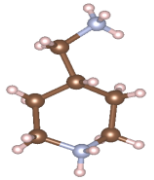

4AMP
4-(aminomethyl)piperidinium

- **High stability**
- **Low but promising power conversion efficiency (PCE)**
- **Highly tunable structure**

Hybrid Organic-Inorganic Lead Halide Perovskites: Promising Materials as Solar Cells

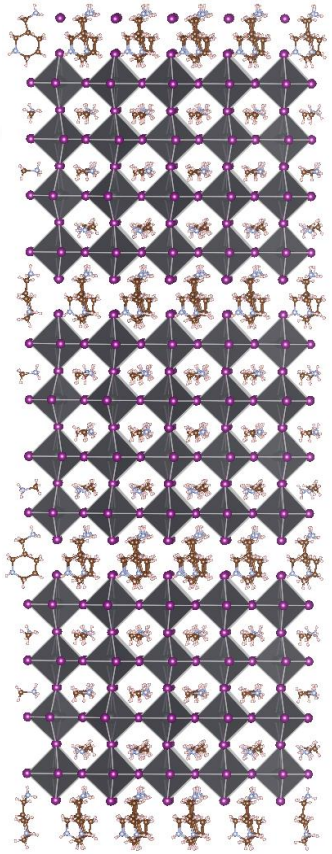

hybrid Dion-Jacobson 2D lead halide perovskites

J|A|C|S JOURNAL OF THE AMERICAN CHEMICAL SOCIETY
Article
Cite This: J. Am. Chem. Soc. 2018, 140, 3775−3783
pubs.acs.org/JACS

Hybrid Dion−Jacobson 2D Lead Iodide Perovskites

Lingling Mao,[†] Weijun Ke,[†] Laurent Pedesseau,[§] Yilei Wu,[†] Claudine Katan,[∥] Jacky Even,[§] Michael R. Wasielewski,[†,‡] Constantinos C. Stoumpos,[*,†] and Mercouri G. Kanatzidis[*,†,‡]

[†]Department of Chemistry, and [‡]Argonne-Northwestern Solar Energy Research (ANSER) Center, Northwestern University, Evanston, Illinois 60208, United States

[§]Univ Rennes, INSA Rennes, CNRS, Institut FOTON − UMR 6082, Rennes F-35000, France

[∥]Univ Rennes, ENSCR, INSA Rennes, CNRS, ISCR (Institut des Sciences Chimiques de Rennes) − UMR 6226, Rennes F-35000, France

- $(3AMP)(MA)_3Pb_4I_{13}$ with the narrowest bandgap and least distorted structure, longer lifetime
- 3AMP-PCE ~7%, 4AMP-PCE~5%

Prediction: $(3AMP)(MA)_3Pb_4I_{13}$ has obviously shorter nonradiative lifetime than $(4AMP)(MA)_3Pb_4I_{13}$

Rationalize the reason of the lifetime difference

Main composition of CBM & VBM

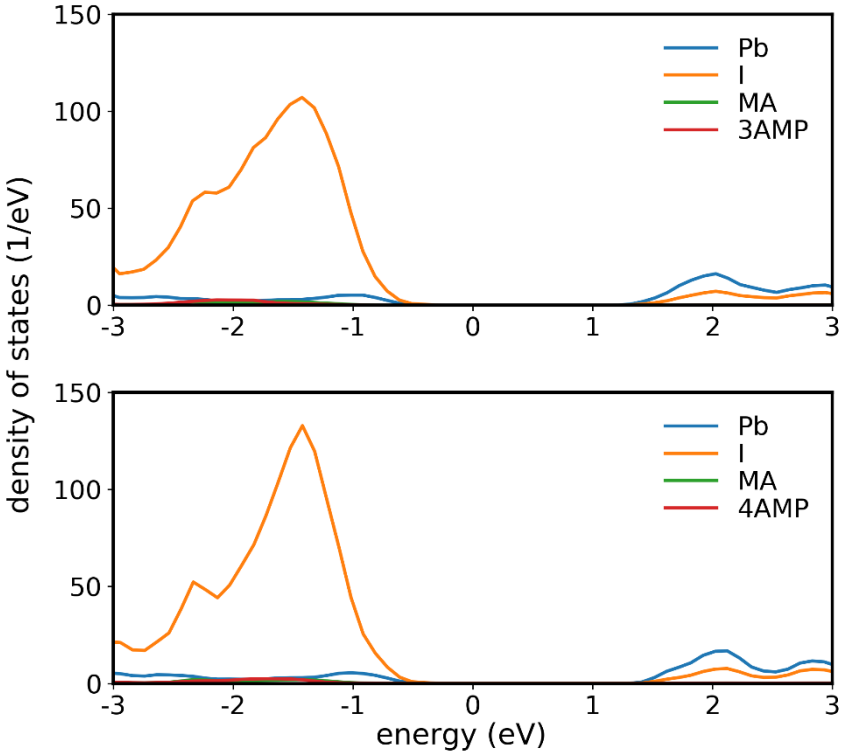

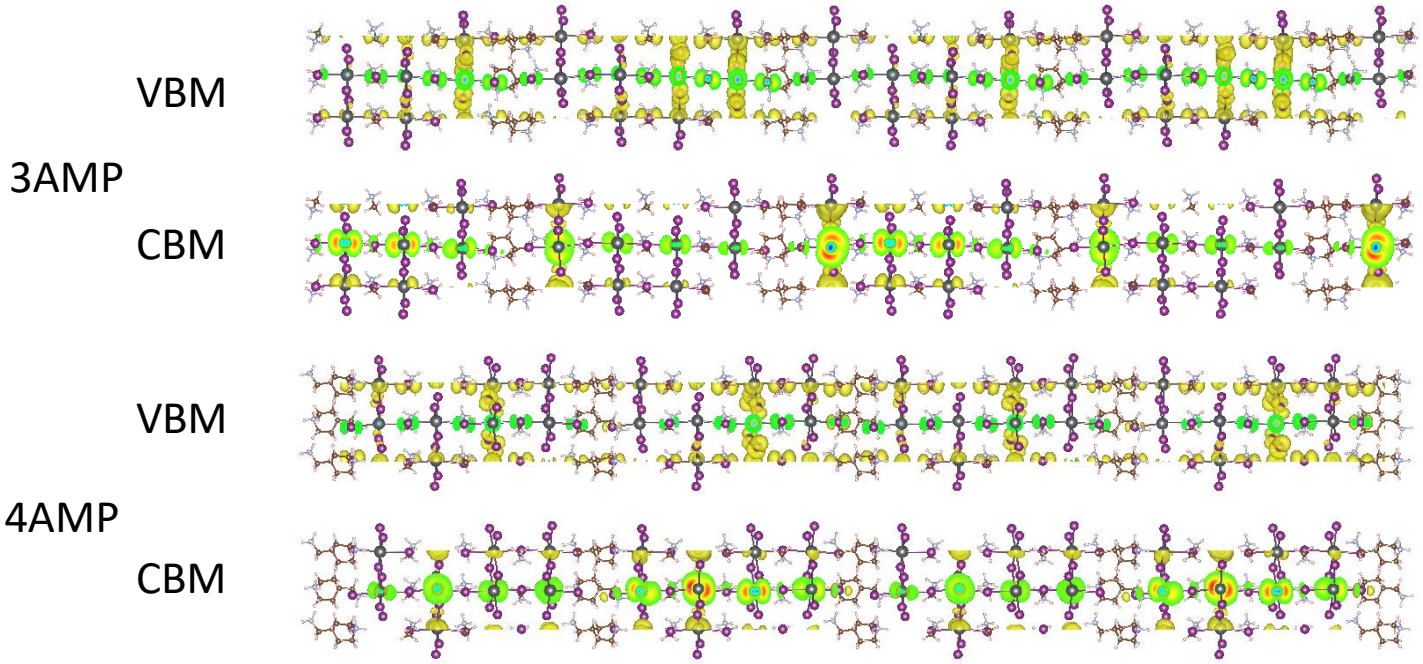

I-5p and Pb-6s dominate VBM (valence band maximum)
Pb-6p and I-5p dominate CBM (conduction band minimum)

Nonadiabatic coupling (NAC) doesn't play an important role in determining nonradiative lifetime

Electron-phonon coupling
- inelastic → NAC
- elastic → Quantum decoherence

- the stronger the NAC, the faster the nonradiative carrier recombination is
- When decoherence time is short enough, the shorter decoherence time induces the slower nonradiative carrier recombination

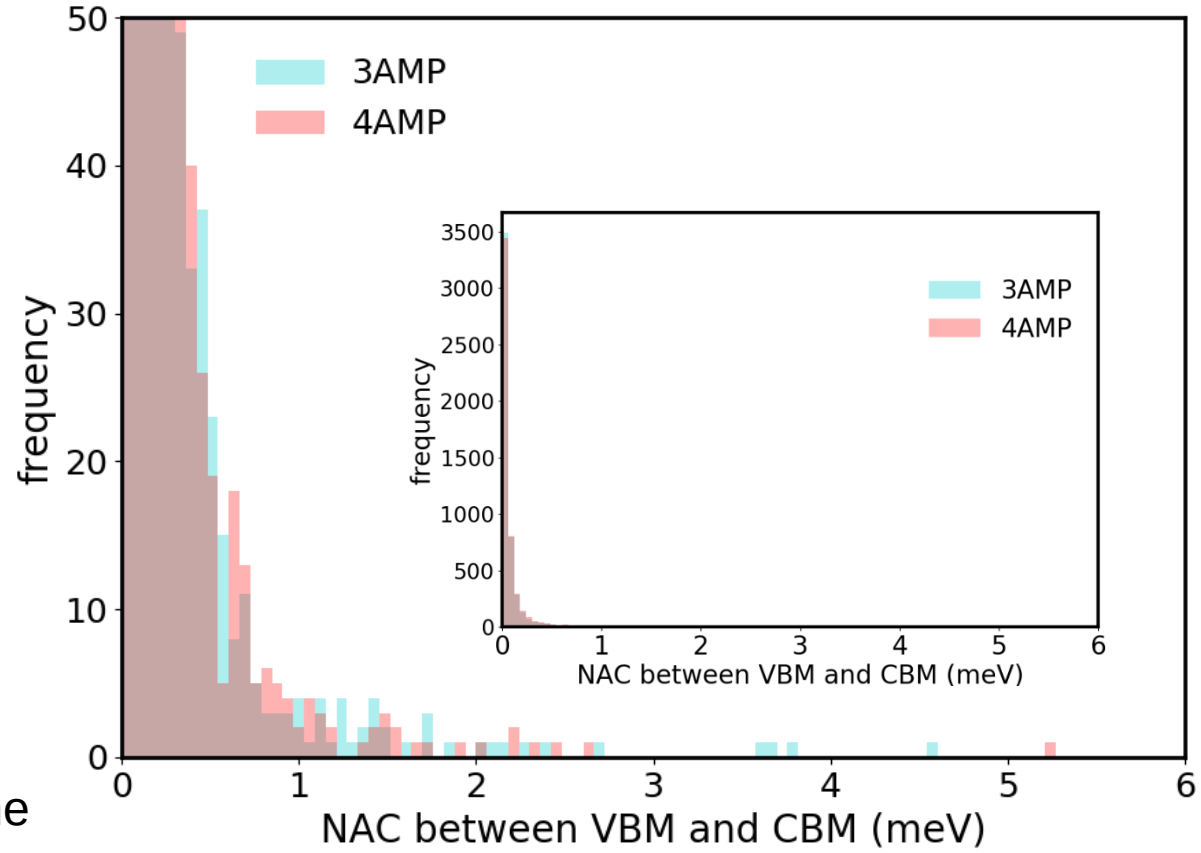

Areas when NAC > 0.1 meV of 3AMP 4AMP is almost the same

Dephasing time decides the nonradiative lifetime difference

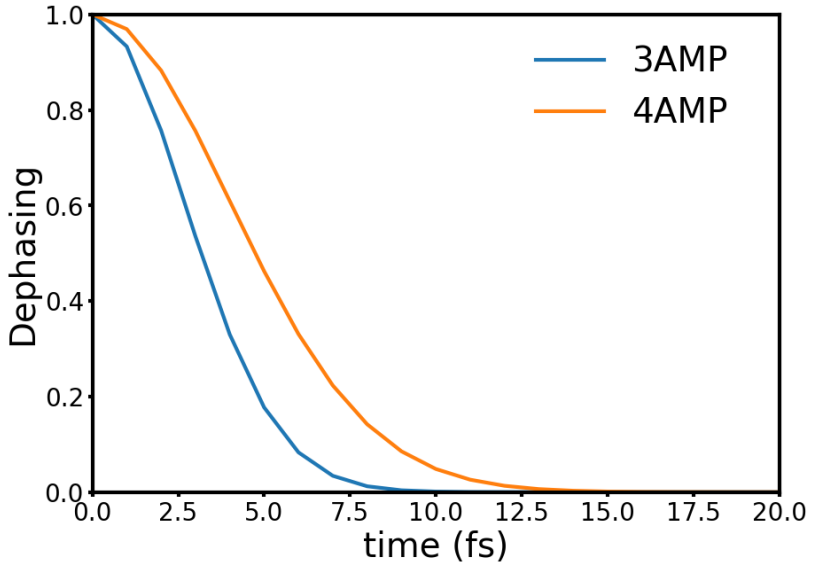

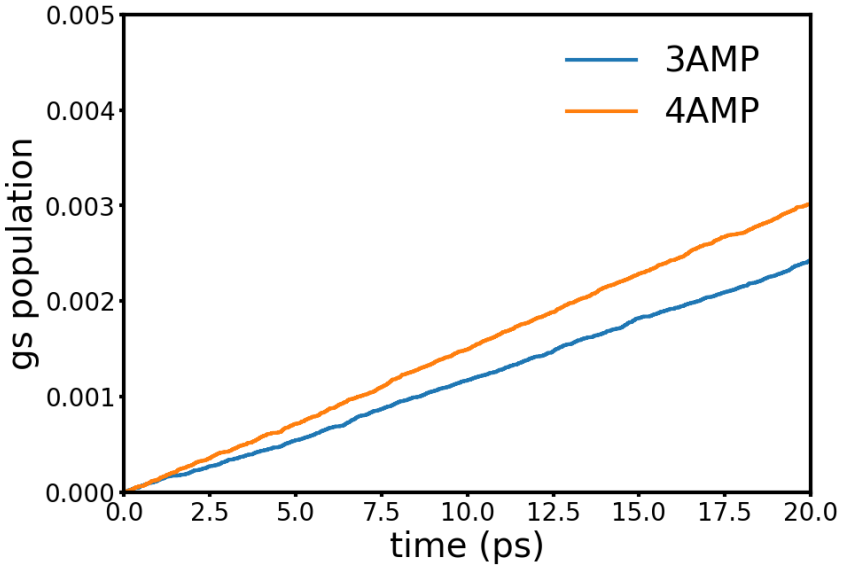

species	Bandgap (eV, 0K)	Bandgap (eV, 300K)	NAC (meV, rms)	Dephasing time (fs)	Radiative lifetime (μs)	Nonradiative lifetime (ns)
3AMP	1.82	1.40	0.21	2.69	1.03	4.12
4AMP	1.89	1.52	0.19	4.03	1.14	3.32

Conclusion

- Nonadiabatic coupling (NAC) doesn't play an important role in determining nonradiative lifetime
- The shorter dephasing time leads to the longer nonradiative lifetime of 3AMP, better solar cell performance

Future:

- Relation between the structures and optoelectronic properties.
- Analyzing the vibrational modes which facilitate electron-phonon coupling

Thank you for your attention

Q & A

References

[1] Mao, Lingling, et al. "Hybrid Dion–Jacobson 2D lead iodide perovskites." *Journal of the American Chemical Society* 140.10 (2018): 3775-3783.

[2] Pedesseau, Laurent, et al. "Advances and promises of layered halide hybrid perovskite semiconductors." *ACS nano* 10.11 (2016): 9776-9786.

[3] Yan, Jielin, et al. "Recent progress in 2D/quasi-2D layered metal halide perovskites for solar cells." *Journal of Materials Chemistry A* 6.24 (2018): 11063-11077.

[4] Zhang, Zhaosheng, et al. "Rapid decoherence suppresses charge recombination in multi-layer 2D halide perovskites: Time-domain ab initio analysis." *Nano letters* 18.4 (2018): 2459-2466.

[5] Zhou, Liujiang, et al. "Density of states broadening in CH3NH3PbI3 hybrid perovskites understood from ab initio molecular dynamics simulations." *ACS Energy Letters* 3.4 (2018): 787-793.

[6] Filip, Marina R., Carla Verdi, and Feliciano Giustino. "GW band structures and carrier effective masses of CH3NH3PbI3 and hypothetical perovskites of the type APbI3: A= NH4, PH4, AsH4, and SbH4." The Journal of Physical Chemistry C 119.45 (2015): 25209-25219.

Appendix

Methodology-nonadiabatic molecular dynamics (NAMD)

Mixed quantum-classical method

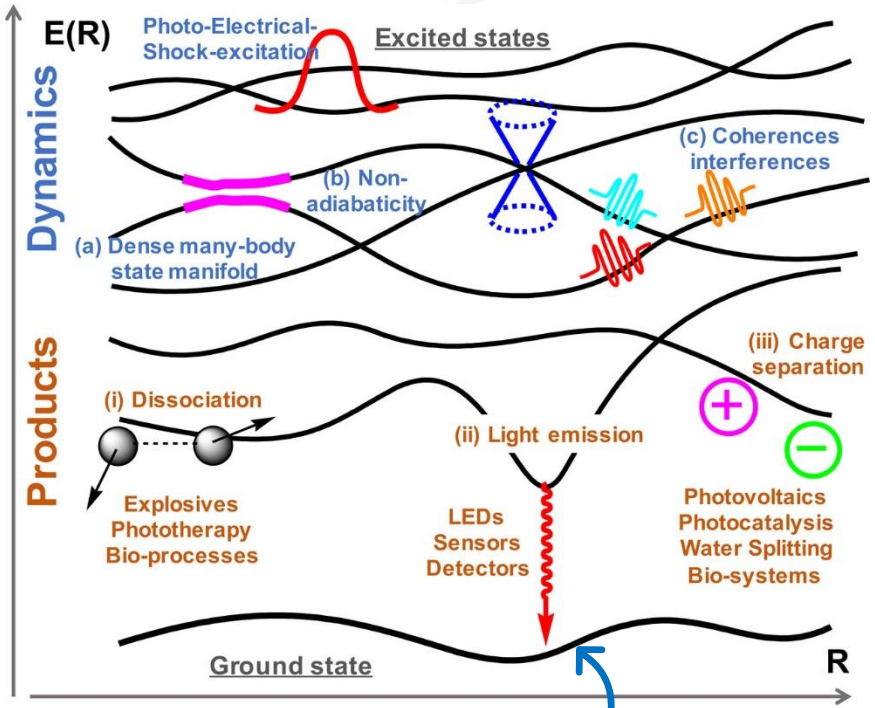

Nuclei are treated classically Molecular dynamics (MD) trajectory is predetermined and independent of electronic evolution

Multielectron adiabatic representation

$\Psi(r,R,t)=\sum_{i=0}^{N_b-1} C_i(t)\,\Phi_i(r|R)$

Time-dependent Schrodinger eq

$$i\hbar\frac{\partial\Psi(r,R,t)}{\partial t}=H(r,R,t)\Psi(r,R,t)$$

Nonadiabatic coupling (NAC)

$$i\hbar\frac{dc_i}{dt}=\sum_{j=0}^{N_b-1}(\in_i \delta_{ij}-i\hbar\vec{d}_{ij})C_j \qquad \vec{d}_{ij}=\left\langle\phi_i\left|\frac{\partial\phi_j}{\partial\vec{R}}\right.\right\rangle,\ -i\hbar\vec{d}_{ij}\equiv\text{NAC}$$

Decoherence-induced surface hopping (DISH)

t>τ_α, the system either hops to that state with probability $|c_\alpha|^2$ or the state is projected out with probability 1-$|c_\alpha|^2$

τ_α -- decoherence time

$$g_{i\to j}=p_{i\to j}\,b_{i\to j},\ b_{i\to j}=\begin{cases}exp\left(-\frac{\varepsilon_j-\varepsilon_i}{k_BT}\right) & \varepsilon_j>\varepsilon_i\\ 1 & \varepsilon_j\le\varepsilon_i\end{cases}$$

Chem. Rev. 2020, 120, 4, 2215-2287

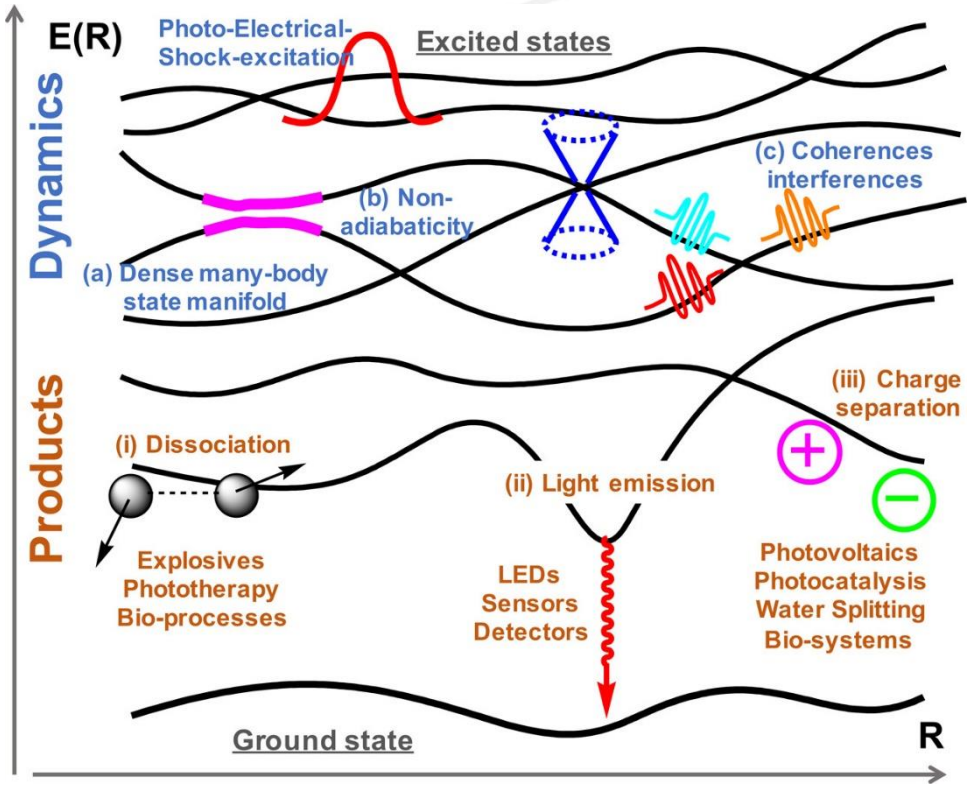

When decoherence time is shorter than the time of coherent electronic transition—including decoherence in surface hopping

$$C_{un}(t) = \langle \delta E(t) \delta E(0) \rangle_T$$

Decoherence function

$$D(t) = exp\left(-\frac{1}{\hbar^2} \int_0^t dt' \int_0^{t'} dt'' C(t'') \right)$$

Gaussian fitting

Decoherence function characterizes the dephasing time.

Long-timescale simulations of morphological changes in ThO_2 nanoparticles

Shanshan Wu
08/13/2020
Mentors: Danny Perez & Ping Yang

Motivation:

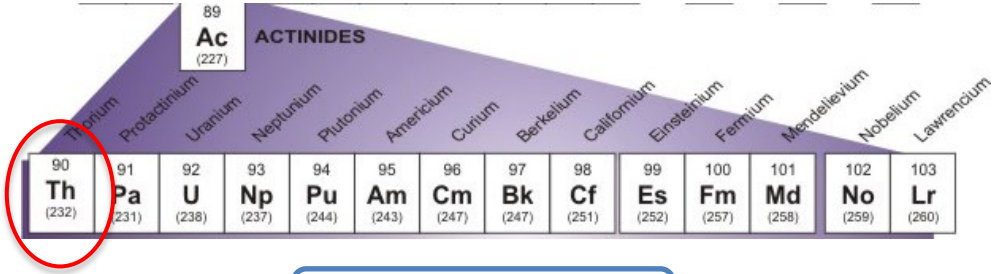

Properties:

Thorium is a naturally radioactive element

Thorium has abundant reserves (3-4 times of U)

ThO_2 is the highest melting point oxide (3390^{o}C)

ThO_2

Applications:

Nuclear reactor fuel pellets

Catalysts, optical glass

Sinter fine high-temperature ceramics

Goal

- Understand the dynamical and morphological properties of ultrasmall ThO_2 nanoparticles(NPs)
- Using accelerated molecular dynamics (AMD) simulations in actinide systems

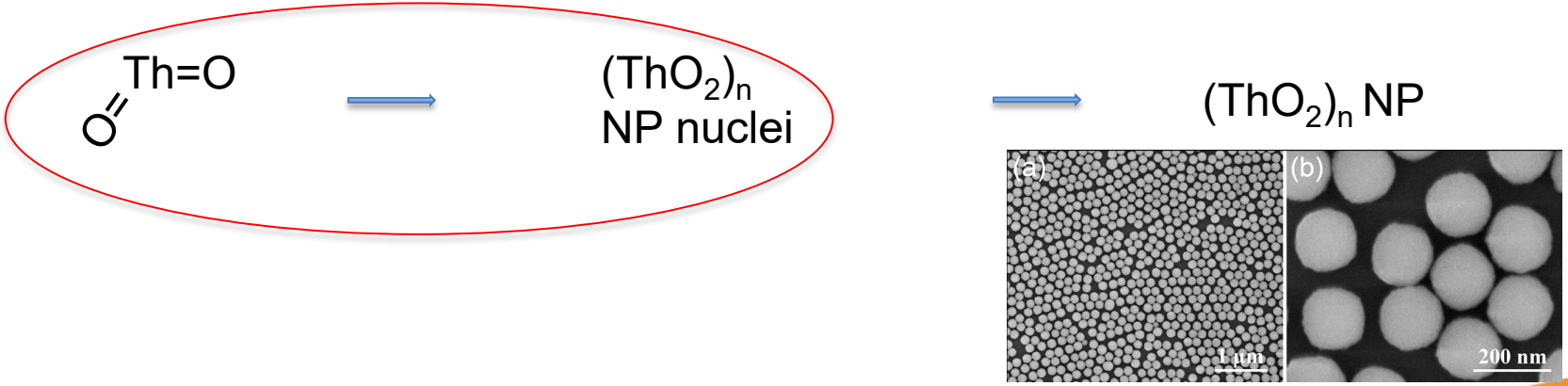

L. Wang, R. Zhao, X. Wang, L. Mei, L. Yuan, S. Wang, Z. Chai, W. Shi. *CrystEngComm* 16, no. 45 (2014): 10469-10475.

Parallel trajectory splicing (ParSplice) – An accelerated MD method

- MD simulation: numerical propagation of Newton's equation $m\ddot{x} = f = -\nabla U$
  - Provides fully-resolved atomistic trajectories
  - But the timescale of traditional MD is limited to ns
- ParSplice: parallelize MD simulation in the time domain to extend timescales to μs, ms

ParSplice

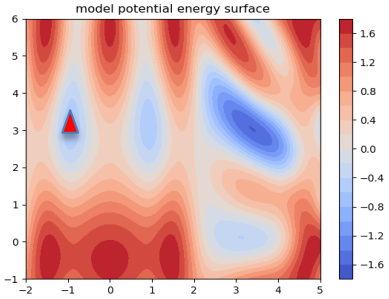

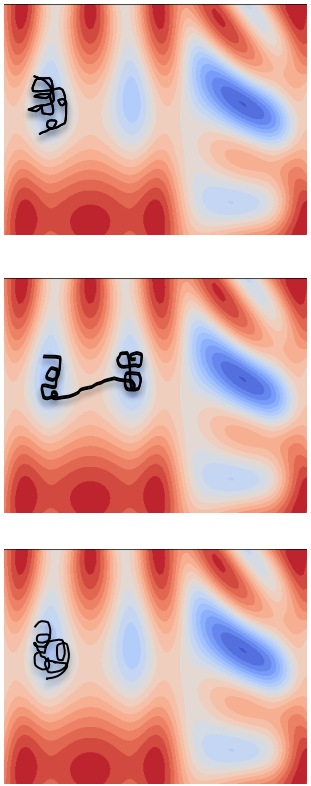

Start with any conformation

Segment database

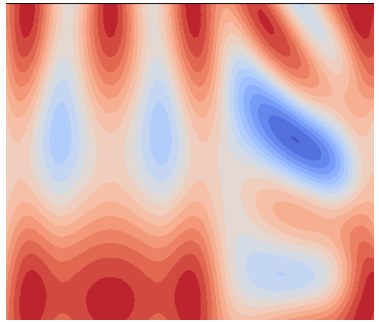

Spliced trajectory

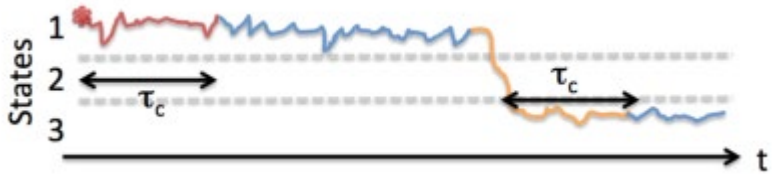

Spliceable segments
T_c: decorrelation time

- Lost strict time continuity
- Generate statistically correct state-to-state trajectories
- Use HPC efficiently

D Perez, ED Cubuk, A Waterland, J. Chem Theory Comput12.1 (2016): 18-28.

AMD simulation of $(ThO_2)_n$ in vacuum

Force field: EAM/alloy
Systems being studied:

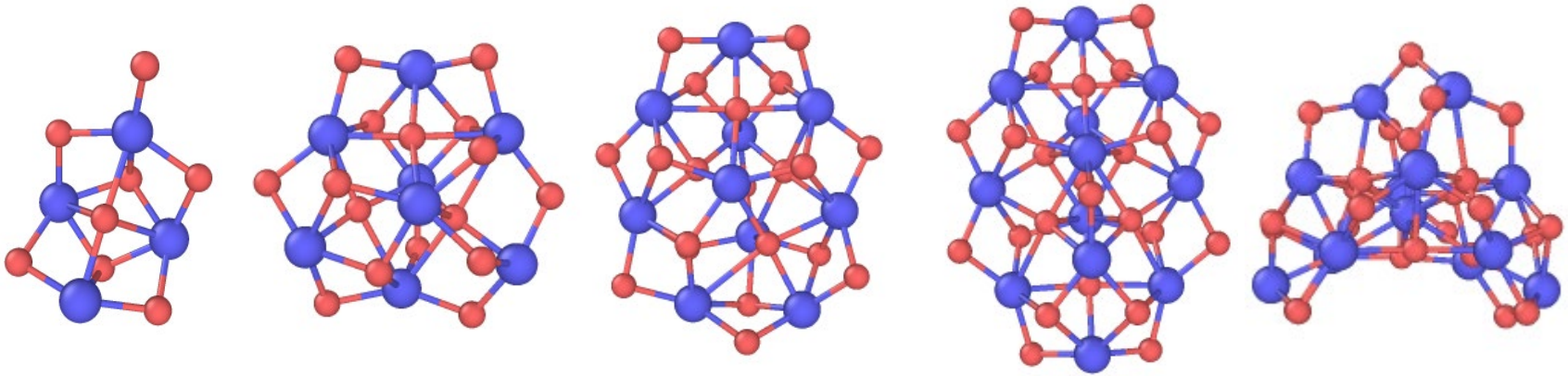

n	4	8	10	12	13
size	0.6nm	0.8nm	1.0nm	1.1nm	0.9nm

M.W.D. Cooper, M.J.D Rushton, R.W. Grimes, *J. Phys. Condens. Matter* **26** (2014) 105401.

AMD simulation of $(ThO_2)_n$ in vacuum at 1000K

n=4

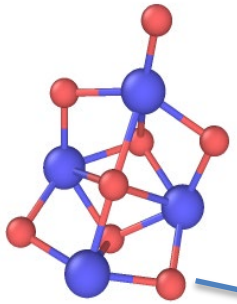

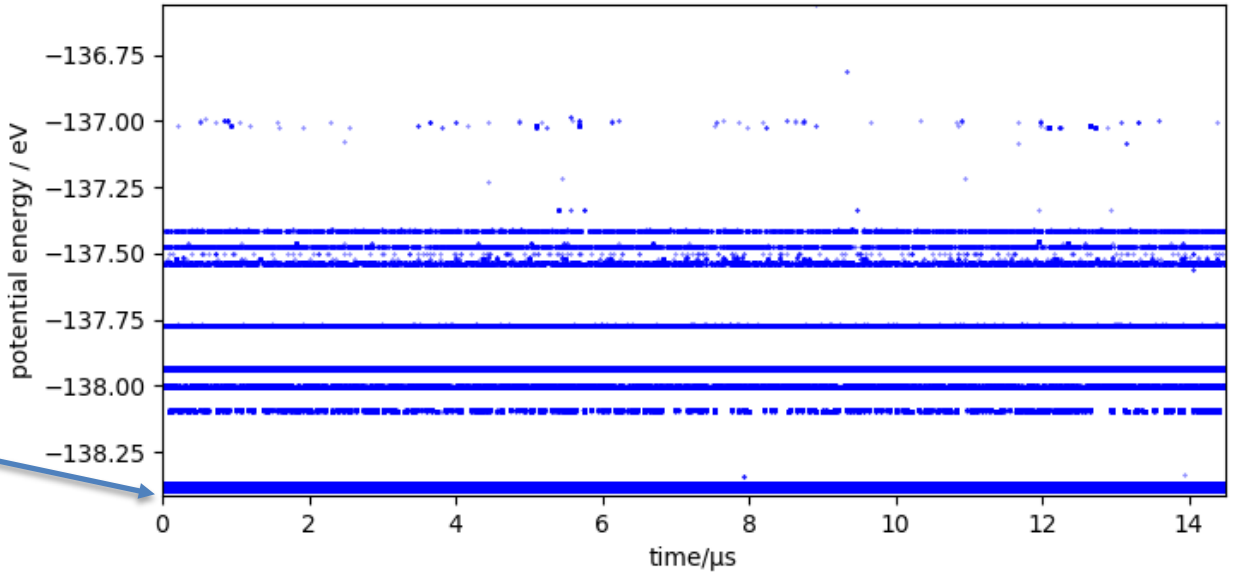

- One global minimum
- Frequent transitions among local minima

AMD simulation of $(ThO_2)_n$ in vacuum at 1000K

n=8

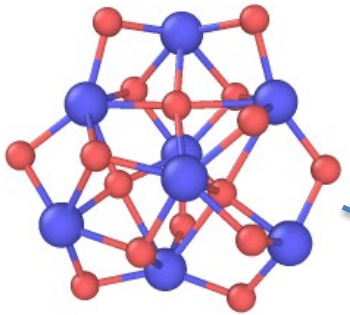

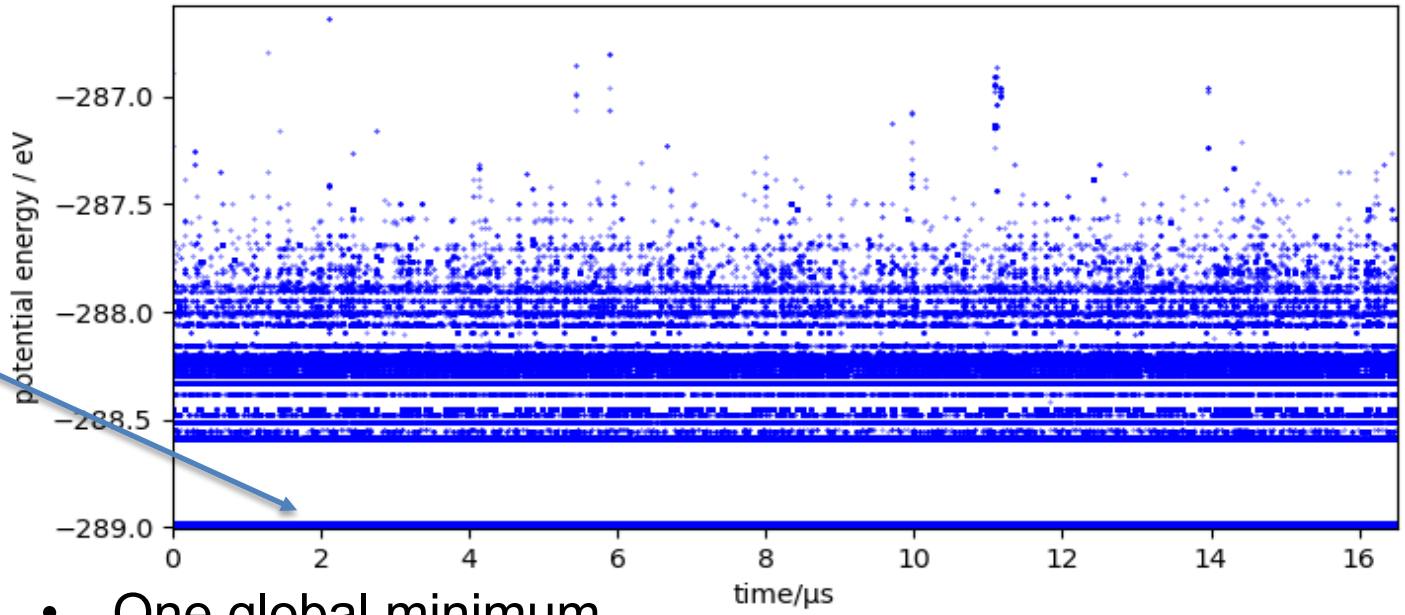

- One global minimum
- Frequent transitions among local minima

AMD simulation of $(ThO_2)_n$ in vacuum at 1000K

n=10

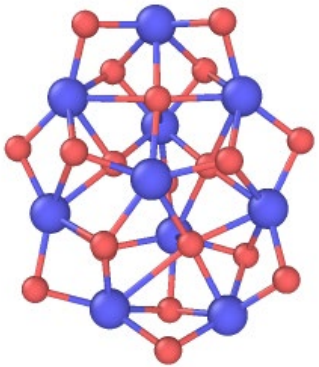

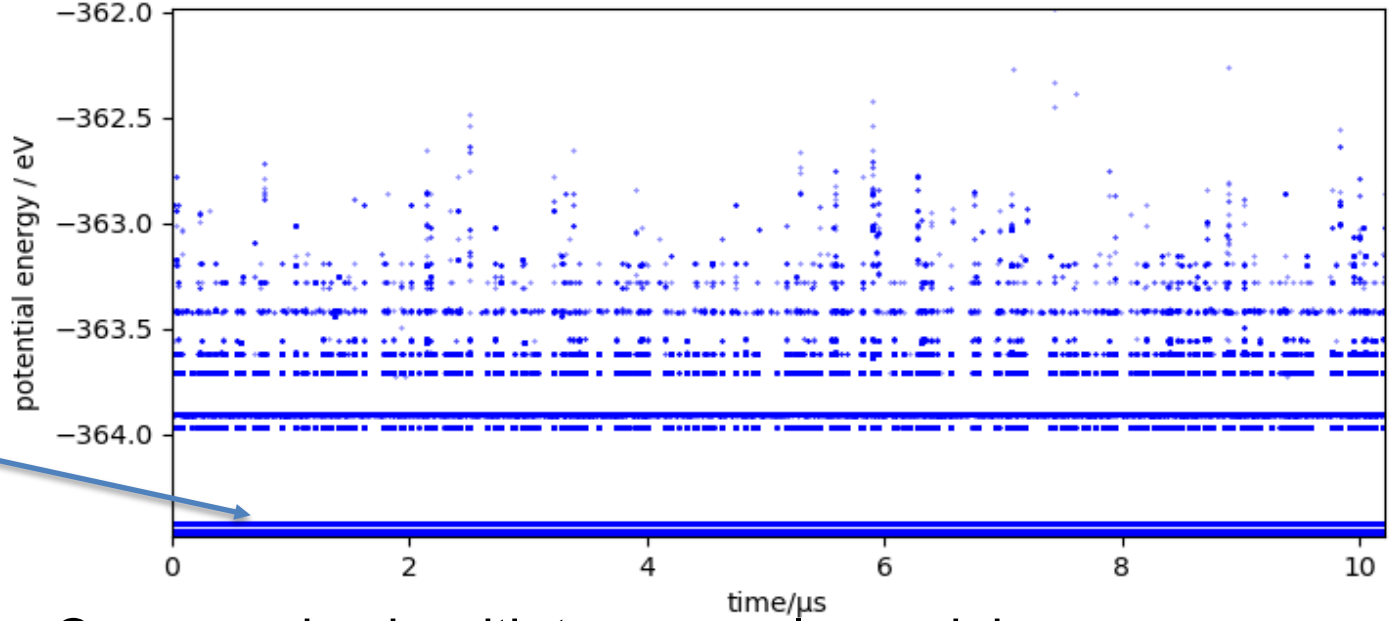

- One superbasin with two very close minima
- Frequent transitions among local minima

AMD simulation of $(ThO_2)_n$ in vacuum at 1000K

n=12

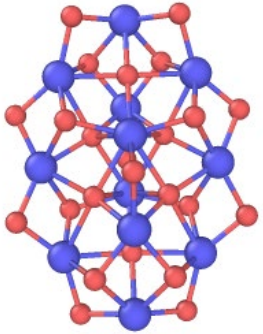

Front view

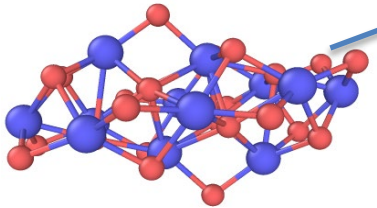

Side view

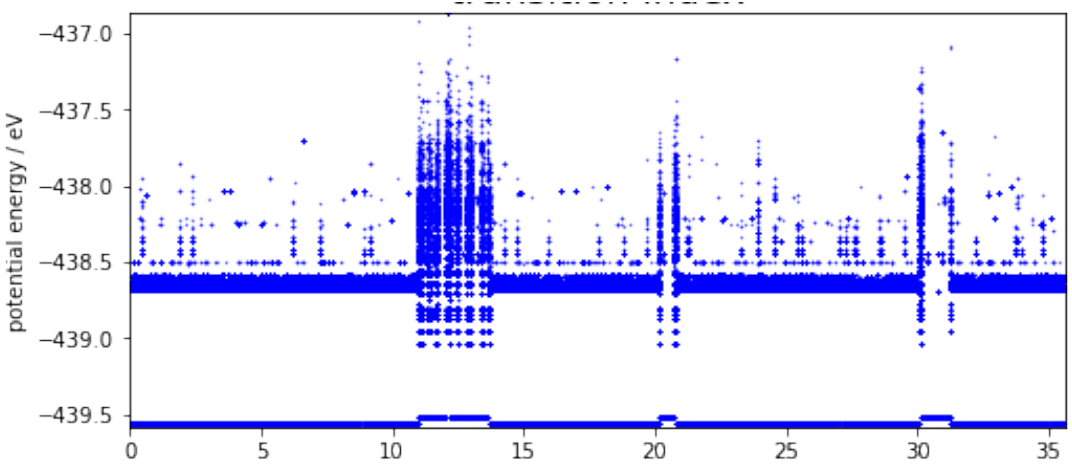

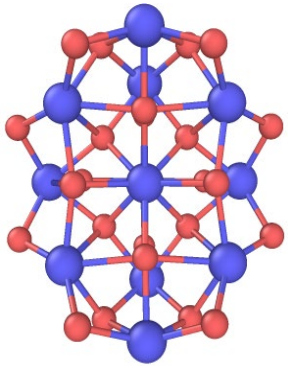

Front view

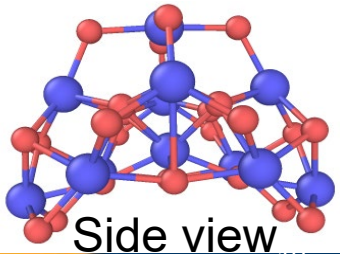

Side view

- T
- A
- S

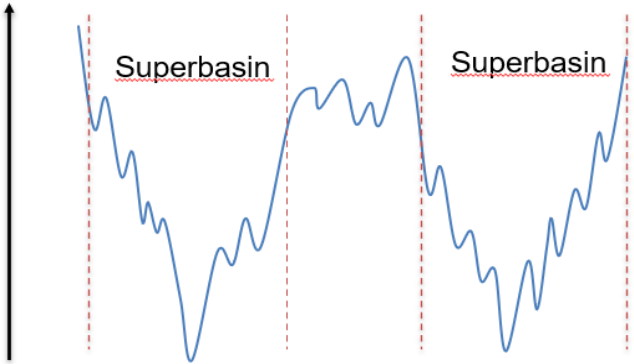

cale
e energy

AMD simulation of $(ThO_2)_n$ in vacuum at 1000K

n=12

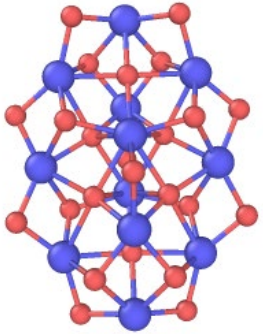

Front view

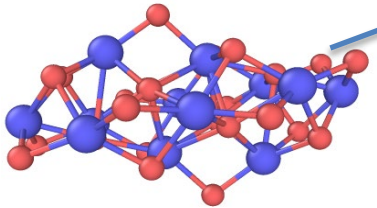

Side view

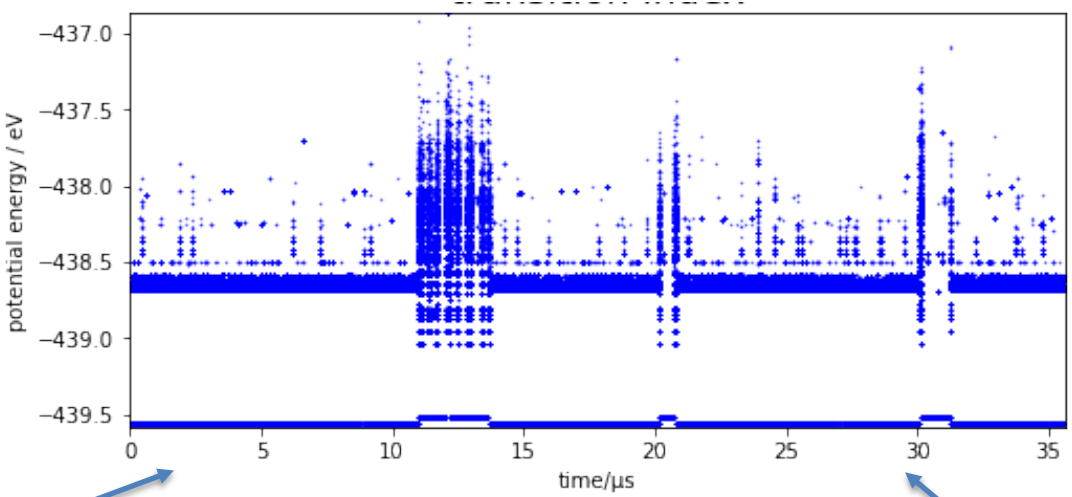

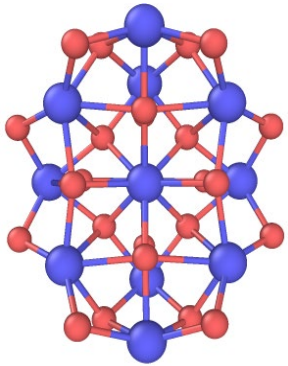

Front view

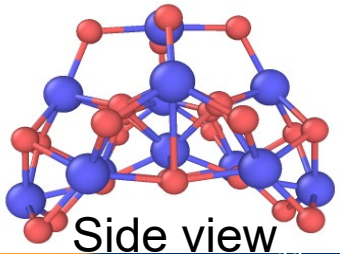

Side view

- Two superbasins were visited
- Activated process occur on μs timescale
- Stretched structure has minimum free energy

Minimum energy pathway of n=12 transition

2.3eV PE barrier

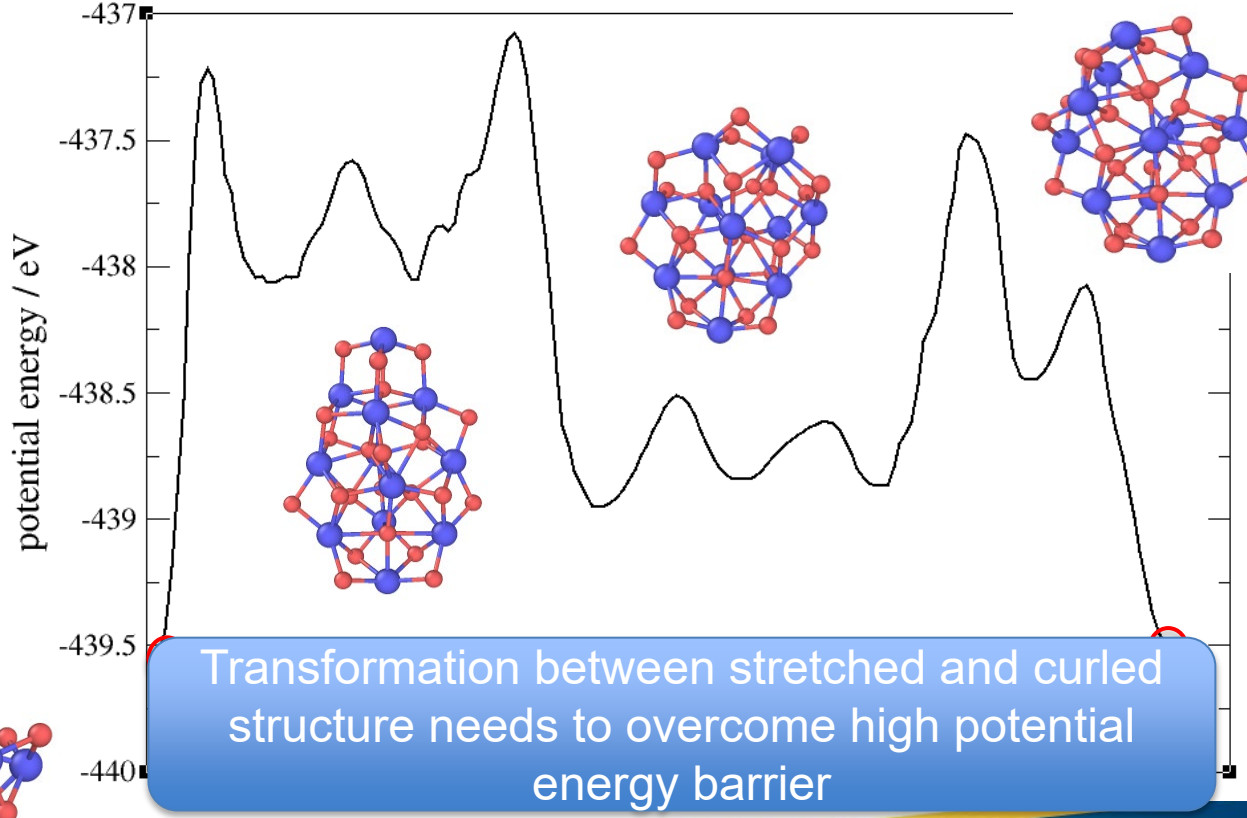

Transformation between stretched and curled structure needs to overcome high potential energy barrier

AMD simulation of $(ThO_2)_n$ in vacuum at 1000K

n=13

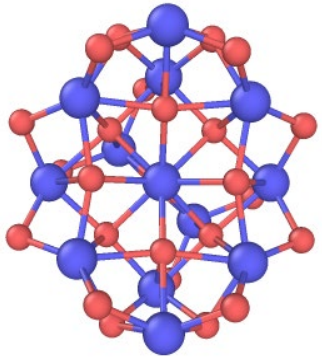

Front view

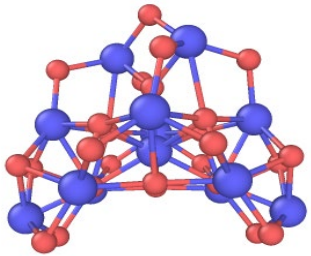

Side view

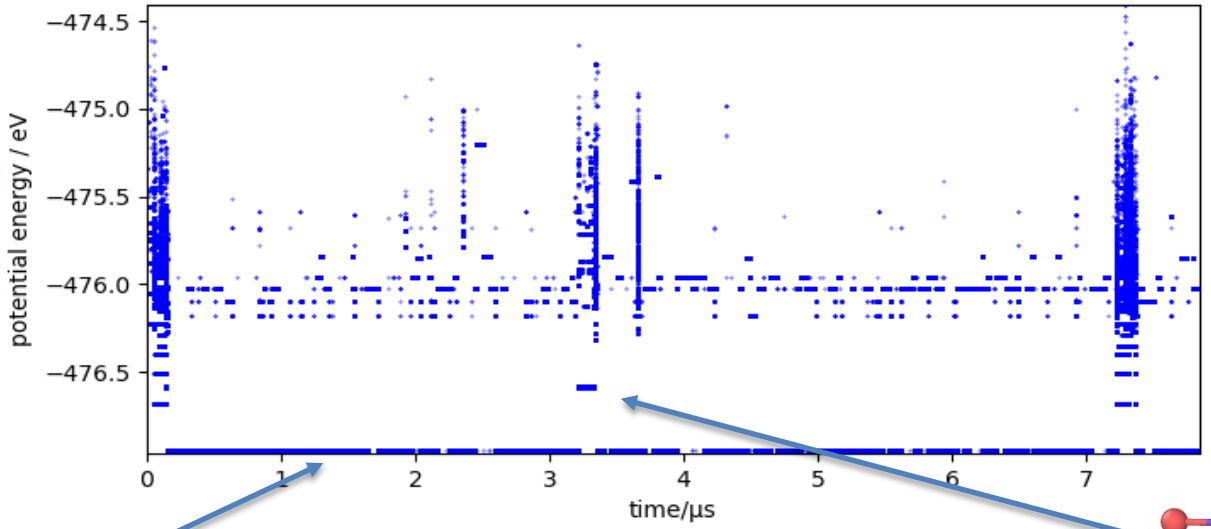

Two superbasins were visited
Curled structure has minimum free energy

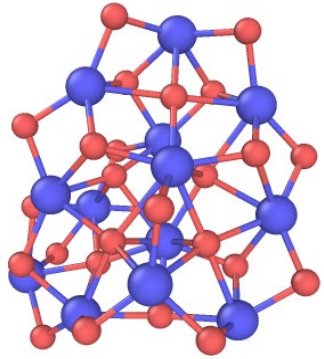

Front view

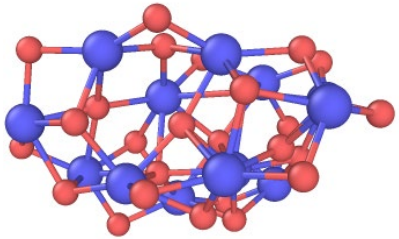

Side view

Conclusion

- This is the first ThO_2 NP system to be studied by the long-timescale dynamics.
- ThO_2 NPs ≤10 units have one superbasin. Local minima will relax to global minimum quickly. At lower temperature, one global conformation may be observed
- ThO_2 NPs with 12 and 13 units have two superbasins. Two types of configurations may be observed. The slow time scale of transition from stretched to curled conformation may affect the growth of small NPs.

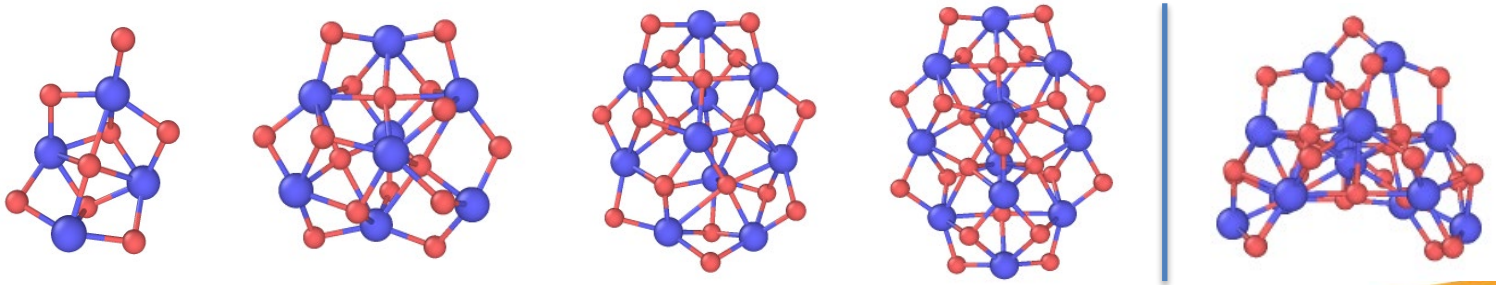

Future work

- Accelerated Quantum MD simulations of ThO_2 NPs
- AMD simulation of larger size clusters to understand the nucleation process

Acknowledgments:

Mentors:

Dr. Danny Perez
Dr. Ping Yang

FUND:

CNLS GRA fellowship
DOE-ECP project

Supercomputers:

CASCADE at PNNL
grizzly at LANL

Thank you

Questions ?